Preparation and Characterisation of Novel Lyotropic Liquid Crystalline Colloidal Systems

A

Thesis

Submitted for the award of degree of

DOCTOR OF PHILOSOPHY

By

Ravi Kumar Shukla

Reg. No. 900812007

Under the supervision of

Dr. K.K. Raina

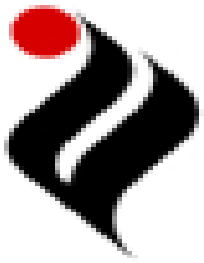

School of Physics and Materials Science,

Thapar University, Patiala - 147004

INDIA.

AUGUST 2012

DECLARATION

I hereby certify that the work which is presented in thesis entitled **"Preparation and characterisation of novel lyotropic liquid crystalline colloidal systems"** in the partial fulfillment of the requirement for award of the degree of DOCTOR OF PHILOSOPHY in the School of Physics and Materials Science, Thapar University, Patiala, is an authentic record of my own work carried out under the supervision of Dr. K. K. Raina. The matter embodied in this report has not been submitted in part or full to any other university or institute for the award of any degree.

(Ravi Kumar Shukla)

This is to certify that the above statement made by the candidate is correct and true to the best of my knowledge.

Date: August 20, 2012

Dr. K.K. Raina

Deputy Director, Thapar University,

Patiala-147004

DEDICATED TO

MY DEAREST GRAND MAA

AND PARENTS

ACKNOWLEDGEMENTS

I find it very difficult to write something in short to acknowledge my research guide, **Dr. K.K. Raina**. His constant inspiration, invaluable, guidance and constructive criticism helped a lot to focus my views in proper perspective. I take this opportunity to express my intense reverence towards him for guiding me in the right direction throughout the course of this work. My deepest personal regards are due for him forever.

I wish to convey my sincere gratitude to **Dr. Kulvir Singh** (Head School of Physics and Materials Science), **Dr. O.P Pandey** and **Dr. P. K. Bajpai** (Dean, R&SP) for helping me in every possible way through fruitful discussions.

I am grateful to **Dr. Rajiv Mehta, Dr. D.P. Singh** for being part of my thesis committee and **Dr. Puneet Sharma, Ms Loveleen Brar, Dr. Rajesh Kumar, Dr. B. N. Chudashama and Dr. H. Bhunia** helping me in many stages for experimentation, data analysis and to raise the quality of my work. Their contribution is invaluable. All the **faculties and staff** of SPMS are acknowledged who never turned me down whenever I approached for any help.

I would also like to thank **Dr. Kiran Singh patyal, Dr. Mukesh Garg, Dr. Manglesh Dixit, Dr. Sanjeev Kumar, Dr. Vishal Chaudhary, Dr. Gurbinder kaur Chaudhary, Dr. Ankush Pathania, Dr. Amit awasthi, Dr. Dinesh Kumar, Dr. Dinesh Pathak, Dr. Mukesh Kumar, Dr. Santosh Pathak, Dr. Shikha Kapila, Dr. Parveen Kumar, Dr. Partibha, Mr. Vishal Mutreja and Mr. Rakesh sharma** for their invaluable help in all my endeavors company at work.

I also take this golden opportunity to convey my earnest respect to my schoolteachers **Mr. Brij lal Sharma** and **Mr. R.K. Bindra** for their extraordinary way of teaching that build up my research career in science.

I would like to express my appreciation to my colleagues and dearest friends **Ranvir Panwar, Akash katoch, Ashok Chaudhary, Renu rani, Rekha Rani,**

Rishi, Ramneek, Gurpreet, Supreet, Gourav Singla, Paramjyot jha, Samita Thakur, Suresh, Mintu Tayagi, Nadeem Vinit, narender and Vikas for their unfailing support and encouragement during many years of studies, that they have shown to me in their own special way.

The Financial support from Defense Research and Development Organization (DRDO) and Department of Science and Technology (DST) India in the form senior research fellowship (SRF) is duly acknowledged.

The thesis could not have been completed without the endless love and blessings of my family. **Dearest Grand Maa, Mother, Father, Sisters and Brothers in law**, I should not be little you by thanking; you taught me how to dream, gave me the skills to chase after those dreams, and encouraged me to reach the goal.

Above all, thanks to the **almighty** beneath the blue sky for bestowing me with his precious blessings!

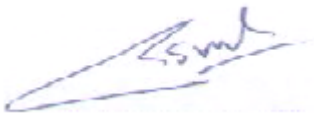

Ravi Kumar Shukla

INDEX

Content		Page no
List of Figure		*(i-vii)*
List of tables		*(viii)*
List of Publications		*(ix-x)*
List of abbreviation and symbols		*(xi-xiv)*
Preface		*(xv-xvi)*
Chapter 1: Introduction and literature review		
1.1	Liquid crystals	2
1.2	Objectives	3
1.3	Lyotropic liquid crystals	3
1.3.1	LLC mesophases derived from aqueous solvents	6
1.3.2	LLC mesophases derived from non-aqueous Solvents	7
1.3.3	Transition Metal Salt based systems	10
1.3.4	Liquid crystalline colloidal systems	10
1.4	Applications prospective of lyotropic phases	14
1.4.1	Soft template	14
1.4.2	Drug delivery systems	15
1.5	References	16
Chapter 2: Experimental methods and characterization techniques		
2.1	Materials	22
2.2	Preparation of lyotropic liquid crystalline materials	23
2.2.1	Binary mixtures	23
2.2.2	Ternary mixtures	24
2.2.3	Synthesis of zinc oxide	24
2.2.4	Colloidal mixtures	25
2.3	Characterization techniques	25
2.3.1	Structural analysis through X-ray diffraction	25
2.3.2	Morphological analysis through Polarizing Optical Microscopy	26
2.3.3	Thermal analysis through Differential scanning calorimetry	27
2.3.4	Dielectric spectroscopy	29
2.3.5	Refractive Index	32
2.4	References	33
Chapter 3: Aqueous and non-aqueous binary lyotropic liquid crystalline mixtures		
3.1	Cationic surfactant	34
3.1.1	Structural analysis	35
3.1.2	Thermal analysis	44

3.1.3	Dielectric spectroscopy	50
3.1.4	Activation energy	56
3.1.5	Refractive index	57
3.2	Anionic surfactant	59
3.2.1	Structural analysis	59
3.2.2	Thermal analysis	69
3.2.3	Dielectric spectroscopy	74
3.2.4	Activation energy	79
3.2.5	Refractive index	80
3.3	Non-Ionic surfactant	81
3.3.1	Structural analysis	82
3.3.2	Thermal analysis	85
3.3.3	Dielectric spectroscopy	91
3.3.4	Activation energy	96
3.3.5	Refractive index	96
3.4	Conclusions	98
3.5	References	99

Chapter 4: Transition metal based Ternary non-aqueous LLC mixtures

4.1	Structural analysis	100
4.2	Thermal analysis	104
4.3	Refractive index	108
4.4	Conclusions	109
4.5	References	110

Chapter 5: Lyotropic colloidal mixtures

5.1	Pure Zinc oxide (ZnO)	111
5.2	Lyotropic colloidal systems	112
5.2.1	Structural analysis	112
5.2.2	Thermal analysis	115
5.2.3	Dielectric spectroscopy	118
5.2.4	Activation energy	123
5.2.5	Refractive index	124
5.3	Conclusions	125
5.4	References	127

Chapter 6: Conclusions and future scope

6.1	Conclusions	128
6.2	Future scope	130

LIST OF FIGURES

Content Page no

Chapter 1: Introduction and literature review

Figure 1.1:	Schematic of self assembly in liquid crystals and their applications.	1
Figure 1.2:	Distinct phases of thermotropic liquid crystals (a) nematic (b) smectic A (c) smectic C (d) chiral nematic (e) chiral smectic.	2
Figure 1.3:	Schematic of amphiphiles.	3
Figure 1.4:	Schematic of critical packing parameter (CPP) of amphiphile.	4
Figure 1.5:	Representation of the packing parameters and the diverse lyotropic liquid crystalline geometries at the expense of increasing surfactant concentration.	6
Figure 1.6:	Phase diagram for the liquid crystalline geometries at the expense of increasing surfactant concentration and temperature.	6
Figure 1.7:	Potential energy curves for stable and unstable dispersions.	12
Figure 1.8:	Growth process of nanostructures in the lyotropic liquid crystalline templates.	14
Figure 1.9:	Structures of (a) reversed bicontinuous cubic and (b) hexagonal Mesophases.	15

Chapter 2: Experimental methods and characterization techniques

Figure 2.1:	Schematic for two dimensionally hexagonally arranged cylindrical micelles.	26
Figure 2.2:	Optical polarizing microscope and thermo-optical set up.	27
Figure 2.3:	Differential scanning calorimeter set up.	28
Figure 2.4:	(a) Schematic for assembly of liquid crystal cell. (b) various capacitor of lyotropic materials.	30
Figure 2.5:	(a) Programmable RCL meter [FLUKE PM6306] used for dielectric studies (b) Block diagram of the experimental set-up to study textures and dielectric properties of lyotropic liquid crystal.	31
Figure 2.6:	Abbe refractrometer used for optical measurements.	32

Figure 3.1: XRD profiles of as prepared mixtures at varying concentration (M1=10:90wt%, M2= 30:70wt%, M3= 40:60 wt%, M4= 50:50wt% and M5= 75:25wt% stands for concentration of respective solute : solvent) at 303K (a) cetyl pyridinium chloride: ethylene glycol series (CEM1-5) (b) cetyl pyridinium chloride : water series (CWM1-5) (c) cetyl pyridinium chloride : formamide series (CFM1-5) respectively. 36

Figure 3.2: XRD profiles of quenched mixtures at varying concentration (M1=10:90wt%, M2= 30:70wt%, M3= 40:60 wt%, M4= 50:50wt% and M5= 75:25wt% stands for concentration of respective solute : solvent) at 303K (a) cetyl pyridinium chloride: ethylene glycol series (CEM1-5) (b) cetyl pyridinium chloride : water series (CWM1-5) (c) cetyl pyridinium chloride : formamide series (CFM1-5) respectively. 39

Figure 3.3: Texture patterns of as prepared mixtures at varying concentration (M1=10:90wt%, M2= 30:70wt%, M3= 40:60 wt%, M4= 50:50wt% and M5= 75:25wt% stands for concentration of respective solute : solvent) at 303K (Col.1) cetyl pyridinium chloride: ethylene glycol series (CEM1-5) (Col.2) cetyl pyridinium chloride : water series (CWM1-5) (Col.3) cetyl pyridinium chloride : formamide series (CFM1-5) respectively. 42

Figure 3.4: Texture patterns of quenched mixtures at varying concentration (M1=10:90wt%, M2= 30:70wt%, M3= 40:60 wt%, M4= 50:50wt% and M5= 75:25wt% stands for concentration of respective solute : solvent) at 303K (Col.1) cetyl pyridinium chloride: ethylene glycol series (CEM1-5) (Col.2) cetyl pyridinium chloride : water series (CWM1-5) (Col.3) cetyl pyridinium chloride : formamide series (CFM1-5) respectively. 43

Figure 3.5: Variation of thermo-dynamical parameters for cetyl pyridinium chloride: ethylene glycol (CPC: EG) mixtures (M1=10:90wt%, M2= 30:70wt%, M3= 40:60 wt%, M4= 50:50wt% and M5= 75:25wt% stands for concentration of respective solute: solvent) (a) heat flow (b) enthalpy (c) thermo-optical analysis. 46

Figure 3.6: Variation of thermo-dynamical parameters for cetyl pyridinium chloride : water (CPC: W) mixtures (M1=10:90wt%, M2= 30:70wt%, M3= 40:60 wt%, M4= 50:50wt% and M5= 75:25wt% stands for concentration of respective solute: solvent) (a) heat flow (b) enthalpy (c) thermo-optical analysis. 48

Figure 3.7:	Variation of thermo-dynamical parameters for cetyl pyridinium chloride: formamide CPC: F mixtures (M1=10:90wt%, M2= 30:70wt%, M3= 40:60 wt%, M4= 50:50wt% and M5= 75:25wt% stands for concentration of respective solute: solvent) (a) heat flow (b) enthalpy (c) thermo-optical analysis.	50
Figure 3.8:	Variation of complex permittivity as function of frequency at 303K (a) cetyl pyridinium chloride: ethylene glycol series (b) cetyl pyridinium chloride: water series (c) cetyl pyridinium chloride: formamide series respectively. Where M1=10:90wt%, M2= 30:70wt% and M4= 50:50wt% stands for concentration of respective solute: solvent.	51
Figure 3.9:	Schematic for the dielectric process in lamellar mesophase	52
Figure 3.10:	Variation of complex permittivity as function of temperature for cetyl pyridinium chloride: ethylene glycol series, cetyl pyridinium chloride: water series and cetyl pyridinium chloride: formamide series respectively (Col.1) real part. (Col.2) imaginary part.	53
Figure 3.11:	Cole-Cole plot at 303K (a) cety pyridinium chloride: ethylene glycol series (b) cetyl pyridinium chloride: water series (c) cetyl pyridinium chloride: formamide series respectively. Where M1=10:90wt%, M2= 30:70wt% and M4= 50:50wt% stands for concentration of respective solute: solvent.	55
Figure 3.12:	Arrhenius plot for CPC: EG series (a) for CEM 1(b) for CEM 2(c) for CEM 4. Where M1=10:90wt%, M2= 30:70wt% and M4= 50:50wt% stands for concentration of respective solute: solvent.	57
Figure 3.13:	Variation of refractive index as a function of temperature (a) cety pyridinium chloride: ethylene glycol series (b) cetyl pyridinium chloride: water series (c) cetyl pyridinium chloride: formamide series respectively. Where M1=10:90wt%, M2= 30:70wt% and M4= 50:50wt% stands for concentration of respective solute: solvent.	58
Figure 3.14:	XRD profiles of as prepared mixtures at varying concentration (M1=10:90wt%, M2= 30:70wt%, M3= 40:60 wt%, M4= 50:50wt% and M5= 75:25wt% stands for concentration of respective solute : solvent) at 303K (a) sodium dodecyl sulfate : ethylene glycol series (SEM1-5) (b) sodium dodecyl sulfate : water series (SWM1-5) (c) sodium dodecyl sulfate : formamide series (SFM1-5) respectively.	61
Figure 3.15:	XRD profiles of quenched mixtures at varying concentration (M1=10:90wt%, M2= 30:70wt%, M3= 40:60 wt%, M4= 50:50wt% and M5= 75:25wt% stands	65

for concentration of respective solute : solvent) at 303K (a) sodium dodecyl sulfate : ethylene glycol series (SEM1-5) (b) sodium dodecyl sulfate : water series (SWM1-5) (c) sodium dodecyl sulfate : formamide series (SFM1-5) respectively.

Figure 3.16: Texture patterns of as prepared mixtures at varying concentration (M1=10:90wt%, M2= 30:70wt%, M3= 40:60 wt%, M4= 50:50wt% and M5= 75:25wt% stands for concentration of respective solute : solvent) at 303K (Col.1) sodium dodecyl sulfate : ethylene glycol series (SEM1-5) (Col.2) sodium dodecyl sulfate : water series (SWM1-5) (Col.3) sodium dodecyl sulfate : formamide series (SFM1-5) respectively. 67

Figure 3.17: Texture patterns of quenched mixtures at varying concentration (M1=10:90wt%, M2= 30:70wt%, M3= 40:60 wt%, M4= 50:50wt% and M5= 75:25wt% stands for concentration of respective solute : solvent) at 303K (Col.1) sodium dodecyl sulfate : ethylene glycol series (SEM1-5) (Col.2) sodium dodecyl sulfate : water series (SWM1-5) (Col.3) sodium dodecyl sulfate : formamide series (SFM1-5) respectively. 68

Figure 3.18: Variation of thermo-dynamical parameters for sodium dodecyl sulfate: ethylene glycol (SDS: EG) mixtures (M1=10:90wt%, M2= 30:70wt%, M3= 40:60 wt%, M4= 50:50wt% and M5= 75:25wt% stands for concentration of respective solute: solvent) (a) heat flow (b) enthalpy (c) thermo-optical analysis. 71

Figure 3.19: Variation of thermo-dynamical parameters for sodium dodecyl sulfate: Water (SDS: W) mixtures (M1=10:90wt%, M2= 30:70wt%, M3= 40:60 wt%, M4= 50:50wt% and M5= 75:25wt% stands for concentration of respective solute: solvent) (a) heat flow (b) enthalpy (c) thermo-optical analysis. 73

Figure 3.20: Variation of thermo-dynamical parameters for sodium dodecyl sulfate: formamide (SDS: F) mixtures (M1=10:90wt%, M2= 30:70wt%, M3= 40:60 wt%, M4= 50:50wt% and M5= 75:25wt% stands for concentration of respective solute: solvent) (a) heat flow (b) enthalpy (c) thermo-optical analysis. 74

Figure 3.21: Variation of complex permittivity as function of frequency at 303K (a) sodium dodecyl sulfate: ethylene glycol series (b) sodium dodecyl sulfate: water series (c) sodium dodecyl sulfate: formamide series respectively. Where M1=10:90wt%, M2= 30:70wt% and M4= 50:50wt% stands for concentration of respective solute: solvent. 76

Figure 3.22: (a) Schematic for the dielectric process in hexagonal 77

mesophase before electric field (b) after electric field.

Figure 3.23: Variation of complex permittivity as function of temperature for sodium dodecyl sulfate: ethylene glycol series, sodium dodecyl sulfate: water series and sodium dodecyl sulfate: formamide series respectively (Col.1) real part. (Col.2) imaginary part. 78

Figure 3.24: Cole-Cole plot at 303K (a) sodium dodecyl sulfate: ethylene glycol series (b sodium dodecyl sulfate: water series (c) sodium dodecyl sulfate: formamide series respectively. Where M1=10:90wt%, M2= 30:70wt% and M4= 50:50wt% stands for concentration of respective solute: solvent. 79

Figure 3.25: Variation of refractive index as a function of temperature (a) sodium dodecyl sulfate: ethylene glycol series (b sodium dodecyl sulfate: water series (c) sodium dodecyl sulfate: formamide series respectively. Where M1=10:90wt%, M2= 30:70wt% and M4= 50:50wt% stands for concentration of respective solute: solvent. 81

Figure 3.26: Texture patterns of as prepared mixtures at varying concentration (M1=10:90wt%, M2= 30:70wt%, M3= 40:60 wt%, M4= 50:50wt% and M5= 75:25wt% stands for concentration of respective solute : solvent) at 303K (Col.1) tween 20 : ethylene glycol series (TEM1-5) (Col.2) tween 20 : water series (TWM1-5) (Col.3) tween 20 : formamide series (TFM1-5) respectively. 83

Figure 3.27: Texture patterns of quenched mixtures at varying concentration (M1=10:90wt%, M2= 30:70wt%, M3= 40:60 wt%, M4= 50:50wt% and M5= 75:25wt% stands for concentration of respective solute : solvent) at 303K (Col.1) tween 20 : ethylene glycol series (TEM1-5) (Col.2) tween 20 : water series (TWM1-5) (Col.3) tween 20: formamide series (TFM1-5) respectively.. 84

Figure 3.28: Variation of thermo-dynamical parameters for tween 20 : ethylene glycol (T20: EG) mixtures (M1=10:90wt%, M2= 30:70wt%, M3= 40:60 wt%, M4= 50:50wt% and M5= 75:25wt% stands for concentration of respective solute: solvent) (a) heat flow (b) enthalpy (c) thermo-optical analysis. 87

Figure 3.29: Variation of thermo-dynamical parameters for tween 20 : Water (T20: W) mixtures (M1=10:90wt%, M2= 30:70wt%, M3= 40:60 wt%, M4= 50:50wt% and M5= 75:25wt% stands for concentration of respective solute: solvent) (a) heat flow (b) enthalpy (c) thermo-optical analysis. 89

Figure 3.30: Variation of thermo-dynamical parameters for tween 20 : formamide (T20: F) mixtures (M1=10:90wt%, M2= 30:70wt%, M3= 40:60 wt%, M4= 50:50wt% and M5= 91

75:25wt% stands for concentration of respective solute: solvent) (a) heat flow (b) enthalpy (c) thermo-optical analysis.

Figure 3.31: Variation of complex permittivity as function of frequency at 303K (a) tween 20 : ethylene glycol series (b tween 20 : water series (c) tween 20 : formamide series respectively. (d) Schematic for dielectric process. Where M1=10:90wt%, M2= 30:70wt% and M4= 50:50wt% stands for concentration of respective solute: solvent. 93

Figure 3.32: Variation of complex permittivity as function of temperature for tween 20: ethylene glycol series, tween 20: water series and tween 20 : formamide series respectively (Col.1) real part. (Col.2) imaginary part. 94

Figure 3.33: Cole-Cole plot at 303K (a) tween 20 : ethylene glycol series (b tween 20 : water series (c) tween 20 : formamide series respectively. Where M1=10:90wt%, M2= 30:70wt% and M4= 50:50wt% stands for concentration of respective solute: solvent. 95

Figure 3.34: Variation of refractive index as a function of temperature (a) tween 20 : ethylene glycol series (b tween 20 : water series (c) tween 20 : formamide series respectively. Where M1=10:90wt%, M2= 30:70wt% and M4= 50:50wt% stands for concentration of respective solute: solvent. 97

Chapter 4: Transition metal based Ternary non-aqueous LLC mixtures

Figure 4.1: XRD profiles of quenched ternary mixtures at 303K (a) $ZnCl_2$ series (b) $CuCl_2$ series respectively. 102

Figure 4.2: Texture patterns of quenched ternary mixtures at 303K (Col.1) $ZnCl_2$ series (Col.2) $CuCl_2$ series (Col.3) aging effect for $CuCl_2$ series respectively. 103

Figure 4.3: Illustration of lamellar- hexagonal- lamellar transition in $CuCl_2$ based non-aqueous ternary mixtures. 104

Figure 4.4: Variation of thermo-dynamical parameters for $ZnCl_2$ series (a) heat flow (b) enthalpy (c) thermo-optical analysis. 106

Figure 4.5: Variation of thermo-dynamical parameters for $CuCl_2$ series (a) heat flow (b) enthalpy (c) thermo-optical analysis. 108

Figure 4.6: Variation of refractive index as function of TMS concentration (a) for $ZnCl_2$ based ternary mixtures (b) for $Cucl_2$ based ternary mixtures. 109

Chapter 5: Lyotropic colloidal mixtures

Figure 5.1:	(a) XRD profile of pure ZnO (b) SEM image of ZnO.	111
Figure 5.2:	XRD profiles of quenched colloidal systems at 303K (a) zinc oxide: cetyl pyridinium chloride: ethylene glycol (b) zinc oxide: sodium dodecyl sulfate: ethylene glycol system (c) zinc oxide: tween 20: ethylene glycol system respectively.	113
Figure 5.3:	Textural variation of quenched colloidal systems at 303K at 100X magnification (a) zinc oxide: cetyl pyridinium chloride: ethylene glycol (b) zinc oxide: sodium dodecyl sulfate: ethylene glycol system (c) zinc oxide: tween 20: ethylene glycol system respectively.	114
Figure 5.4:	Variation of thermo-dynamical parameters for zinc oxide: cetyl pyridinium chloride: ethylene glycol based colloidal mixtures (a) heat flow (b) enthalpy respectively.	115
Figure 5.5:	Thermo-optical analysis for the ZnO dispersed colloidal systems (a) zinc oxide: cetyl pyridinium chloride: ethylene glycol (b) zinc oxide: sodium dodecyl sulfate: ethylene glycol system (c) zinc oxide: tween 20: ethylene glycol system respectively.	117
Figure 5.6:	Variation of complex permittivity as a function of frequency for colloidal systems at 303 K (a) zinc oxide: cetyl pyridinium chloride: ethylene glycol (b) zinc oxide: sodium dodecyl sulfate: ethylene glycol system (c) zinc oxide: tween 20: ethylene glycol system respectively.	119
Figure 5.7:	Variation of complex permittivity as a function of temperature for zinc oxide: cetyl pyridinium chloride: ethylene glycol, zinc oxide: sodium dodecyl sulfate: ethylene glycol system and zinc oxide: tween 20: ethylene glycol system respectively Col.1 real part Col. 2 Imaginary part .	120
Figure 5.8:	Cole-Cole plots for colloidal systems at 303 K (a) zinc oxide: cetyl pyridinium chloride: ethylene glycol (b) zinc oxide: sodium dodecyl sulfate: ethylene glycol system (c) zinc oxide: tween 20: ethylene glycol system respectively.	122
Figure 5.9:	Arrhenius plot for zinc oxide: cetyl pyridinium chloride: ethylene glycol colloidal systems (a) 0.05wt% ZnO (b) 0.1wt% ZnO (c) 0.5wt% ZnO respectively.	124
Figure 5.10:	Variation of refractive index as function of temperature (a) zinc oxide: cetyl pyridinium chloride: ethylene glycol (b) zinc oxide: sodium dodecyl sulfate: ethylene glycol system (c) zinc oxide: tween 20: ethylene glycol system.	125

LIST OF TABLES

Content Page no

Chapter 1: Introduction and literature review

Table 1.1: Some colloidal dispersions. 11

Chapter 2: Experimental methods and characterization techniques

Table 2.1: Properties of precursor materials. 23

Chapter 3: Aqueous and non-aqueous binary lyotropic liquid crystalline mixtures

Table 3.1: Physicochemical parameters of various solvents. 35
Table 3.2: Geometrical parameters for quenched CPC: EG mixtures. 39
Table 3.3: Structural parameters for quenched CPC:W mixtures at 303K. 40
Table 3.4: Structural parameters for the quenched CPC:F systems at 303K. 41
Table 3.5: Thermal parameters for CPC: EG, CPC: W and CPC:F series. 47
Table 3.6: Relaxation parameters for CPC: EG, CPC: W and CPC:F series. 56
Table 3.7: Structural parameters for as prepared SDS: EG systems. 60
Table 3.8: Structural parameters for as prepared SDS: W systems. 60
Table 3.9: Structural parameters for as prepared SDS: F systems. 62
Table 3.10: Structural parameters for quenched SDS: EG systems. 63
Table 3.11: Structural parameters for quenched SDS: W systems. 63
Table 3.12: Structural parameters for quenched SDS: F systems. 64
Table 3.13: Thermal parameters for SDS: EG, SDS: W and SDS: F series. 71
Table 3.14: Relaxation parameters for SDS: EG, SDS: W and SDS: F series. 80
Table 3.15: Thermal parameters for T20: EG, T20: W and T20: F series. 88
Table 3.16: Relaxation parameters for T20: EG, T20: W and T20: F series. 96

Chapter 5: Lyotropic colloidal mixtures

Table 5.1: Thermal parameters for the colloidal systems. 116
Table 5:2: Relaxation parameters for colloidal systems. 122

LIST OF PUBLICATIONS

[1] Observation on lyotropic liquid crystalline behaviour of a cationic surfactant and polar solvent in non-aqueous medium, **Ravi K. Shukla** and K. K. Raina, *International Journal of Modern Physics B*, Vol. 23, No.25 (2009) 5075-5083.

[2] Dielectric behaviour of the composite system: multiwalled carbon nanotubes dispersed in ferroelectric liquid crystalline material, **Ravi K. Shukla** and K. K. Raina, *Phase Transitions*, Vol.84, No.9-10, (2011) Page 850-857.

[3] On the observation of lyotropic liquid crystalline mesophase in non-aqueous and aqueous media: Effects of transition metal salt, **Ravi K. Shukla** and K. K. Raina, *Advances in Condensed Matter Physics*, Volume 2011, Article ID 174786, 8.

[4] Observation of lyotropic liquid crystalline phases in some transition metal salt dispersed soft non queous systems, **Ravi K. Shukla** and K. K. Raina, *AIP conf. Proc.*1393, (2011) pp. 341-342.

[5] Observations of lyotropic liquid crystalline behaviour of $C_{21}H_{38}NCl$:$ZnCl_2$:OH- CH_2-CH_2-OH complexes, **Ravi K. Shukla** and K. K. Raina, *Journal of Molecular Liquids*, **under review**.

[6] Effects of electric field on the ionic non-aqueous lyotropic liquid crystalline phases , **Ravi K. Shukla** and K. K. Raina, *Journal of Colloid and Interface Sciences* **under review**.

[7] Dielectric dynamics of non-aqueous lyotropic liquid crystalline phases in solvent rich Region, **Ravi K. Shukla** and K. K. Raina (in pipeline).

CONFERENCES ATTENDED

[1] Formation of hexagonal phase of lyotropic liquid crystal in the dilute region of cationic surfactant and polar solvent, **Ravi K. Shukla** and K.K. Raina, presented in *National conference on liquid Crystal, 2008.*

[2] Phase identification in novel soft materials using thermal polarizing microscopy, K.K. Raina, Pankaj Kumar, Shikha Kapila, Neeraj and **Ravi K. Shukla**, *presented in EMSI09, 2009.*

[3] Topological defect in soft matter, K.K. Raina and **Ravi K. Shukla** presented in *National Conference on Advanced Materials and Radiation Physics (AMRP-2009),2009.*

[4] Some investigations on nano dispersed liquid crystalline colloidal systems, K.K. Raina, **Ravi K. Shukla** and Neeraj, presented in *National Conference on Recent Advances in Condensed Matters Physics (RACMP-2009), 2009.*

[5] Investigation on TMS dispersed soft lyotropic liquid crystalline phases derived from non-aqueous media, **Ravi K. Shukla** and K. K. Raina, presented in *Conference on Advances in Chemical Engineering (AChemE 2011), 2011.*

[6] Investigations on the transition metals salt based new lyotropic liquid crystalline non-aqueous complexes, **Ravi K. Shukla** and K. K. Raina, *presented in Soft Matter Chemistry Workshop 2011.*

LIST OF ABBREVIATION AND SYMBOLS

LC	Liquid crystal
TLC	Thermotropic liquid crystal
LLC	Lyotropic liquid crystal
CPC	Cetyl pyridinium chloride
CTAB	Cetyltrimethylammonium bromide
SDS	Sodium dodecyl sulfate
CMC	Critical miceller concentration
CPP	Critical packing parameter
l	length
v	volume
L_α	Lamellar mesophase
$2DH_\alpha$	Two dimensional hexagonal mesophase
NMA	N-msthylacetamide
DMF	N,N'-di- methylformamide
CPBr	Cetylpyridinium bromide
NMS	N-methylsydnone
WSS	Water, salt and surfactant
TMS	Transition metal aqua complex salts
XRD	X-ray diffraction
POM	Polarizing optical microscopy
DSC	Differential scanning calorimetric
T20	Tween 20
EG	Ethylene glycol
W	Water
F	Formamide

M_w	Molecular weight
CPC: EG	Cetylpyridinuium chloride: Ethylene glycol
CPC: F	Cetylpyridinuium chloride: formamide
CPC: W	Cetylpyridinuium chloride: water
SDS: EG	Sodium dodecyl sulfate: ethylene glycol
SDS: W	Sodium dodecyl sulfate: water
SDS: F	Sodium dodecyl sulfate: formamide
T20: EG	Tween 20: ethylene glycol
T20: W	Tween 20: water
T20: F	Tween 20: formamide
$ZnCl_2$: CPC: EG	Zinc chloride: cetylpyridinuium chloride: ethylene glycol
$CuCl_2$: CPC: EG	Cupric chloride: cetylpyridinuium chloride: ethylene glycol
ZnO: CPC: EG	Zinc oxide: cetylpyridinuium chloride: ethylene glycol
ZnO: SDS: EG	Zinc oxide: sodium dodecyl sulfate: ethylene glycol
ZnO: T20: EG	Zinc oxide: tween 20: ethylene glycol
CEM	Cetylpyridinuium chloride: ethylene glycol: mixture
CWM	Cetylpyridinuium chloride: water: mixture
CFM	Cetylpyridinuium chloride: formamide: Mixture
SEM	Sodium dodecyl sulfate: ethylene glycol: Mixture
SWM	Sodium dodecyl sulfate: water: mixture
SFM	Sodium dodecyl sulfate: formamide: mixture
TEM	Tween 20: ethylene glycol: mixture
TWM	Tween 20: water: mixture
TFM	Tween 20: formamide: mixture
ZnO	Zinc Oxide

$CuCl_2$	Cupric Chloride
$ZnCl_2$	Zinc Chloride
ITO	Indium tin oxide
ΔH	Enthalpy
ΔG	Gibbs free energy
n	Refractive index
$C_{benzene}$	Capacitance of benzene
C_{air}	Capacitance of air
ε'	Dielectric permittiity
ε''	loss Dielectric
σ_{ac}	**ac** conductivity
E_a	Activation energy
ω	Cyclic frequency
T	Temperature
K	Kelvin
P	Pressure
λ	Wave length
R	Gas constant
Cp	Heat capacity
D_{ce}	Density of cohesive energy
μ_D	Charge Dipole moment
a_0	Lattice parameter
d_L	Thickness of surfactant bilayer
φ_s	Mole fraction of the surfactant
d_{EG}	Thickness of ethylene glycol channel
r_H	Radius of the cylinder
ε_0	Static permittivity

ε_∞	High frequency permittivity
τ	Relaxation time
α	Distribution parameter
f_r	Relaxation frequency
$\Delta\varepsilon$	Dielectric strength

PREFACE

Lyotropic liquid crystals (LLC) constitute almost half the area in soft matter science. The key areas in the lyotropes like binary and ternary mesophases transition metal based mesophases and the lyotropic colloidal systems gain considerable interest and facilitate applications in diverse fields (biology, cosmetics, pharmaceutical) as a soft template, drug delivery vehicles and active components of optical, capacitive and electrical devices The present study deals with the synthesis, structural, thermal, dielectric and electro-optical characterizations of binary, ternary and colloidal LLC systems. The prepared mixtures were studied in as prepared and quenched conditions at 303K and elevated temperatures (303-400K).The entire work is presented in the **six chapters**. **Chapter 1** deals with background of LLC systems, their diverse classes and physiochemical parameters which play vital role to engineer LLC materials for diverse applications. The importance and need of binary non-aqueous, transition metal salt (TMS) based ternary and colloidal LLC mixtures under different conditions have been discussed. This section also summarize the detailed description of the milestones and fundamental aspects achieved in the concerned research area so far including their future applications considering fundamental and technological view points. **Chapter 2** gives the detailed description of experimental route implemented for the synthesis of binary, ternary and colloidal LLC mixtures. Fundamental techniques like X-ray diffraction (XRD) and Polarization optical microscopy (POM) were used to explicate the structural behaviour of the as prepared and quenched mixtures. Thermal, thermo-optical, dielectric and optical behaviour have been studied using differential scanning calorimetry (DSC), LCR meter and Abbe refractrometer. **Chapter 3** demonstrates the structural and morphological analysis of aqueous and non-aqueous binary LLC mixtures obtained from ionic and non-ionic amphiphiles in the higher and lower concentration regime of varying polarity solvents. The origin of diverse lyotropic crystalline phases and phase transitions have been explored and discussed for non-aqueous and aqueous LLC mixtures in as prepared and quenched conditions on the basis of XRD and textural analysis. In addition thermal, dielectric and thermo-optical behaviour of these binary LLC mixtures are described in this chapter. Thermal parameters and order of the transitions have also been discussed inferring about the melting and nucleation of new phases at elevated temperature. Frequency and temperature dependent dielectric dynamics of these LLC mixtures were explored and correlated with structural analysis. The higher dielectric constant observed for these systems is one of the key finding of the thesis. The optical behaviour was also discussed for all the mixtures at 303K and higher temperature. **Chapter 4**

represents the fabrication, structural, textural, thermal and optical investigations of transition metal salts [($ZnCl_2$ and $CuCl_2$): cetyl pyridinium chloride: ethylene glycol] based ternary mixtures at room and higher temperature in as prepared and quenched conditions. XRD and POM characterizations demonstrate the growth of new phases and structural phase transition with TMS addition at lower and higher content. Interestingly dispersion of $CuCl_2$ gives rise to the growth of cubic rods at lower concentration is one of the important finding of this work. Thermal and thermo-optical analysis of these systems were done to examine the various phase transitions and the nucleation of new phases. Some hypothetical models have been applied to describe the solute-solvent interactions in these systems. The optical properties of these systems were also examined and correlated with the structural and thermal analysis. **Chapter 5** gives insight about the preparation, structural, morphological, thermal, dielectric and optical behaviours of colloidal systems derived from ionic and non-ionic surfactant systems (at very low concentration 10:90 wt%) via dispersion of Zinc oxide (ZnO) particles at varying concentrations(0.05,0.1 and 0.5wt%). XRD and POM analysis were employed to examine the various structural changes and phase transition with the addition of these particles. DSC profiles of these systems were explained to ascertain the thermal stability of the observed phases and phase transitions. A dielectric measurement reveals the enhancement in permittivity in the mesophases derived from cationic amphiphiles and decrease in other two. Such behaviour of these colloidal mixtures infers that physical properties of these systems not only depend upon the colloidal particles but also on the nature of the basic building blocks and the structure of mesophase. **Chapter 6** includes the conclusion and significance of the systems prepared along with the future scope.

Chapter 1

Introduction and literature review

Soft matter is the field of science which brings cohesiveness of ideas among of physicists chemists and biologists on one platform to define the novelties of this delicate state of matter. This chapter summarizes the development in self assembled soft systems and various aspects which enable self assembly phenomena in them. Various chemical and physical properties of the neat lyotropic liquid crystalline and colloidal systems have been discussed along with their importance in the technological applications. In addition, this chapter includes the detailed literature review on the experimental and theoretical facet of the soft matter research till date. Various breakthrough and milestones in this field and their technological and industrial applications have been discussed in detailed.

Soft matter is a subfield of condensed matter comprising a variety of physical states that are easily deformed by thermal stresses or corresponding fluctuations. They include liquids, colloids, polymers, foams, gels, granular materials, liquid crystals and a number of biological materials. These materials share an important common feature in the predominant physical behaviors occur at an energy scale comparable with room temperature thermal energy [1]. Basically soft matter is the physics of macromolecules: how do suspensions of macromolecules interact with each other and move around (dynamics)? The basic constituent molecules of soft matter can be broadly classified as:

- Colloidal suspensions
- Polymers
- Amphiphilic molecules capable of self assembly

Liquid crystalline materials also considered a special case of the soft matter systems and have attracted interest of material society and technologists. The various classes of liquid crystalline phases and their technological applications are reviewed in the figure 1.1.

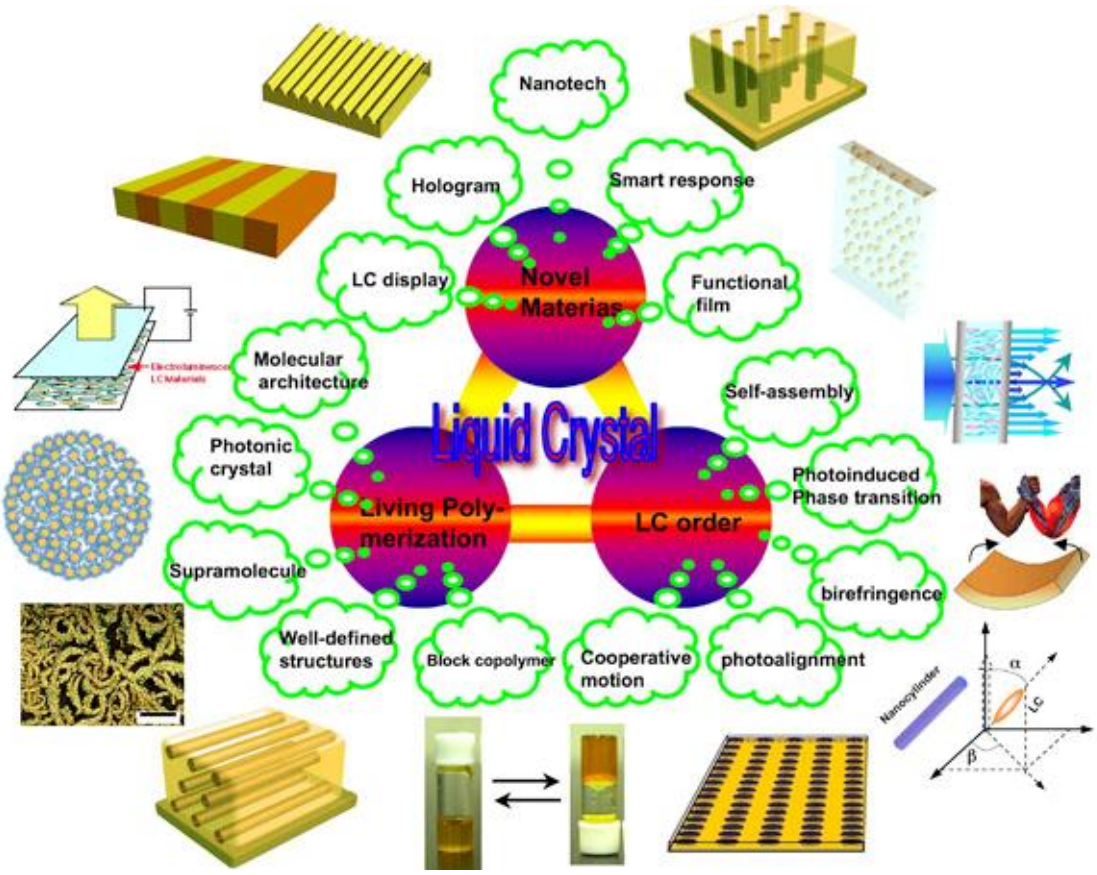

Figure 1.1: Schematic of self assembly in liquid crystals and their applications [Image curtsey of Prof. Haifeng Yu, China].

1.1: Liquid crystals

Liquid crystals (mesophase) are organic substances that pure, or in aqueous and some polar non aqueous solutions are capable to form a special state of aggregation, intermediate between liquid and solid state. They possess both the flow properties of a liquid as well as ordering of a crystal and present multiple anisotropies. The existence domain is very well defined by two distinct temperatures melting interface at solid state border and the higher one is the clearing point at the isotropic liquid [2]. Pure organic substances, providing liquid crystals reach the mesomorphic domain by varying temperature and have been named thermotropic Liquid Crystals (TLC). They can be made up of either rod-shaped molecules (calamitic mesophases) or disc-shaped mesogens named as discotic mesophases. The calamitic liquid crystalline phases further classified into nematic (possess orientational order but no positional order) and smectic A and C phases (both these mesophases possess positional as well as directional order). The chiral smectic C mesophases are also included in this category of liquid crystals (The mesogens in these phases possess chirality which results in a gradual change in the orientation of the director from one layer of mesogens to the other)[2-5]. The distinct phases of thermotropic liquid crystals are presented in the figure 1.2. Discotic thermotropic liquid crystals exhibit nematic and columnar phases. These liquid crystalline phases facilitate numerous applications ranging from display world to the biomedical application, sensor, actuator, and spatial light modulators etc.

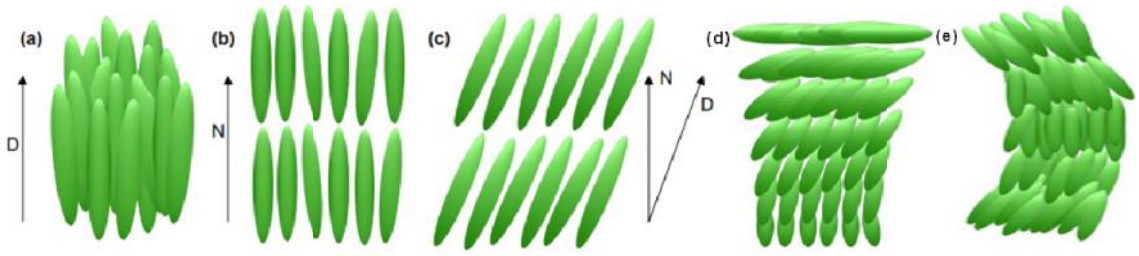

Figure 1.2: Distinct phases of thermotropic liquid crystals (a) nematic (b) smectic A (c) smectic C (d) chiral nematic (e) chiral smectic [Image curtsey of Mr. K.Tamhane].

Other organic substances, in aqueous and non aqueous solutions, reach the mesomorphic domain by varying temperature and concentrations have been named Lyotropic Liquid Crystals (LLC) [2-5].

1.2: Objectives

On the basis of fundamental aspects and experimental facts of the lyotropic liquid crystalline phase we intended to develop as pure non-aqueous LLC and colloidal systems and understand their structure-property correlations, stability on temperature and time scale to replace water based lyotropic liquid crystalline systems. The laid down objectives for this study were

- ❖ Preparation of lyotropic liquid crystalline (LLC) phases using ionic and non ionic surfactants in aqueous and non aqueous medium.
- ❖ Thermal and structural characterization of prepared LLC phases.
- ❖ Optical and electro-optic behavior investigations of liquid crystalline colloidal systems.

1.3: Lyotropic liquid crystals

Considering the scope and the objectives laid down, we focus on lyotropic liquid crystalline systems in detail. Lyotropes are basically derived from amphiphilic compounds [contains dual character hydrophilic (head group) and a hydrophobic (tail) regions]. The schematic of amphiphilic molecule is presented in the figure 1.3.

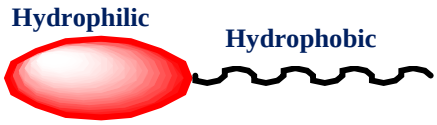

Figure 1.3: Schematic of amphiphiles.

This dual character of the surfactant molecule ensures solubility in organic solvents and water. One of the basic surfactant characteristics is their tendency to absorb at surfaces and interfaces. Surfactants decrease the interfacial tension between water and oil lowering the free energy at the interface. The surfactant molecules are classified as

- Cationic
- Anionic
- Zwitter ionic
- Non ionic

Basically there are two main categories of surfactants: ionic and non-ionic. Ionic surfactants include anionic, cationic and Zwitterionic species. Anionic surfactants like sodium dodecyl sulfate (SDS), alkylbenzene sulfonates, alkyl phosphates, dialkyl sulfosuccinates, fatty acid salts, etc. have a negatively charged head group [6]. Whereas, cationic surfactants like cetyltrimethylammonium bromide (CTAB), cetylpyridinium chloride (CPC), benzalkonium chloride (BAC), etc. have a positively charged head group. Cationic surfactants adsorb strongly to surfaces because the majority of surfaces carry a net negative charge. Zwitterionic surfactants have both positive and negative charges. Phospholipids, the most abundant of the amphiphiles in the body, are examples of Zwitterionics. These surfactants extensively used to develop binary and ternary lyotropes. In general mechanism, surfactant when dissolved in a solution reach to the some specific aggregates, called "micelles". This aggregation process termed as micellization starts just above the critical miceller concentration (CMC). The value of the CMC is the highest possible concentration of non- aggregated surfactant molecules, unimers, in a solution. The variety of geometries seen for the micelles ranging from spherical, rod like, disc like or branched (in rare cases). Micellization is initialized by the hydrophobic effect, which means that the hydrophobic part of the surfactant tries to avoid contact with water [7-8]. Minimization of Gibbs free energy is responsible for formation of structural order [9]. At higher surfactant concentration, the micelles packed in ordered geometries with long range orientational order, so-called liquid crystalline mesostructures.

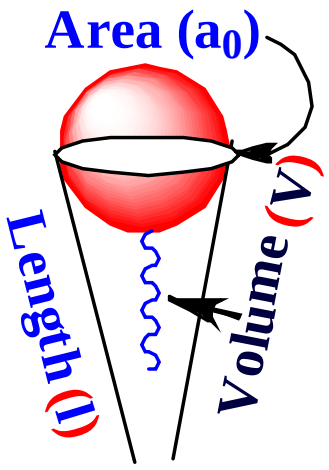

Figure 1.4: Schematic of critical packing parameter (CPP) of amphiphile.

The aggregate structure is basically determined by the surfactant geometry. This can be expressed by a dimensionless number called critical packing parameter (CPP), which relates the head group area (a_0) to the extended length (l) and the volume (v) of the hydrophobic part of a surfactant molecule as shown in figure 1.4. The liquid crystals are of different types like

miceller cubic, hexagonal, lamellar, bicontinuous cubic and reversed hexagonal as depicted in the figure 1.5. The liquid crystalline phases typically have long range order but short range disorder, which is contrary to normal crystals, which have both long and short range order. In spite of the diversity of structures, in all liquid crystalline phases the surfactants are arranged in such a way that the ends of the hydrophobic tails of two surfactant films come together. Due to the presence of both a hydrophilic and a hydrophobic domain, liquid crystalline phases can solubilize polar, water soluble substances as well as non polar, oil soluble compounds [12]. The phase diagram for distinct liquid crystalline structures is shown in figure 1.6.

v/al<1/3

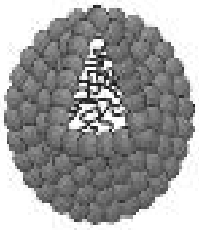

Micelles

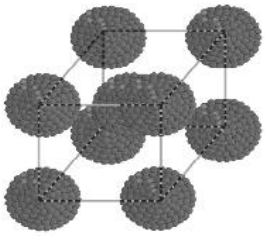

Cubic

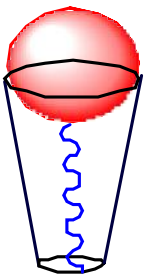

1/3<v/al<1/2

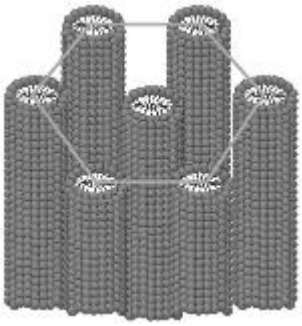

Hexagonal

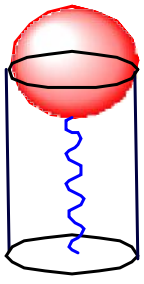

v/al=1

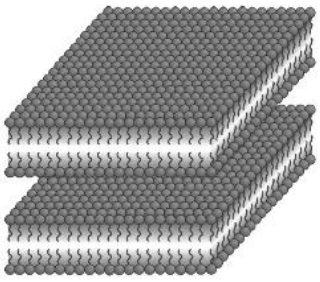

Lamellar

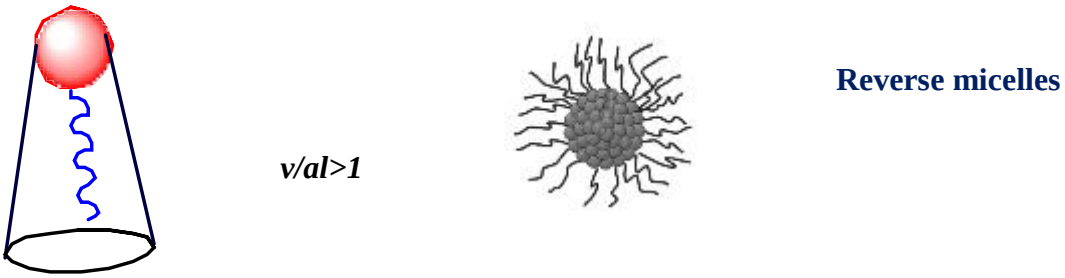

Figure 1.5: Representation of the packing parameters and the diverse lyotropic liquid crystalline geometries at the expense of increasing surfactant concentration [Redrawn from ref.6,10-11].

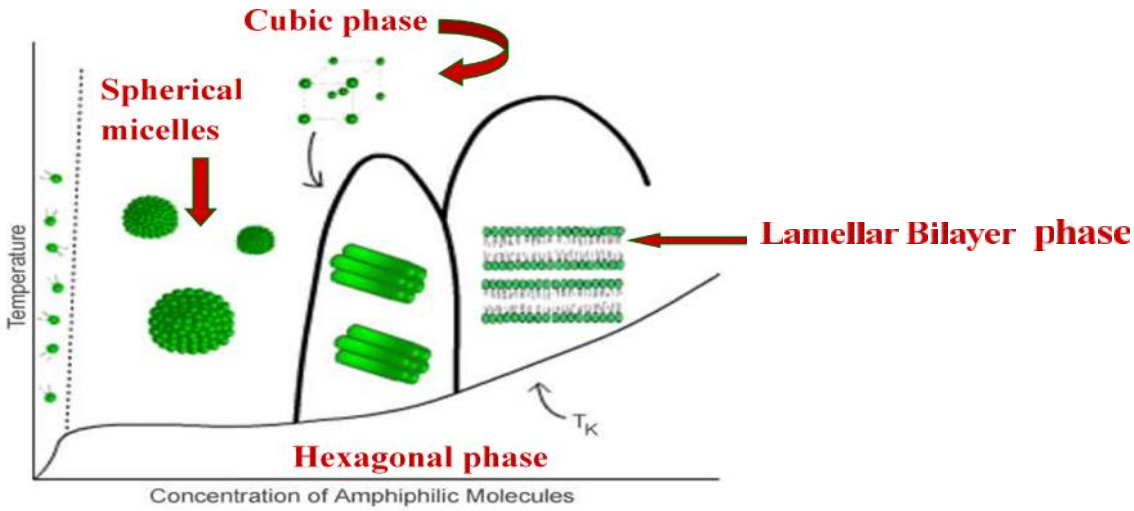

Figure 1.6: Phase diagram for the liquid crystalline geometries at the expense of increasing surfactant concentration and temperature [Image courtesy of Physics Today (Pershan, 1982)].

The whole mechanism discussed above attributed to the self-assembly process. During self-assembly, the molecules organize through non-covalent interactions like dipole moments, Van der Waals forces, hydrogen bonds etc. [13-16]. All biological assemblies are created through the process of self-assembly or self-organization. We ourselves are products of the process of self-assembly. It is thus extremely important to study and understand self-assembly if we hope to understand the origin of life. The extensive literature review on various aspects and milestones achieved in the field of lyotropics is discussed below.

1.3.1: LLC mesophases derived from aqueous solvents

The self assembly known for the many decades attributed to the hydrophobic effect. The first published oil/water experiments were those of Benjamin Franklin in 1773, who put a drop of oil on the pond to test the idea [17]. In 1890, Lord Rayleigh repeated Franklin's experiment

[18] knowing the volume of a spoonful of oil and the surface area of the body of water, and assuming that oil forms a monolayer film on water, Rayleigh was one of the first experimentalist made a mark to determinations of the size of a molecule, at a time when the existence of atoms and molecules was still in doubt. The word “hydrophobic” appeared in 1915 [19]. In 1920, J.W. McBain and C.S. Salmon [20] demonstrated reversible formation of micelles in soap solutions. In 1925, Gorter and Grendel [21] proposed that lipid molecules from red blood cells could form “bilayers”, i.e., a pair of opposed monolayers, based on careful Langmuir trough experiments that showed twice the surface concentrations of surfactant molecules as in monolayer experiments. Later, in 1954, Walter Kauzmann coined the term “hydrophobic bonding” to refer to the tendency of oils to associate in aqueous solutions [22]. The first X-ray structures of proteins appeared in 1958, showing cores of buried hydrophobic amino acids similar to the structures of micelles [23]. Although he emphasized that the driving force was the avoidance of the aqueous phase by the oil, his terminology drew criticism. Joel Hildebrand objected to the term “bonding”, which he preferred to reserve for covalent interactions. Hildebrand also objected to the term “hydrophobic” on the grounds that oil has a favorable enthalpy of interaction with water [24]. However, the alternative view has ultimately prevailed, [25-27] namely (1) that it is the free energies, not enthalpies, that define affinities, (2) that “bond” is a term that is widely accepted to also refer to certain types of non-covalent interactions, and (3) that it is useful to have a word for the types of interactions between non polar molecules and water. “Hydrophobic” has now become common usage [24, 28-30]. Further the advancement in the self assembly from 1970 to recent years has been summarized by the recent reviews [31-35].

1.3.2: LLC mesophases derived from non-aqueous Solvents

After the well establishment of the aqueous self assembled systems and the lyotropic mesophases, it was Ray who claimed the first report on the self assembly of surfactant molecules in the non-aqueous domains of ethylene glycol at ambient temperature in 1969 [36]. His idea was based on the resemblance of the ethylene glycol molecule with water and other alcohol as it contain both inter and intra molecular hydrogen bonding enable it to facilitate the self assembly. He concluded the micellization in the protic non-aqueous domains of the ethylene glycol, though, the exact size of the micelles was not predicted at that moment. With more understanding of the concept and passage of time later Ray published a paper in the nature demonstrating the solvophobic effect responsible for the self assembly in the ethylene glycol and several cationic detergents [37]. Micelle formation of

two ionic surfactants, viz. sodium dodecyl sulfate (SDS) and cetyltrimethylammonium bromide (CTAB), in organic solvents of various dielectric constant and intermolecular H-bonding capability, viz. N-msthylacetamide (NMA), formamide (FA), dimethyl sulfoxide (Me_2SO), and N,N'-di- methylformamide (DMF), at different temperatures by conductance measurements were reported by Singh *et al.* in 1980[38]. The references cited in this report also demonstrates the various inverse and direct micelles assembly in non-polar and polar solvents owing to the solvophobic interactions examined during the time period 1970 to1980. Few years later Lattes *et al.* [39-40] explored the micelles aggregation and Critical micelle concentrations (cmc) of cetyltrimethylammonium bromide (CTAB) and sodium dodecyl sulfate (SDS) at 60^{O}C in formamide. The CMC were considerably higher in formamide than in water, and the corresponding Krafft temperatures for these surfactants were also higher in formamide than in water. This report presented a new substitute for water. In 1988 Canet *et al.* [41] presented a comparative report on the micellization of CTAB in water and formamide via nuclear magnetic relaxation at different frequencies. A year later Rico *et al.* [42] explored the CTAB and formamide based non-aqueous micro-emulsion. Diverse mesomorphic phases have been explored via small angle X-ray scattering studies and also present the comparative scenario with the existing results. Lyotropic liquid crystalline phase of SDS derived from various polar solvents were reported by Lattes *et al.* [43-44]. Complex 2-3 and 1-dimensional ordered phases were observed for the SDS-water system which displays sequence of hexagonal (p6m) ↔ centered rectangular (cmm) ↔ rhombohedral ↔centered tetragonal ↔lamellar. The rhombohedral structure turns into a cubic phase Im3m. In the other polar solvents (formamide, glycerol, ethylene glycol, N-methylformamide), the phase sequence is very different. The SDS/formamide system exhibited the sequence hexagonal ↔cubic (Ia3d) ↔lamellar. Only lamellar structures were observed in the other less structured solvents. This report hints that geometric constraints and head polar-solvent interactions play a vital role in the aggregation of LLC phases. In similar way Lattes *et al.* [45] presented other report demonstrating liquid crystals phases from CTAB and cetylpyridinium bromide (CPBr) in water protic solvents [glycerol, formamide, ethylene glycol and N-methylformamide (NMF)], and the aprotic solvents [DMF and N-methylsydnone (NMS)] at the expanse of head group nature of two surfactant and the cohesive energy of the solvent. The Krafft temperature CMC of N-alkylpyridinium halides (CmPyX, m = 12, 16, or 20 and X = Cl, Br, or I) in formamide were explored by Lattes *et al.* [46]. The effects of size, structure, and charge of the micelles as a function of chain length and nature of counter ion were computed from the small angle neutron scattered intensity.

They found that the micelles bear a higher charge in formamide than in water, but similar solvation effects were noted in the two solvents on changing the counterion (I-, Br-, or Cl-). Aggregation of ionic surfactants in formamide was reported by Akhter *et al.* in 2000 [47]. They presented the electric conductivity and surface tension measurements of various ionic surfactants, such as Na caprylate, Na laurate, Na palmitate, and Na stearate, in formamide. It was suggested that the self assembly in these systems owe to the solvophobic interactions. After three year Akhter *et al.*[48] made another successful attempt to demonstrate the CMC measurements from electric conductivity and surface tension techniques of various ionic surfactants like sodium caprylate, sodium laurate, sodium palmitate and sodium stearate, in formamide (FA), in N-methylformamide (NMF) and in N,N-dimethylformamide (DMF) at 25°C. Both methods confirm the micellization in FA, in NMF and in DMF solutions. The CMC was considerably lower in FA, and in NMF, and higher in DMF, than in water. A report published by Lattes *et al.*[49] also hints at the self assembly in non-aqueous media. They reviewed the various aspects and micellization in the formamide and comparative study with water. Mixed and pure LLC mesophases of cetyl pyridinium chloride [$C_{21}H_{38}NCl$ (CpCl)] and ethylene glycol [OH-CH_2-CH_2-OH (EG)] under quenched condition were reported by Raina *et al.* in 2009 [50]. Recent advancement in non-aqueous lyotropic phases, self assembly in ionic liquid and the various physical effects are well covered in the review presented by Drummond *et al.* [51-52] and various reference cited in them. Several research groups have attempted to explain structural and thermal properties of these systems and their possible potential application in the diverse field as discussed above, but, their molecular dynamics phenomena needs better understanding in order to explore them for possible applications. Ishai *et al.* [53-54] suggested the dielectric spectroscopic approach to explain the molecular dynamics at the LLC surface. They predicted that the counter ion gets dissociate in solvent which form layers around the micelles at the interface via columbic interactions. These ions in turn form dipoles with head group of amphiphile under the influence of electric field and thus encourage higher polarization and relatively high dielectric constant [55-57]. Chien *et al.* [58] studied dielectric behaviour in chromonic lyotropic liquid crystals, isotropic fluids and hinted at the possibility of developing a high density electrolytic capacitor from these systems.

1.3.3: Transition Metal Salt based systems

The most advantageous prospective of soft phases is their easy tailoring to desired mesophase by modulating the internal dimension of building blocks (head group and hydrophobic chain) via utilizing the variety of hydrophilic and hydrophobic additives. Such additives enhance the internal dimensions (like head group area and chain length), thus producing new stable and ordered LLC geometry. Miceller phase or normal liquid crystalline phase containing a vast amount of water [59-61] or water and oil [62-64] have been known for a long time. New kinds of ternary systems like water, salt and surfactant (WSS) have also been synthesized and characterized to facilitate the development of modified meso-structured, meso-porous materials via self assembly of ionic and non-ionic amphiphilic molecules [65-70]. They could offer confinement of the metal ions in definite ordered geometry even at lower concentration, better control on shape and size with higher yield [71-74]. However, due to the lack of stability at higher metal density and evaporation of water content from the media, these systems could not be exploited for the industrial applications [75]. To overcome these fundamental difficulties, Dag *et al.* discovered a new lyotropic liquid crystalline system, composed of transition metal aqua complex salts (TMS) and Oligo(ethylene type) surfactants in 2001 [76]. These new systems demonstrate that TMSs can be dissolved up to 3.2 mole ratio (metal ion/surfactant) by keeping the LLC mesophase. The system has been further extended to Pluronic type surfactants, which have much longer ethoxy chains as compared to Oligo surfactants, therefore the metal ion/surfactant mole ratio could be increased up to 15.0 mole ratio [76, 77, 78-79]. The structure directing force in these systems owing to the hydrogen bonding between coordinated water molecules of the TMS and the oxygens of the ethoxy groups of the hydrophilic parts of the surfactants [80,81-82]. Several transition metal salts were used including; Ni(II), Mn(II), Cd(II), Zn(H), Co(II) with Hofmcistcr counterions such as ClO_4^-, NO_3^-, Cl and $COCI_4^{2-}$ [72-75]. Cubic, 2D-Hexagonal, 3D-Hexagonal and tetragonal mesostructures are common. The new system has many advantages in true-liquid crystalline templating processes of mesoporous metals, metal sulfides and metal selenides [77]. Recently, Raina *et al.* [83-84] reported the transition metal salt based non-aqueous LLC systems. Diverse neat and mixed phase have been observed in these systems along with the growth of the some micro structure.

1.3.4: Liquid crystalline colloidal systems

Colloid means glue-like, originating from the Greek, it describes materials that are predominantly liquid but which have other properties: either optical, giving rise to turbidity

such as milk, or viscous, with characteristics of mucus, gelatin or wet clay. These effects arise from the presence of macromolecules dissolved in liquid and/or by mixing two or more solid, liquid or gas phases. Colloid science can therefore be described the study of dispersions of one phase in another, for example emulsions (oil in water or water in oil), solid in liquid, foams and the complex lyotropic liquid crystal dispersions of soap or synthetic detergents. Alternatively, colloid science is the study of systems in which one or more dimensions is in the range of approximately 1nm to 10µm. For example, synthetic polymers with a molecular weight of 100,000 adopt a random coil dimension of ~40nm in solution, emulsion droplets are typically 1 to 10µm in diameter, and foam films are typically 10 to 100nm thick [85].

Colloidal dispersions are two-phase systems contains the dispersed phase and the continuous medium. The mixture is homogeneous over an appreciable time period. Domestic dispersions such as paint and abrasive cleaners will have a shelf-life of several months or years. The properties of the dispersion are determined to a large extent by the nature of the dispersed phase-dispersion medium interface. Colloid science and surface science are therefore closely linked. The selected examples shown in Table 1.1 illustrate the scope and importance of colloidal dispersions.

Table 1.1: Some colloidal dispersions [85-87]

Dispersed phase	***Medium***	***Type***	***Examples***
Liquid	Gas	Aerosol	Fog, sprays
Liquid	Liquid	Emulsion	Salad dressing
Liquid	Solid	Solid emulsion	Pearl, opal
Solid	Solid	Solid suspension	Pigmented plastics
Solid	Liquid	Sol or paste	Ink, toothpaste
Solid	Gas	Aerosol	Inhalers, smoke
Gas	Liquid	Foam	Fire extinguisher, detergent foam
Gas	Solid	Solid foam	Pumice stone, expanded polystyrene

In general, emulsions and sols are termed lyophobic colloidal dispersions. Lyophobic (liquid hating) dispersions cannot be prepared by dissolving the dispersed phase in the dispersion medium.

A colloidal dispersion of sub-µm particles may be stable or unstable to aggregation. Brownian motion ensures that the particles are in continual motion, giving rise to collisions at a rate determined by diffusion theory. Owing to the high interfacial free energy, lyophobic

colloids are thermodynamically unstable and tend to aggregate. In a stable dispersion the particle collisions do not lead to aggregation because inter-particle repulsion forces dominate. It will remain dispersed indefinitely, although particles bigger than about 0.1µm will sediment depending on their density. In an unstable dispersion, the collisions lead to aggregate formation; larger aggregates either sediment or cream depending on their relative density [85-87].

The repulsive forces in a stable dispersion were long ago identified as being electrical in origin. A surface potential exists at the interface between the solid particle and the surrounding liquid due to the presence of a surface charge. To maintain electrical neutrality, ions of opposite charge present in the medium are attracted closer to the particle surface, resulting in a diffuse layer of highly concentrated counter ions. The concentration of counter ions in this layer decays exponentially from the surface over a distance of tens of nano meters. The resulting ionic cloud is called the diffuse region of the electric double layer. On particle-particle collision, overlap of the ionic clouds gives rise to an osmotic repulsion that pushes the particles apart [85-87]. A positive resultant (figure 1.7 a) corresponds to an energy barrier and repulsion, while a negative resultant (figure 1.7 b) corresponds to attraction and hence aggregation. It is generally considered that the basic theory and its subsequent modifications provide a sound basis for understanding colloid stability.

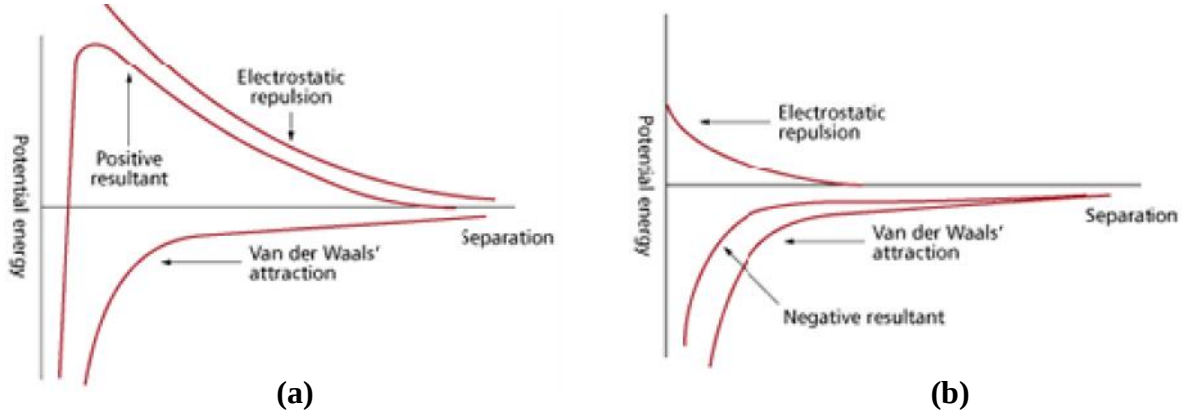

Figure 1.7: Potential energy curves for stable and unstable dispersions [85].

Liquid crystals are known for their anisotropic mechanical and optical properties which originate from the long-range orientational molecular ordering. If a liquid crystal is used as a host liquid in a colloidal suspension, this ordering gives rise to additional long-range interactions between the colloidal particles. The type of the interaction is controlled by the presence and symmetry of topological defects of the director field. Particle clustering,

formation of superstructures, and even new phases are immediate consequences of these anisotropic interactions [85-87].

Anisotropic liquid crystal (LC) fluids are being used as host media for such colloidal self assembly is currently perhaps one of the most promising approaches. It facilitate control of the medium-mediated inter particle forces by means of varying temperature, applying external fields, and utilizing the response of LC alignment to the presence of various chemical substances [88-97] and also enable one to achieve long range self assembly at the expanse of the long range orientational order of LC molecules. Most of the reports available in the literature dedicated to the nematic LC colloidal systems. Poulin *et al.* [95] in 2000 reported nematic emulsion with anisotropic liquid (silicon oil). In the similar way in 2001 Yamamoto *et al.* [98] reported nematic emulsions using surfactant and water. Their observations demonstrate that liquid crystalline colloidal systems gives batter electro-optic response as compared to pure LC. Fukuda *et al.* [99] in 2002 reported the liquid-crystal emulsion, consisting of water, surfactants, and cholesteric liquid crystals. Stark *et al.* [100] in 2002 reported the analogy between confined geometries and magnetic field on saturn-ring defects around microspheres suspended in nematic liquid crystals. Monte Carlo simulation of topological defects in the nematic liquid crystal matrix around a spherical colloid particle has been reported by Ruhwand *et al.* [101]. In 2003 Rudhardt *et al.* [102] presented a report on the phase switching of ordered arrays of liquid crystal emulsions. They reported the fabrication method for producing the interface-based electro-optic phase grating that switch between diffracting and transparent sates. Zhang *et al.* [103] in 2006 reported first time the nonaqueous suspensions of rod like particles based on the natural clay sepiolite. Zummer *et al.* [93] presents some reports on the self assembly of gold nano rods and mesoscopic modeling of the colloides in chiral nematics. In the continuum growth of the field Smalyukh *et al.* [91,104] reported the opto-elastic manipulation of colloidal particles in liquid crystal. Recently, Jung and Lavrentovich *et al.* presented some interesting aspects of liquid crystal-based colloid ordering [105,106]. Rather than nematic hosts they work with smectics and they confine the phase inside narrow channels micro fabricated in a silicon wafer. They treated the channels with a fluorinated polymer in order to ensure planar director anchoring along the side walls as well as bottom of the channel. The channels were kept open from the top and the air interface induces strong homeotropic alignment there. The conflict in alignment between the top and bottom forced the smectic phase to develop a regular array of toric focal conic defects, in each of which the layers curve around a central defect line. Colloidal particles introduced to the liquid crystals can be trapped in these defect lines and

fluorescent particles along hexagonal patterns with very long-range fidelity solely by liquid crystal self-assembly [107]. The regular smectic liquid crystal defect array can also be used in general as a soft lithographic template [108] or as a basis for fabricating super hydrophobic surfaces [109]. Very recently, Scalia *et al.* [110] presented a review well covered the dispersion of the nano impurities in liquid crystals, liquid crystalline colloidal systems and variety of applications of liquid crystals in soft matter nano-, bio- and micro technology.

1.4: Applications prospective of lyotropic phases

Lyotropic liquid crystals play an extremely important role in the industrial, pharmaceutical and biological applications.

1.4.1: Soft template

Lyotropes are wieldy used to developed variety of mesoporous and nanostructured materials of pure metals, metal oxides and metal sulfides via self assembly of the metallic ions at the interface (via hydrogen bonding between the inorganic ions and the surfactant head group) or into the channel as shown in the figure 1.8 [111-120].

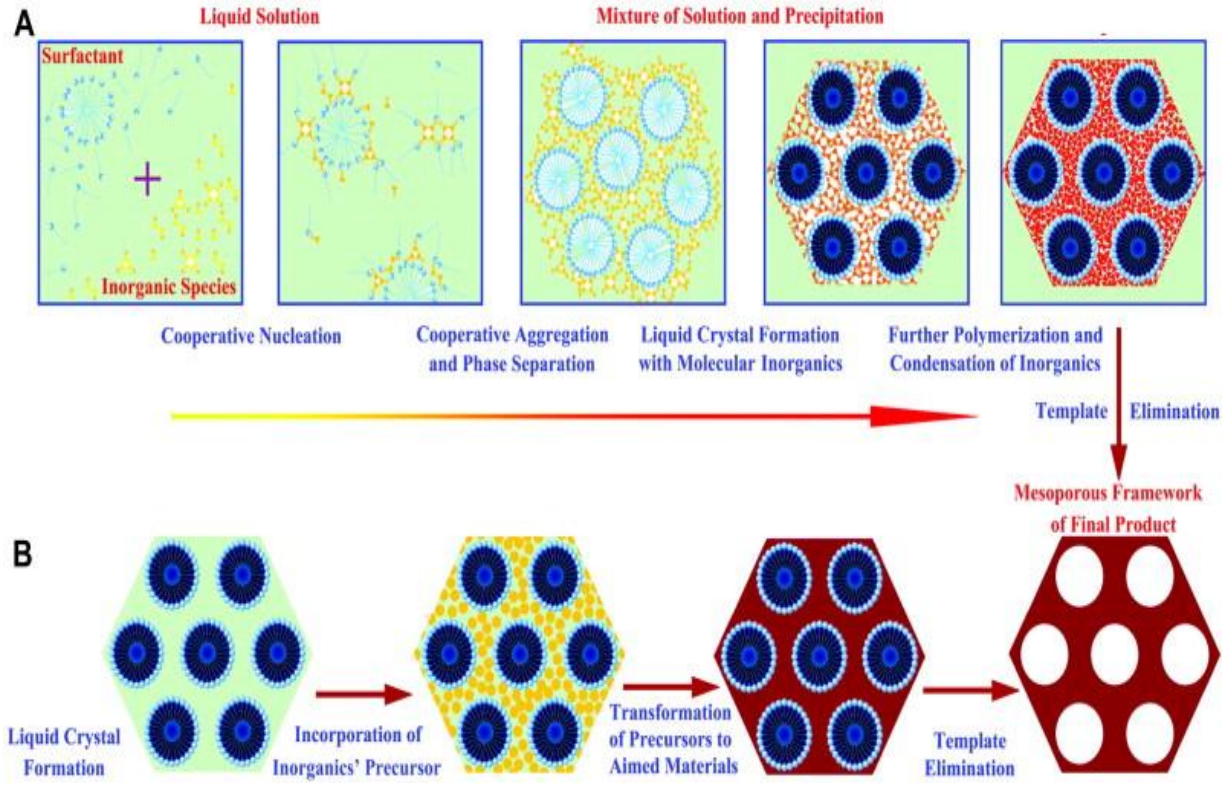

Figure 1.8: Growth process of nanostructures in the lyotropic liquid crystalline templates [121-122].

1.4.2: Drug delivery systems

Lyotropic liquid crystal systems, such as reversed bicontinuous cubic and hexagonal mesophases, are attracting more and more attention because of their unique microstructures and physicochemical properties. Various bioactive molecules such as chemical drugs, peptides and proteins can be solubilized in either aqueous or oil phase and be protected from hydrolysis or oxidation. Furthermore, several studies have demonstrated sustained release of bioactive molecules from reversed cubic and hexagonal mesophases [123].

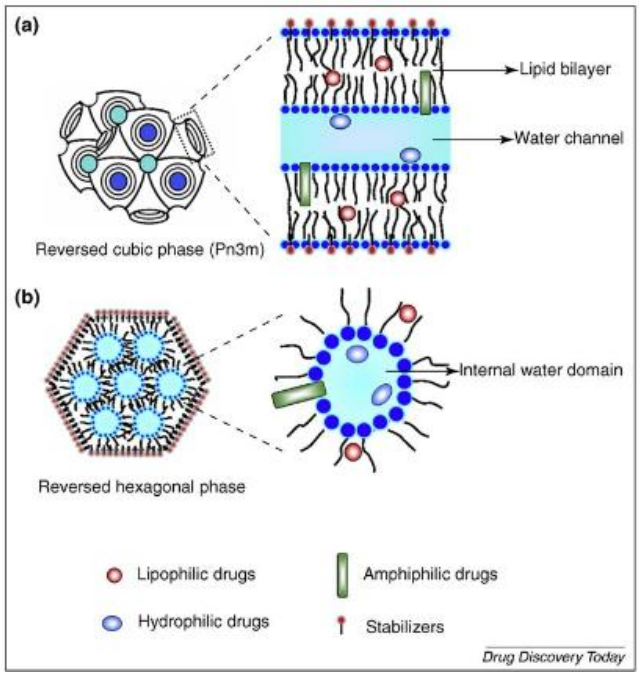

Figure 1.9: Structures of (a) reversed bicontinuous cubic and (b) hexagonal mesophases, inspired by Sagalowicz et al. [124].

Some examples of drug attachment in the lyotropic systems are presented in the figure 1.9 (a-b). On the basis of above discussed application of the existing lyotropic systems it could be predicted that the non-aqueous lyotropic mixture can act as more stable template and drug vehicle than that of aqueous systems as they are stable up to higher temperature and longer time.

1.5: References

[1] http://en.wikipedia.org/wiki/Soft_matter.

[2] B. Gabriela, Romanian Reports in Physics, 56 (2004) 66.

[3] P. G. De Gennes, Oxford University Press, Oxford, (1993).

[4] S. Chandrasekhar, Liquid crystals, Cambridge Univ. Press, Cambridge, (1977).

[5] P. J. Collings, Liquid crystals, nature's delicate phase of matter, Princeton University.

[6] T. Witula, Ph.D thesis "Organic Reactions in Organized Media", (2007).

[7] C. Tanford, "The hydrophobic effect" Wiley Publishers: New York, (1973).

[8] D. Chandler, Nature, 437 (2005) 640.

[9] J. K. Hurst, R. F. Khairutdinov, Electr. Trans. Chem., 4 (2001) 578.

[10] A. M. F. Neto, S. R. A. Salinas "The Physics of Lyotropic Liquid Crystals" Oxford University Press, ISBN: 9780198525509.

[11] K. Holmberg, B. Jonsson, B. Kronberg. B. Lindman, Surfactants and Polymers in Aqueous Solution; 2nd ed.; Wiley: Chichester, (2003) 84.

[12] P. Alexandridis, D. Zhou, A. Khan, Langmuir, 12 (1996) 2690.

[13] G. Whitesides, B. Grzybowski, Science, 295 (2002) 2418.

[14] D. G. Oakenfull, L. R. Fisher, J. Phys. Chem., 81 (1977) 1838.

[15] P. Venkatesan, Y. Cheng, D. Kahne, J. Am. Chem. Soc., 116 (1994) 6955.

[16] K. Tamhane, M.Sc. Thesis "formation of lyotropic liquid crystals through the self-assembly of bile acid building blocks" (2007).

[17] A. A. Collyer, Mater. Sci. Technol., 6 (1990) 981.

[18] S. T. Hyde, "Identification of Lyotropic Liquid Crystalline Mesophases" John Wiley & Sons, Ltd, (2001).

[19] Simpson, J., Weiner, E., 2nd Eds. Oxford University Press: New York, (1989).

[20] J. W. McBain, C. S. Salmon, J. Am. Chem. Soc., 42 (1920) 426.

[21] E. Gorter, F. Grendel, J. Exp. Med., 41 (1925) 439.

[22] W. Kauzmann, "The Mechanism of Enzyme Action" McElroy, W. D., Glass, B., Eds.; The John Hopkins Press: Baltimore, (1954) 70110.

[23] J. C. Kendrew, G. Bodo, H. M. Dintzis, R. G.Parrish, H. Wyckoff, D. C. Phillips, Nature, 181 (1958) 662.

[24] J. H. Hildebrand, J. Phys. Chem., 72 (1968) 1841.

[25] J. H. Hildebrand, Proc. Natl. Acad. Sci. U.S.A., 76 (1979) 194.

[26] G. Nemethy, H. A. Scheraga, W. Kauzmann, J. Phys. Chem., 72 (1968) 1842.

[27] C. Tanford, Proc. Natl. Acad. Sci. U.S.A., 76 (1979) 4175.

[28] K. A. Dill, Science, 250 (1990) 297.

[29] K. P. Murphy, P. L. Privalov, S. J.Gill, Science, 247 (1990) 559.

[30] J. Herzfeld, Science, 253 (1991) 88.

[31] N. T. Southall, K. A. Dill, A. D. J. Haymet, J. Phys. Chem. B, 106 (2002) 521.

[32] E. E. Meyer, K. J. Rosenberg, J. Israelachvili, Proc. Natl. Acad. Sci. U. S. A., 103 (2006) 15739.

[33] S. B. Johnson, C. J. Drummond, P. J. Scales, S. Nishimura, Langmuir, 11 (1995) 2367.

[34] A. J. Ward and C. du Reau "Surfactant Association in Nonaqueous Media" in Surface and Colloid Science, ed. E. Matijevic, Plenum Press, New York, (1993)15.

[35] T. L. Greaves, C. J. Drummond, Chem. Soc. Rev., 37 **(**2008) 1709.

[36] A. Ray, J. Am. Chem. Soc., 91 (1969) 6511.

[37] A. Ray, Nature, 231(1971) 313.

[38] H. N. Singh, S. M. Saleem, R. P. Singh, K. S. Birdi, J. Phys. Chem., 84 (1980) 2191.

[39] I. Rico, A. Lattes, J. Phys. Chem., 90 (1986) 5870.

[40] X. Auvray, C. Petipas, R. Anthore, I. Rico, A. Lattes, A. A. Z. Samii, A. Desavignac, Colloid Polym. Sci., 265 (1987) 925.

[41] A. Belmajdoub, K. Elbayed, J. Brondeau, D. Canet, I. Rico, Lattes, J. Phys. Chem., 92 (1988) 3569.

[42] A. Lattes, I. Rico, Colloids Surf., 35(1989) 221.

[43] X. Auvray, C. Petipas, R. Anthore, I. Rico, A. Lattes, J. Phys. Chem., 93 (1989) 7458.

[44] X. Auvray, T. Perche, R. Anthore, C. Petipas, I. Rico, Lattes, Langmuir, 7 (1991) 2385.

[45] X. Auvray, T. Perche, C. Petipas, R. Anthore, M. J. Marti, Rico, A. Lattes, Langmuir, 8 (1992) 2671.

[46] T. Perche, X. Auvray, C. Petipas, R. Anthore, E. Perez, I. R. Lattes, A. Lattes, Langmuir, 12 (1996) 863.

[47] M. S. Akhter, S. M. Alawi, Colloids Surf. A, 173 (2000) 95.

[48] M. S. Akhter, S. M. Alawi, Colloids Surf. A, 219 (2003) 281.

[49] A. Lattes, E. Perez, I. R. Lattes, C. R. Chimie, 12 (2009) 45-53.

[50] R.K Shukla, K.K. Raina, Int. J. Mod. Phys. B., 23 (2009) 5075.

[51] T. L. Greaves, C. J. Drummond, Chem. Soc. Rev., 37 (2008) 1709.

[52] C. Fong, T. Le, C. J. Drummond, Chem. Soc. Rev., 41(2012) 1297.

[53] P. B. Ishai, D.Libster, A. Aserin, N. Garti, Y. Feldman, J. Phys. Chem. B., 113 (2009) 12639.

[54] P. B. Ishai, D. Libster, A. Aserin, N. Garti, Y. Feldman, J. Phys. Chem. B., 114 (2010) 12785.

[55] R. Buchner, C. Baar, P. Fernandez, S. Schrfdle, W. Kunz, J, Mol. Liq., 118 (2005) 179.

[56] P. Fernandez, S. Schödle, R. Buchner, W. Kunz, Chem. Phys. Chem., 4 (2003) 10.

[57] L. Lanzi , M. Carlà , L. Lanzi , C. M.C. Gambi, J. Colloid and Interface Sci., 330 (2009)156.

[58] L. C. Chien, A.B. Golovin, Patent, US 2008/0165472 A1.

[59] D. J. Mitchell, G. J. T Tiddy, L. Waring, T. Bostock, M. P. McDonald, J Chem. Soc. Faraday Trans., 79 (1983) 975.

[60] G. G. Chemik, Curr. Opin. in Coll. & inter. Sci., 4 (1999) 381.

[61] P.Sakya, J. M. Seddon, R. H. Templer, R. J. Mirkin, G. J. T. Tiddy, Langmuir, 13 (1997) 3706.

[62] T. Iwanaga, M. Suzuki, H.Kunieda, Langmuir, 14 (1998) 5775.

[63] H. Kunieda, K. Shigcta, M. Suzuki, Langmuir, 15 (1999) 3118.

[64] H. Kunieda, G.Umizu, K. Aramaki, J. Phys. Chem. B, 104 (2000) 2005.

[65] T. Imura, Y. Hikosaka, W. Worakitkanchanakul, H. Sakai, M. Abe, M. Konishi, H. Minamikawa, D. Kitamoto, Langmuir, 23 (2007) 1659.

[66] H. Kawasaki, A. Sasaki, T. Kawashima, S. Sasaki, R. Kakehashi, I. Yamashita, K. Fukada, T. Kato, H. Maeda, Langmuir, 21 (2005) 5731.

[67] V. Percec, D. Tomazos, J. Heck, H. Blackwell, G. Ungar, J. Chem. Soc., Perkin Trans., 2 (1994) 31.

[68] M. Lee, B.K. Cho, Chem. Mater., 10 (1998) 1894.

[69] T. Otake, M. Ogasawara, K. Ito-Akıta, N. Nishina, S. Ujiie, H. Ohno, T. Kato, Chem. Mater., 12 (2000) 782.

[70] B. Donnio, Curr. Opin. Colloid Interface Sci., 7 (2002) 371.

[71] O. Dag, A. Verma, G.A. Ozin, C.T. Kresge, J. Mater. Chem., 9 (1999) 1475.

[72] F. Schuth, Chem. of Mat., 13 (2001) 3184.

[73] G.S. Attard, P.N. Barlett, N.R.B. Coleman, J.M. Elliott, J.R. Owen, J. H. Wang, Science, 278 (1997) 838.

[74] Y. Yamauchi, T. Momma, T. Yokoshima, K. Kuroda, T. Osaka, J. Mater. Chem. 15 (2005) 1987.

[75] C. Albayrak, A.M. Soylu, O. Dag, Langmuir, 24 (2008) 10592.

[76] A. Shiloach, D. Blankschtein, Langmuir, 14 (1998) 1618.

[77] Y. Turker, O. Dag, J. Mat. Chem. 18 (2008) 3467.

[78] A. F. Demirors, B. E. Eser, O. Dag, Langmuir, 21(2005) 4156.

[79] A. F. Demirors, M. Arslan, O. Dag, Micro. and Meso. Mat., 98 (2007) 249.

[80] O. Celik, O. Dag, Ange. Chem. Inter. Ed., 40 (2001) 3800.

[81] O. Dag, S. Alayoglu, I. Uysal, J. Phy. Chem. B, 108 (2004) 8439.

[82] O. Dag, O. Samarskaya, C. Tura, A. Gunay, O. Celik, Langmuir, 19 (2003) 3671.

[83] R.K. Shukla, K.K. Raina, Adv. Cond. Matt. Phys. Article ID 1747861 (2011) 1.

[84] R. K. Shukla, K. K. Raina, AIP conf. Proc., 1393 (2011) 341.

[85] http://www.rsc.org/chemistryworld/Issues/2003/February/science.asp.

[86] D. F. Evans, H. Wennerstrom, The colloidal domain, 2nd Edn. Weinheim: VCH, (1999).

[87] D. J. Shaw “Introduction to colloid and surface chemistry” 4th Edn. London: Butterworth-Heinemann, (1992).

[88] P. Poulin, S. Holger, T.C. Lubensky, D.A. Weitz, Science, 275 (1997) 1770.

[89] M. Musevic, Skarabot, U. Tkalec, M. Ravnik, S. Zumer, Science, 313 (2006) 954.

[90] T.C. Lubensky, D. Pettey, N. Currier, H. Stark, Phys Rev E., 57 (1998) 610.

[91] C.P. Lapointe, T.G. Mason, I.I. Smalyukh, Science, 326 (2009)1083.

[92] L. Ramos, M. Zapotocky, T.C. Lubensky, D.A .Weitz, Phys Rev E, 66 (2002) 031711.

[93] M. Ravnik, G.P. Alexander, J.M. Yeomans, S. Zumer, Faraday Discuss, 144 (2010) 159.

[94] T. Yamamoto, H. Yokoyama, Y. Tabe, Mol. Cryst. Liq. Cryst., 478 (2007) 967.

[95] J.C. Loudet, P. Barois, P. Poulin, Nature, 407 (2000) 613.

[96] M. Zapotocky, L. Ramos, P. Poulin, T.C. Lubensky, D.A. Weitz, Science, 283 (1999) 209.

[97] O.P. Pishnyak, S. Tang, J.R. Kelly, S.V. Shiyanovskii, O.D. Lavrentovich, Phys. Rev. Lett., 99 (2007) 127802.

[98] J.Yamamoto, H.Tanaka , Nature, 409 (2001) 321.

[99] J. Fukuda, B.I.Lev, H.Yokoyama, Phys. Rev. E, 65 (2002) 1710.

[100] H. Stark, Phys. Rep., 351 (2001) 387.

[101] R.W. Ruhwand, E. M. Terentjev, Phys. Rev. E, 56 (1997) 5561.

[102] D.Rudhardt, A. Ferna, N. Nieves, D. R.Link, D. A.Weitz, App. Phy. Lett., 82 (2003) 2610.

[103] Z. X.Zhang , S.Jeroen, V. Duijneveldt, J. Chem. Phy., 124 (2006) 154910.

[104] A. Martinez, H. C. Mireles, I. I. Smalyukh, PANS, 52 (2011) 20891.

[105] H. Kikuchi, M. Yokota, Y. Hisakado, H. Yang, T. Kajiyama, Nat. Mater., 1 (2002) 64.

[106] D. Yoon, M. Choi, Y. Kim, M. Kim, O. Lavrentovich, H. Jung, Nat. Mater., 6 (2007) 866.

[107] Y. Kim, D. Yoon, H. Jeong, O. Lavrentovich, H. Jung, Adv. Funct. Mater., 21 (2011) 610.

[108] Y. Kim, D. Yoon, H. Jeong, H. Jung, Soft Matter, 6 (2010) 1426.

[109] Y.H. Kim, D.K. Yoon, H.S. Jeong, J.H. Kim, E.K. Yoon, H.-T. Jung, Adv. Funct. Mater., 19 (2009) 3008.

[110] J. P.F. Lagerwall, G. Scalia, Cur. App. Phys., 12 (2012) 1387.

[111] T. Sun, J. Y. Ying, Nature, 389 (1997)704.

[112] Z. R. Tian, W. Tong, J. Y. Wang, N. G. Duan, V. V. Krishnan, S. L. Suib, Science, 276 (1997) 926.

[113] P. D.Yang, D. Y.Zhao, D. I. Margolese, B. F. Chmelka, O. D. Stucky, Nature, 396 (1998)152.

[114] X. D. Zou, T. Conradsson, M. Klingstcdt, M. S. Dadachov, M. Keeffe, Nature, 437 (2005) 716.

[115] O. Dag, S. Alayoglu, C. Tura, O. Celik, Chem. of Mat., 15 (2003) 2711.

[116] P. V. Braun, P. Osenar, S. I. Stupp, Nature, 380 (1996) 325.

[117] M. J. MacLachlan, N. Coombs, O. A. Ozin, Nature, 397(1999) 681.

[118] P. N. Trikalitis, K. K. Kangan, Bakas, T. M. Kanatzidlis, Nature, 410 (2001) 671.

[119] Y. Yamauchi, K. Kuroda, Chem.-an Asian J., 3 (2008) 664.

[120] C. Albayrak, M.Sc. Thesis “Investigation of two new lyotropic liquid crystalline systems: [Zn $(H_2O)_6$]$(NO_3)_2$-$C_{12}EO_{10}$-CTAB-H_2O and [Zn$(H_2O)_6$]$(NO_3)_2$-$C_{12}EO_{10}$-SDS- H_2O”, (2008).

[121] L. Wang, X. Chen, J. Zhan, Y. Chai, C. Yang, L. Xu, W. Zhuang, B. Jing, J. Phys. Chem. B, 109 (2005) 3189.

[122] Y. Wan, D. Y. Zhao, Chem. Rev., 107 (2007) 2821.
[123] C. Guo, J. Wang, F. Cao, R. J. Lee, G. Zhai, Drug Disc. Today, 15 (2010) 1032.
[124] L. Sagalowicz, Trends Food Sci. Technol., 17 (2006) 204.

Chapter 2

Experimental methods and characterization techniques

The detailed description about the selection of precursor materials (surfactant and solvents), experimental methodologies for synthesis and characterization techniques used for the variety of binary, ternary and colloidal systems is presented in this chapter. X-ray diffraction (XRD) and polarizing optical microscopy (POM) techniques were used to identify the structural phases of the prepared LLC mixtures. Differential scanning calorimetric (DSC) measurements were used to evaluate thermal parameter like heat flow, enthalpy and also to predict the order of the phase transition. Dielectric spectroscopy was used to study the effects of electric field on ordering, nature and physical properties of the prepared mixtures. Abbe refractrometer was employed to measure the refractive index of the prepared mixtures.

2.1: Materials

The various amphiphilic molecules reach to the lyotropic liquid crystalline state at the expense of increasing concentration in aqueous medium and in some polar non-aqueous solvents. The liquid crystalline behaviour of these phases depend upon the micellization, reaction medium, thermodynamic equilibria, counter ion effect, optimal surface area of head group and alkyl chain length and the physicochemical interactions of solvent and solute. The main aim of the present study is to understand effect of varying polarity of the solvent on the self assembly of cationic, anionic and non-ionic surfactants of diverse chain lengths and head group area in as pure and quenched conditions. Cetyl pyridinium chloride [($C_{21}H_{38}NCl$) Merck, 99 % purity], Sodium dodecylsulfate [(SDS) $NaC_{12}H_{25}SO_4$, purity 99%], Polyoxyethylene (20) sorbitan monolaurate [(Tween 20) $C_{58}H_{114}O_{26}$, purity 99%] were purchased from LOBA Chemie used as received without any further purification. The various solvents used were ethylene glycol [EG] (SD Fine chemicals, 99 % purity), water [(H_2O) (purified with the Millipore direct Q3 system)], formamide [(F) CH_3NO (SD Fine chemicals, 99 % purity)].

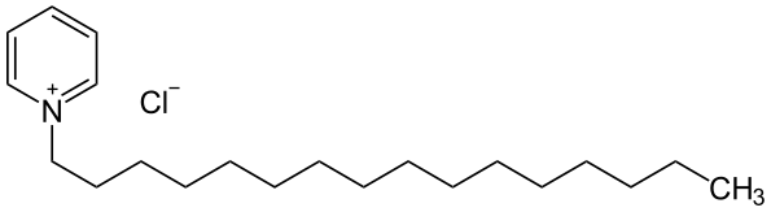

Cetylpyridinuium chloride ($C_{21}H_{38}ClN$)

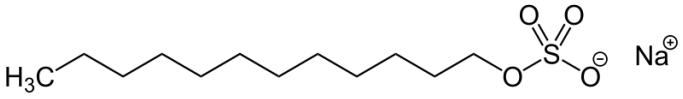

Sodium dodecyl sulfate [$CH_3 (CH_2)_{11}OSO_3Na$]

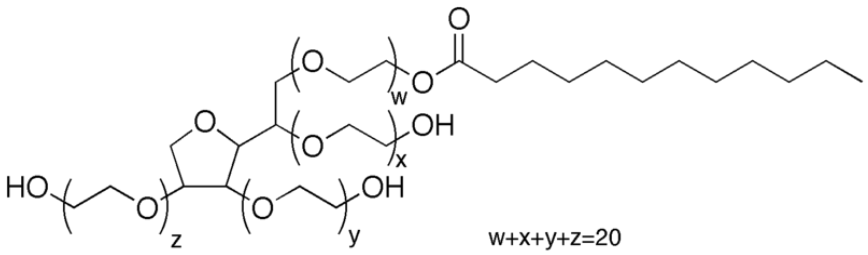

Polysorbate 20 [Tween 20($C_{58}H_{114}O_{26}$)]

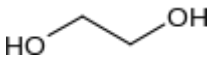

Ethylene Glycol

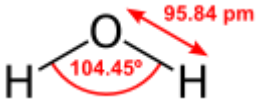

Water (H_2O)

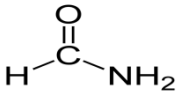

Formamide CH_3NO

Table 2.1: Properties of precursor materials [1]

System	Chemical Formula	Mw (g/mol)	Density (g/cm^3)	Melting point (K)	boiling point
Cetylpyridinuium chloride	$C_{21}H_{38}ClN$	339.00	1.10	360.00	--
Sodium dodecyl sulfate	$CH_3(CH_2)_{11}OSO_3Na$	288.00	1.01	479.00	--
Polysorbate 20 (Tween 20)	$C_{58}H_{114}O_{26}$	1227.00	1.01	368.00	--
Ethylene Glycol	$C_2H_6O_2$	62.00	1.10	260.00	197.00
Water	H_2O	18.00	1.00	273.00	373.00
Formamide	CH_3NO	45.00	1.10	275.00	483.00

2.2: Preparation of lyotropic liquid crystalline mixtures

2.2.1: Binary mixtures

Cetylpyridinuium chloride (CPC) was used as precursor material to synthesize various mesophasic materials in the aqueous and non-aqueous medium of varying polarity solvents. In typical procedure varying concentrations of solute and solvent (10:90, 30:70, 40:60, 50:50, 75:25 wt %) were taken in glass vials. The reaction mixtures were mixed via mechanical shaking (via vertex meter) and the heating and cooling cycle (between 30^0C-80^0C) to homogenize the mixture. In final step the reaction mixtures were sonicated (37 KHz) for about an hour at 80^0C and kept at rest at room temperature for a week to attained the thermal equilibrium. Same experimental procedure was followed for the synthesis of the following systems

- Cetylpyridinuium chloride: water [CPC: W (10:90, 30:70, 40:60, 50:50, 75:25 wt %)]
- Cetylpyridinuium chloride: formamide [CPC: F (10:90, 30:70, 40:60, 50:50, 75:25wt %)]
- Sodium dodecyl sulfate: ethylene glycol [SDS: EG (10:90, 30:70, 40:60, 50:50, 75:25wt %)]
- Sodium dodecyl sulfate: water [SDS: W (10:90, 30:70, 40:60, 50:50, 75:25 wt %)]
- Sodium dodecyl sulfate: formamide [SDS: F (10:90, 30:70, 40:60, 50:50, 75:25 wt %)]
- Tween 20: ethylene glycol [T20: EG (10:90, 30:70, 40:60, 50:50, 75:25 wt %)]
- Tween 20: water [T20: W (10:90, 30:70, 40:60, 50:50, 75:25 wt %)]
- Tween 20: formamide [T20: F (10:90, 30:70, 40:60, 50:50, 75:25 wt %)]

2.2.2: Ternary mixtures

Transition metal salts [(TMS) Zinc chloride and cupric chloride] were employed as third component to prepare the ternary non-aqueous LLC systems. Ternary mixtures were derived via dispersing varying concentrations of the TMS in the binary mixture CPC: EG. The studied series are given below

- $ZnCl_2$: CPC: EG [$ZnCl_2$=1, 2, 4, 6 and10 wt % on CPC: EG (40:60wt %)]
- $CuCl_2$: CPC: EG [$CuCl_2$=1, 2, 4, 6 and10 wt % on CPC: EG (40:60wt %)

The reaction mixtures of appropriate concentrations were mixed via mechanical shaking (via vertex meter) and the heating and cooling cycle (between 30^0C-80^0C). In final step the reaction mixtures were sonicated (37 KHz) for about an hour at 80^0C and rested at room temperature for a week to attain the thermal equilibrium.

2.2.3: Synthesis of zinc oxide

Zinc Acetate (Loba Chemie, purity 98.0%), Ethanol (Merck, purity 99.9%) and Sodium Hydroxide (Loba Chemie, purity 98.0%) were used as a precursor, solvent and base for the synthesis of ZnO. Co-precipitation method was employed to synthesize zinc oxide. In typical procedure 0.01 moles of Zinc Acetate [$Zn(CH_3CO_2)_2.2H_2O$] were dissolved in 100 ml of ethanol at 70^0c by continuous stirring for 2 hours. Further about 0.02 moles of NaOH were added in the solution to adjust pH in basic region (10.82) which results precipitation. The

precipitate thus obtained were filtered out and washed with ethanol many times. Finally, the obtained product was heated in the oven at 90^0c for 4 hours to remove the excess solvent and other residue material. The dried product was collected and grinded to make fine powder and finally characterized with many techniques.

2.2.4: Colloidal mixtures

Non-aqueous colloidal mixtures were prepared via mixing ZnO particles of 1µm in the binary mixtures of CPC: EG, SDS: EG, T20: EG (10:90wt% in all systems) at varying concentration as listed below

- ZnO: CPC: EG (ZnO =0.05, 0.1 and 0.5wt %)
- ZnO: SDS: EG (ZnO =0.05, 0.1 and 0.5wt %)
- ZnO: T20: EG (ZnO =0.05, 0.1 and 0.5wt %)

Same experimental procedure (as described in the section 2.2.1 and 2.2.2) was followed for the preparation of the colloidal mixtures. Colloidal suspensions were rested for several weeks and consistently examined weather the particles are suspended or settled down. The stable colloidal suspensions were further characterized using various techniques discussed below.

2.3: Characterization techniques

As prepared and quenched binary, ternary and colloidal mixtures were characterized by using various techniques to examine the diverse lyotropic liquid crystalline mesophases and their thermal, dielectric and optical properties at 303K and elevated temperature (300K-400K).

2.3.1: Structural analysis through X-ray diffraction

X-ray crystallography is a method of determining the arrangement of atoms within a crystal, in which a beam of X-rays strikes a crystal and diffracts into many specific directions. From the angles and intensities of these diffracted beams, a crystallographer can produce a three-dimensional picture of the density of electrons within the crystal. From this electron density, the mean positions of the atoms in the crystal can be determined, as well as their chemical bonds, their disorder and various other information. Larger is the angle lower is the atomic distance to be probed; the liquid crystalline systems are aggregates of the micelles in the definite geometries and hence exhibit larger size and scanned at lower angle of the 2θ scale. To ascertain the phase behaviour of the prepared mixtures (binary, ternary and colloidal) XRD patterns were recorded in the $2\theta = 1\text{-}10^0$ range at slow scan at 303 K in as prepared and

quenched conditions. The sample for XRD measurement were made via placing appropriate amount of sample in the glass cavity, which further exposed to the X-ray beam of PANalytical X'Pert-PRO MPD [(Cu Kα radiation source λ=1.54Å)].

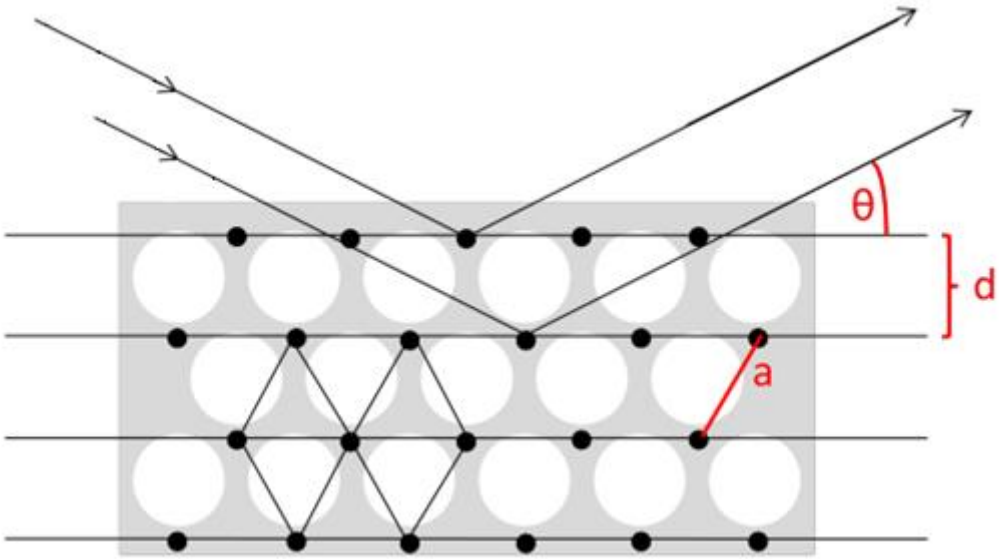

Figure 2.1: Schematic for two dimensionally hexagonally arranged cylindrical micelles.

Similar procedure was used to scan the quenched, ternary and colloidal systems. The schematic for the diffraction of X-ray from cylindrically array of two dimensional LLC hexagons along with various structural lengths are shown in figure 2.1. The obtained XRD profiles were indexed with the standard mesophases and used to deduce various structural and geometrical parameters via utilizing some standard equations. All the structural parameters and equations are discussed in the chapter 3.

2.3.2: Morphological analysis through Polarizing Optical Microscopy

Polarizing optical microscopy is one of the versatile technique employed to identify the distinct liquid crystalline phases. Morphological and phase behaviour studies were carried out through polarizing microscope (Olympus BX-51P) coupled with CCD camera. The micro texture were recorded in the transmission mode, under crossed polarizer's using convergent white light at 303K and elevated temperature at 100X by placing the small amount of sample in between the cover glasses or by filling the liquid crystal sample cells to identify the various phases and the phase transition occurred in the lyotropic systems at the expanse of varying temperature. The whole experimental set up was interfaced with the computer as shown in the figure 2.2. All the textures were acquired via Linksys software and further analyzed with the OLYSIA BIO REPORT software. Thermo optical measurements were done by using the

Linkam temperature programmable hot stage (Model TP 94-THMS 600). This hot stage is the particularly designed for broad range (-196-600^{0}C) of the thermal measurement purpose with an accuracy of ±0.1^{0}C.

Figure 2.2: Optical polarizing microscope and thermo-optical set up.

The precise coding of the heating rate in the instrument facilitates the accurate heating and cooling rate ranging 0.1 to 0.9^{0}C/min at 0.1degree interval from 1.0 to 9.0^{0}C/min at 1.0 degree interval and from 10 to 90^{0}C degree intervals. The optical textures of the various LLC mixtures were recorded at the expanse of increasing temperature with heating and cooling rate of 1^{0}C/min to understand the effects of temperature on the self assembly of the surfactant molecules into distinct mesophase. Various liquid crystalline to liquid crystalline, crystalline to liquid crystalline and liquid crystalline to crystalline and liquid crystalline transition were also noticed on the basis of thermo-optical textural analysis which further discussed in the result and discussion section.

2.3.3: Thermal analysis through Differential scanning calorimetry

Differential scanning calorimetry (DSC) is an inexpensive and rapid method to measure heat capacities of condensed phases. From these measurements, enthalpy changes for phase transitions can easily be determined. DSC has been applied to a wide variety of problems, fromcoal combustion, organic and inorganic materials to protein denaturation to understand thermal behaviour and variation thermo-dynamical constraints. DSC provides a convenient and moderately accurate method of measuring heat capacities and enthalpy changes. Commercial instruments provide a recorder output of the constant pressure heat capacity,

$$Cp = \left(\frac{dq}{dT}\right)_P = \left(\frac{\partial H}{dT}\right)_P$$

as a function of temperature. The area under such a curve between any two temperature limits yields an enthalpy change [2-3]:

$$\Delta H = \int_{T_1}^{T_2} \left(\frac{\partial H}{dT}\right)_P dT = \int_{T_1}^{T_2} CpdT$$

Experimental set up used for the measurements of various samples is presented in the figure 2.3. Thermo-dynamical behaviour of various lyotropic systems was investigated using differential scanning calorimeter (DSC model LINSEIS L- 63) with heating @ 2 degree/ minute for each case. The calculation of heat flow and enthalpy were made by using the LINSEIS software to examine the various phase transitions and the absorption or evolution of the heat during reaction. Further on the basis of these two thermal parameters, the orders of transitions were predicted via examine variation of the ΔH on the temperature scale. There are many ways to classify phase transitions. One is a formal definition usually taught in statistical physics courses. There are two different states of the same substance two phases. One is stable at lower temperatures; another

Figure 2.3: Differential scanning calorimeter set up.

one is stable at higher temperatures. At the transition temperature, the free energy (ΔG) of both phases must be the same. The first derivatives of the free energy, for instance, the entropy, may experience a jump at the transition; in this case, one speaks of the first order phase transition. The most well-known examples are liquid-solid and liquid-gas transitions. It

could also be that the first derivatives are continuous, but the second derivatives, for instance, the specific heat, have a jump. Then one speaks of the second order phase transition. Examples are superconducting, magnetic, pyroelectric, and some structural phase transitions in solids. Generally speaking, the transition order is the order of the derivatives that experience a jump at the transition temperature. The thermal behavior of studied systems and the obtained phase transition are discussed in next chapter.

2.3.4: Dielectric spectroscopy

Dielectric spectroscopy is one of the powerful technique facilitate the deep insight of the molecular, dipolar and surface interactions at lower and higher frequency regimes and widely used for examine the variety of materials ranging from solid, liquid polymeric and liquid crystals. The dielectric measurements of lyotropic binary and colloidal mixtures were performed via making the parallel plate capacitor. Indium tin oxide (ITO) coated glass substrates were prepared by first thoroughly cleaning and then inducing a planer alignment with polyamide. They were sandwiched in the form of a cell of thickness 6µm using mylar spacer and sample was filled in between via capillary action. The schematic of the cell assembly is presented in the figure 2.4(a), the various capacitor of lyotropic materials made during this study are also depicted in the figure 2.4(b).

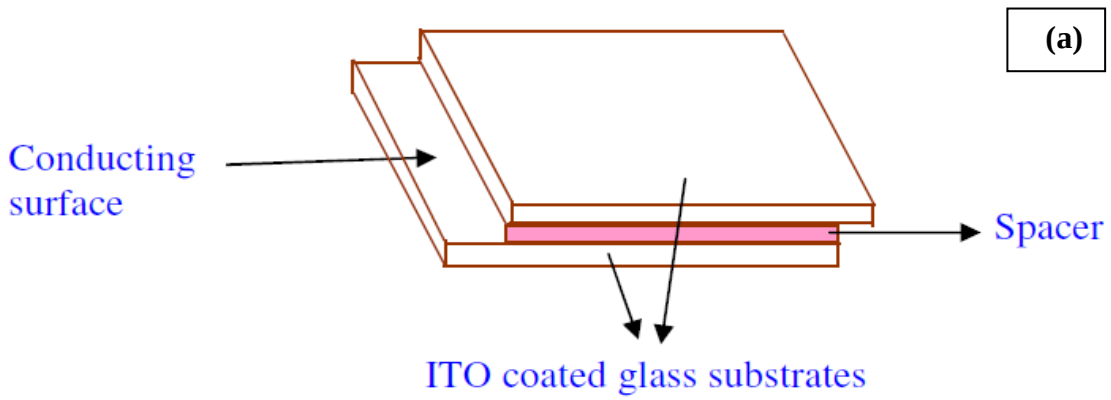

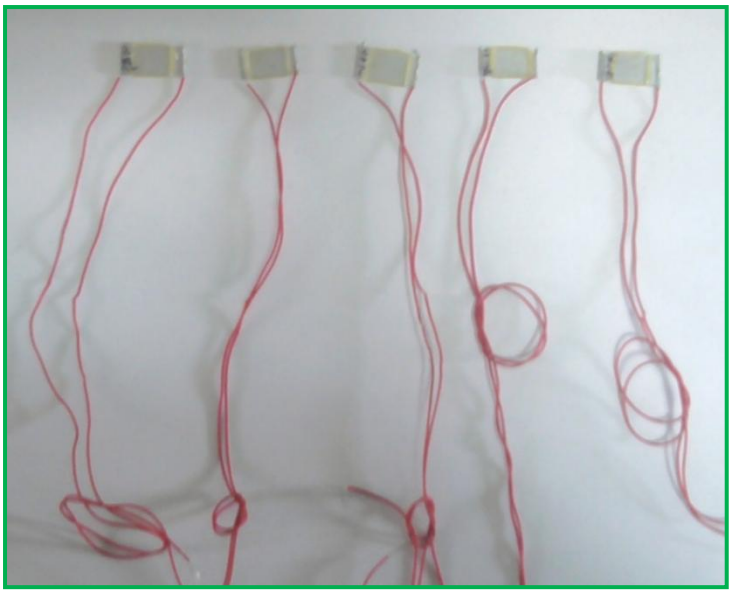

(b)

Figure 2.4: (a) Schematic for assembly of liquid crystal cell (b) various capacitor of lyotropic materials.

Dielectric spectroscopy measurements were carried out using RCL meter (Fluke PM6306) in the frequency range 50 Hz to 1 MHz at 303K and elevated temperature (300-400K). Schematic representation experimental set up is shown in the figure 2.5 (a-b) dielectric cells were calibrated by using the benzene as a reference media.The calculation of dielectric constant of lyotropic liquid crystals can be done through equations listed below [4]

$$C_{effective} = \frac{C_{benzene} - C_{air}}{1.254} \qquad 2.1$$

$$\varepsilon' = \left(\frac{C_{LLC} - C_{air}}{C_{effective}}\right) + 1 \qquad 2.2$$

$$\varepsilon'' = D \times \varepsilon' \qquad 2.3$$

Where, $C_{benzene}$, C_{air} and C_{LLC} are the capacitance values in benzene, air and lyotropic liquid crystals medium respectively. D is Dissipation factor, ε' is the dielectric constant of the material, also known as the dielectric permittivity, and it is used to define the ability of the material to store electrical charge. ε'' is the imaginary part, which is related to the loss and

(a)

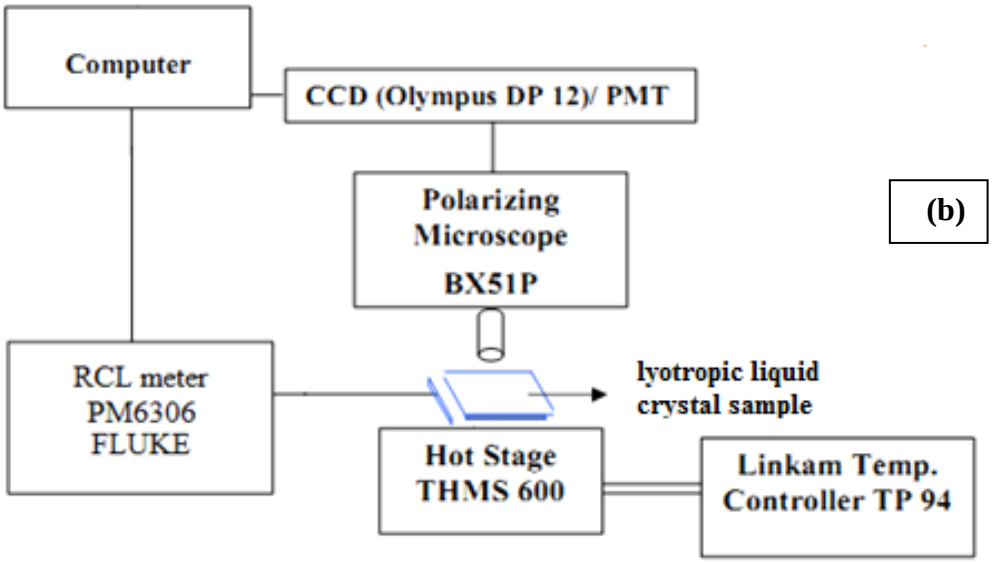

(b)

Figure 2.5: (a) Programmable RCL meter [FLUKE PM6306] used for dielectric studies (b) Block diagram of the experimental set-up to study textures and dielectric properties of lyotropic liquid crystal.

known as the dielectric loss. Certain parameters like **ac** conductivity and activation energy of the different LLC phases were derived from the complex dielectric permittivity using following equations were associated with the dielectric parameters were estimated using [5]

$$\sigma_{ac} = \varepsilon_0 \varepsilon'' \omega \qquad 2.4$$

Where ε_0 is absolute permittivity, ε'' is imaginary part of the permittivity and $\omega=2\pi f$ is cyclic frequency.

$$E_a = -R\left[\frac{\partial l_n \sigma}{\partial(1/T)}\right]_P \qquad 2.5$$

E_a is activation energy, R is gas constant, σ is ac conductivity, T is temperature and P is constant pressure [6].

2.3.5: Refractive Index

Refractive indices for these binary ternary and colloidal liquid crystalline mixtures were measured at room temperature by using Abbe refractrometer at 303K with λ=589nm. Experimental set used for the refractive index measurement is shown in the figure 2.6. In other measurement we deduce the refractive index (**n**) for these systems from the dielectric permittivity with an assumption that the surfactant molecules are non-interacting in nature. With this assumption we use the standard direct relation between refractive index and the dielectric permittivity as given below

$$\mathbf{n} = \sqrt{\varepsilon'}$$

Where **n** is refractive index and ε′ is real part of dielectric permittivity [7-8]. The variation of the refractive index has also been studied with the rise in temperature for these systems.

Figure 2.6: Abbe refractrometer used for optical measurements.

2.4: References

[1] http://en.wikipedia.org.

[2] www.dartmouth.edu/~pchem/75/pdfs/DSC.pdf.

[3] Manual of LINSEIS L- 63 DSC.

[4] J. B. Briks, J. Hart, properties in deielctric vol 3, Heywood and Company Ltd., London (1961).

[5] A. K. Chuk, L. Dolgov, O. Yaroshchuk**,** Semi. Phys., Quantum Ele.s & Opto., 11 (2008) 337.

[6] http://en.wikipedia.org/wiki/Arrhenius_equation.

[7] http://en.wikipedia.org/wiki/Refractive_index.

[8] Manual Abbe refractrometer.

Chapter 3

Aqueous and non-aqueous binary lyotropic liquid crystalline mixtures

This chapter summarizes the structural, morphological, thermal, dielectric and optical analyses of aqueous and non-aqueous binary lyotropic liquid crystalline mixtures. The preliminary goal of present thesis is to explicate diverse lyotropic phases developed in as-prepared and quenched conditions. The origin of diverse lyotropic crystalline phases and phase transitions have been explored and discussed in the non-aqueous and aqueous regime of varying polarity solvents at lower and higher amphiphilic concentrations at room temperature. In addition dielectric dynamics of these mixtures have been examined to understand the interfacial interaction. Refractive index was also explored to find the suitable application of investigated systems in technological areas.

3.1: Cationic Surfactant

Cetylpyridinuium chloride [($C_{21}H_{38}ClN$) CPC] is the quaternary pyridinium salt derived from alkylation of pyridine with cetyl chloride. The presence of positively charged nitrogen atom with pyridine ring and hydrophobic tail makes CPC amphiphilic in nature which facilitates the self assembly characteristics with number of solvents.

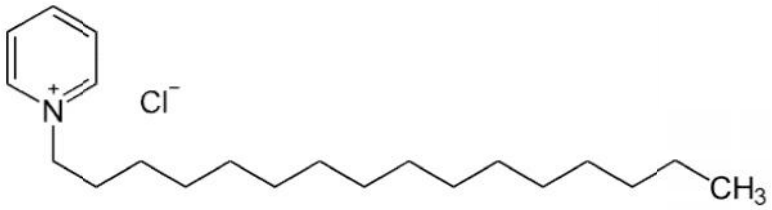

Three solvents of varying polarity used in the present study were ethylene glycol (ethylene glycol is a protic solvent do possess cohesive energy, dielectric constant and hydrogen bonding ability to initialize the micellization. Presences of both inter and intra molecular hydrogen bonding provoked aggregation of amphiphilic molecules in its non-aqueous domains), water (water molecule contains one oxygen and two hydrogen atoms connected by covalent bonds and exhibit enough higher dielectric constant and hydrogen bonding ability to initiate self organization of amphiphiles) and formamide (derived from the formic acid having higher dielectric constant (109) sufficient to dissociate the surfactant molecule and drive their self assembly). The necessary conditions recognized for the self assembly attributed to the physicochemical approach are listed below

- **High polarity:** The dielectric constant must be sufficiently high to dissociate ions of amphiphilic molecules and hinder self-agglomeration.
- **High solvating power:** In combination with the high dielectric constant, favors dipole interactions over associations between opposite charge ions.
- **Highly structured:** Conception of structure is based on the strength of intermolecular bonds and the geometry of the molecules. Both chemical (hydrogen bonds) and non-chemical (polar and non-polar) interactions must be taken into account. Structured nature further associated with the internal pressure and cohesive energy density.

Solvents forming hydrogen bonds were well reported in the literature to drive the self assembly, although, if aprotic molecules could be found of sufficient polarity (dipole) to structure the medium they could also replace the aqueous solvents. Physicochemical properties of the utilized solvents are given in Table 3.1. However there is another empirical approach which supports the self organization of variety materials [1-9].

Table 3.1: Physicochemical parameters of various solvents

Solvents	Chemical formula	D_{ce} (J cm^{-3})[1]	$\varepsilon/\varepsilon_0$[2]	μ_D[3]
Ethylene glycol	$C_2H_6O_2$	0892	037.70	2.00
Water	H_20	2302	078.50	1.80
Formamide	CH_3NO	1575	109.50	3.40

[1] Density of cohesive energy, [2] Dielectric constant,[3] Charge Dipole moment .

The binary mixtures of Cetyl pyridinium chloride and various solvents [ethylene glycol (EG), water(W) and formamide (F)] at varying concentrations 10:90, 30:70, 40:60, 50:50 and 75:25wt% were prepared. They were characterized via X-ray diffraction (XRD), polarizing optical microscopy (POM), differential scanning calorimetry (DSC), dielectric spectroscopy and optical techniques to investigate the development of diverse phase in the varying concentration regime in as prepared and quenched systems and to understand their physical properties at 303K and elevated temperature range of 300-400K. Cetyl pyridinium chloride: ethylene glycol series named as CEM 1[CPC: EG (10:90)], CEM 2[CPC: EG (30:70)], CEM 3[CPC: EG (40:60)], CEM 4[CPC: EG (50:50)] and CEM 5[CPC: EG (75:25)], in similar way Cetyl pyridinium chloride: water series designated as CWM 1[CPC: W (10:90)], CWM 2[CPC: W (30:70)], CWM 3[CPC: W (40:60)], CWM 4[CPC: W (50:50)] and CWM 5[CPC: W (75:25)], series of Cetyl pyridinium chloride: formamide was denoted as CFM 1[CPC: F (10:90)], CFM 2[CPC: F (30:70)], CFM 3[CPC: F (40:60)], CFM 4[CPC: F (50:50)] and CFM 5[CPC: F (75:25)].

3.1.1: Structural analysis

To ascertain the validity of structural phases of the prepared mixtures X-ray diffraction measurement were done in the low angle (2θ=1-10^0) range at 303K. The XRD patterns of the as prepared mixture for the various series CPC: EG, CPC: W and CPC: F are presented in the figure 3.1 (a-c). As prepared mixtures of CPC:EG series did not diffract at any angle over the 2θ (2θ =1-7^0) scale at lower and higher amphiphilic concentration indicates the disordered state which may be due to the lack of thermal equilibrium in these systems in as prepared conditions or systems require some external thermal energy to initialize the self assembly. In CPC: W series as prepared mixtures exhibit mixed lyotropic and neat crystalline phase at

lower and higher band of surfactant concentration. Diffraction peaks observed at 2θ =3.1 and 6.2 represent the crystalline phase of neat CPC at all concentrations, though some un indexed

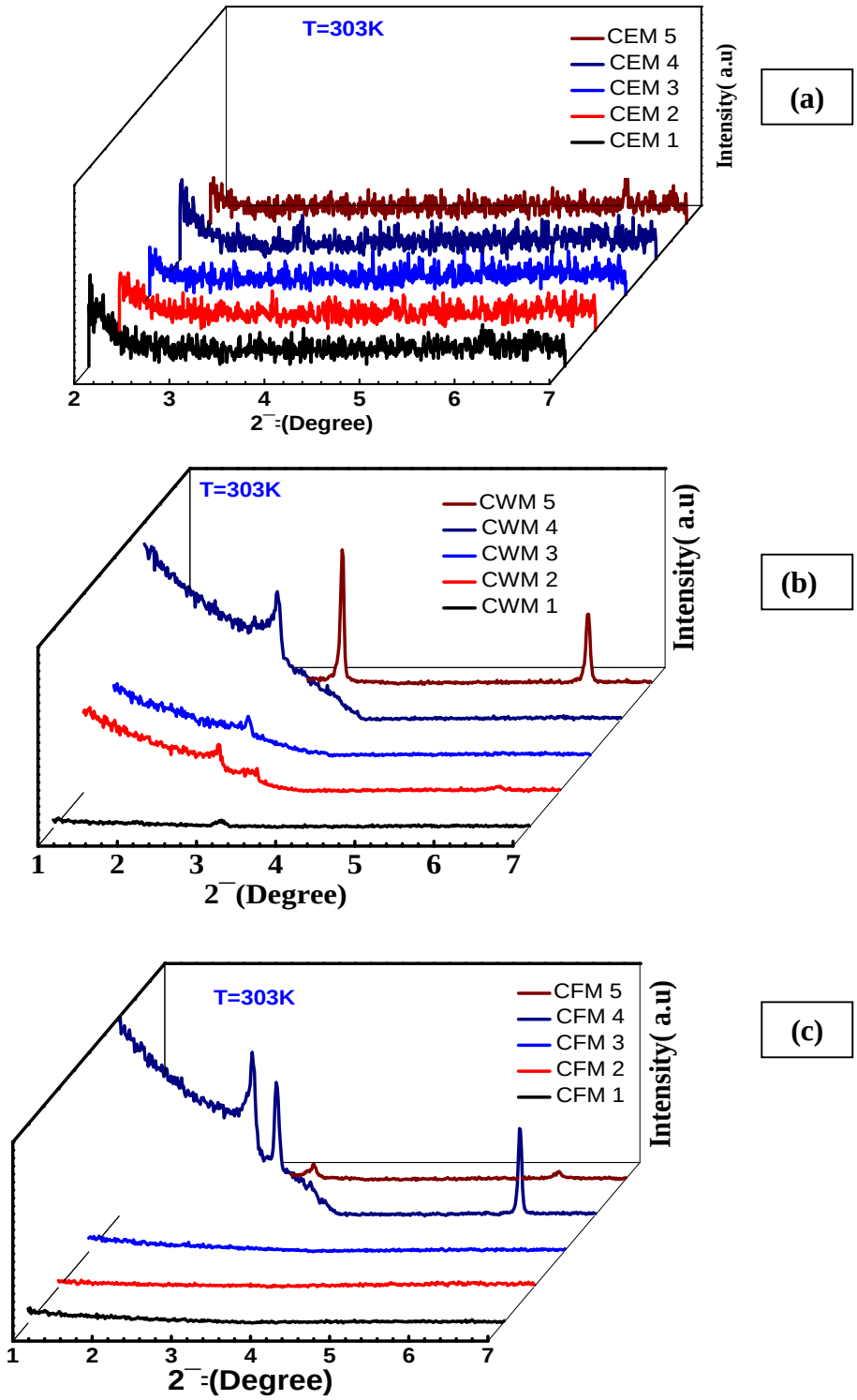

Figure 3.1: XRD profiles of as prepared mixtures at varying concentration (M1=10:90wt%, M2= 30:70wt%, M3= 40:60 wt%, M4= 50:50wt% and M5= 75:25wt% stands for concentration of respective solute : solvent) at 303K (a) cetyl pyridinium chloride: ethylene glycol series (CEM1-5) (b) cetyl pyridinium chloride : water series (CWM1-5) (c) cetyl pyridinium chloride : formamide series (CFM1-5) respectively.

reflections observed for CWM 2,3 and 4 may attributed to the liquid crystalline mesophase as evident from the figure 3.1(b), and further needs to be confirmed from textural analysis. CPC:F series did not diffract at any angle of 2θ scale over the scanned range (2θ =1-7^0) up to 40 wt% (CFM 3) concentration reveals lack of ordering in these systems or the richness of the solvent at the lower concentration range. However at higher concentrations these systems show well defined peaks. Peaks obtained for the CFM 4 are found to be in 1:√2: √4 (corresponding to the 2θ= 1.3, 2.6, and 3.07) are the characteristics of the bicontinuous LLC mesophase along with one crystalline peak at 2θ=6.2 (characteristic of neat CPC). However the systems procured higher amphiphilic content depicts crystalline phase (peaks at 2θ= 3.1 and 6.2) as evident from the figure 3.1 (c).

In order to achieve the thermal equilibria and examine the effect of heat treatment, prepared systems were heated up to the 353K just below the melting of the neat surfactant and quenched to the 300K. XRD patterns of the quenched mixtures of various series are shown in the figure 3.2 (a-c). XRD profiles for quenched CPC: EG series are shown in figure 3.2(a). Strong reflection at 2θ = 3.05^0 (corresponds to 28.8 nm) and 6.1^0 (corresponds to 14 nm) noticed at lower concentrations (<40 wt %) were found in ratio1:2 indicative of a lamellar LLC phase. In addition very low intensity diffraction peaks at 2θ = 2.7^0 (corresponds to 32.6 nm), 5.7^0 (corresponds to 15.3 nm) in the lower concentration range (<40 wt %) are in 1: $4^{1\backslash 2}$ ratio indicative of a two dimensional direct hexagonal LLC phase ($2D_H$). At higher concentration diffraction peaks observed at 2θ = 3.05^0 (corresponds to 28.8 nm) and 6.1^0 (corresponds to 14 nm) showed the occurrence of a lamellar phase having relatively lower intensity with some un indexed peaks. The geometrical parameters [a_0 is the lattice parameter, thickness of surfactant bilayer (d_L), mole fraction of the surfactant (φ_s), thickness of ethylene glycol channel (d_{EG}) and the area per molecule (a_s)] of observed LLC mesophases were computed from the standard equations [10-12]

For lamellar mesophase

$$d_{L\alpha} = a_0 / l \qquad (3.1)$$

$$¤_S = \frac{W_S / °_S}{W_S / °_S + W_{EG} / °_{EG}} \qquad (3.2)$$

$$2 \cdot d_L = (\varphi_S).a_0 \quad (3.3)$$

$$d_{EG} = a_0 - 2 \cdot d_L \quad (3.4)$$

$$a_S = \frac{2V_L}{d_L} \cdot ¤_S \quad (3.5)$$

For hexagonal mesophase

$$r_H = a_0 \cdot \left(\frac{2}{\sqrt{3®}} \cdot (¤_S) \right)^{1/2} \quad (3.6)$$

$$d_W = \frac{2}{\sqrt{3}} a_0 - 2r_H \quad (3.7)$$

$$a_S = \frac{2V_L}{r_H} \cdot ¤_S \quad (3.8)$$

Where φ_s is the mole fraction of the surfactant, r_H is radius of the cylinder. V_L= 27.4+29.9N [4]

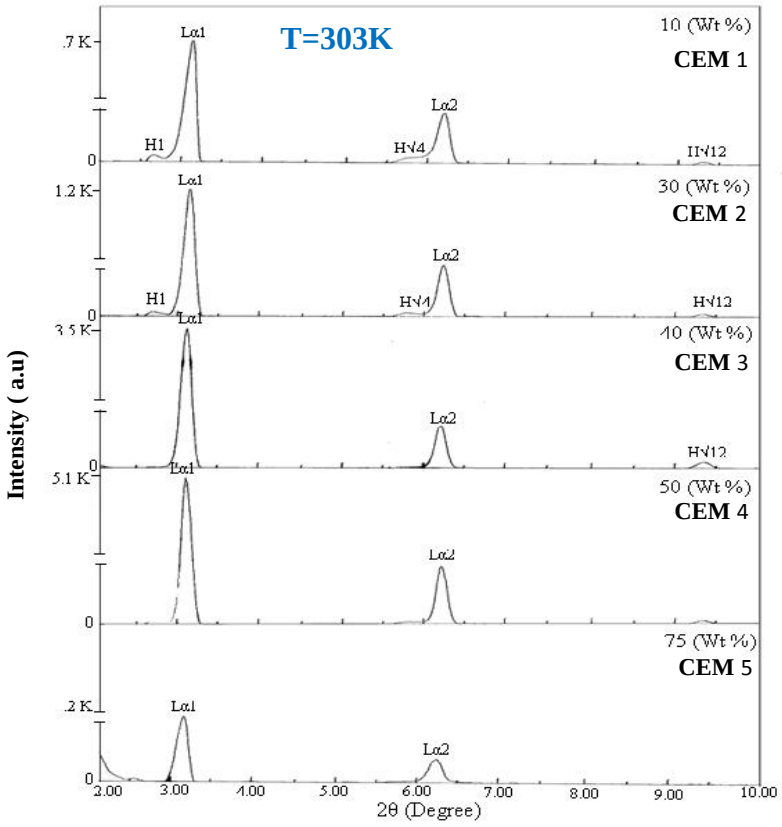

(a)

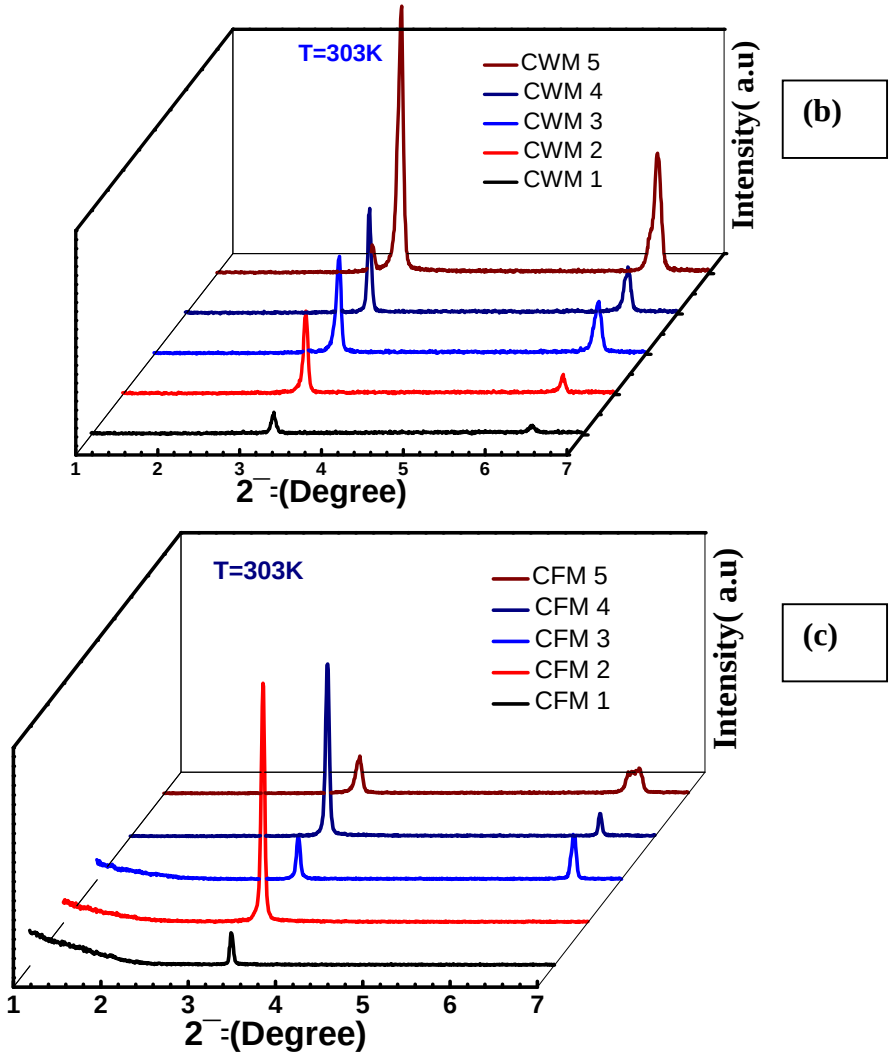

Figure 3.2: XRD profiles of quenched mixtures at varying concentration (M1=10:90wt%, M2= 30:70wt%, M3= 40:60 wt%, M4= 50:50wt% and M5= 75:25wt% stands for concentration of respective solute : solvent) at 303K (a) cetyl pyridinium chloride: ethylene glycol series (CEM1-5) (b) cetyl pyridinium chloride : water series (CWM1-5) (c) cetyl pyridinium chloride : formamide series (CFM1-5) respectively.

Table 3.2: Geometrical parameters for quenched CPC: EG mixtures

Sample	Phase	a_0(Å)	d_L(Å)	d_{EG}(Å)	a_s(Å)
CEM 1	$2D_H+L_\alpha$	--	--	--	--
CEM 2	$2D_H+L_\alpha$	--	--	--	--
CEM 3	L_α	28.80	5.760	17.30	205
CEM 4	L_α	28.80	7.20	14.40	164
CEM 5	L_α	28.80	10.80	7.20	108

The obtained structural parameters are listed in the Table 3.2. CEM 1 and 2 exhibits the mixed phase and not considered for the calculation of the structural parameters. No change

has been seen in the lattice a_0 with the variation of the concentration from CEM 3 to CEM 5. The bilayer thickness found to be increased with rise in CPC concentration which consequently decreases the thickness of ethylene glycol channel and a_s indicates that at intermediate and higher concentration region large number of amphiphiles self assembled in layered stacking at the expense of solvophobic interactions between solute and solvent and facilitate ordered mesostructure. XRD patterns obtained for the quenched mixtures of CPC: W series are depicted in the figure 3.2(b). Mixtures CWM 1-CWM 5 displayed two diffraction lines corresponding to 2θ = 3.25 and 6.4 were in ratio 1:2 characteristics of lamellar L_α phase. A characteristic peak observed at 2θ = 2.7 for CWM 4 and CWM 5 remains unmatched. The structural parameters obtained using the equations 3.1 to 3.5 for the quenched LLC phases (CPC: W based systems) are listed in the Table 3.3.

Table 3.3: Structural parameters for quenched CPC: W mixtures at 303K

Sample	Phase	a_0(Å)	d_L(Å)	d_{EG}(Å)	a_s(Å)
CWM 1	L_α	27.40	1.37	24.60	864
CWM 2	L_α	27.30	4.09	19.00	289
CWM 3	L_α	27.25	4.45	18.30	266
CWM 4	L_α	27.20	6.80	13.60	174
CWM 5	L_α	27.10	10.1	6.70	115

It was noticed that the lattice parameter a_0 decreased at the expense of the increasing CPC concentration, in similar fashion the thickness of the water channel and the a_s also follow the same behaviour, however the bilayer thickness found to be increased with increasing concentration. These findings hint that with the increment of amphiphilic concentration the aggregation number of the micelles also increased which results the closed packed and highly ordered bilayer structures. Note that bilayer thickness was found very less at lower band of the concentration which may be due to the less aggregates in the solvent rich region results less ordered geometries as also evident from the XRD profiles. Well defined diffraction peaks observed at all concentrations of CFM: F series (CFM 1-CFM 5) hints at the ordering in these systems as evident from the figure 3.2(c). Reflections seen at 2θ= 1.9 and 3.3 at very low concentration (CFM 1) are found in 1: √3 ratio corresponds to the two dimensional hexagonal phase ($2D_H$) similarly strong reflection observed for CFM 2 at 2θ=3.3 was also index with $2D_H$ mesophase though, first reflection was absent in this case. At higher concentrations sample procured the lamellar LLC phase as the diffraction peaks are in 1:2 ratio up to 75wt%. The structural and geometrical parameters for the hexagonal lattice of CFM 1and 2 were computed with an assumption that infinite long cylinder are arranged in two dimensional

hexagonal array using equations 3.1-3.8. The lattice parameter and the different length computed for these systems are given in Table 3.4. We noticed that the lattice parameter and radius of the cylinder increased with rise in the surfactant concentration for hexagonal mesophase in CFM1 and 2. However the radius observed for these mixtures were much less than the total length of the hydrocarbon chain (27Å) indicates that the chains were shrunk in these cylindrical micelles. The thickness of the solvent channel and the a_s decline as the CPC concentration increased. In similar fashion the lattice constant obtained for the Lα phases (CFM 3-5) also shows increase with the variation of concentration and depicts higher thickness of the bilayer at 75wt% concentration. The d_{EG} and a_s were found to be decline at higher Surfactant content as evident from the Table 3.4

Table 3.4: Structural parameters for the quenched CPC: F systems at 303K

Mixtures	Phase	a_0(Å)	d_L(Å)	r_H(Å)	d_{EG}(Å)	a_s(Å)
CFM 1	H_α	53.4	--	10.7	40.00	110
CFM 2	H_α	54	--	18.7	25.00	063
CFM 3	L_α	26.7	5.30	--	16.00	221
CFM 4	L_α	27.1	7.00	--	13.10	169
CFM 5	L_α	27.3	10.23	--	6.840	046

Morphological analysis of various series (CPC: EG, CPC: W and CPC: F) is shown in the figure 3.3(Col. 1corresponds to the CPC: EG series, Col.2 corresponds to the CPC: W series and Col.3 corresponds to the CPC: F series). We noticed well aligned lamellas at CEM 2, 3, 4, however no ordered morphology has been observed at lower and higher region of surfactant concentrations (CEM1 and CEM5) as evident from the figure 3.3 (Col.1). Lack of ordered texture at lower CPC (CEM 1) content and disordered domains appeared at CEM 5 may attributed to the less number of aggregates at the lower concentration and steric hindrance in between the amphiphiles head groups at higher CPC content respectively. Textural variation of CPC: W systems at varying concentration is shown in figure 3.3 (Col.2). Nucleation of small lamellas has been observed in solvent rich regions (CWM 1) which further grow as the concentration reached to the intermediate region (CWM 4). The black region in the textures represents the layer of unbound solvent. The growth mechanism of such phases attributed to the aggregation number which could be quit less at the lower region of the surfactant concentration, however, increment in the CPC concentration raised the

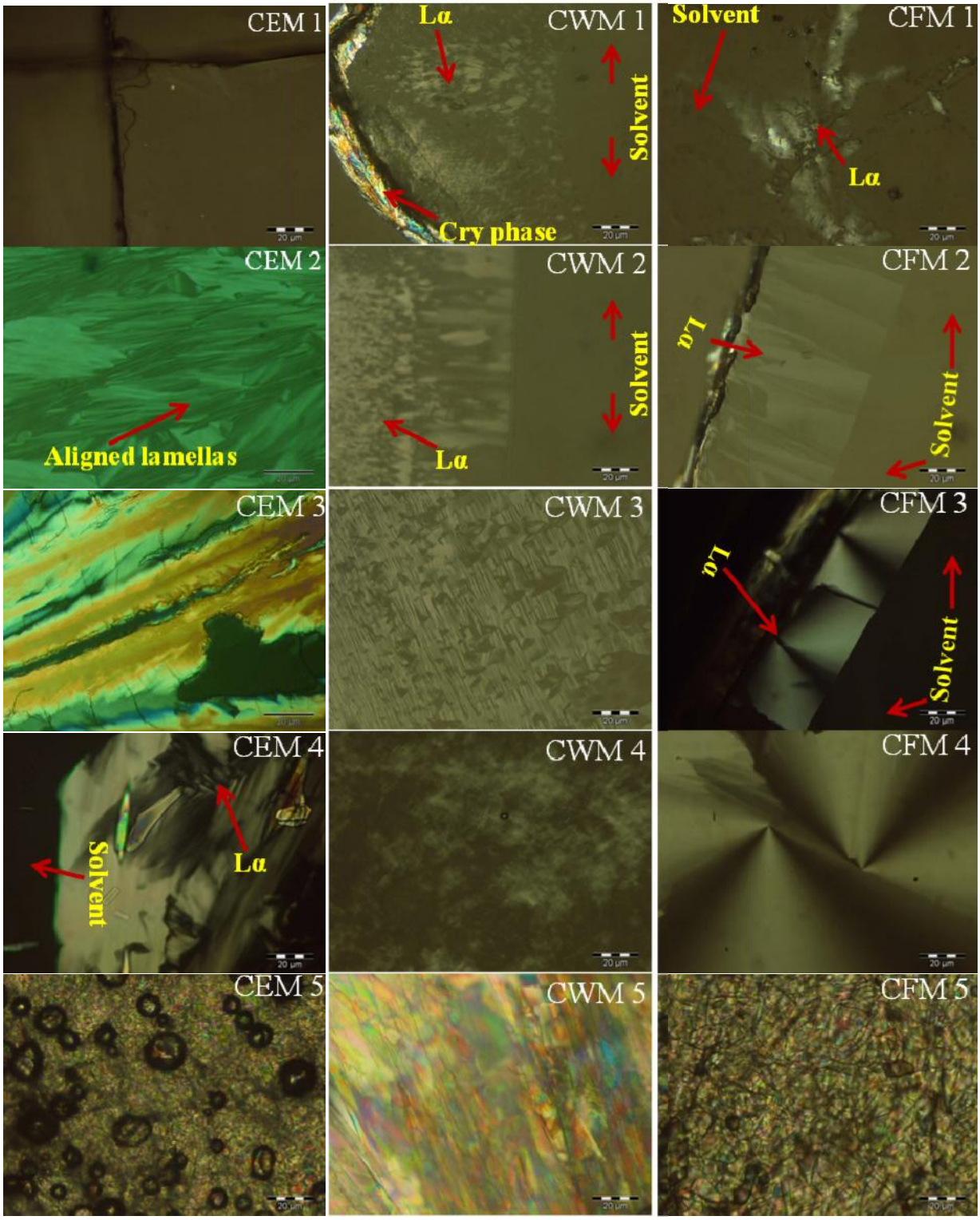

Figure 3.3: Texture patterns of as prepared mixtures at varying concentration (M1=10:90wt%, M2= 30:70wt%, M3= 40:60 wt%, M4= 50:50wt% and M5= 75:25wt% stands for concentration of respective solute : solvent) at 303K (Col.1) cetyl pyridinium chloride: ethylene glycol series (CEM1-5) (Col.2) cetyl pyridinium chloride : water series (CWM1-5) (Col.3) cetyl pyridinium chloride : formamide series (CFM1-5) respectively.

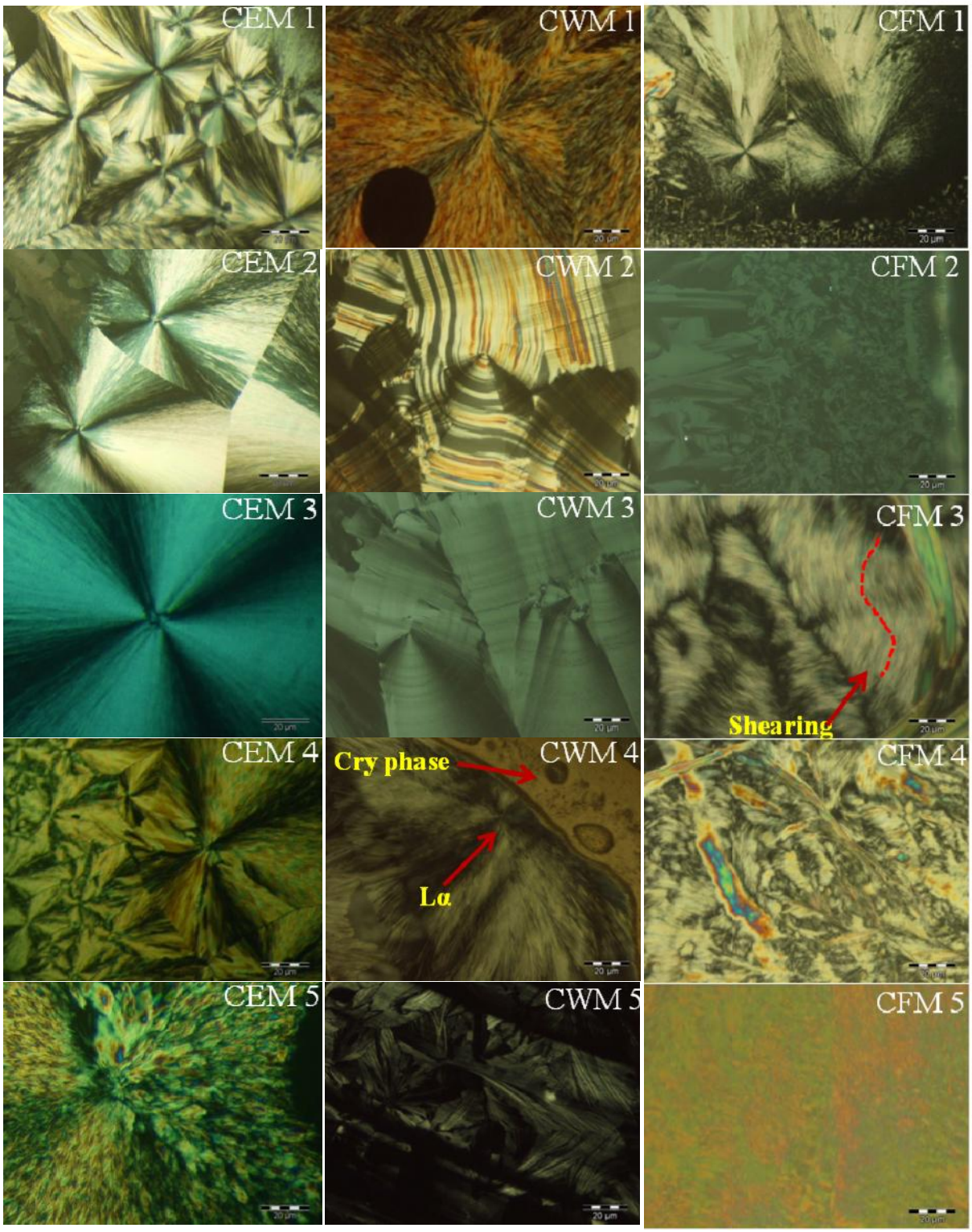

Figure 3.4: Texture patterns of quenched mixtures at varying concentration (M1=10:90wt%, M2= 30:70wt%, M3= 40:60 wt%, M4= 50:50wt% and M5= 75:25wt% stands for concentration of respective solute : solvent) at 303K (Col.1) cetyl pyridinium chloride: ethylene glycol series (CEM1-5) (Col.2) cetyl pyridinium chloride : water series (CWM1-5) (Col.3) cetyl pyridinium chloride : formamide series (CFM1-5) respectively.

aggregation number and hence facilitates the more ordered mesostructure at intermediate concentrations. Crystalline nature of the CWM 5 owes to the less availability of water molecules to prop up the self assembly in the system. Textural variation for as prepared CPC:F series is shown in the figure 3.3 (Col 3). Nucleation of the focal conic domains has been observed at lower concentration region which further fully developed and facilitate the focal conic parabolic defect at 50:50 wt% concentration (CFM 4). However, mixture contains higher surfactant content displayed the birefringent crystalline texture as evident from figure 3.3 (Col.3). Textural variations for the quenched mixtures of various series are presented in the figure 3.4. Col. 1 corresponds to the CPC: EG series, Col.2 corresponds to the CPC: W series and Col.3 corresponds to the CPC: F series). For quenched CPC: EG series at CEM 1(10wt %) we could observe the nucleation of fan like texture. With increasing concentration (30, 40 and 50 wt %) the surfactant molecules could have got assembled in more ordered fashion giving rise to ordered geometry as illustrated in figure 3.4 Col.1 (up to CEM 4). CEM 4 was found most ordered system. However, we observed some distorted morphologies at higher concentrations. On the other hand quenched CPC: W mixture shows well ordered focal conic texture at all concentrations corresponding to the lamellar LLC phase as presented in the figure 3.4 Col.2. Sample procured 30 and 40 wt% concentration exhibit parabolic focal conic defects and helicoids structures. Quenched systems demonstrate the four lobe focal conic defect texture of $2D_H$ mesophase up to 30 wt% concentrations in CPC: F series as shown in the figure 3.4 Col.3, afterwards the sheared defused textures were seen at CFM 3 and CFM 4 stands for the lamellar (Lα) LLC phase. Hexagonal to lamellar phase transition in these systems has also been discussed in the XRD analysis. These structural investigations demonstrate that the CPC amphiphiles show self assembly in as synthesized condition at the expense of varying amphiphilic concentration and the polarity of the solvent, though the quenching has its pronounced effect as these systems result highly ordered geometries in quenched conditions. Solvent with higher polarity gives single and more ordered phases. In most of the cases we observed the lamellar layered ordering in these systems, which attributed to the higher chain length of the CPC amphiphilic molecule. In conclusion polarity of the solvent plays an important role or the self assembly process.

3.1.2: Thermal analysis

The calorimetric profiles of CPC: EG series scanned in the temperature span of 300 - 400K at the rate 2^0/ min are shown in the figure 3.5(a). The sharp and broad transition observed at 360K and 342K corresponding to the melting of the pure surfactant and structural change in

ethylene glycol (melting and boiling points of ethylene glycol are 260 K and 470K respectively). In CEM 1 a broad transition observed at 340K represents the unbinding of the micelles aggregates or structural transformation of EG as this concentration regime was solvent rich (ethylene glycol) and transition temperature is very close to the neat EG transition. The broad transition found at 331, 334, 338, 337K for CEM 2 to CEM 5 represents the phase change in these systems, however, the defuse transition at 360 K refer to the melting of parent amphiphiles. The variation of enthalpy (ΔH) for these mixtures is depicted in the figure 3.5 (b). The continuous variation of ΔH for CEM 1to CEM 4 at transition temperature inferring about the second order phase transition up to 50 wt%, though, discontinuous variation found at transition in higher surfactant concentration represents (CEM 5) first order phase transition. Figure 3.5(c) presents the thermo-optical analysis for all the CPC: EG Mixtures. No optical change has been seen at CEM1 before and after transition, which might be due to the richness of the solvent in this region. At intermediate and higher surfactant concentrations (CEM 2-CEM 5) LLC mixtures depicts deformation and nucleation of LLC phase (In range 335-345K). These results are in well accordance with the thermo dynamical transition and hints that these transitions are liquid crystal to liquid crystal transition (LC-LC). Thermal behaviour of CPC: W and CPC: F series is presented in the figure 3.6 (a-c) and figure 3.7(a-c), and the corresponding thermal parameters are listed in the table 3.4. The transition temperatures obtained for these series found to be decrease with the rise in the amphiphilic concentrations, inferring the disordering in the systems with rise in concentration.

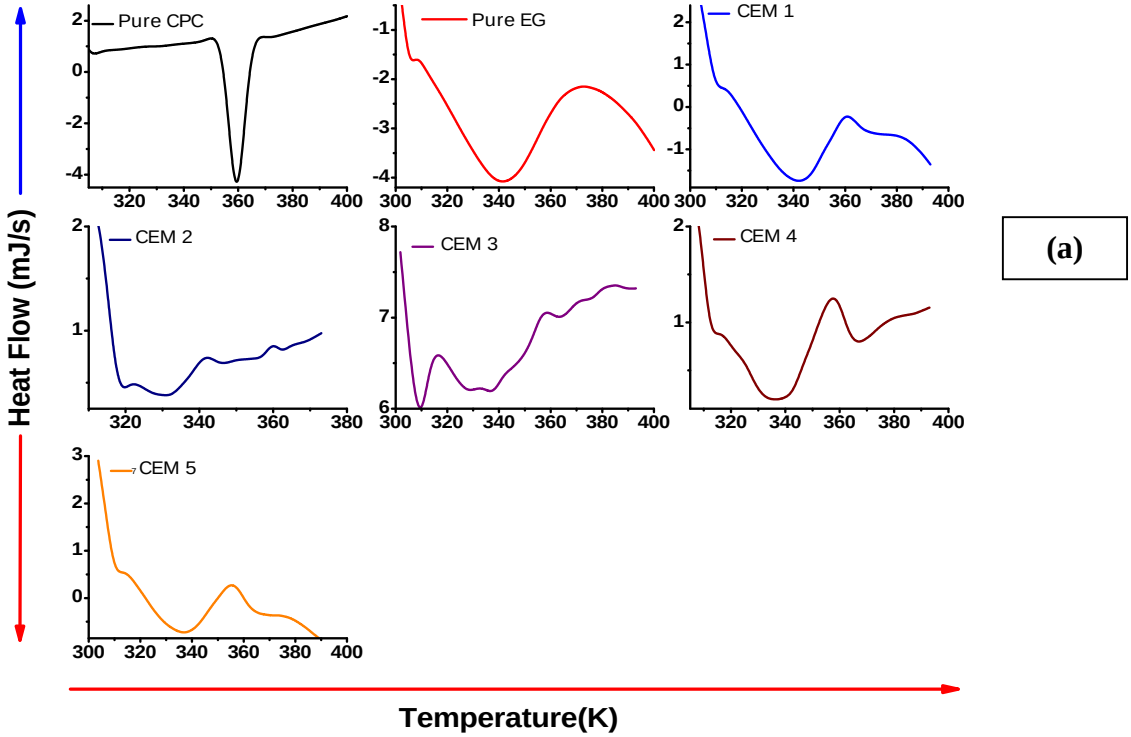

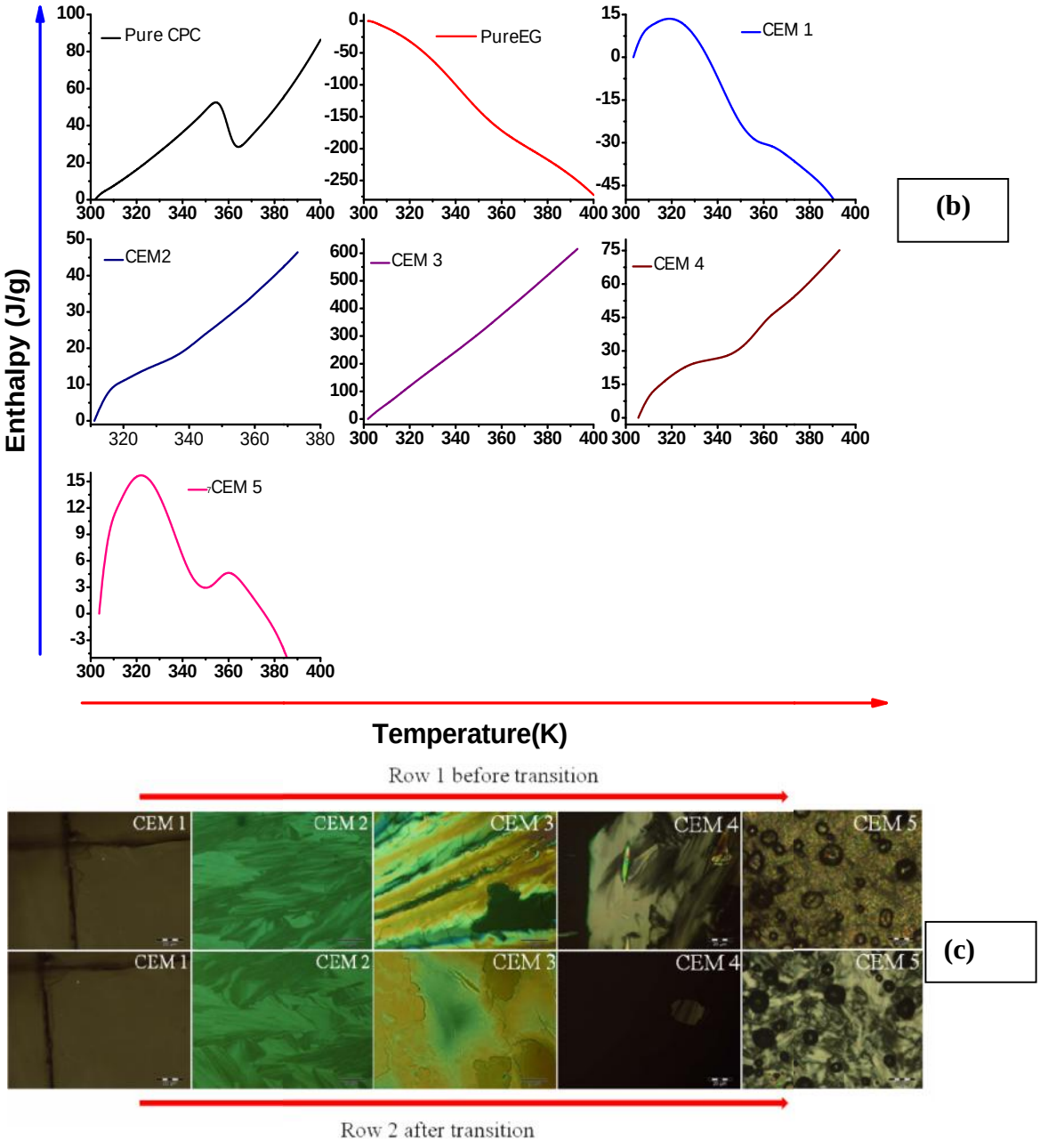

Figure 3.5: Variation of thermo-dynamical parameters for cetyl pyridinium chloride: ethylene glycol (CPC: EG) mixtures (M1=10:90wt%, M2= 30:70wt%, M3= 40:60 wt%, M4= 50:50wt% and M5= 75:25wt% stands for concentration of respective solute: solvent) (a) heat flow (b) enthalpy (c) thermo-optical analysis.

Some peaks seen in the CPC: W series at higher temperature around 360K attributed to the melting of the un-reacted amphiphilic content. The variation of enthalpy for these systems also shows continuous and discontinues variation at the transition temperature. The corresponding orders for the phase transitions are listed in the Table 3.5. All the mixtures of CPC: W series shows 2nd order phase transition at lower and higher amphiphilic content

except CWM 5which exhibit 1st order phase transition. On the other hand all the mixtures of the CPC: F series exhibit 2nd order phase transition at lower and higher amphiphilic

Table 3.5: Thermal parameters for CPC: EG, CPC: W and CPC: F series

Cetylpyridinuium chloride: Ethylene glycol			
Mixtures	**Phase**	**T_C**	**Order**
CEM 1	$2D_H+L_\alpha$	341.00	2^{nd}
CEM 2	$2D_H+L_\alpha$	331.00	2^{nd}
CEM 3	L_α	334.00	2^{nd}
CEM 4	L_α	338.00	2^{nd}
CEM 5	L_α	337.00	2^{nd}
Cetylpyridinuium chloride: Water			
CWM 1	L_α	346.00	2^{nd}
CWM 2	L_α	341.00	2^{nd}
CWM 3	L_α	338.00	2^{nd}
CWM 4	L_α	335.00	2^{nd}
CWM 5	L_α	337.00	1^{st}
Cetylpyridinuium chloride: Formamide			
CFM 1	H_α	343.00	2^{nd}
CFM 2	H_α	343.00	2^{nd}
CFM 3	L_α	343.00	2^{nd}
CFM 4	L_α	340.00	2^{nd}
CFM 5	L_α	331.00	2^{nd}

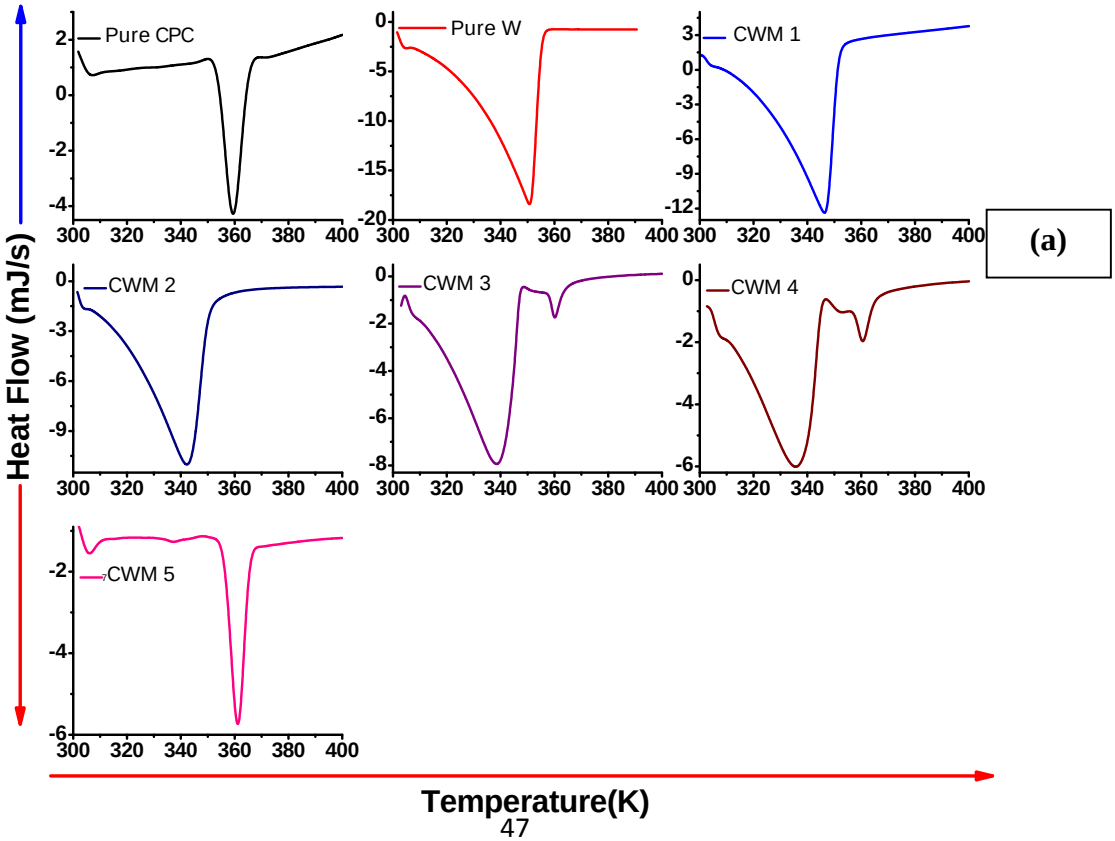

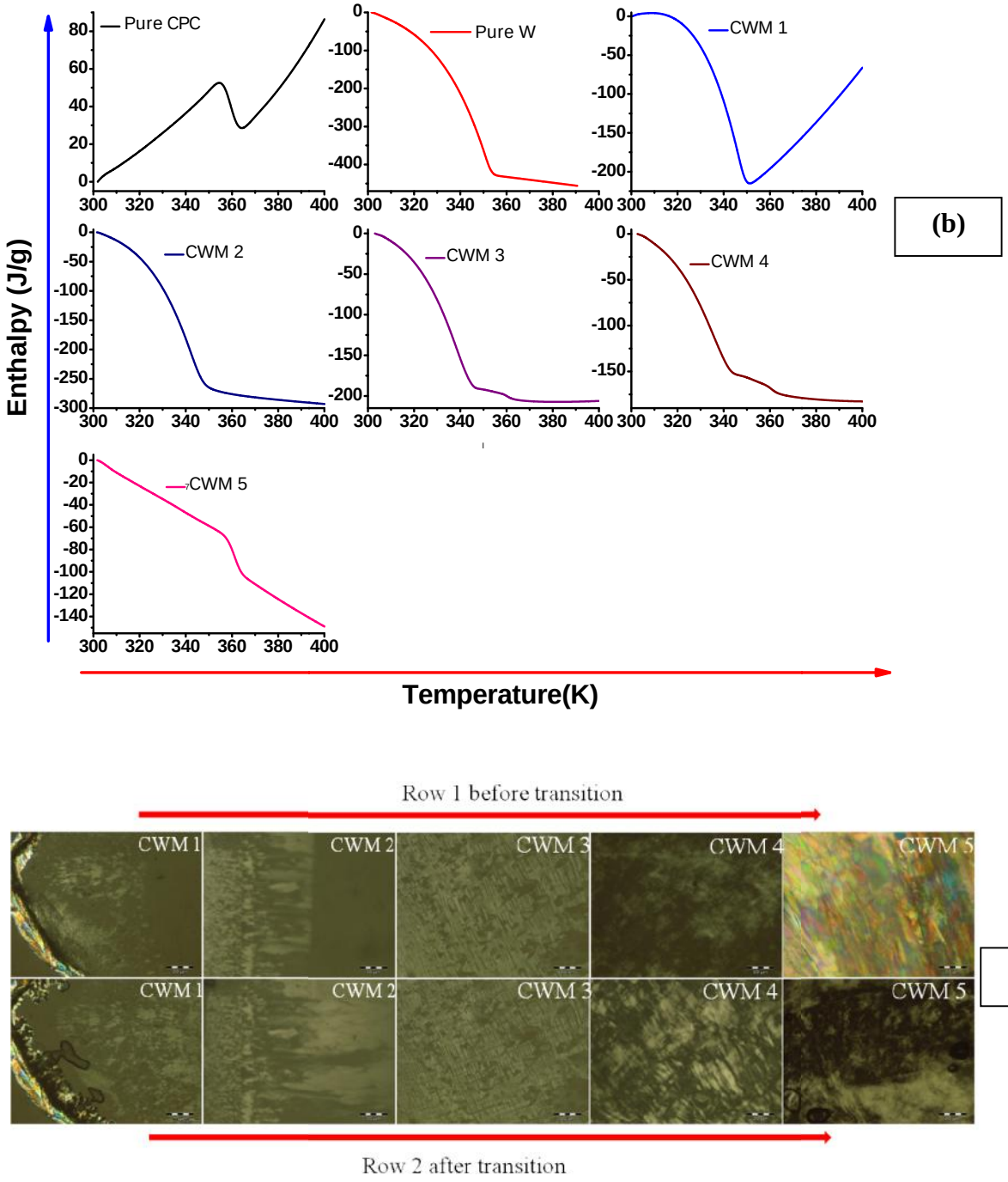

Figure 3.6: Variation of thermo-dynamical parameters for cetyl pyridinium chloride : water (CPC: W) mixtures (M1=10:90wt%, M2= 30:70wt%, M3= 40:60 wt%, M4= 50:50wt% and M5= 75:25wt% stands for concentration of respective solute: solvent) (a) heat flow (b) enthalpy (c) thermo-optical analysis.

concentrations. Thermo optical analysis shown in figure 3.6 (c) and 3.7(c) demonstrates the nucleation of the new phase after transition which, implies that transition observed in the calorimetric studies are liquid crystalline to liquid crystalline transition.

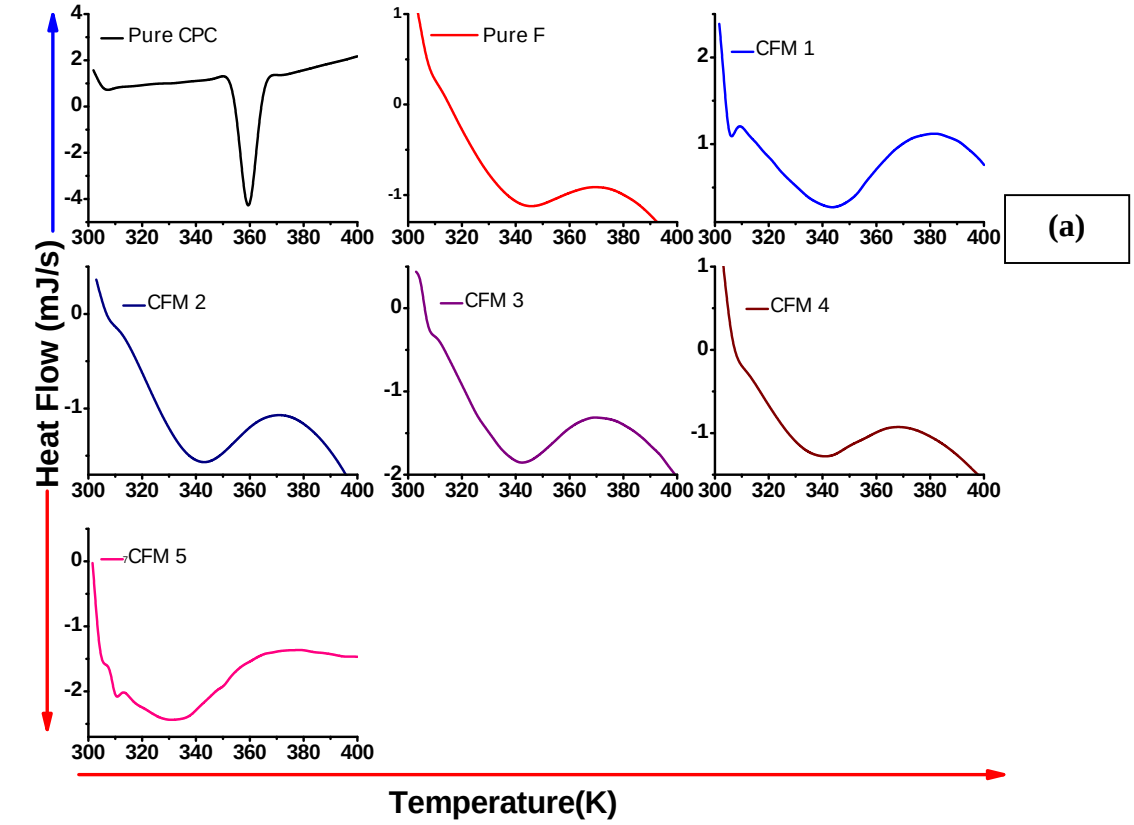

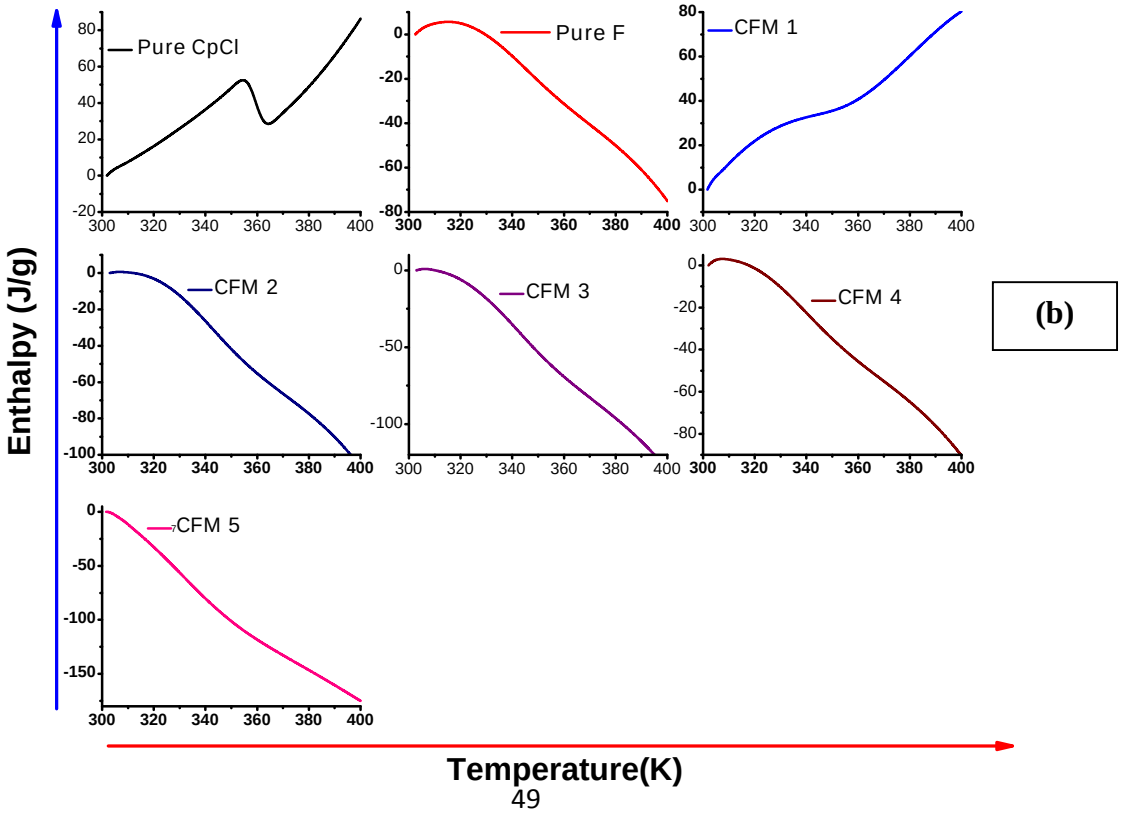

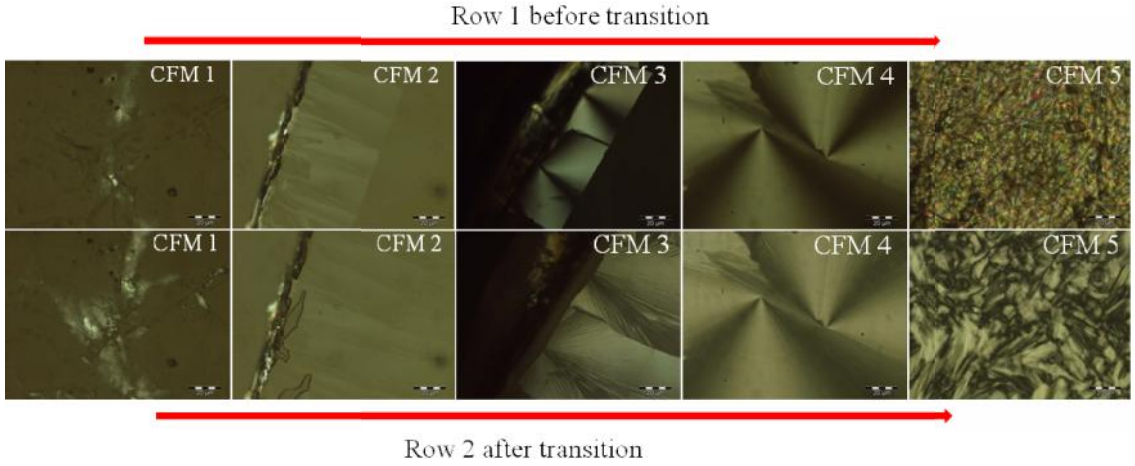

(c)

Figure 3.7: Variation of thermo-dynamical parameters for cetyl pyridinium chloride: formamide CPC: F mixtures (M1=10:90wt%, M2= 30:70wt%, M3= 40:60 wt%, M4= 50:50wt% and M5= 75:25wt% stands for concentration of respective solute: solvent) (a) heat flow (b) enthalpy (c) thermo-optical analysis.

3.1.3: Dielectric Spectroscopy

Structural studies infer that the quenched mixtures exhibit more stable and ordered mesophase than that of as prepared mixture. Among these phases three concentrations (CEM 1, 2 and 4) were selected for the dielectric measurements to get deep insight of the interfacial interactions at the molecular level and their correlation with the structural and thermal properties. The selected LLC mixtures were examined in the wide frequency (50Hz-1MHz) and temperature range (300-380K) to elucidate the stability, interfacial interactions, type of relaxation and the various relaxation parameters. The frequency dependent complex dielectric permittivity (ε´ and ε´´) for CPC: EG, CPC: W and CPC: F series is shown in the figure 3.8 (a-c). In CPC: EG series well defined exponential decay behaviour was seen for the all the mixtures CEM 1, 2 and 4. Dielectric permittivity was found maximum at lower range of the frequency and present large dispersion at the expense of increasing CPC concentration. With the rise in the amphiphilic concentration anomalous behaviour has been noticed for the dielectric permittivity (ε´) as it first decreased and then increased at higher amphiphilic concentrations (CEM 4) in this series. Such behaviour observed for these systems owes to the mixed to single phase transition with the variation of CPC concentration as already discussed in the structural analysis. The corresponding loss factor for these systems was found minimum at low frequency range which further increase with the progression of the frequency and decline to the lower value after reaching the relaxation frequency, however some fluctuation at higher frequency also seen. Whole frequency range divided into the three different processes to explain the obtained behaviour and the role of the different interfacial

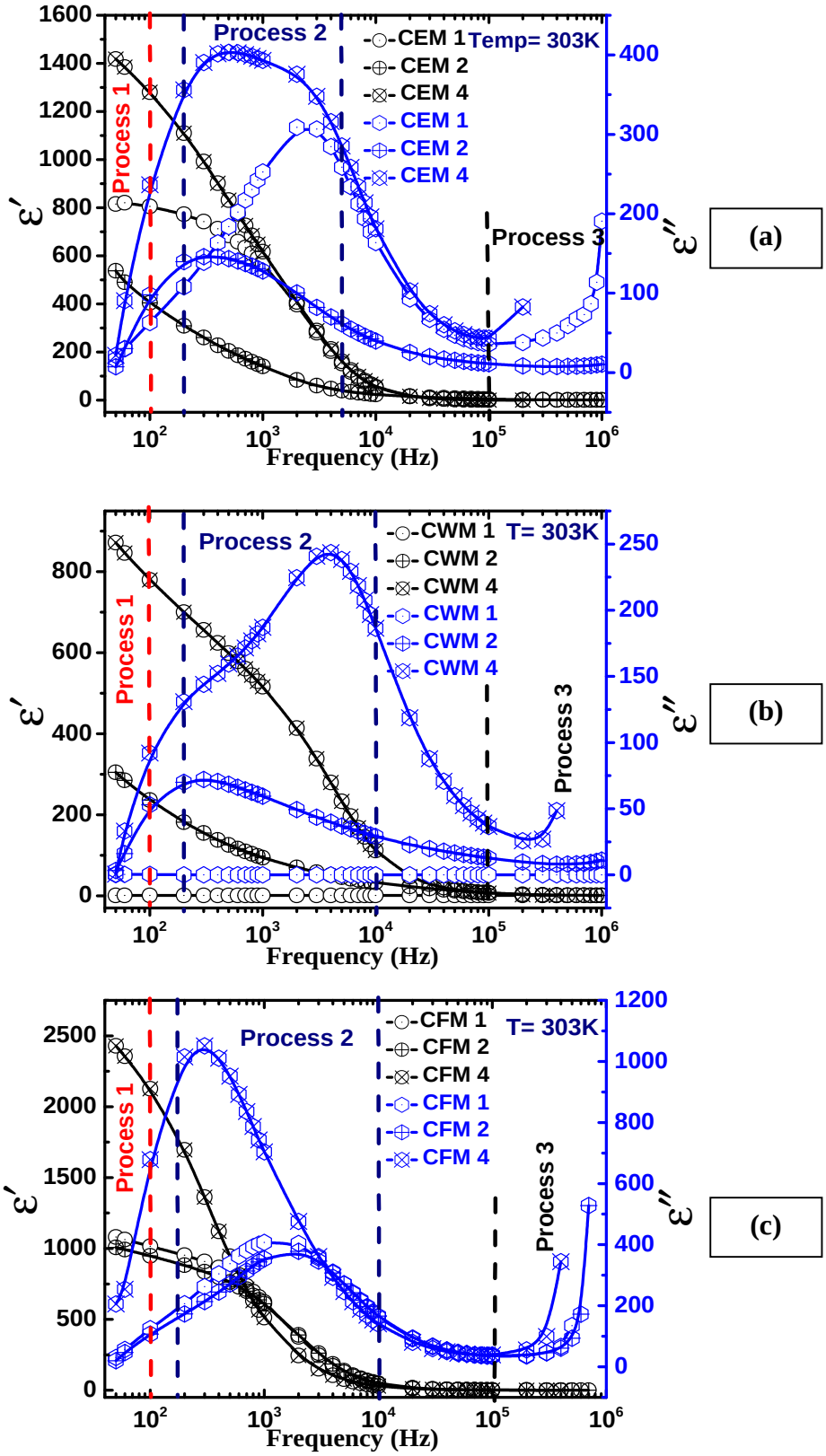

Figure 3.8: Variation of complex permittivity as function of frequency at 303K (a) cetyl pyridinium chloride: ethylene glycol series (b) cetyl pyridinium chloride: water series (c) cetyl pyridinium chloride: formamide series respectively. Where M1=10:90wt%, M2= 30:70wt% and M4= 50:50wt% stands for concentration of respective solute: solvent.

phenomenon responsible for such dielectric behaviour. Process 1 represents the lower frequency region at which LLC phases depicts higher magnitude of the ε´ which arise from the various polarization processes owing to the motion of amphiphilic head group and the counter ion in the charged layer with the application of applied field. Process 2 demonstrates the relaxation behaviour which mainly refers to the relaxation of the counter ion in the charged layer at intermediate frequencies (KHz range). However the third process represents the electronic contribution in the systems and also dangling of the hydrophobic chain of the micelles at higher frequencies. The complex permittivity for CPC: W and CPC: F series is depicted in the figure 3.8 (b-c). We observed the increase in the dielectric permittivity with the variation of amphiphilic concentration in CPC: W series, however the CPC: F series shows the irregular trend (as permittivity is first decreased at CFM 2 and then attained maxima at CFM4). The loss factor for these systems shows the same trend as discussed for the CPC: EG series. Among all series formamide based mixtures display the higher dielectric permittivity reveals that the polarity of the solvent play an important role in the self assembly of these lyotropic systems as well as demonstrates better properties. The schematic for this process is shown in the figure 3.9. Organization of the counter ion in the layer and tangential motion of the counter ion with the application of field is depicted below.

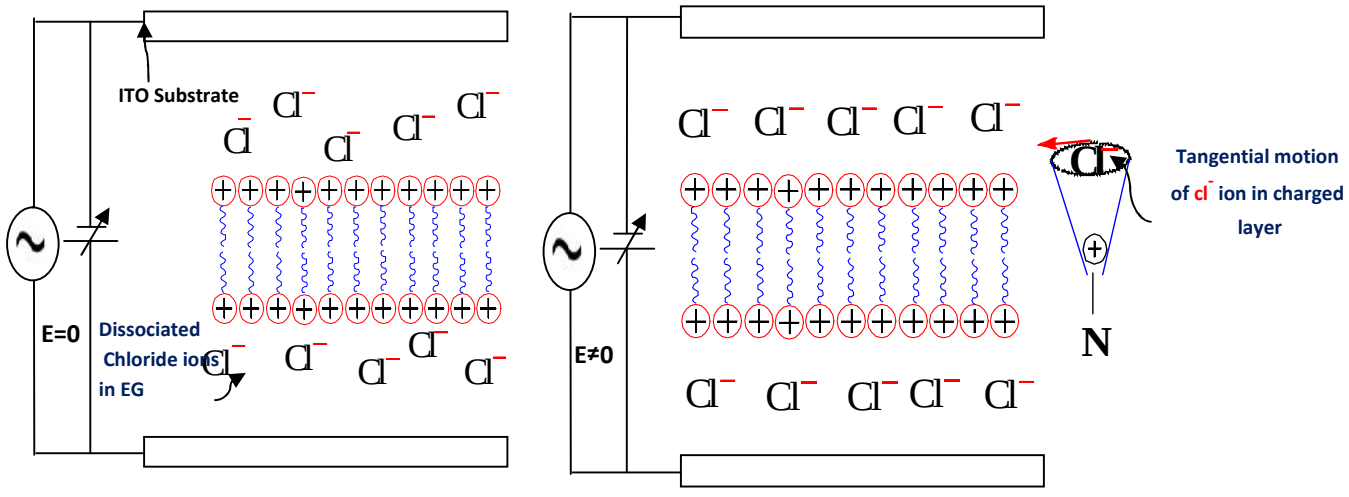

Figure 3.9: Schematic for the dielectric process in lamellar mesophase.

Temperature dependent complex permittivity for these series is shown in the figure 3.10 (Col.1-Col. 3). We observed the increment in the permittivity with the increase in the temperature for all the mixtures in all the series. Such behaviour reveals that these mixtures remain in the liquid crystalline state before and after the transition as described in the thermal

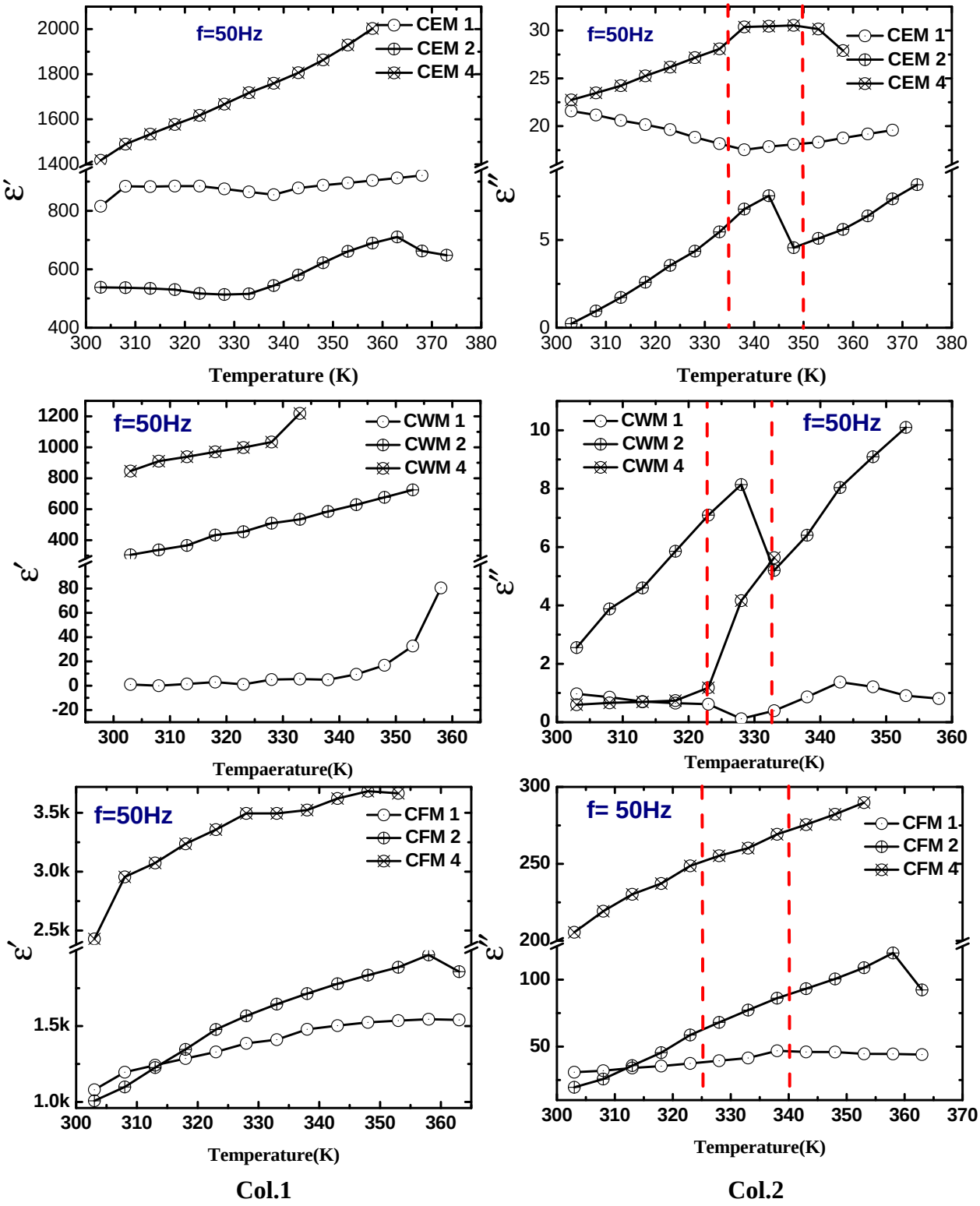

Figure 3.10: Variation of complex permittivity as function of temperature for cetyl pyridinium chloride: ethylene glycol series, cetyl pyridinium chloride: water series and cetyl pyridinium chloride: formamide series respectively (Col.1) real part. (Col.2) imaginary part.

analysis. Variation of loss factor as function of temperature also follows the same trend as discussed for the dielectric permittivity. Various two phase region seen in the loss factor at

the expense of increasing temperature attributed to the structural phase transition in these systems. Single relaxation peak seen in the loss factor at all concentration represents Cole – Cole relaxation process which further confirmed from the semicircle obtained via plotting ε´ vs ε´´. The Cole-Cole plots for all the series are presented in the figure 3.11 (a-c). The obtained semicircle was fitted with the equation 3.9 to obtain the various relaxation parameters.

$$\varepsilon^* = \varepsilon_\infty + \frac{\varepsilon_0 - \varepsilon_\infty}{1+(i\omega\tau)^{1-\alpha}} \qquad (3.9)$$

Where, ε_0 and ε_∞ corresponds to static and high frequency permittivity, τ and α represents relaxation time and the distribution parameter respectively. v and u are two vectors drawn from two points on the semicircle, used to measure the relaxation frequency f_r and relaxation time corresponding to the Cole-Cole relaxation process. The magnitude of *v* and *u* can be computed from

$$v = [(\varepsilon_0 - \varepsilon')^2 + (\varepsilon'')^2]^{1/2} \qquad (3.10)$$

$$u = [(\varepsilon' - \varepsilon_\infty)^2 + (\varepsilon'')^2]^{1/2} \qquad (3.11)$$

A plot of $\log_{10}$ (v/u) versus $\log_{10}$f gives a straight line (graph not shown here). The intercept on abscissa corresponds to the relaxation frequency, whereas, slope gives the magnitude of distribution parameter.

The computed values of relaxation frequency (f_r), relaxation time (τ) and dielectric strength (Δε) are given in Table 3.6.

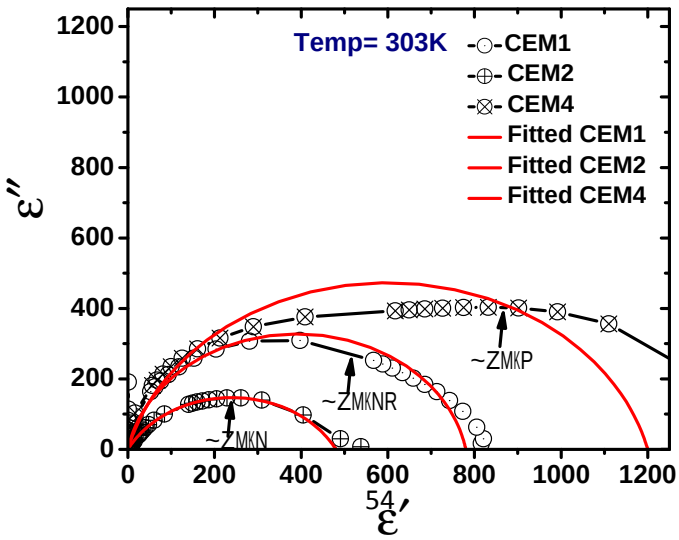

(a)

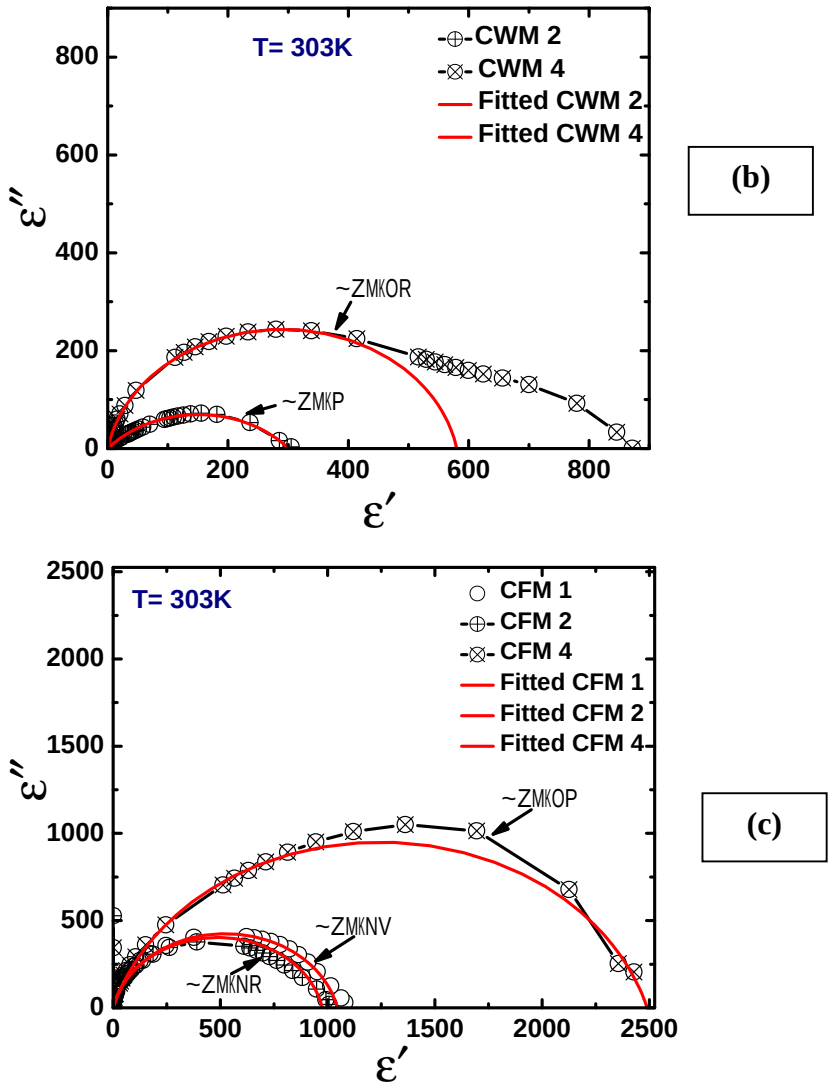

Figure 3.11: Cole-Cole plot at 303K (a) cety pyridinium chloride: ethylene glycol series (b) cetyl pyridinium chloride: water series (c) cetyl pyridinium chloride: formamide series respectively. Where M1=10:90wt%, M2= 30:70wt% and M4= 50:50wt% stands for concentration of respective solute: solvent.

Dielectric strength for these systems found to be increased with rise in the CPC concentration for the CPC: W series, however, it follows the irregular trend in the CPC: EG and CPC: F series. Relaxation frequency for these systems was found higher (around 2-2.4KHz) at lower amphiphilic concentrations in CPC: EG and CPC: F series, while reverse trend was seen in CPC: W series as it depicts higher relaxation frequency at higher concentration (CPW 4). Relaxation time for these systems was found to be very low (in µs); however, magnitude is higher for some cases as evident from the Table 3.6.

Table 3.6: Relaxation parameters for CPC: EG, CPC: W and CPC: F series

Cetylpyridinuium chloride: Ethylene glycol								
Mixtures	**ε′**	**Δε**	**f_r(Hz)**	**τ (μs)**	**Ea**			**n**
					Ist phase	**2nd phase**	**3rd phase**	
CEM 1	0815	0797	2400	066	05.00	03.30	--	1.42
CEM 2	0537	0479	0328	485	58.00	22.20	--	1.43
CEM 3	--	--	--	--	--	--	--	1.44
CEM 4	1418	1414	0481	331	06.00	00.08	--	1.45
CEM 5					--	--		1.46
Cetylpyridinuium chloride: Water								
CWM 1	0001	--	--	--	18.00	147.00	38	1.35
CWM 2	0305	0297	0300	530	36.00	33.00	--	1.38
CWM 3	--	--	--	--	--	--	--	1.40
CWM 4	0871	0558	4000	039	10.80	141.00	--	1.42
CWM 5	--	--	--	--	--	--	--	1.42
Cetylpyridinuium chloride: Formamide								
CFM 1	1080	1014	2000	079	08.00	02.40	--	1.44
CFM 2	1007	0937	2000	079	53.00	17.00	--	1.45
CFM 3	--	--	--	--	--	--	--	1.46
CFM 4	2428	2376	0300	530	07.80	05.00	--	1.47
CFM 5	--	--	--	--	--	--	--	1.46

3.1.4: Activation energy

The Arrhenius plots for the CPC: EG series is shown in the figure 3.12 (a-c). The obtained two phase regions were linearly fitted to compute the amount of the activation energy required for the phase transition. The magnitude of the obtained activation energy of various phases is tabulated in the Table 3.6. We observed that activation energy of all mixtures of

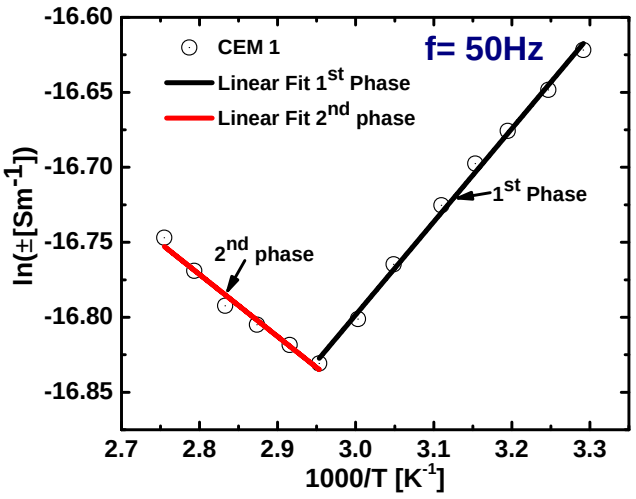

(a)

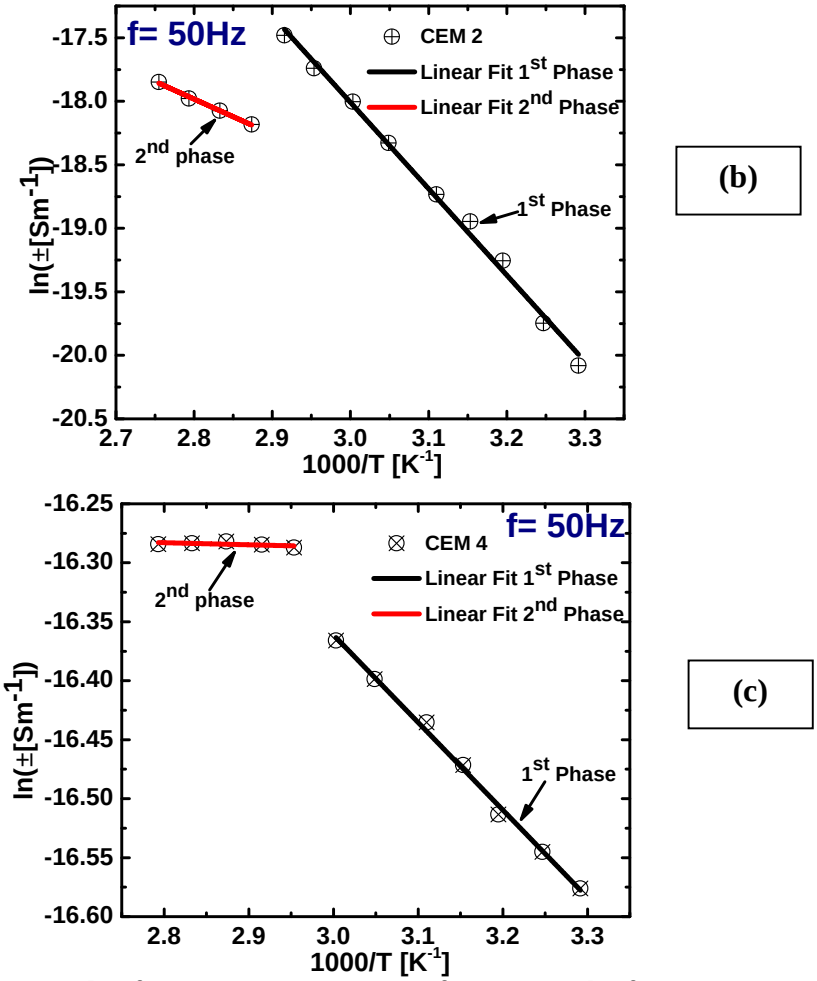

Figure 3.12: Arrhenius plot for CPC: EG series (a) for CEM 1(b) for CEM 2(c) for CEM 4. Where M1=10:90wt%, M2= 30:70wt% and M4= 50:50wt% stands for concentration of respective solute: solvent.

CPC: EG series are higher than that of the second phase, hints at the higher stability of the first phase. In similar fashion the activation energy also calculated for the CPC: W and CPC: F series (graphs not shown here) as listed in the Table 3.6. In the CPC: W series activation energy of the second phase was found prominent than first one, though activation energy calculated for various phases in CPC: F series show some irregular trend.

3.1.5: Refractive index

The refractive index (**n**) of these mixtures was measured using abbey refractrometer and from dielectric calculations via considering the non-interacting nature of the constituent particle which result the direct proportion of n on the $\sqrt{\varepsilon'}$. The magnitude of the refractive index for the various samples of distinct series is given in the Table 3.6. We found that value of **n** increases with the rise in the amphiphilic concentration for all the series except CPC: F

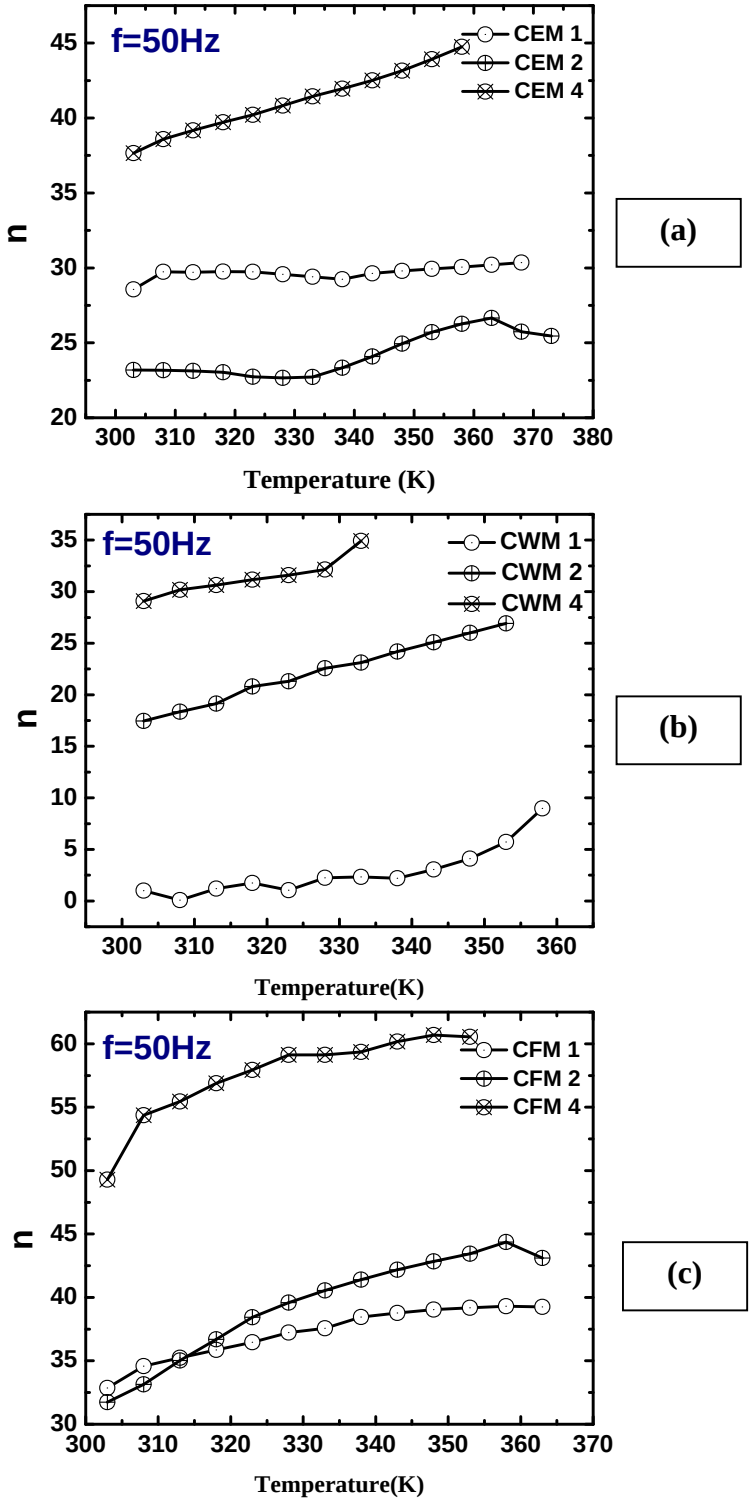

Figure 3.13: Variation of refractive index as a function of temperature (a) cety pyridinium chloride: ethylene glycol series (b) cetyl pyridinium chloride: water series (c) cetyl pyridinium chloride: formamide series respectively. Where M1=10:90wt%, M2= 30:70wt% and M4= 50:50wt% stands for concentration of respective solute: solvent.

which shows decline in refractive index at higher surfactant content. Such behaviour of the refractive index owes to the increase in the viscosity of the systems. Variation of **n** as a function of temperature at fixed frequency (50Hz) is presented in the figure 3.13 (a-c) for all

three series. The refractive index follows the same trend as discussed for the temperature dependent permittivity as it found to be increase with the rise in temperature and show various fluctuation regions as discussed earlier in dielectric behaviour.

3.2: Anionic Surfactant

Anionic surfactants contain sulfate, sulfonate, phosphate and carboxylates anionic functional groups at their head. Sodium dodecyl sulfate (SDS) is an organic compound with the formula CH_3 $(CH_2)_{11}OSO_3Na$. SDS is salt of an organosulfate consisting of a 12-carbon tail attached to a sulfate group; giving the material amphiphilic character facilitates many applications in industrial, chemical and biological fields.

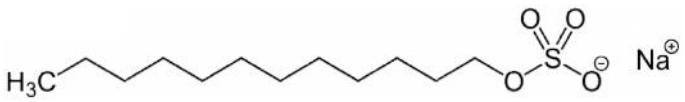

The binary mixtures of sodium dodecyl sulfate and various solvents [ethylene glycol (EG), water (W) and formamide (F)] at varying concentrations 10:90, 30:70, 40:60, 50:50 and 75:25wt% were prepared. They were characterized via X-ray diffraction (XRD), polarizing optical microscopy (POM), differential scanning calorimetry (DSC), dielectric spectroscopy and optical techniques to investigate the development of diverse phase in the varying concentration regime in as prepared and quenched systems and to understand their physical properties at 303K and elevated temperature range of 300-400K. Sodium dodecyl sulfate : ethylene glycol series named as SEM 1[SDS: EG (10:90)], SEM 2[SDS: EG (30:70)], SEM 3[SDS: EG (40:60)], SEM 4[SDS: EG (50:50)] and SEM 5[SDS: EG (75:25)], in similar way sodium dodecyl sulfate : water series designated as SWM 1[SDS: W (10:90)], SWM 2[SDS: W (30:70)], SWM 3[SDS: W (40:60)], SWM 4[SDS: W (50:50)] and SWM 5[SDS: W (75:25)], series of sodium dodecyl sulfate : formamide was denoted as SFM 1[SDS: F (10:90)], SFM 2[SDS: F (30:70)], SFM 3[SDS: F (40:60)], SFM 4[SDS: F (50:50)] and SFM 5[SDS: F (75:25)].

3.2.1: Structural analysis

XRD profiles of as prepared SDS: EG, SDS: W and SDS: F based series are shown in the figure 3.14(a-c). In SDS: EG series at very low concentration (SEM 1), mixture did not direct at any angle in the scanned range inferring about the lack of ordering or miceller phase. Peaks obtained at 2θ= 2.2, 3.7 and 4.4 for SEM 2 and 3 were found in 1:√3:√4 ratio attributed to the two dimensional hexagonal ($2D_H$) mesophase. System procured 50 wt% surfactant

content diffract at 2θ = 1.9, 3.8 corresponds to the lamellar mesophase, although, peaks found at SEM 5 indexed with crystalline phase of neat SDS (2θ = 2.35 and 4.6). All the structural parameters for these systems were computed using equation 3.1-3.8. The structural parameters for these systems are given in the Table 3.7. It was found that in these systems the lattice constant was found to be decreased with the increase in the surfactant concentration. The radius of the cylinder calculated for the SEM 2 and 3 was found just above the fully extended chain length indicating that these phase are distorted and near to the phase

Table 3.7: Structural parameters for as prepared SDS: EG systems

Mixtures	Phase	a_0(Å)	d_L(Å)	r_H(Å)	d_{EG}(Å)	a_s(Å)
SEM 1	L	--	--	--	--	--
SEM 2	H_α	50.00	--	17.30	23.20	40.00
SEM 3	H_α	48.20	--	19.28	17.14	36.00
SEM 4	L_α	46.40	11.60	--	23.20	60.00
SEM 5	Crystal	--	--	--	--	--

transition, the thickness of the solvent channel and a_s shows decrement as we move from SEM 2 to3. Further increase in the concentration give rise to the Lα phase as expected from the dimension of the hexagonal cylinder of SEM 3.On the other hand, lamellar layered mesophase has been seen at the lower concentrations (SWM 1-2) in SDS: W series (as mixture exhibit three diffraction lines at 2θ = 2.2, 4.4 and 6.6 were found in 1:2:3 ratios) as shown in the figure 3.14 (b). Samples procured 40 and 50 wt% (SWM 3 and 4) did not diffract at any angle reflect the lack of liquid crystallinity or miceller phase. Single diffraction peak seen at 2θ =2.35 in SWM 5 corresponding to the crystalline structure of SDS. The geometrical parameters for these systems are tabulated in the Table 3.8. It was noticed that the lattice constant and thickness of water channel computed for these mixtures was decreased with the rise in the SDS concentration, however the thickness of the SDS layer and a_s found to be increased. The magnitude of the bilayer thickness is very less than that of the

Table 3.8: Structural parameters for as prepared SDS: W systems

Mixtures	Phase	a_0(Å)	d_L(Å)	d_W(Å)	a_s(Å)
SWM 1	L_α	40.00	2.00	36.00	35.00
SWM 2	L_α	39.20	5.90	27.40	118.60
SWM 3	No Phase	--	--	--	--
SWM 4	No Phase	--	--	--	--
SWM 5	Crystal	--	--	--	--

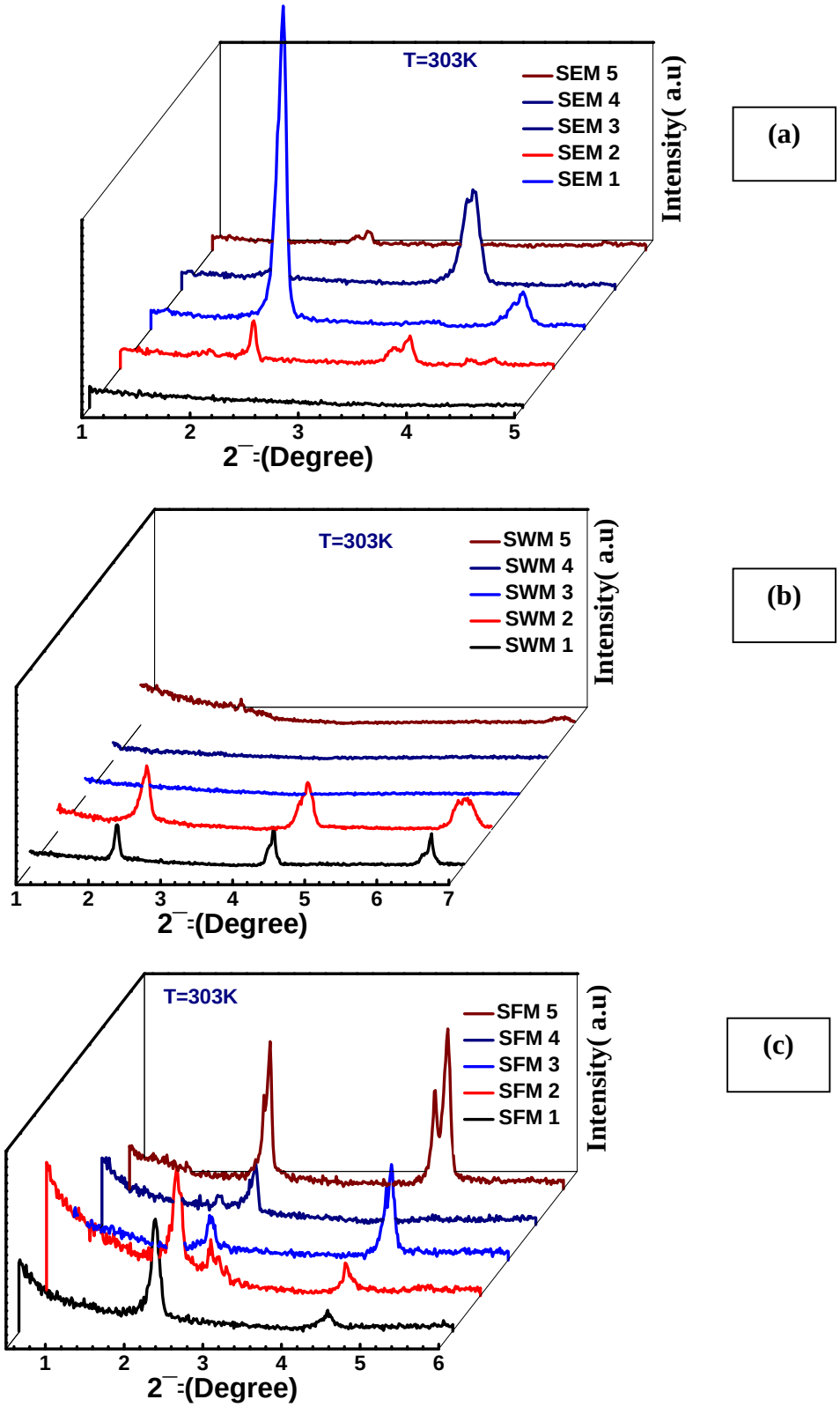

Figure 3.14: XRD profiles of as prepared mixtures at varying concentration (M1=10:90wt%, M2= 30:70wt%, M3= 40:60 wt%, M4= 50:50wt% and M5= 75:25wt% stands for concentration of respective solute : solvent) at 303K (a) sodium dodecyl sulfate : ethylene glycol series (SEM1-5) (b) sodium dodecyl sulfate : water series (SWM1-5) (c) sodium dodecyl sulfate : formamide series (SFM1-5) respectively.

fully extended chain length of the SDS amphiphiles (16.7Å) hints that either these phases are not fully developed or hydrocarbon chains are shrunk in the bilayer structure. Well ordered sharp reflections were seen for all the as prepared mixtures of SDS: F series as shown in the figure 3.14(c). Two sharp lines found at 2θ= 2.2 and 4.4 for SFM 1 to 3 were in 1:2 ratio, a characteristics of lamellar structure. At higher surfactant concentrations peak seen at 50 wt% are in ratio 1:√2 corresponding to bicontinuse LLC phase, though, the systems procured 75wt% surfactant indexed with the neat crystalline phase of SDS (peak at 2θ= 2.35 and 4.6). These systems show some splitting in the XRD peak in some cases corresponds to the secondary reflection or the mixed ordering (if phase not transit completely) in the systems. The structural parameters for these systems are given below in the Table 3.9. We noticed the

Table 3.9: Structural parameters for as prepared SDS: F systems

Mixtures	Phase	a_0(Å)	d_L(Å)	d_F(Å)	a_s(Å)
CFM 1	L_α	39.90	2.00	35.90	350
CFM 2	L_α	40.10	6.00	28.08	116
CFM 3	L_α	40.10	8.00	24.06	087
CFM 4	Crystal	--	--	--	--
CFM 5	Crystal	--	--	--	--

increase in the lattice parameters and bilayer thickness of Lα phase as the concentration increased to the higher extent. Though the thickness of the bilayer is much less than that of the fully extent chain length attributed to the shrinkage of the hydrocarbon chain in the lattice. Thickness of the solvent channel and a_s was found to be decreased as we raised the SDS content.

XRD patterns for the quenched mixtures of various series SDS: EG, SDS: W and SDS: F is shown in the in figure 3.15 (a-c). In SDS: EG series Bragg reflection seen at 2θ = 2.2, 3.67, 4.5 for SEM 1 were found in the ratio 1:√3:√4 corresponding to the two dimensional hexagonal ($2D_H$). We noticed that systems possesses hexagonal symmetry up to 50wt % SDS concentration (SEM 4) as prominent reflections were in the ratio of 1:√3:√4 (2θ = 2.2, 3.73, and 4.5). Mixture contain 75wt% SDS content diffract at 2θ= 2.4 and 4.8 were in ratio 1:2 reflect the lamellar mesophase. It is interesting to note that the 30, 40 and 50 wt% concentration possess hexagonal symmetry in as prepared mixture and under quenching condition which implies that temperature does not affect the ordering in these systems under varying condition and reflects their higher ordering and stability. Various structural parameters computed using equation 3.1 to 3.8 are given in the table 3.10. Lattice parameters

for these systems decreased with the increment of amphiphilic concentration. Further we found that r_H and a_s increases, while, thickness of the ethylene glycol channel decreases. At low concentration (SEM 1), the magnitude of r_H is about half of the fully extended chain length of the SDS molecules ($16.7A^0$) thereby reflecting shrinkage in the chain and hence, densely packed ordered structure. Although, in SEM 2 and SEM, r_H approaches almost the extended chain length, which clearly indicates the increase in the size of micelles,

Table 3.10: Structural parameters for quenched SDS: EG systems

Mixtures	Phase	a_0(Å)	d_L(Å)	r_H(Å)	d_{EG}(Å)	a_s(Å)
SEM 1	H_α	41.00	--	08.20	30.90	4.40
SEM 2	H_α	39.00	--	13.00	18.85	16.10
SEM 3	H_α	38.40	--	15.36	13.00	45.50
SEM 4	H_α	38.00	--	16.10	11.70	21.70
SEM 5	L_α	36.40	13.65	--	09.10	51.00

which probably attributed to the increase in the internal steric repulsion in the amphiphilic head groups at higher concentration and system leads the structural transition. XRD profiles of quenched SDS: W series are shown in the figure 3.15 (b). Four diffused reflections observed in solvent rich region (SWM 1) were index as the characteristic reflection of $2D_H$ LLC phase (2θ=1.3, 2.2, 2.6 and 3.9 are in ratio 1:√3:√4:√7:√9). Similarly five reflection observed at SWM 2 corresponding to 2θ= 2.2, 2.6, 4.5, 5.3 and 6.7 attributed to the $2D_H$. However, amorphous and neat crystalline phases (no diffraction at SWM3 and peak at 2θ= 2.35 corresponds to crystalline SDS at SWM 4 and 5) were found at intermediate and higher concentration range of SDS. Structural parameters for these quenched systems are tabulated in the Table 3.11. These systems exhibit hexagonal ordering at lower concentrations depicts the increment in the lattice constant, r_H and a_s at the expanse of the increasing concentration of

Table 3.11: Structural parameters for quenched SDS: W systems

Mixtures	Phase	a_0(Å)	r_H(Å)	d_W(Å)	a_s(Å)
SWM 1	H_α	39.70	07.94	29.90	44.00
SWM 2	H_α	39.80	13.70	12.40	51.00
SWM 3	No Phase	--	--	--	--
SWM 4	Crystal	--	--	--	--
SWM 5	Crystal	--	--	--	--

SDS. The radius of the cylindrical micelles at lower concentration is about half of the fully extended length of the hydrocarbon chain inferring the close packing of the amphiphiles and shrinkage in the hydrocarbon chain. However, further increment in the amphiphilic concentration, increased the radius of the cylinder which may be due to the increase in the size of the micelles at expanse of increasing steric hindrance in the head group of the amphiphiles. Thickness of the solvent layer found to be decreased as the concentration increased.

XRD profiles for the quenched SDS: F series are presented in the figure 3.15 (c). Diffused reflection obtained at 2θ= 1.6 and 2.75 for SFM 1 and 2θ= 1 and 1.7 for SFM 2 were found in1:√3 ratio attributed to the two dimensional hexagonal lyotropic mesophase. Three diffraction lines observed at 40 wt % (SFM 3) were in ratio 1:√9:√12 characteristics of $2D_H$ LLC phase. However, at higher concentrations systems exhibit bicontinuse ordering as the four reflection obtained in the diffraction patterns are in ratio of 1:√6:√8:√10 (2θ= 0.9,2.3,2.4,2.8) and 1:√4:√5:√6 (2θ= 1.1,2.2,2.4,2.7) at 50 and 75wt% (SFM 4-5) respectively. One characteristic reflection seen at 2θ =4.6 for 50wt% indexed as reflection of crystalline SDS. The geometrical parameters for these systems are given in the Table 3.12. In quenched mixtures lattice parameters and radius of the cylinder show the increment with the rise in SDS content. As the concentration reached to the 30wt% the radius of the cylindrical micelles approach the length of the fully extended hydrocarbon chain of the SDS amphiphiles which cause the structural transition in these systems at higher concentration as evident from the XRD profiles. Thickness of the formamide channel and the a_s found to be decreased at the expanse of increasing SDS concentration.

Table 3.12: Structural parameters for quenched SDS: F systems

Mixtures	Phase	a_0(Å)	r_H(Å)	d_F(Å)	a_s(Å)
CFM 1	H_α	32.40	06.50	24.40	100.00
CFM 2	H_α	45.00	15.50	21.00	45.00
CFM 3	H_α	41.20	16.40	07.40	42.00
CFM 4	Bi	--	--	--	--
CFM 5	Bi	--	--	--	--

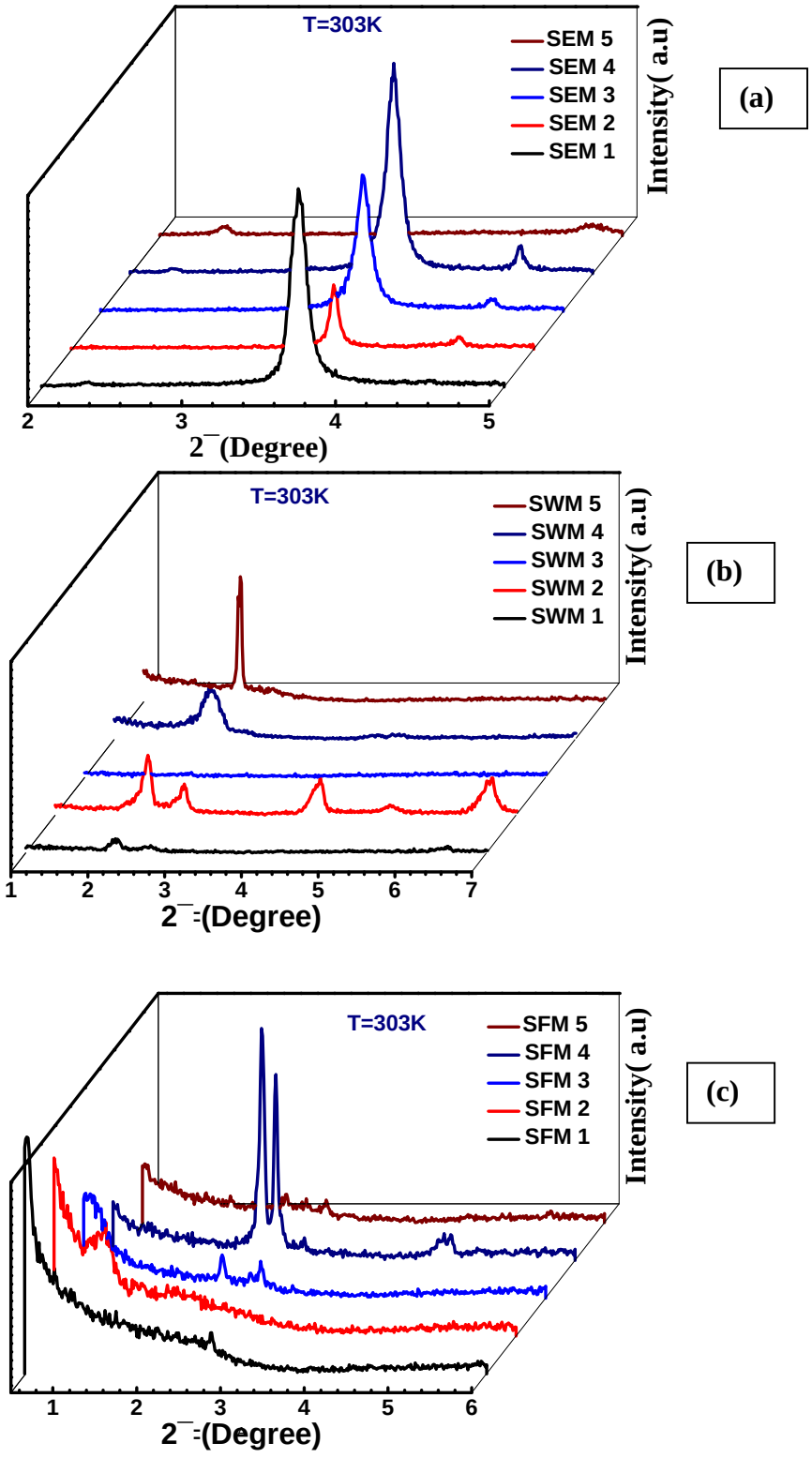

Figure 3.15: XRD profiles of quenched mixtures at varying concentration (M1=10:90wt%, M2= 30:70wt%, M3= 40:60 wt%, M4= 50:50wt% and M5= 75:25wt% stands for concentration of respective solute : solvent) at 303K (a) sodium dodecyl sulfate : ethylene glycol series (SEM1-5) (b) sodium dodecyl sulfate : water series (SWM1-5) (c) sodium dodecyl sulfate : formamide series (SFM1-5) respectively.

Texture patterns for the as prepared mixtures of various series are shown in the figure 3.16 (Col. 1 for SDS: EG, Col.2 for SDS: W and Col.3 for SDS: F). Growth of tiny needle like domains has been observed at very low concentration (SEM 1) in the isotopic media of the ethylene glycol in the SDS: EG series. However, diffused textures were seen at rest of the concentrations as evident from the figure 3.16 (Col.1). Well aligned lamellas were seen at SWM 1 represent the layered lamellar mesophase as evident from the figure 3.16 (Col.2). Coaxial droplet morphology has been seen at 40 and 50 wt% concentrations (SWM 3 and 4) representing the lamellar ordering, while, solid crystal like flakes were observed at higher SDS content (SWM5). Textural behaviour of SDS: F based as prepared mixtures is shown in figure 3.16 Col. 3. No definite morphology has been seen at very low concentration (SFM 1), however, at intermediate concentration region (SFM 2 and 3) growth of well aligned lamellas has been observed reflects the presence of layered ordering in these systems along with the black isotropic solvent pool. However, SFM 4 and 5 did not depict any ordered texture.

The textural variation for the quenched mixtures for three series are presented in the figure 3.17(Col. 1 for SDS: EG, Col.2 for SDS: W and Col.3 for SDS: F). Quenched mixtures show the characteristic texture of hexagonal mesophase up to SEM 4 in the SDS: EG series as evident from the figure 3.17 Col.1. While texture appeared at 75 wt% (SEM 5) represents the lamellar LLC phase. In SDS: W series focal conic domains were observed at 10 and 30 wt% concentration matched with the hexagonal mesophase. Flakes like birefergent domains seen at SWM 3 to 5 may correspond to LLC mesophase or crystalline phase as evident from the figure 3.17 Col.2. Well ordered four lobe focal conic domains found up to 40 wt% concentration in SDS: F series attributed to the $2D_H$ lyotropic mesophase as shown in the 3.17 Col.3. However the mesh texture and oily streaks have been observed for SFM 4 and 5 respectively. From above structural measurements it could be concluded that the non-aqueous present more salvation to the SDS amphiphiles as we observed more ordered structures in non –aqueous media than that of aqueous. Most of the cases we observed the hexagonal ordering in these systems which attributed to the lower chain length of the SDS amphiphiles. Quenched systems were found more ordered than that of the as prepared.

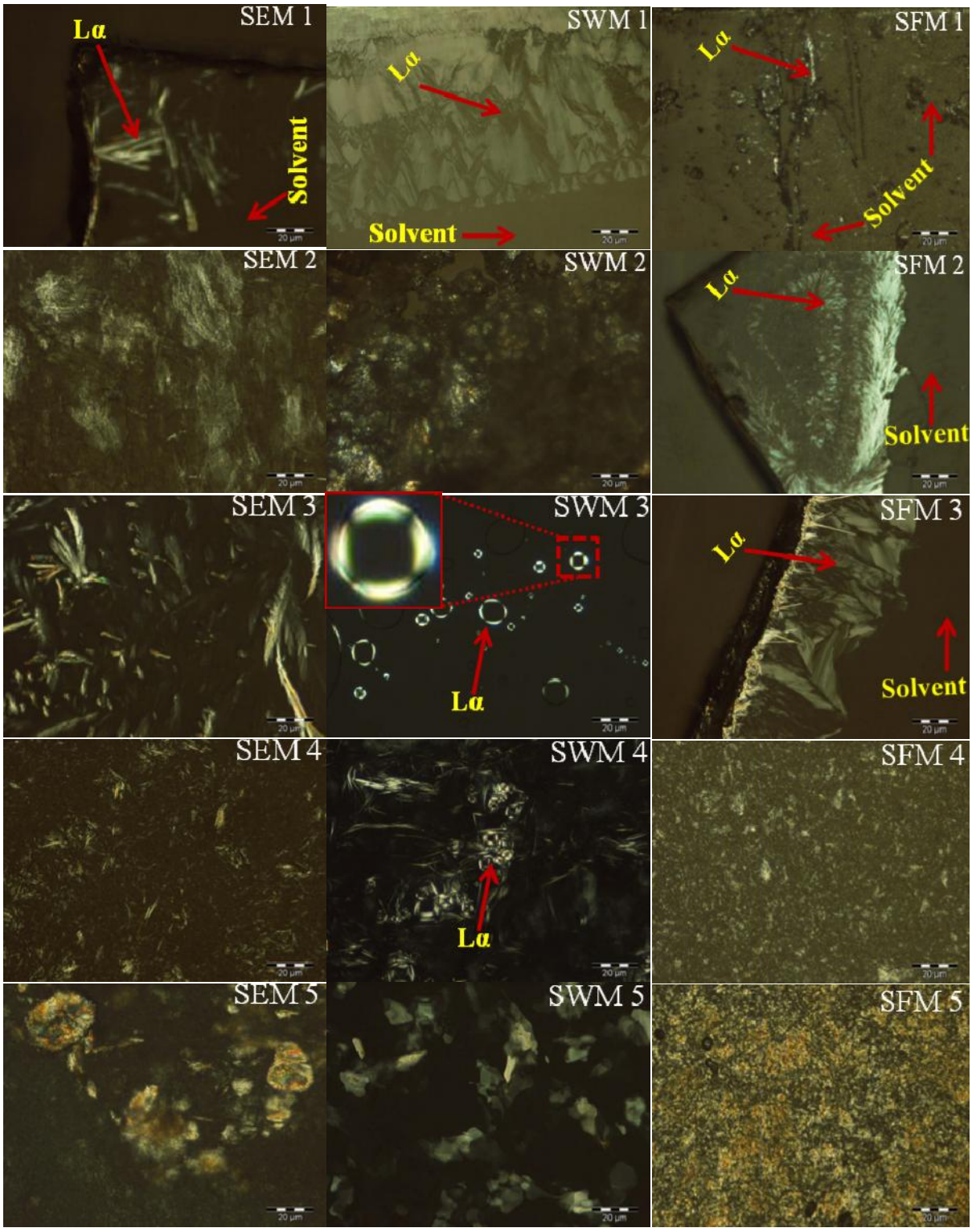

Col.1 **Col.2** **Col.3**

Figure 3.16: Texture patterns of as prepared mixtures at varying concentration (M1=10:90wt%, M2= 30:70wt%, M3= 40:60 wt%, M4= 50:50wt% and M5= 75:25wt% stands for concentration of respective solute : solvent) at 303K (Col.1) sodium dodecyl sulfate : ethylene glycol series (SEM1-5) (Col.2) sodium dodecyl sulfate : water series (SWM1-5) (Col.3) sodium dodecyl sulfate : formamide series (SFM1-5) respectively.

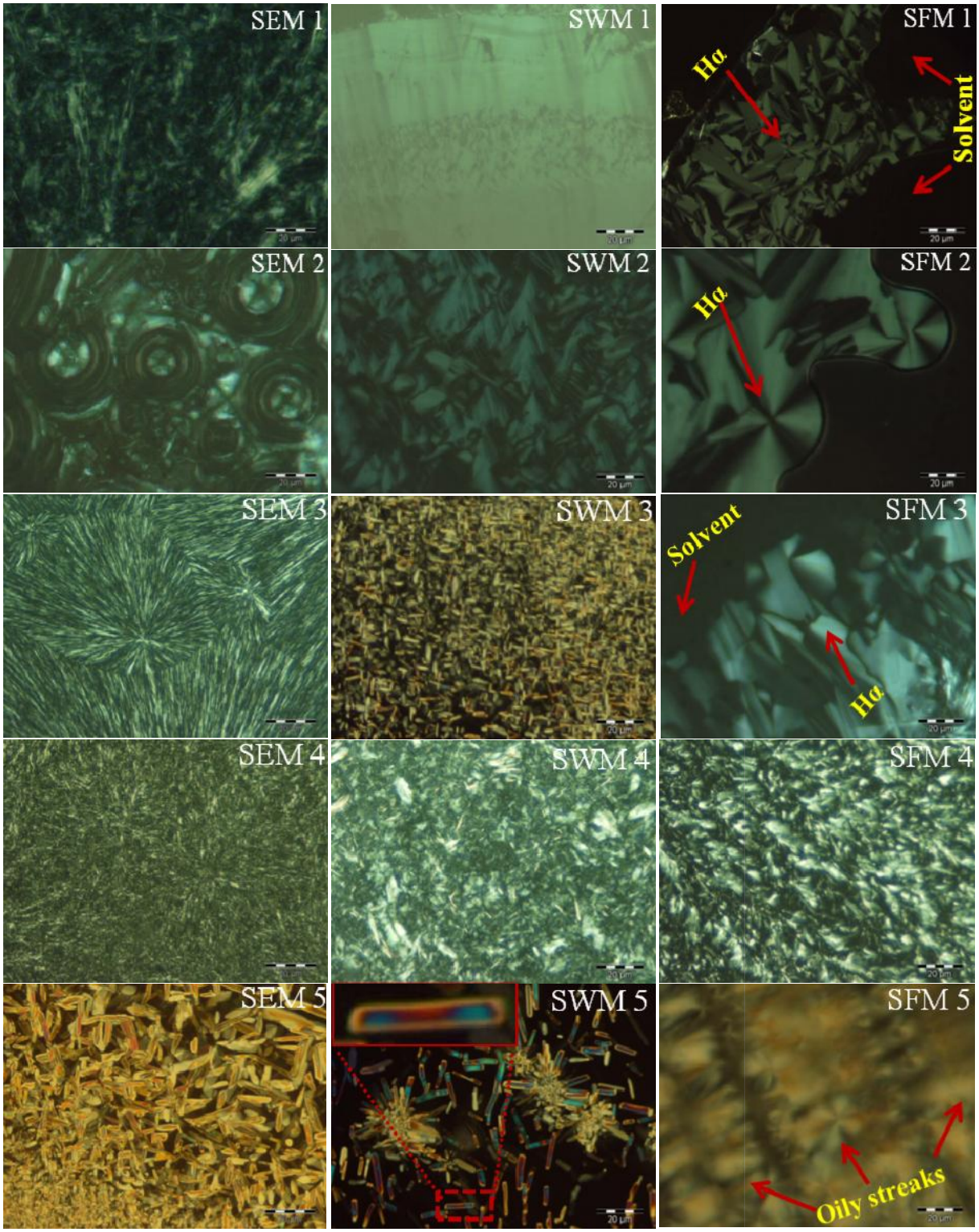

Figure 3.17: Texture patterns of quenched mixtures at varying concentration (M1=10:90wt%, M2= 30:70wt%, M3= 40:60 wt%, M4= 50:50wt% and M5= 75:25wt% stands for concentration of respective solute : solvent) at 303K (Col.1) sodium dodecyl sulfate : ethylene glycol series (SEM1-5) (Col.2) sodium dodecyl sulfate : water series (SWM1-5) (Col.3) sodium dodecyl sulfate : formamide series (SFM1-5) respectively.

3.2.2: Thermal analysis

DSC profiles of as pure SDS, ethylene glycol and SDS: EG series are shown in the figure 3.18 (a). Single transition were observed for the neat SDS and EG at 380 and 342 K representing the structural transition in the precursor materials as their melting points (SDS for 479K and M.P and B.P of EG are 260 K and 470K respectively) are much different than that of these transitions. Single transition peak was seen for the SEM 1, 3 and 5 at 340, 317 and 332K respectively, however SEM 2 and SEM 4 display two calorimetric transition at lower (334 and 333K) and higher temperature range (364 and 384K). The first transition observed for these systems may correspond to the LC to LC phase transition and the second hints at the melting of un reacted SDS. Further to ascertain the order of the phase transition the variation enthalpy for SEM 1-SEM 5 is presented in the figure 3.18 (b). It was found that the pure SDS, ethylene glycol and the SEM 1, 2 and 4 showed the exothermic nature, however, the SEM 3 and 5 exhibits the endothermic nature. It was noticed that the variation of the ΔH was discontinues at the transition of pure SDS and second peak observed for the mixture 3 and 5, demonstrates the first order transition in these systems. However, the single peak observed in the lower temperature zone showed continuous variation of the enthalpy at transition hints at the second order phase transition. These orders of these transitions give an idea about the structural transition (LC to LC) and nucleation of new lyotropic phases. The thermo-optical analysis of these mixtures gives more close insight to identify the nucleation LLC phase before and after the transition on the basses of textural morphologies as shown in the figure 3.18(c). We noticed nucleation of new LLC phases for SEM 2- 4after transition as evident from the textures shown in the figure 3.18(c). Focal conic texture noticed at SEM 2 and 3 indexed as characteristic texture of hexagonal mesophase. These findings hint at the higher ordering in quenched systems because in as prepared systems ordered phase developed at higher temperature when quenched to the room temperature systems acquired same ordering of the LC domains and hence results highly ordered phase at room temperature. Similarly the thermo-dynamical parameters obtained for the SDS: W and SDS: F series are shown in the figure 3.19 (a-c) and 3.20 (a-c). Computed value of T_c and corresponding phase transitions obtained for these systems is tabulated in the Table 3.13. For SDS:W series the first transition occurred at 345, 326,325,331 and 328 K may corresponds to the liquid crystalline to liquid crystalline transitions, however, second transition (364 and 371 K) observed at higher concentration corresponds to the melting of the amphiphilic chains. The first transition observed for these systems demonstrates the 2^{nd} order phase transition;

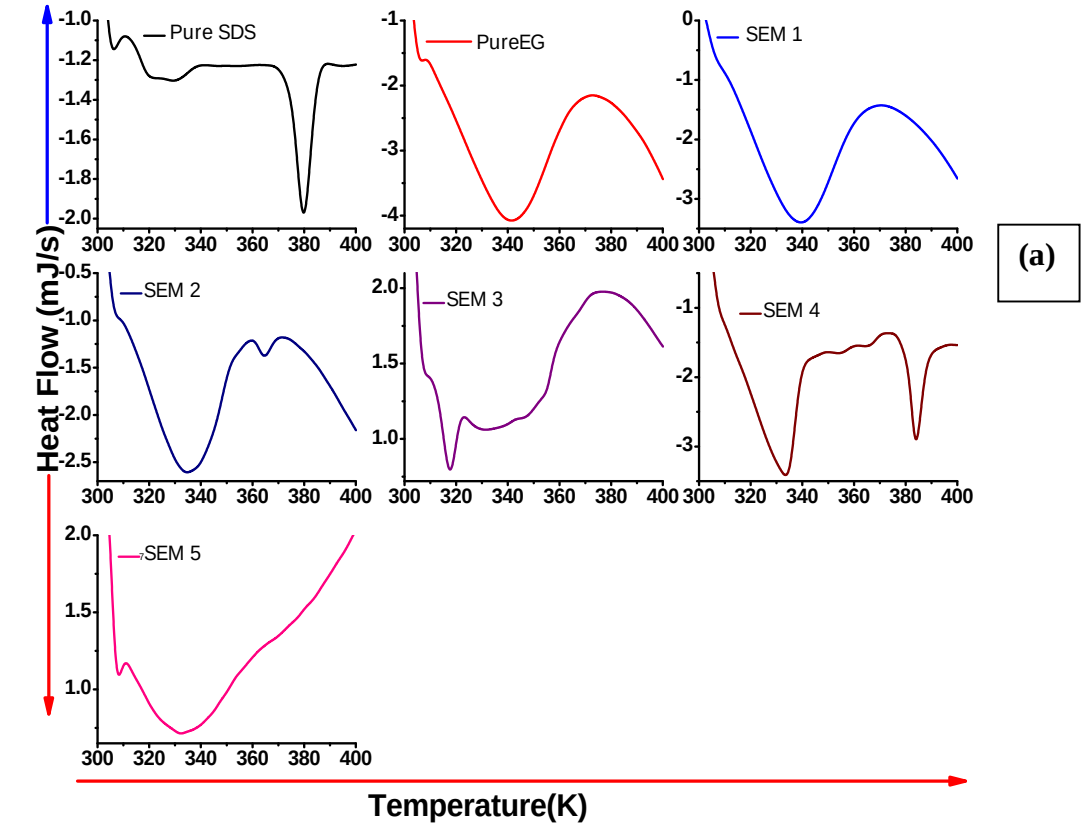
Pure SDS
PureEG
SEM 1
SEM 2
SEM 3
SEM 4
SEM 5
Heat Flow (mJ/s)
Temperature(K)

(a)

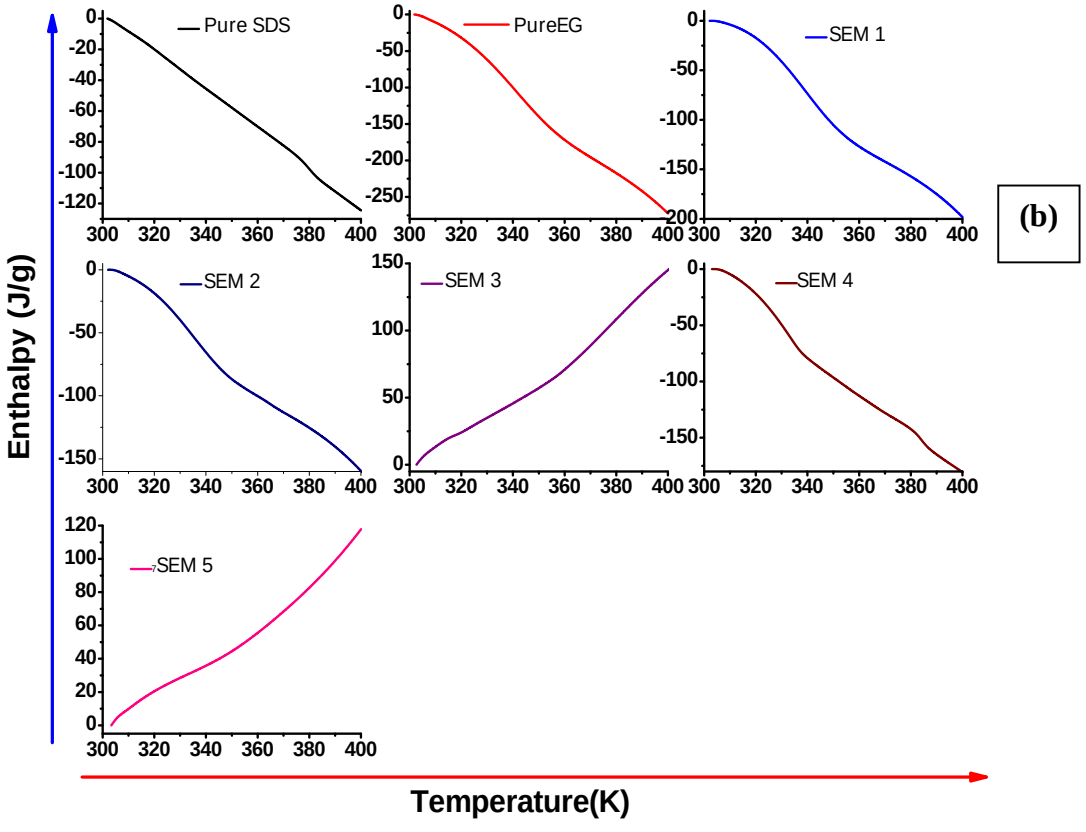
Pure SDS
PureEG
SEM 1
SEM 2
SEM 3
SEM 4
SEM 5
Enthalpy (J/g)
Temperature(K)

(b)

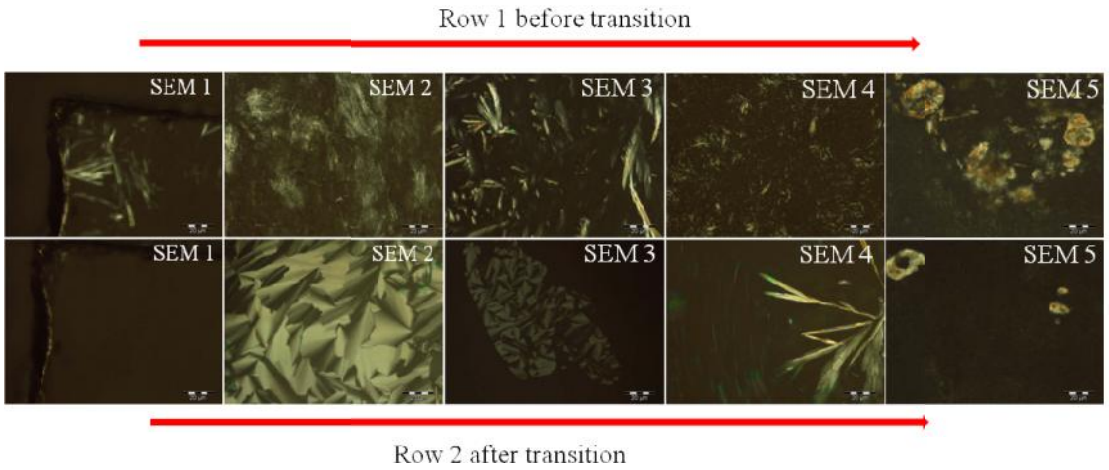

(c)

Figure 3.18: Variation of thermo-dynamical parameters for sodium dodecyl sulfate: ethylene glycol (SDS: EG) mixtures (M1=10:90wt%, M2= 30:70wt%, M3= 40:60 wt%, M4= 50:50wt% and M5= 75:25wt% stands for concentration of respective solute: solvent) (a) heat flow (b) enthalpy (c) thermo-optical analysis.

Table 3.13: Thermal parameters for SDS: EG, SDS: W and SDS: F series

Sodium dodecyl sulphate: Ethylene glycol					
Mixtures	**Phase**	**T_C**		**Order**	
		1st peak	**2nd peak**	**1st peak**	**2nd peak**
SEM 1	H_α	340.00		2nd	
SEM 2	H_α	334.00	364.00	2nd	1st
SEM 3	H_α	317.00		2nd,	
SEM 4	H_α	333.00 384.00		2nd	1st
SEM 5	L_α	332.00		1st	
Sodium dodecyl sulphate : Water					
SWM 1	H_α	345.00		2nd	
SWM 2	H_α	326.00	371.00	2nd	1st
SWM 3	No Phase	325.00		2nd,	
SWM 4	Cry	331 .00	364.00	2nd	1st
SWM 5	Cry	328.00		1st	
Sodium dodecyl sulphate : Formamide					
SFM 1	H_α	342.00		2nd	
SFM 2	H_α	341.00		2nd	
SFM 3	H_α	341.00		2nd	
SFM 4	Bi	337.00		2nd	
SFM 5	Bi	322.00	344.00	2nd	

however the 2nd transition represents the first order phase transition. The thermo-optical analysis of these systems also hints at the nucleation of new phase and LC to LC transition in

these systems. In SDS:F based series SFM 1-3 depicts the single transition peak at 342, 341 and 341K respectively, however, at higher SDS concentration two peaks are found for SFM 4 and 5 at 321, 337K , 322 and 340K respectively. Small shift in transition temperature towards lower side have been seen with the increment in the SDS concentration.

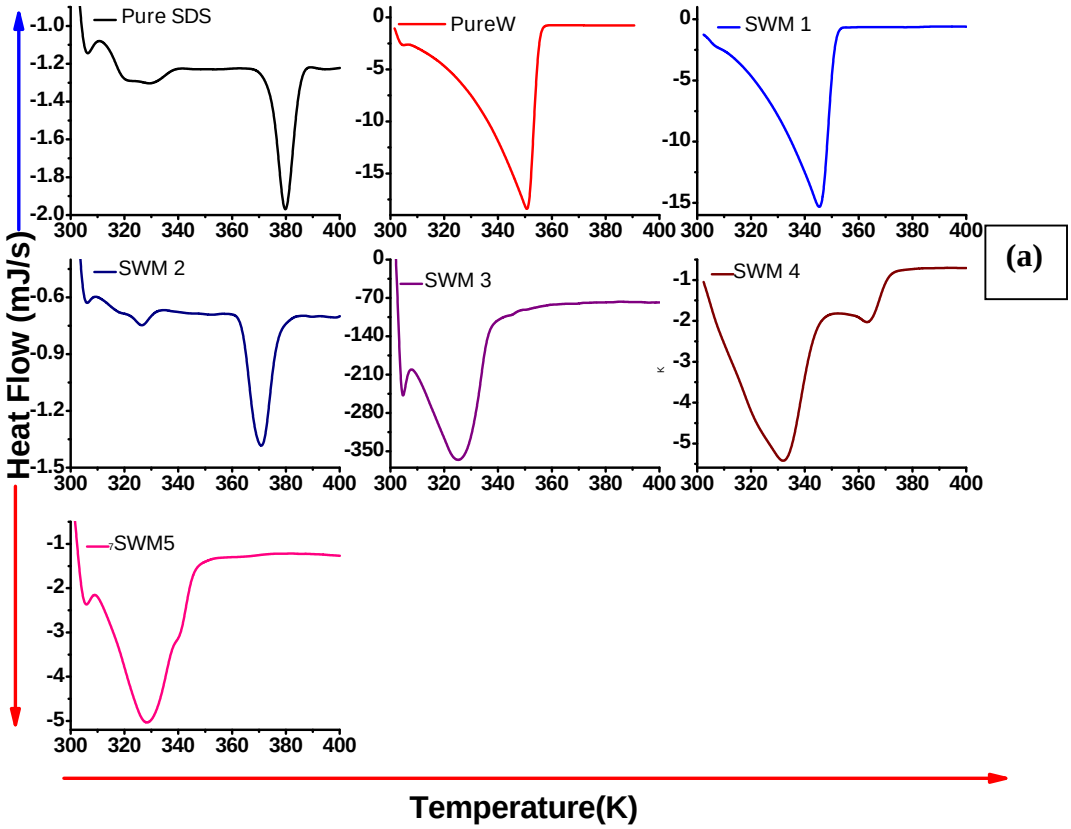

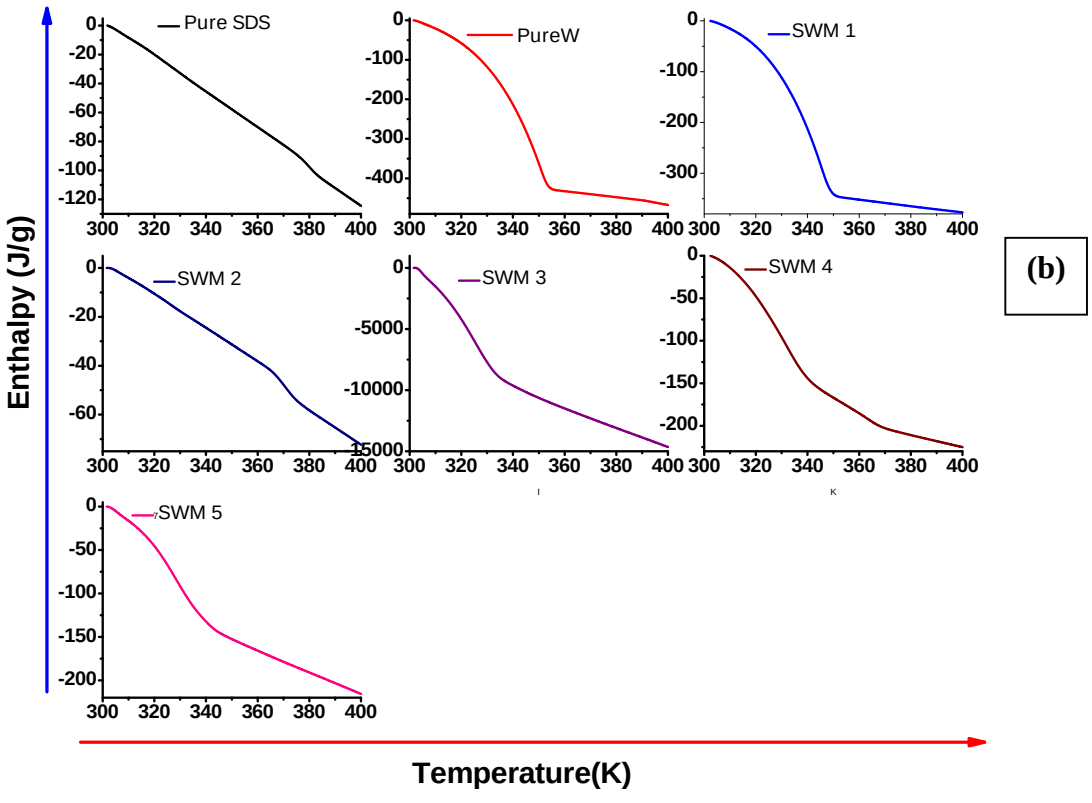

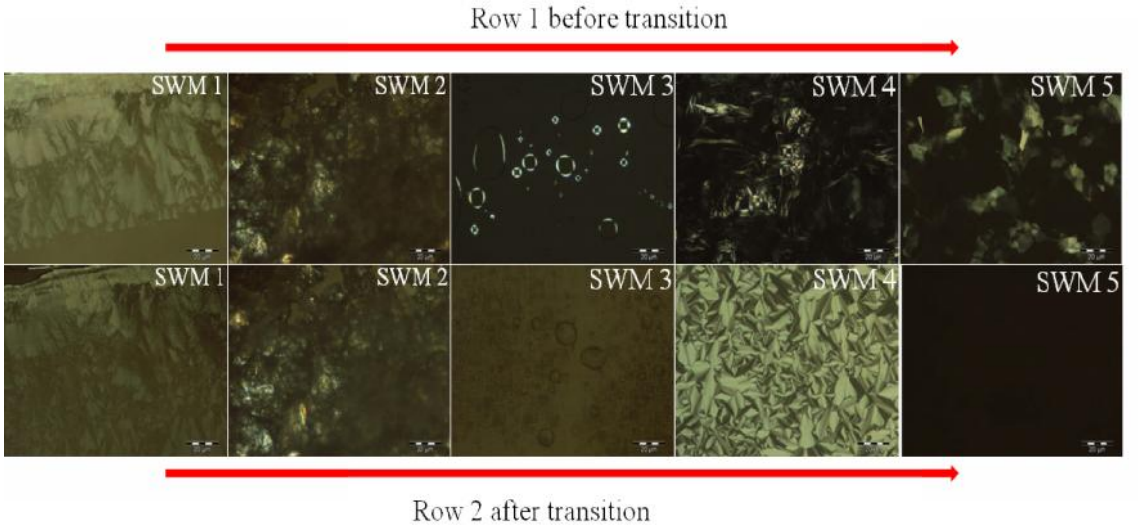

Figure 3.19: Variation of thermo-dynamical parameters for sodium dodecyl sulfate: Water (SDS: W) mixtures (M1=10:90wt%, M2= 30:70wt%, M3= 40:60 wt%, M4= 50:50wt% and M5= 75:25wt% stands for concentration of respective solute: solvent) (a) heat flow (b) enthalpy (c) thermo-optical analysis.

The transitions in these phases are of 2nd order as evident from the variation of enthalpy [figure 3.20(b)]. Thermo optical analysis of these systems also depicts the growth of new phases at higher temperature.

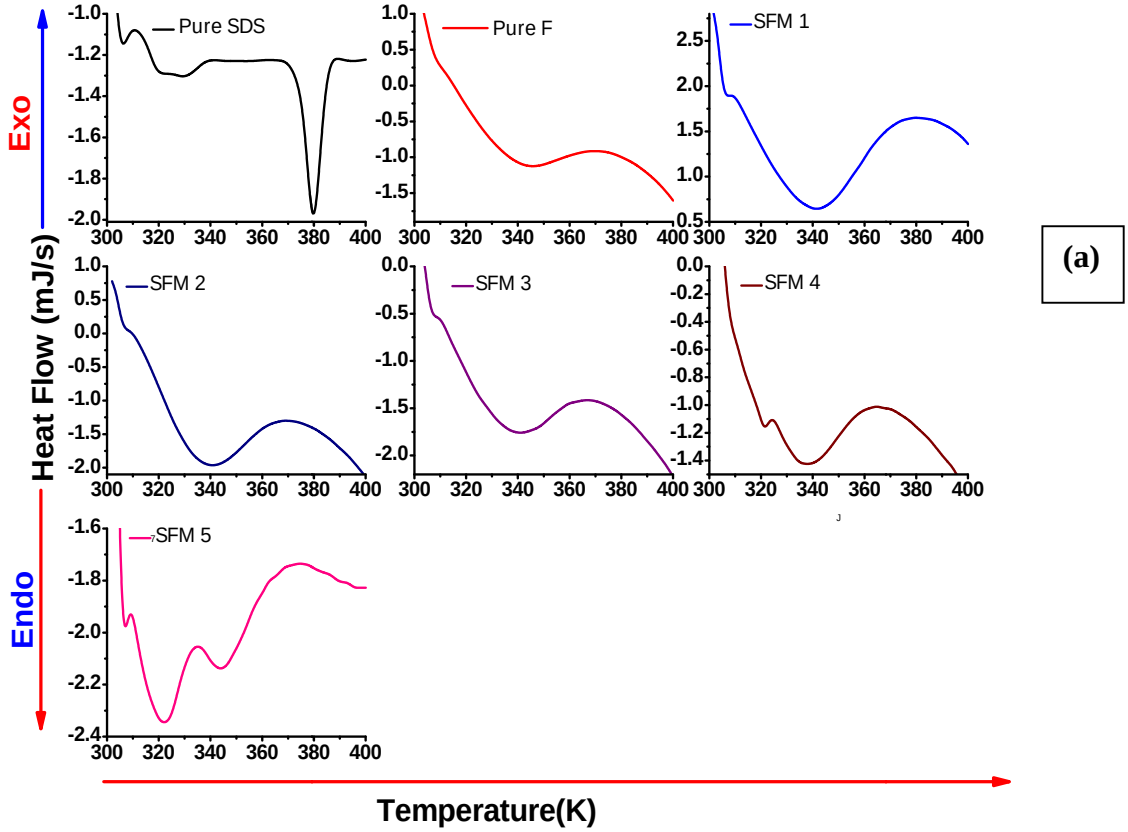

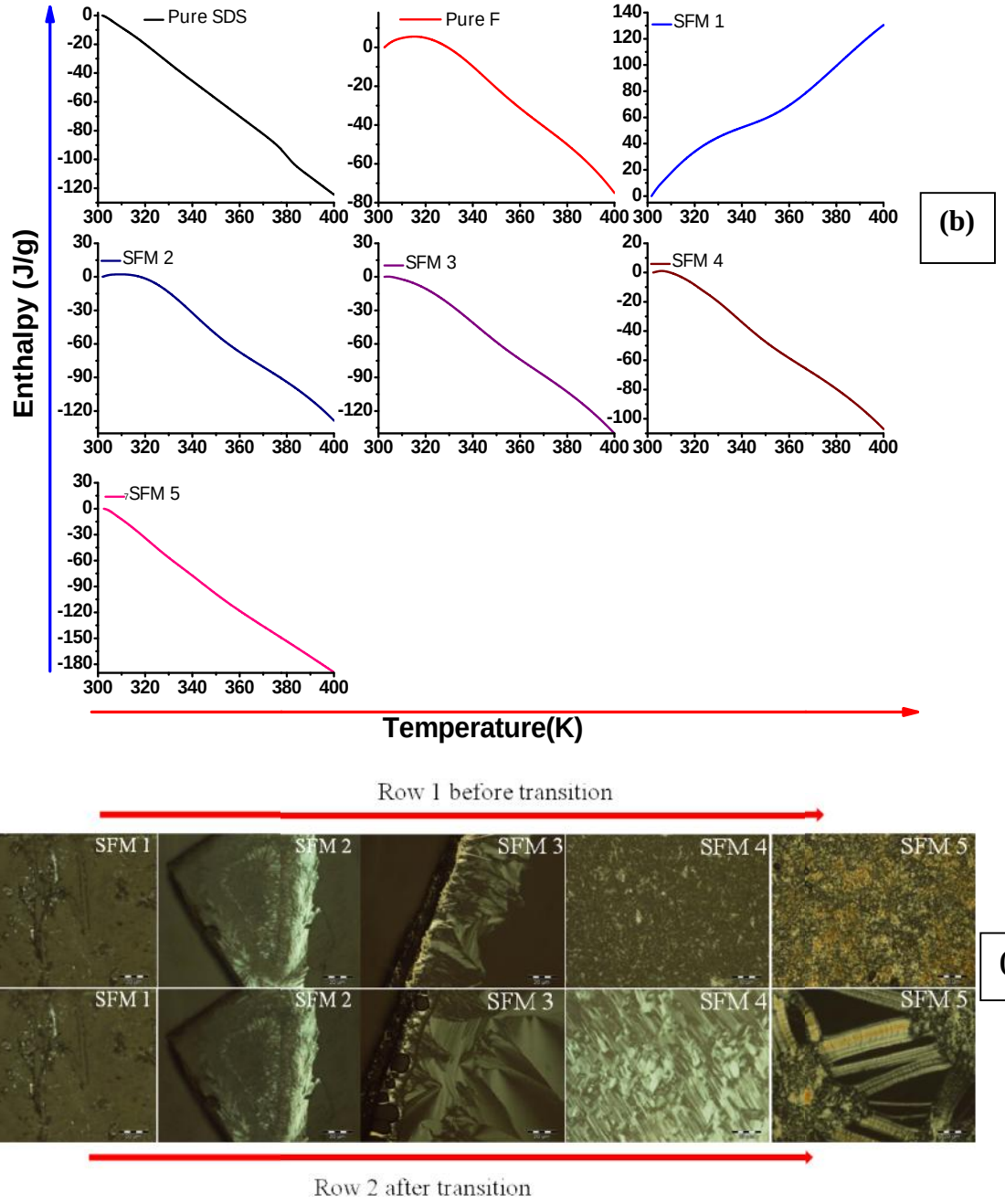

Figure 3.20: Variation of thermo-dynamical parameters for sodium dodecyl sulfate: formamide (SDS: F) mixtures (M1=10:90wt%, M2= 30:70wt%, M3= 40:60 wt%, M4= 50:50wt% and M5= 75:25wt% stands for concentration of respective solute: solvent) (a) heat flow (b) enthalpy (c) thermo-optical analysis.

3.2.3: Dielectric spectroscopy

Variation of complex permittivity as a function of frequency for various series (SDS: EG, SDS: W and SDS: F) is shown in figure 3.21 (a-c). In SDS: EG series dielectric permittivity

was found higher in the lower frequency zone. Large dispersion in the permittivity has been seen at the expense of increasing amphiphilic concentration. Permittivity decreased from 1495 to 559 as the concentration reached to the higher site. Such reduction in the permittivity in these systems attributed to the evolution of the micelles size with the rise in the concentration. Dielectric loss spectra shows well accentuated single peak in all samples attributed to the single relaxation process .The apparent broadening and lower frequency shift for SEM 2 and SEM 3 indicates the disorder in the system. Similarly the dielectric behaviour of SDS: W and SDS: F series shows well defined behaviour with the progression of frequency. These systems show the reverse trend for the permittivity than that of the SDS: EG series with variation of amphiphilic concentration as we observed increase in dielectric permittivity increasing. Such behaviour of these systems owes to the stable hexagonal structure and higher polarity of solvent media. The loss factor follow the same trend for these systems as discussed in the SDS: EG series.

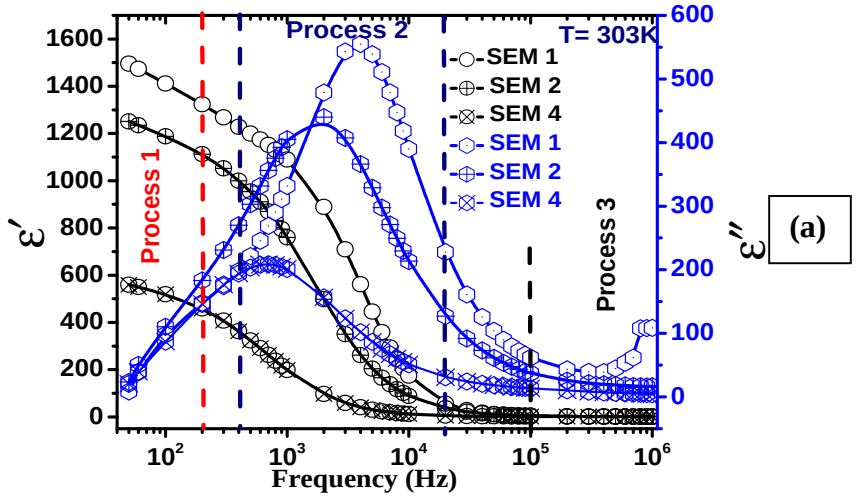

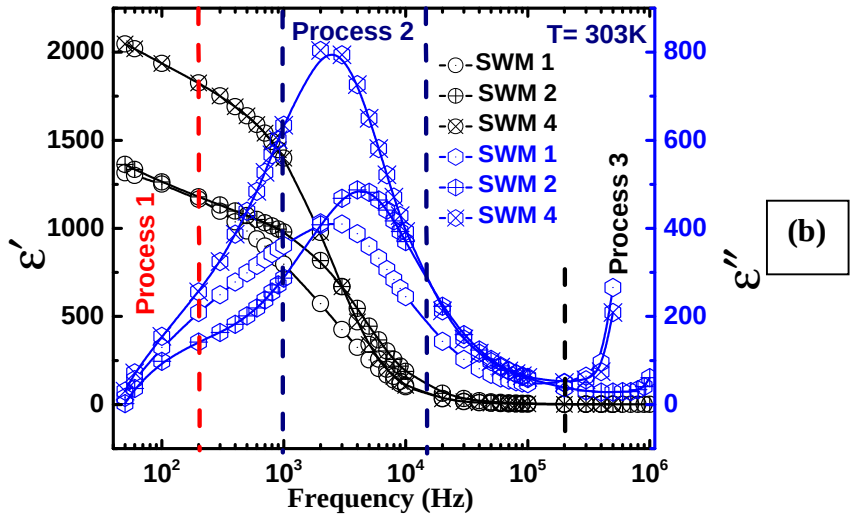

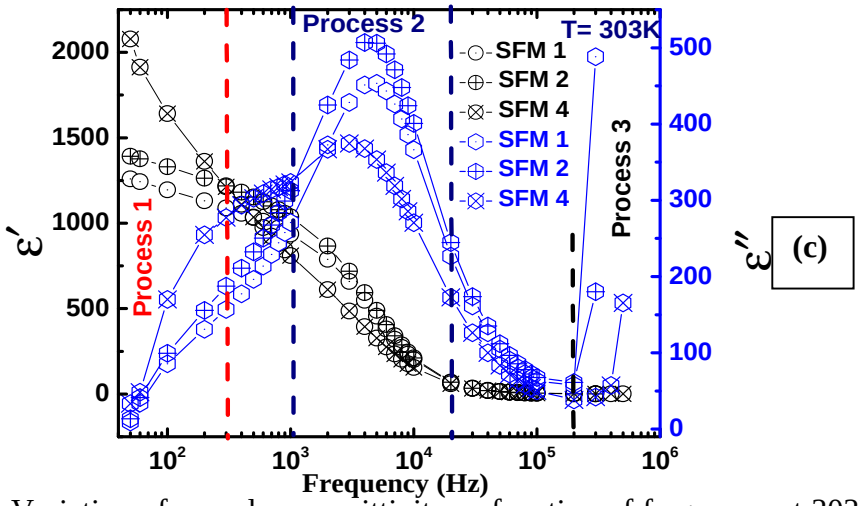

Figure 3.21: Variation of complex permittivity as function of frequency at 303K (a) sodium dodecyl sulfate: ethylene glycol series (b) sodium dodecyl sulfate: water series (c) sodium dodecyl sulfate: formamide series respectively. Where M1=10:90wt%, M2= 30:70wt% and M4= 50:50wt% stands for concentration of respective solute: solvent.

The schematic diagram for the dielectric process in the hexagonal mesophase of SDS based systems is shown in the figure 3.22 (a-b). We demonstrate the effects of applied electric field on the orientation of charged ions at the interface of hexagonal array. Temperature dependent complex permittivity for these systems is presented in the figure 3.23(Col.1 and Col.2). The dielectric permittivity was found to be increased with the variation of the temperature for these systems in all series. SFM4 systems of SDS: F series shows some unusual behaviour, it demonstrates large reduction in the permittivity with the small increment in the temperature (310K), and further regains the higher value as temperature raised to higher site. Such increasing behaviour of permittivity in these systems indicates that the increment in the temperature induces more ordering in the lyotropic phases or development of ordered mesophases at higher temperature. Loss factor shows decrease with the progression of the temperature and also indicating the biphasic region the temperature range of 325-330K in the SDS;EG and SDS:W series, however reverse trend have been seen in the formamide based series.

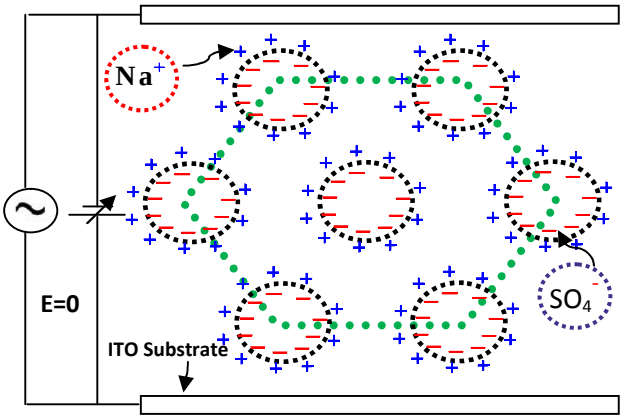

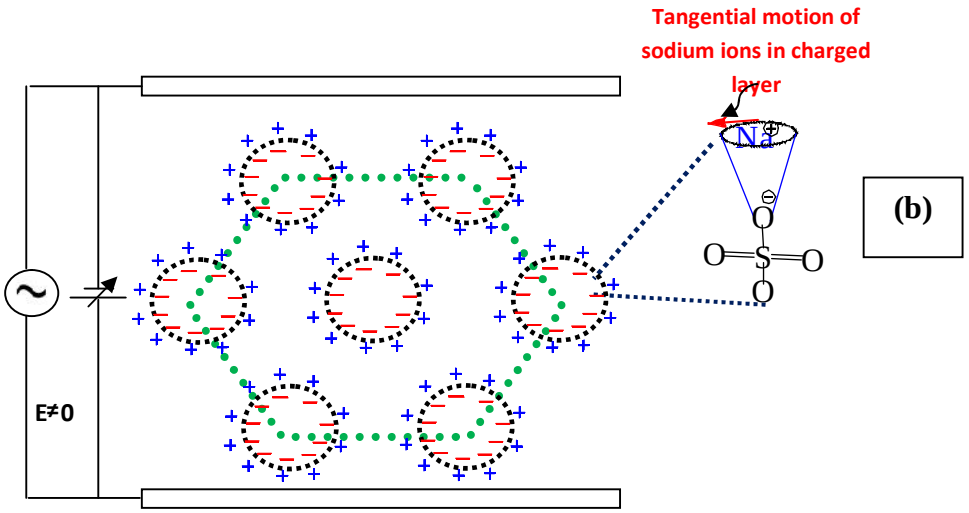

Figure 3.22: Schematic for the dielectric process in hexagonal mesophase (a) before electric field (b) after electric field.

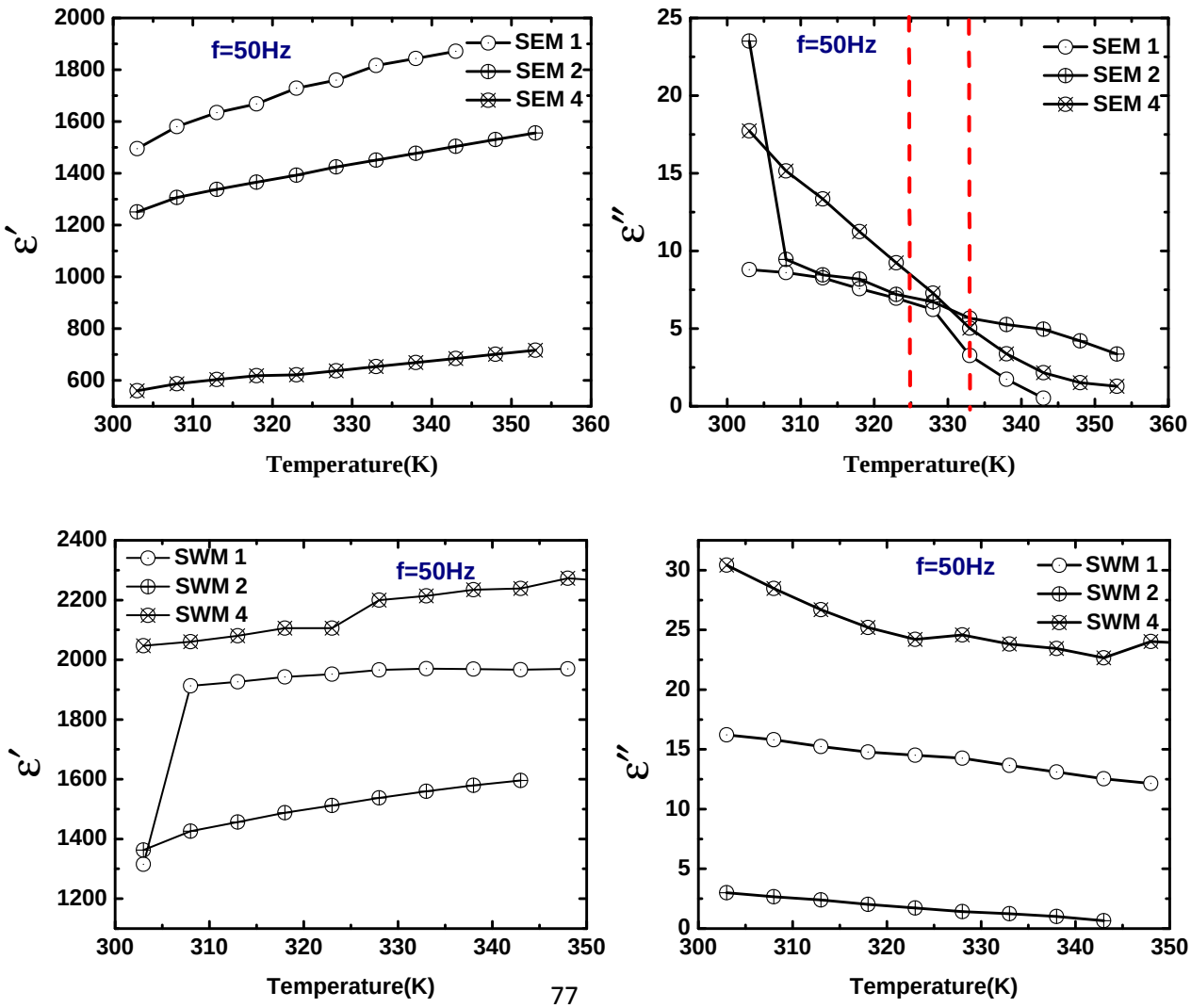

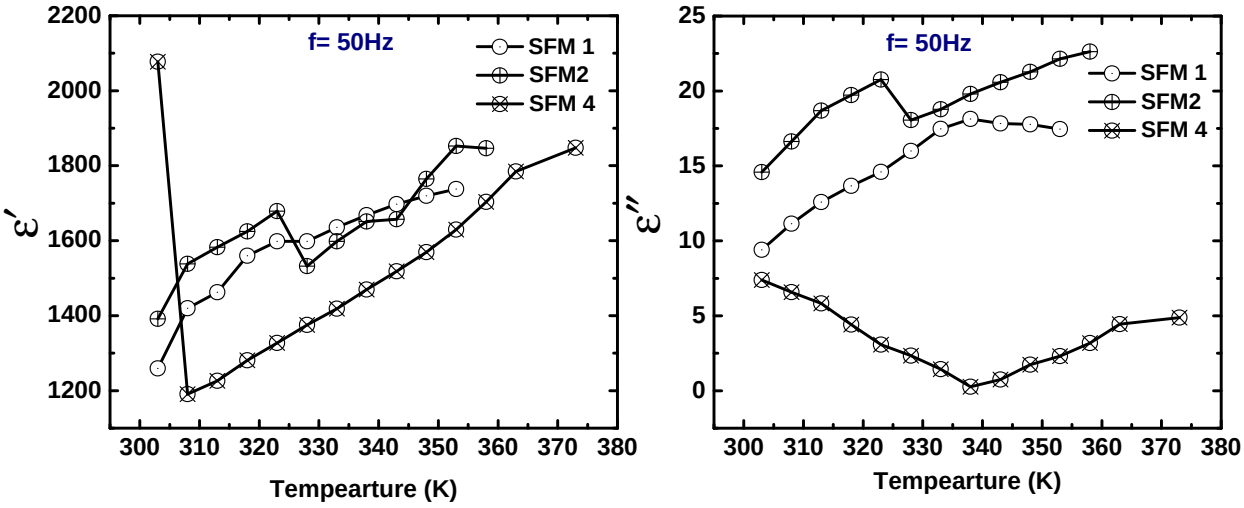

Col. 1 **Col. 2**

Figure 3.23: Variation of complex permittivity as function of temperature for sodium dodecyl sulfate: ethylene glycol series, sodium dodecyl sulfate: water series and sodium dodecyl sulfate: formamide series respectively (Col.1) real part. (Col.2) imaginary part.

These single relaxation process seen for various mixtures of three series was best fitted with the Cole-Cole relaxation process as evident from the figure 3.24 (a-c). The variation of distribution parameter (α) ranging from 0.2 to 0.2 for SDS: EG series, 0.1-0.2 for SDS: W series and 0.12-0.2 for SDS: F series. The corresponding relaxation parameters for these systems were computed by using the standard equations 3.9-3.11. The obtained magnitude of the relaxation parameters are given in the Table 3.14. We observed that these systems exhibit higher dielectric strength and higher relaxation frequency of KHz range along with the very low relaxation time as evident from the table 3.14. The relaxation time was found minimum for SDS: F series and maximum for SDS: EG series.

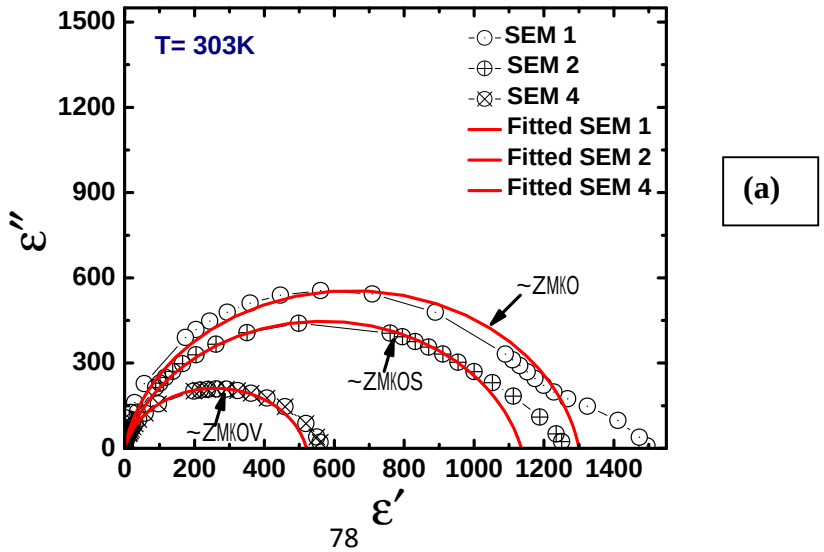

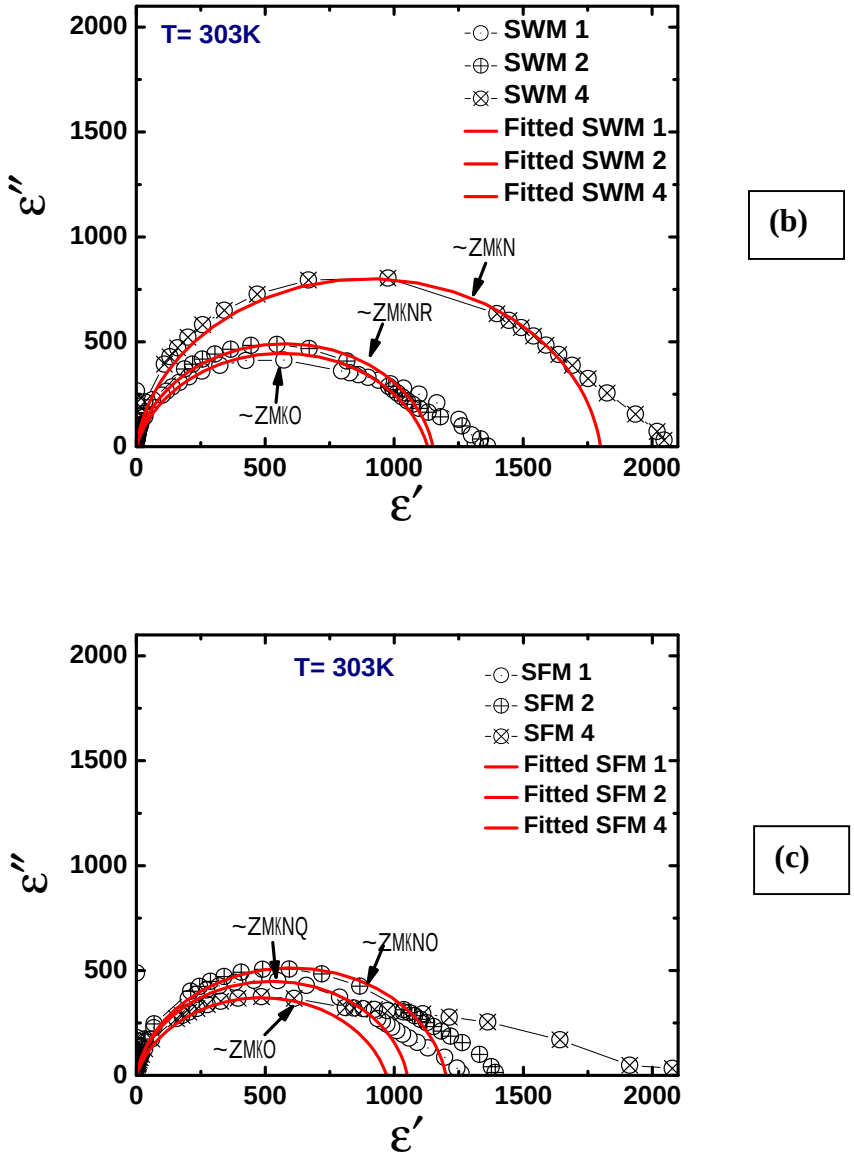

Figure 3.24: Cole-Cole plot at 303K (a) sodium dodecyl sulfate: ethylene glycol series (b) sodium dodecyl sulfate: water series (c) sodium dodecyl sulfate: formamide series respectively. Where M1=10:90wt%, M2= 30:70wt% and M4= 50:50wt% stands for concentration of respective solute: solvent.

3.2.4: Activation energy

Activation energy for the biphasic region on various series (SDS: EG, SDS: W and SDS: F) was computed from the Arrhenius plot (graphs not shown here) is given in the table 3.14. The activation energy for the various phases of non-aqueous (SDS: EG and SDS: F series) was found higher than that of the aqueous, reveals that the LLC phase derived from the non-aqueous media are more stable.

Table 3.14: Relaxation parameters for SDS: EG, SDS: W and SDS: F series

Sodium dodecyl sulphate: Ethylene glycol							
Mixtures	**ε′**	**Δε**	**f_r(Hz)**	**τ (μs)**	**Ea**		**n**
					Ist phase	**2nd phase**	
SEM 1	1495	1169.70	4000	39.00	25.20	076.00	1.41
SEM 2	1250	1148.70	1700	93.00	10.80	174.00	1.42
SEM 3	--	--	--	--	--	--	1.43
SEM 4	0559	0588.20	0600	260.00	18.60		1.44
SEM 5	--	--	--	--	--		1.44
Sodium dodecyl sulphate : Water							
SWM 1	1315	0995.00	2500	63.00	03.60	07.20	1.34
SWM 2	1362	1024.00	4000	39.00	27.00		1.35
SWM 3	--	--	--	--	--	--	1.36
SWM 4	2047	1577.00	2500	63.00	09.00	04.20	1.37
SWM 5					--	--	1.43
Sodium dodecyl sulphate : Formamide							
SFM 1	1259	1008.00	4534	35.00	09.60	01.20	1.44
SFM 2	1391	1185.00	4521	33.00	13.80	07.20	1.44
SFM 3	--	--	--	--	--	--	1.44
SFM 4	2077	0910.00	3000	53.00	44.50	105.00	1.45
SFM 5	--	--	--	--	--	--	1.47

3.2.5: Refractive index

The magnitude of the refractive index for the various series is given in the Table 3.14. We found that value of **n** increased with the rise in the amphiphilic concentration for all the series, such behaviour of the refractive index owes to the increase in the viscosity of the systems. However, the magnitude of the variation is very small. Variation of **n** as a function of temperature is presented in the figure 3.25 (a-c) for three series. The refractive index follows the same trend as discussed for the temperature dependent permittivity as it found to be increase with the rise in temperature and show various fluctuation regions as discussed earlier in dielectric behaviour.

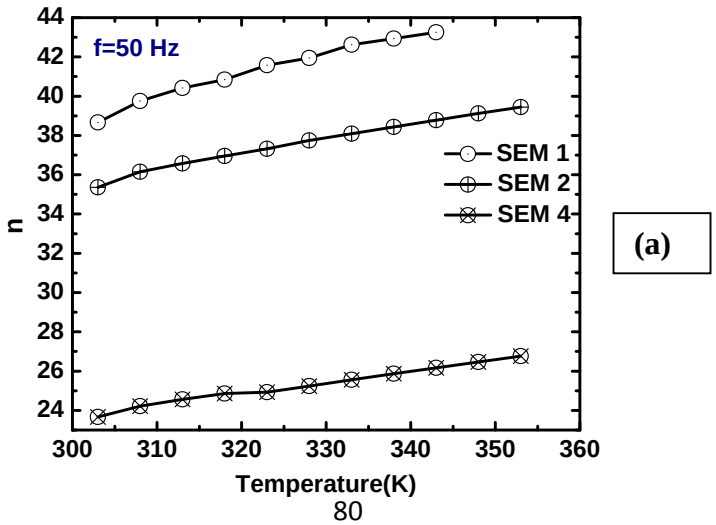

(a)

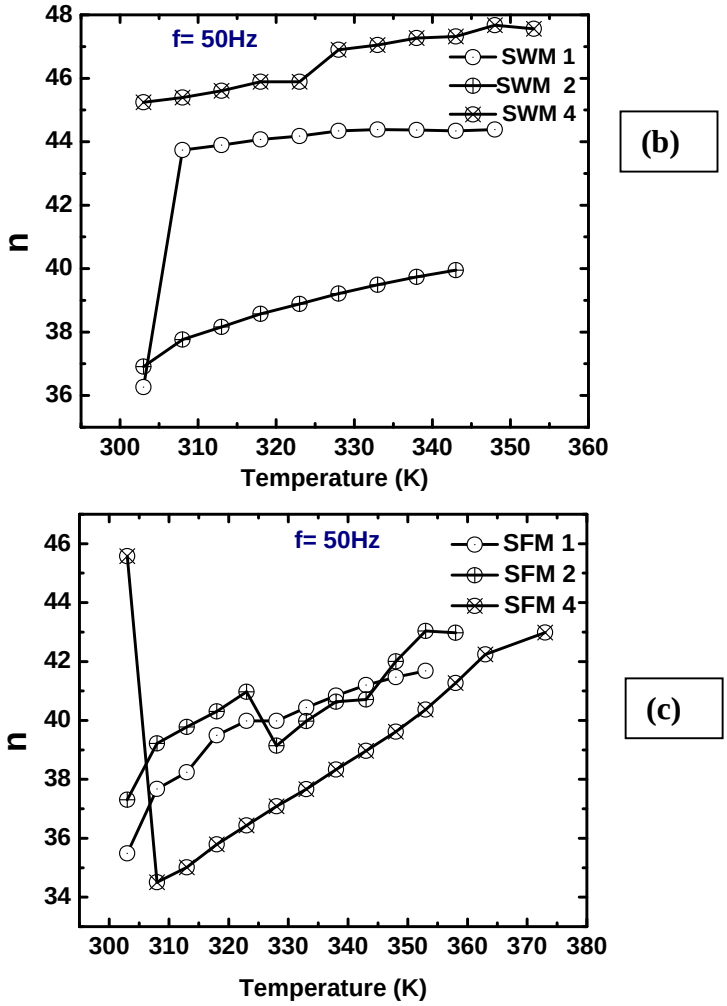

Figure 3.25: Variation of refractive index as a function of temperature (a) sodium dodecyl sulfate: ethylene glycol series (b) sodium dodecyl sulfate: water series (c) sodium dodecyl sulfate: formamide series respectively. Where M1=10:90wt%, M2= 30:70wt% and M4= 50:50wt% stands for concentration of respective solute: solvent.

3.3: Non-Ionic surfactant

Nonionic surfactants are mainly the long chain alcohols exhibit some surfactant character. Prominent among these are the fatty alcohols, cetyl alcohol, stearyl alcohol, cetostearyl alcohol (consisting predominantly of cetyl and stearyl alcohols), and oleyl alcohol. Polysorbate 20 (common commercial brand name Tween 20) is a polysorbate surfactant whose stability and relative non-toxicity makes its use as a detergent and emulsifier in a numeral domestic, scientific, and pharmacological applications. It is a polyoxyethylene derivative of sorbitan monolaurate, and is distinguished

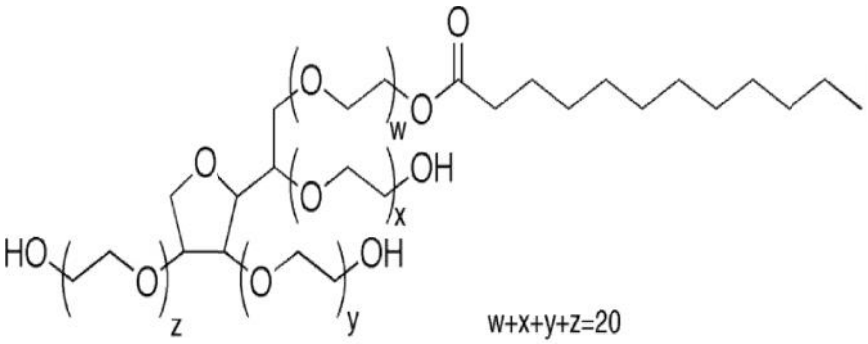

from the other members in the polysorbate range by the length of the polyoxyethylene chain and the fatty acid ester moiety.

The binary mixtures of tween 20 and various solvents [ethylene glycol (EG), water (W) and formamide (F)] at varying concentrations 10:90, 30:70, 40:60, 50:50 and 75:25wt% were prepared. They were characterized via X-ray diffraction (XRD), polarizing optical microscopy (POM), differential scanning calorimetry (DSC), dielectric spectroscopy and optical techniques to investigate the development of diverse phase in the varying concentration regime in as prepared and quenched systems and to understand their physical properties at 303K and elevated temperature range of 300-400K. Tween 20 : ethylene glycol series named as TEM 1[T20: EG (10:90)], TEM 2[T20: EG (30:70)], TEM 3[T20: EG (40:60)], TEM 4[T20: EG (50:50)] and TEM 5[T20: EG (75:25)], in similar way tween 20 : water series designated as TWM 1[T20: W (10:90)], TWM 2[T20: W (30:70)], TWM 3[T20: W (40:60)], TWM 4[T20: W (50:50)] and TWM 5[T20: W (75:25)], series of tween 20 : formamide was denoted as TFM 1[T20: F (10:90)], TFM 2[T20: F (30:70)], TFM 3[T20: F (40:60)], TFM 4[T20: F (50:50)] and TFM 5[T20: F (75:25)].

3.3.1: Structural analysis

To determine the structure of the various mixtures of T20: EG, T20: W and T20: F series XRD measurement was done at low angle range. It was observed that these T20 based mixture did not diffract at any angle over 2θ scale in as prepared and quenched conditions. We did not observe any peak in any series (graphs not shown here). Such behaviour reflects the lack of ordering, or miceller and vessels like structures in these systems. Though, efforts are on to investigate the region behind the absence of diffraction peaks in these systems. The structural phases of these systems were further confirmed from the POM analysis. The optical textures for as prepared mixtures of various series are shown in the figure 3.26 (Col. 1 for T20: EG, Col.2 for T20: W and Col.3 for T20: F). Interestingly ring like texture patterns were

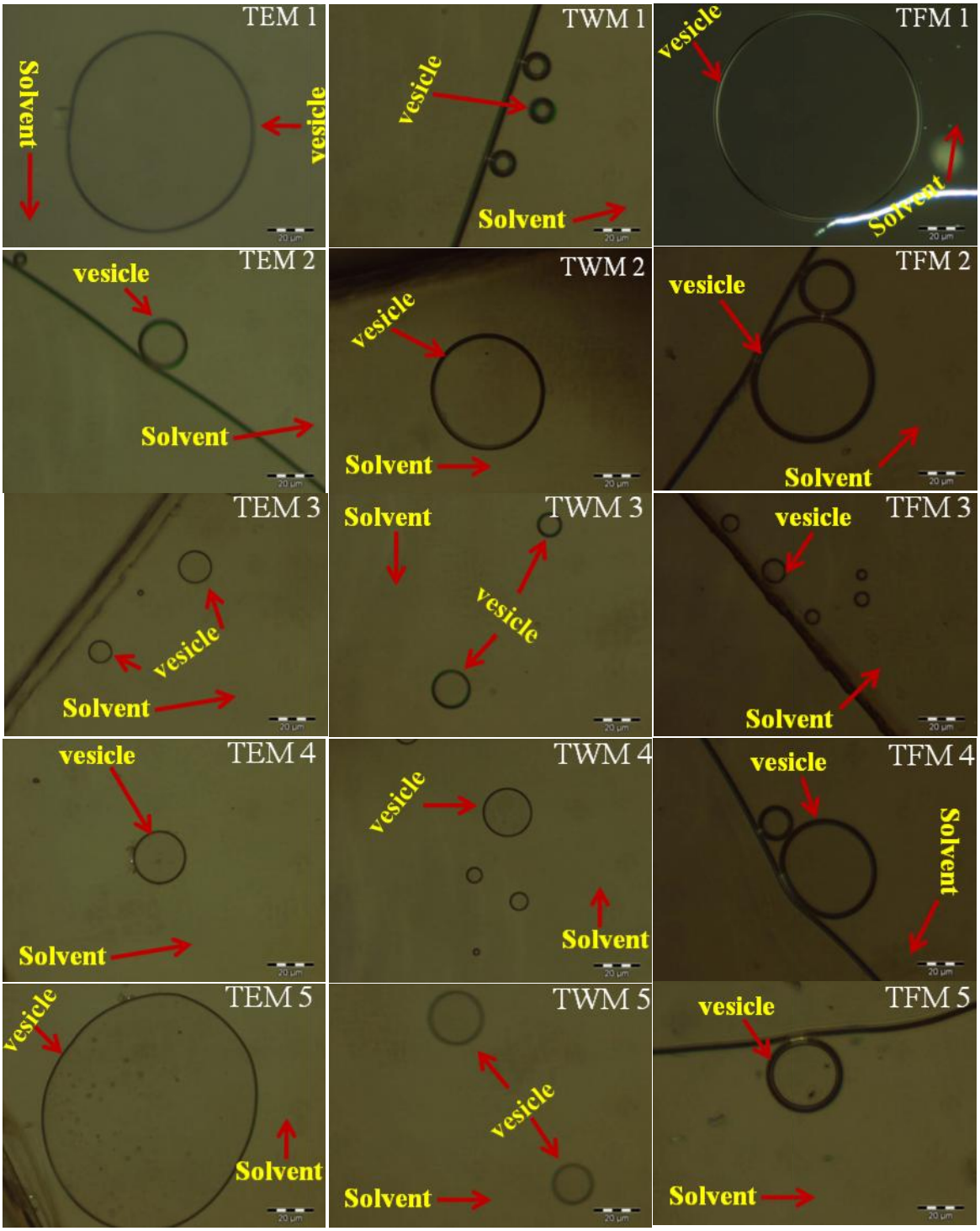

Col.1 **Col.2** **Col.3**

Figure 3.26: Texture patterns of as prepared mixtures at varying concentration (M1=10:90wt%, M2= 30:70wt%, M3= 40:60 wt%, M4= 50:50wt% and M5= 75:25wt% stands for concentration of respective solute : solvent) at 303K (Col.1) tween 20 : ethylene glycol series (TEM1-5) (Col.2) tween 20 : water series (TWM1-5) (Col.3) tween 20 : formamide series (TFM1-5) respectively.

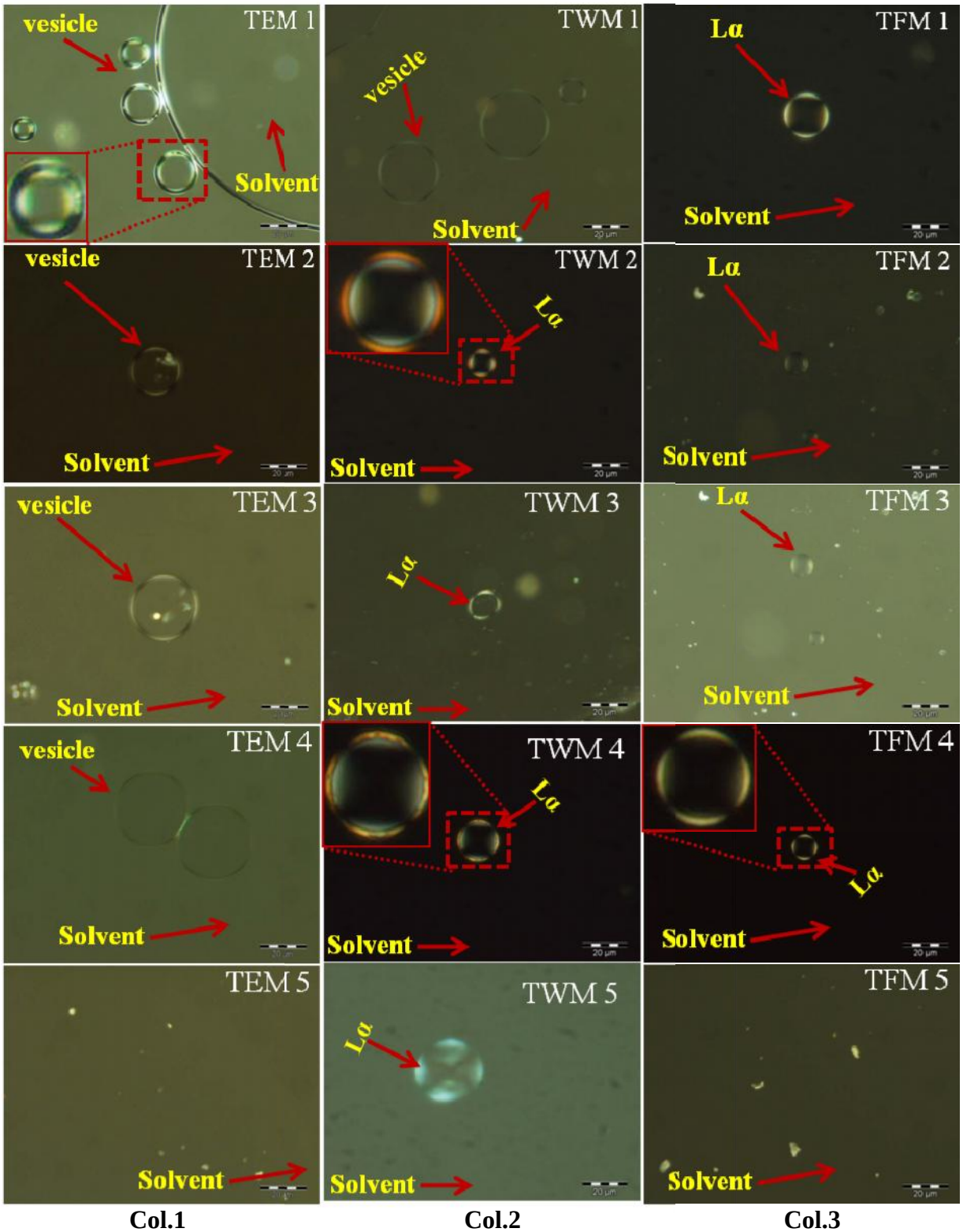

Figure 3.27: Texture patterns of quenched mixtures at varying concentration (M1=10:90wt%, M2= 30:70wt%, M3= 40:60 wt%, M4= 50:50wt% and M5= 75:25wt% stands for concentration of respective solute : solvent) at 303K (Col.1) tween 20 : ethylene glycol series (TEM1-5) (Col.2) tween 20 : water series (TWM1-5) (Col.3) tween 20 : formamide series (TFM1-5) respectively.

seen in as prepared mixtures of T20: EG series (TEM1-TEM5) resembled with the typical texture of vesicles as evident from the figure 3.26 (Col.1). In general, the formation of the vesicles structures associated with small head group area and long bulky chains, such structures are generally arises because in closed bilayer the energetically unfavorable edges are eliminated at a finite rather than infinite aggregation number, which is also entropically favored. In similar fashion vesicles of diverse size have been observed at lower and higher concentrations (TWM1-TWM 5) of T20: W and T20: F series in as prepared mixtures as shown in figure 3.26 Col2 and Col.3.Texture patterns for the quenched mixtures of various series are presented in the figure 3.27 (Col. 1 for T20: EG, Col.2 for T20: W and Col.3 for T20: F). No pronounced effects of quenching have been seen on the texture development of these phases as we observed the vesicles like geometries in the quenched T20: EG series at lower and higher content of amphiphiles (figure 3.27 Col.1). In T20: W series vesicles like structures appeared at low surfactant concentration. However, coaxial droplet in the isotropic media were observed at TWM 2-4 representing the lamellar phase, although, these mixtures did not diffract over 2θ scale in the XRD measurement. Focal conic domains obtained at higher T20 content (TWM 5) may correspond to the hexagonal mesophase. On the other hand in T20: F series quenched mixture developed well ordered coaxial droplet up to 50 wt% concentrations corresponding to the lamellar mesophase. However, isotropic texture has been seen at 75wt% concentration. On the basis of these structural measurements it can be concluded that the most of these systems exhibit layered ordering either bilayer lamellar or vesicular. Vesicles to bilayer transition have been seen with the change in the polarity of the solvent (as water and formamide gives lamellar structures but EG shows only vesicles). Such layered ordering in these systems owing to the higher chain length of T20 molecules which generally preferred layered geometries than others.

3.3.2: Thermal Analysis

The calorimetric profiles of T20: EG series (TEM 1-TEM5) are presented in the figure 3.28 (a). Two broad transitions were noticed for the pure surfactant in the lower (326K) and higher temperature range (387K) attributed to the structural change and melting respectively. Single broad transition was noticed up to TEM 5 at 339,344,341, 333and 326K. No regular trend in the transition temperature has been seen as it first decreased and then increased and again becomes minimum at TEM 4. The transition observed in these systems may correspond to the

unbinding of the mesophases or nucleation of the new structure which further confirmed from the thermo-optical analysis. The variation of ΔH obtained for these mixtures are depicted in

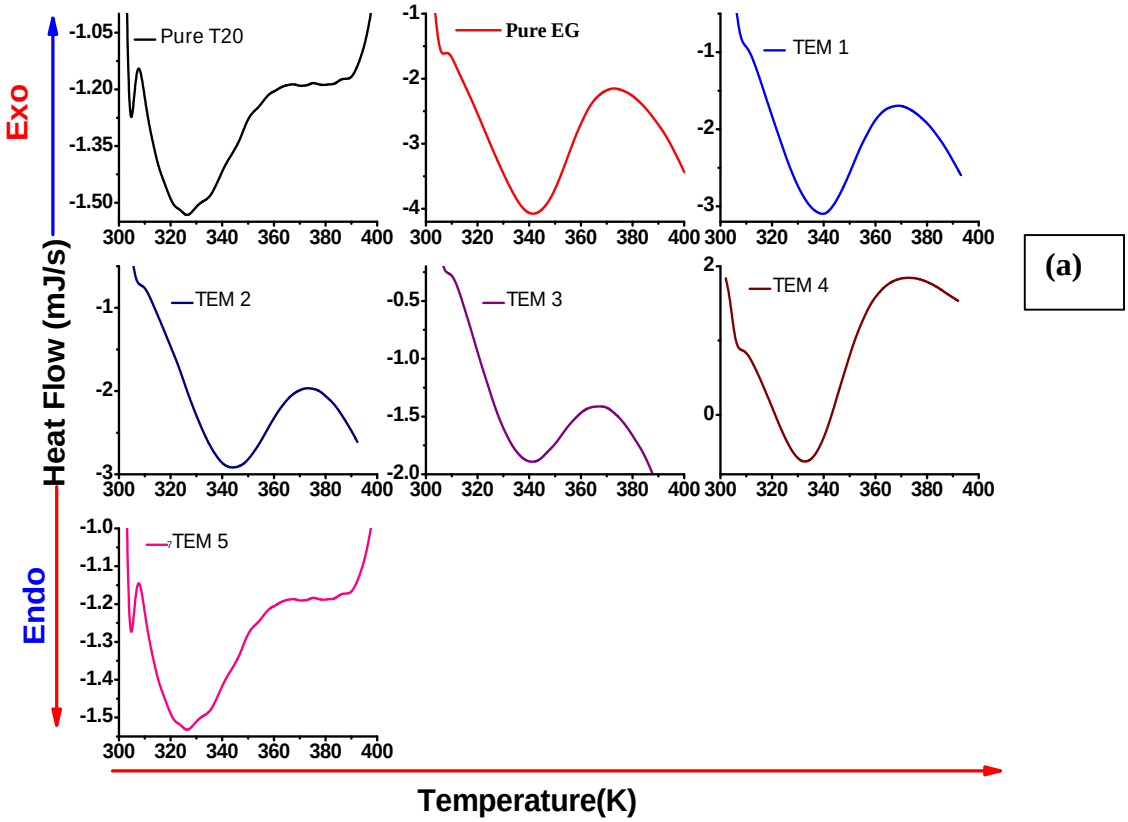

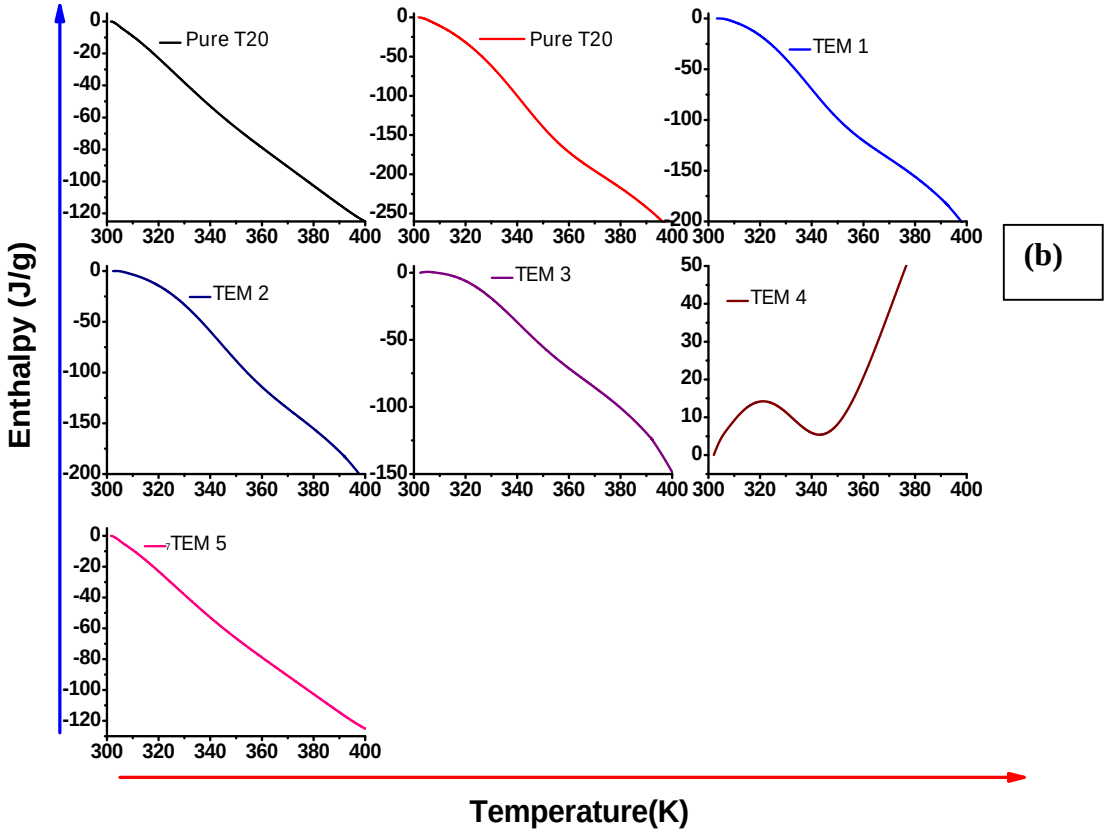

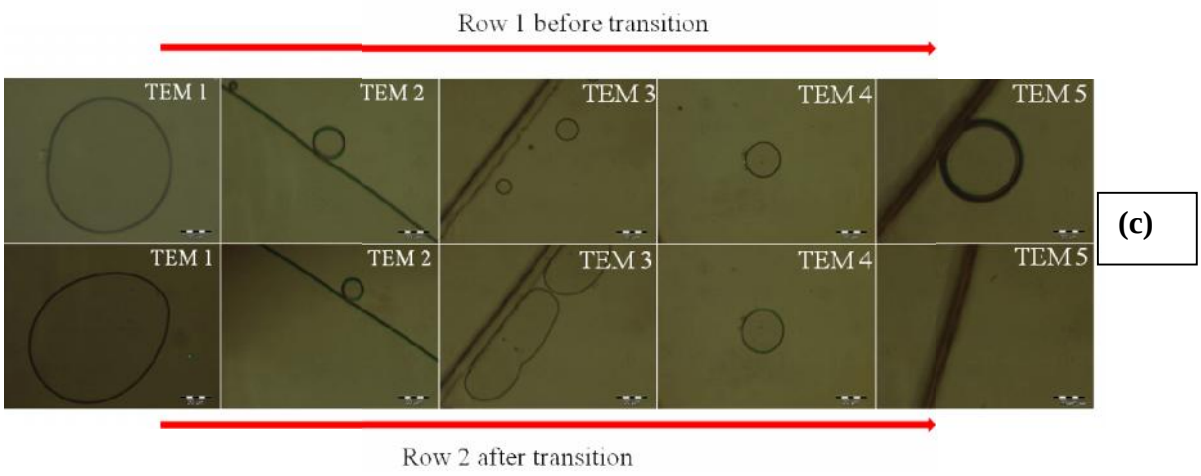

Figure 3.28: Variation of thermo-dynamical parameters for tween 20 : ethylene glycol (T20: EG) mixtures (M1=10:90wt%, M2= 30:70wt%, M3= 40:60 wt%, M4= 50:50wt% and M5= 75:25wt% stands for concentration of respective solute: solvent) (a) heat flow (b) enthalpy (c) thermo-optical analysis.

the figure 3.28 (b). Neat precursor and LLC mixture possess exothermic nature, however, sample contain TEM 4 demonstrate the endothermic character. All the systems show the continuous variation of enthalpy at the transition except the 50wt% mixture (TEM 4) which shows the discontinuous change at the transition separating two phase region. These discontinuous and continuous variations of enthalpy represent the first and second order phase transition in these systems respectively. Thermo-optical analyses of these phases are presented in the figure 3.28 (c). The structure transformation, unbinding, clustering and melting of vesicles have been observed at different T 20 concentrations. TEM 1and 4 shows the increase in the vesicles structures with rise in the temperature, however, mixture 2 shows the decrease in the vesicles size with the increment in the temperature. TEM 3 and 5 reflects the clustering and melting of the vesicles geometries. These studies are found in good correlation with the calorimetric analysis and confirm that the transition seen the calorimetric profiles corresponds to one mesophase to another. In similar fashion the thermo-dynamical behaviour of T20: W and T20: F series are presented in the figure 3.29 (a-c) and 3.30 (a-c). The corresponding thermal parameters are listed in the Table 3.15. Transition temperature (340,339,338 327,326K for TW1 to TW5) were found to be decreased at the expense of increasing surfactant concentration in T20: W series. The continuum decrease in the transition temperature reflects that the phases formed at higher concentrations are less stable than that of the lower concentration phases. In T20: F series a similar trend have been seen as we seen a single broad transition at346, 340, 339, 334, 326 K for TF1 to TF5 may attribute to the structural change in these systems. Apparent shift towards lower temperature side in the

transition temperatures of TFM1-TFM5 with the rise in T20 concentration infer that phase at higher concentration are less stable than that of the lower one. The thermo optical analysis of these series demonstrates the unbinding of the vesicles structures in the intermediate region of the temperature, though, at higher temperature region systems show the isotropic texture which may corresponds to the LC to isotropic transition or miceller phase.

Table 3.15: Thermal parameters for T20: EG, T20: W and T20: F series

Tween 20: Ethylene glycol			
Mixtures	**Phase**	**T_C**	**Order**
TEM 1	Vesicles	339.00	2^{nd}
TEM 2	Vesicles	344.00	2^{nd}
TEM 3	Vesicles	341.00	2^{nd}
TEM 4	Vesicles	333.00	1^{st}
TEM 5	Vesicles	326.00	2^{nd}
Tween 20: Water			
TWM 1	L_α	340.00	2^{nd}
TWM 2	L_α	338.00	2^{nd}
TWM 3	L_α	339.00	2^{nd}
TWM 4	H_α	327.00	2^{nd}
TWM 5	Vesicles	326.00	2^{nd}
Tween 20: Formamide			
TFM 1	L_α	346.00	2^{nd}
TFM 2	L_α	340.00	2^{nd}
TFM 3	L_α	339.00	2^{nd}
TFM 4	L_α	334.00	2^{nd}
TFM 5	H_α	326.00	2^{nd}

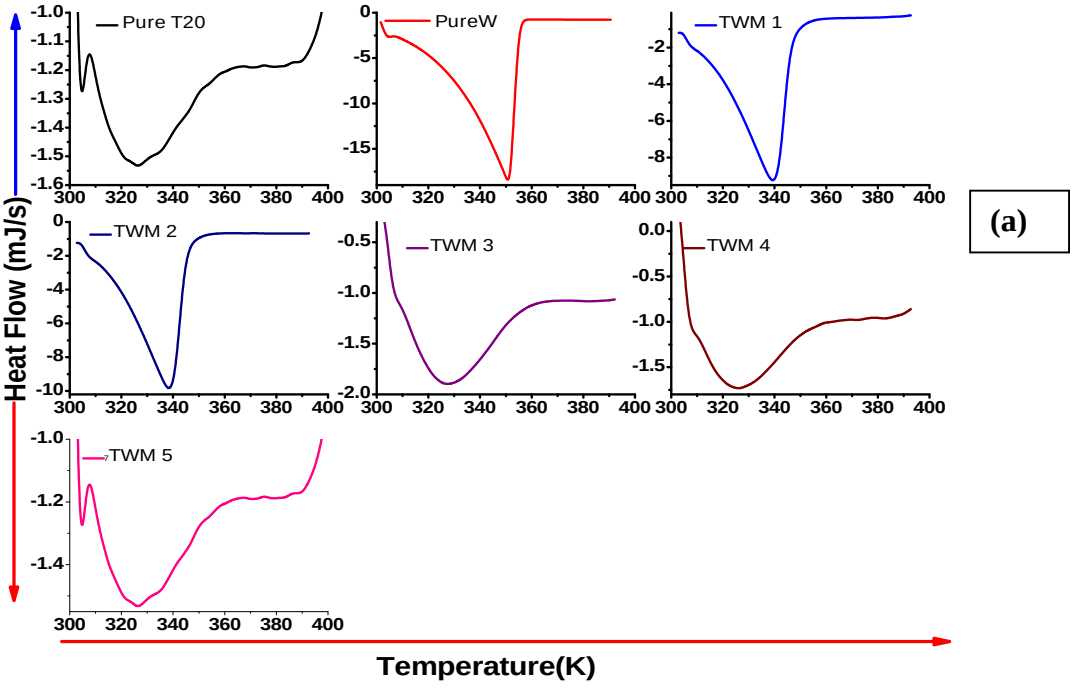

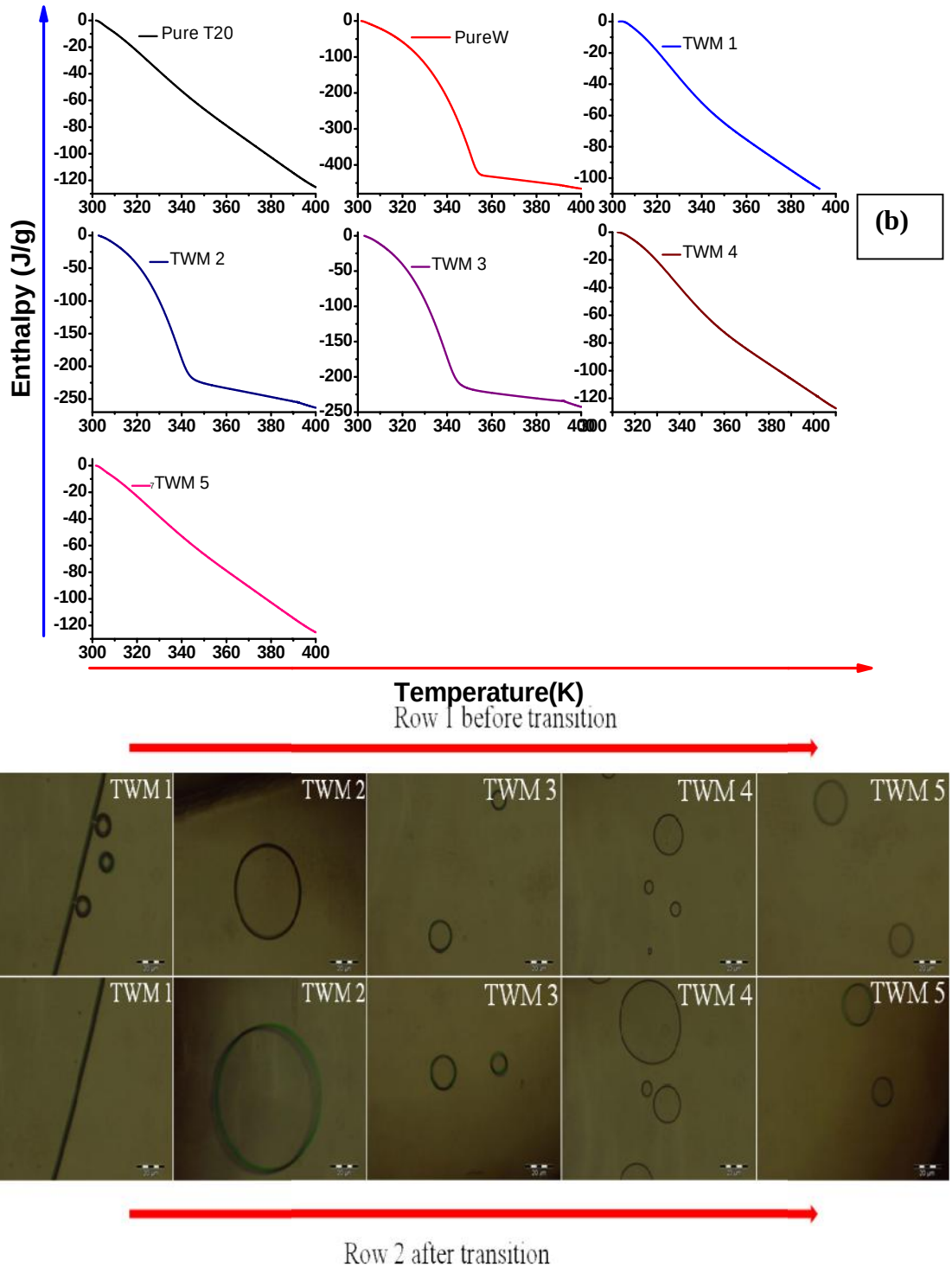

Figure 3.29: Variation of thermo-dynamical parameters for tween 20 : Water (T20: W) mixtures (M1=10:90wt%, M2= 30:70wt%, M3= 40:60 wt%, M4= 50:50wt% and M5= 75:25wt% stands for concentration of respective solute: solvent) (a) heat flow (b) enthalpy (c) thermo-optical analysis.

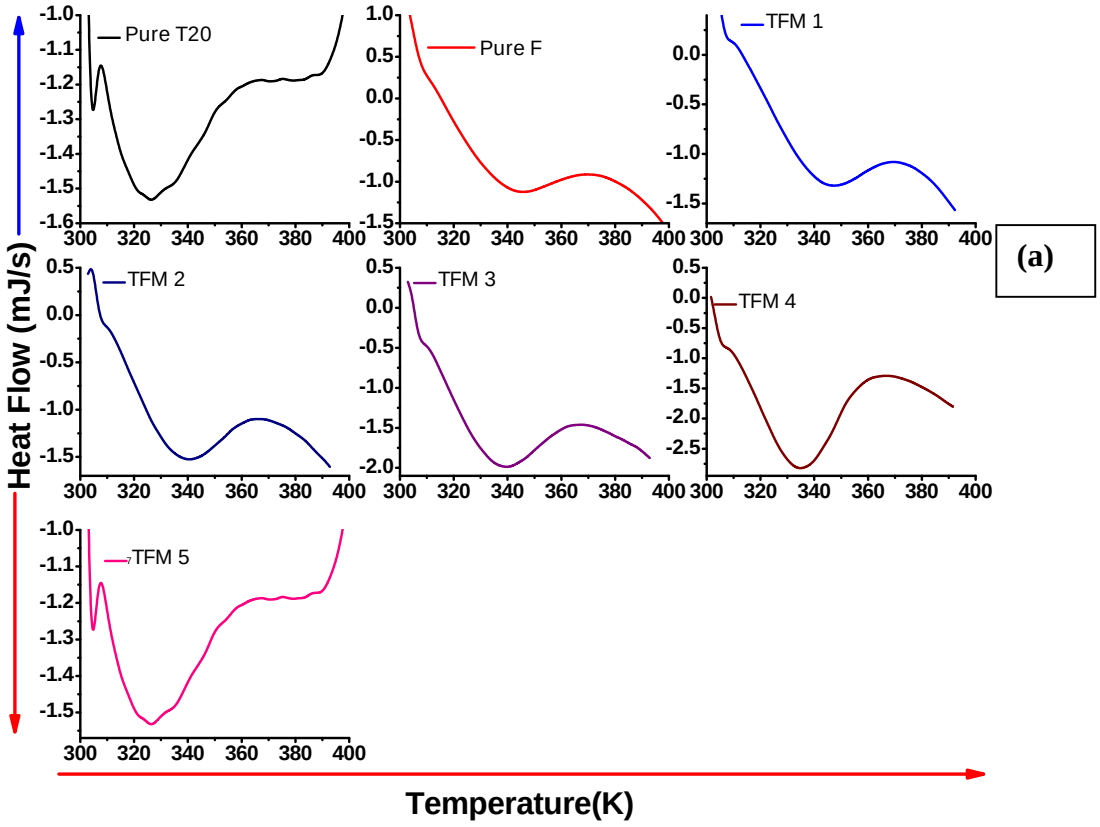
Pure T20
Pure F
TFM 1
TFM 2
TFM 3
TFM 4
TFM 5
Heat Flow (mJ/s)
Temperature(K)
(a)

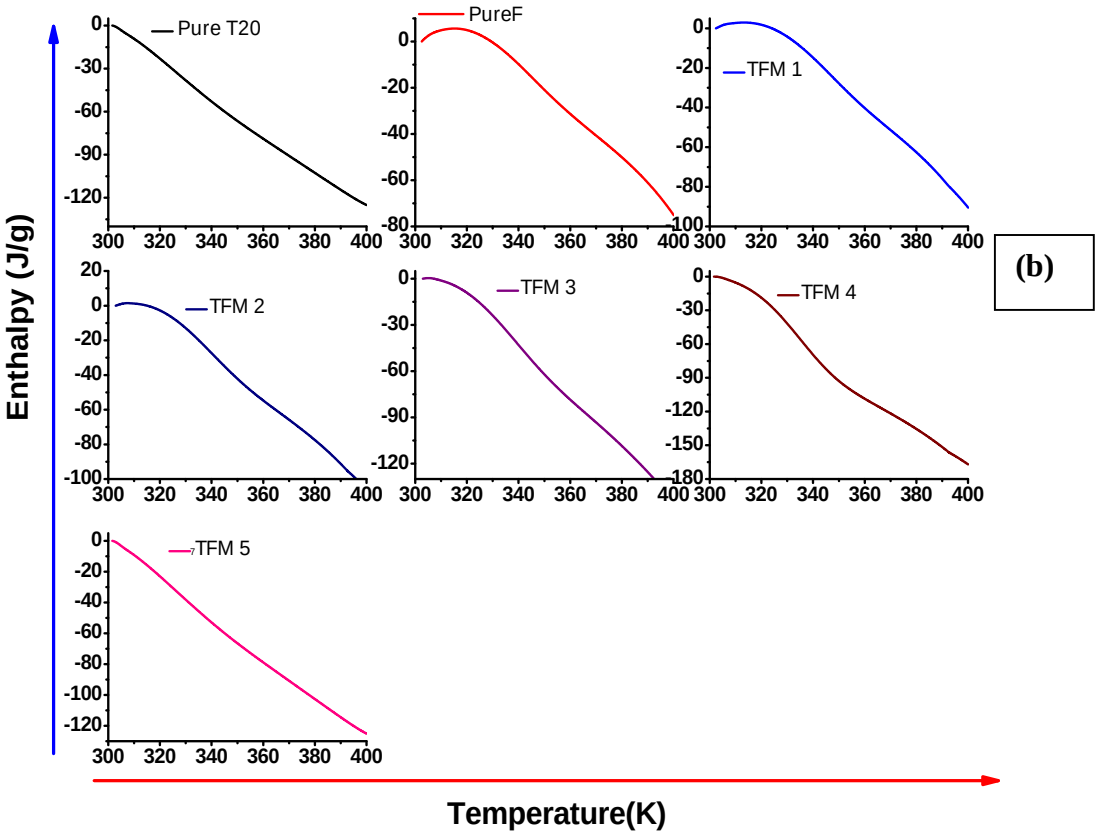
Pure T20
PureF
TFM 1
TFM 2
TFM 3
TFM 4
TFM 5
Enthalpy (J/g)
Temperature(K)
(b)

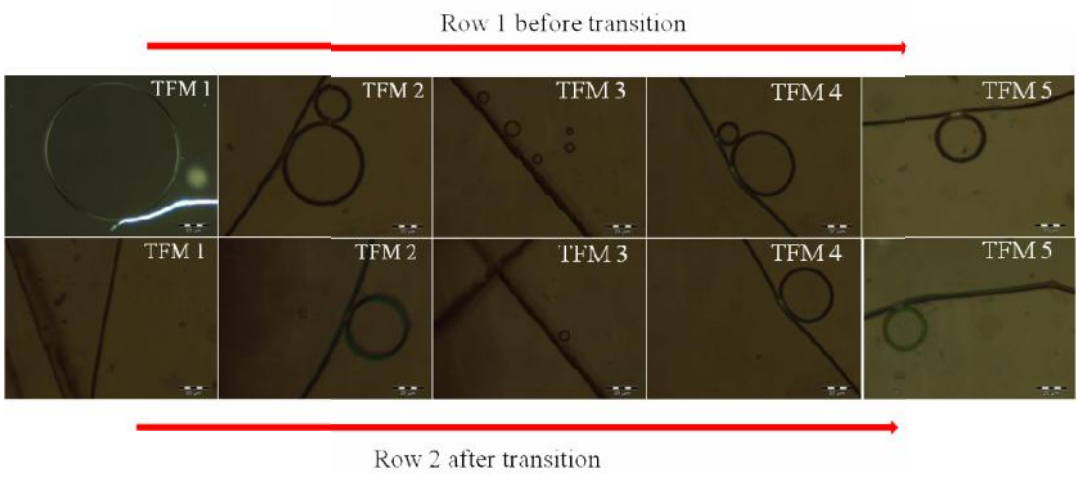

(c)

Figure 3.30: Variation of thermo-dynamical parameters for tween 20 : formamide (T20: F) mixtures (M1=10:90wt%, M2= 30:70wt%, M3= 40:60 wt%, M4= 50:50wt% and M5= 75:25wt% stands for concentration of respective solute: solvent) (a) heat flow (b) enthalpy (c) thermo-optical analysis.

3.3.3: Dielectric spectroscopy

Frequency dependent complex dielectric permittivity for series T20: EG, T20: W and T20: F is shown in the figure 3.31(a-c). Large dispersion in the dielectric permittivity was noticed at the expanse of the varying T20 concentration as TEM1exhibit lower magnitude than that of the other two however at higher concentration variation is small as evident from the figure 3.31(a). Anomalous trend of permittivity have been seen at the expense of increasing concentration of the T20 amphiphiles. Higher permittivity observed for these mixtures attributed to the dipolar motion of the head group and interfacial polarization at low frequency region (process 1). Low loss and single relaxation peak have been seen for all the mixtures results from the low frequency conduction phenomena in these non-ionic systems. Similarly well-defined dielectric behaviours were seen for T20: W and T20: F series as shown in the figure 3.31(b-c). Dielectric permittivity was found to be decreased with the rise in the T20 concentration for T20: W series, however, reverse trend have been seen for the T20: F series as we observed increase in the permittivity with increasing amphiphilic concentration. The schematic diagram to show the orientation of the dipoles and origin of the dipole moment in these non-ionic systems with the application of the field is shown in the figure 3.31(d). The relaxation phenomena in systems attributed to the interfacial polarization and change in the low frequency electric conduction

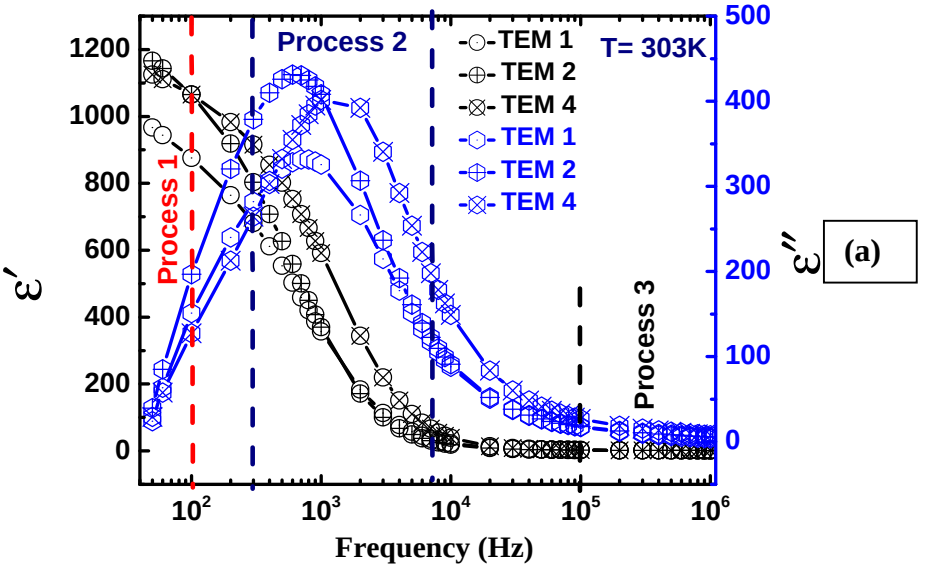
Process 2
-○-TEM 1
-⊕- TEM 2
-⊗- TEM 4
-⬡- TEM 1
-⊕- TEM 2
-⊗- TEM 4
T= 303K
Process 1
Process 3
ε′
ε″
(a)
Frequency (Hz)

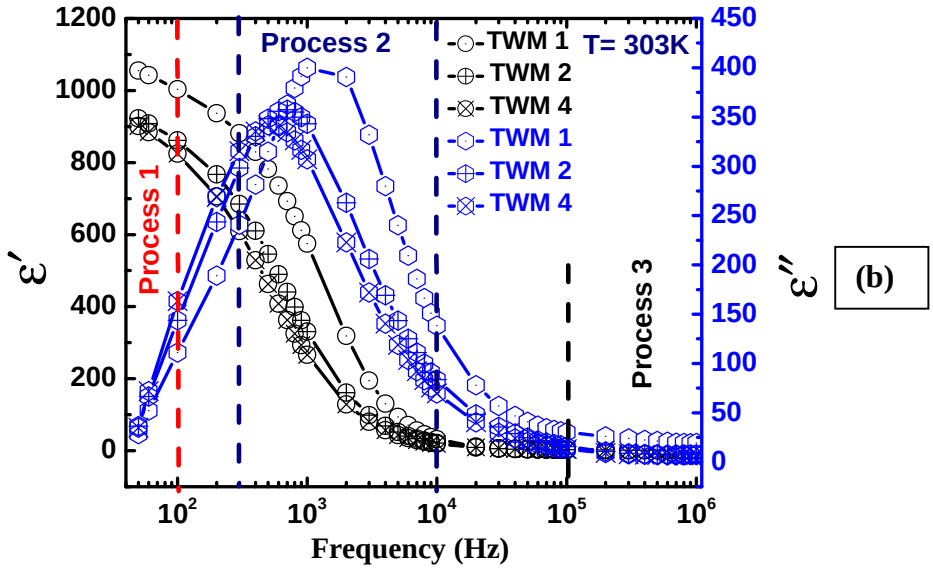
Process 2
-○-TWM 1
-⊕- TWM 2
-⊗- TWM 4
-⬡- TWM 1
-⊕- TWM 2
-⊗- TWM 4
T= 303K
Process 1
Process 3
ε′
ε″
(b)
Frequency (Hz)

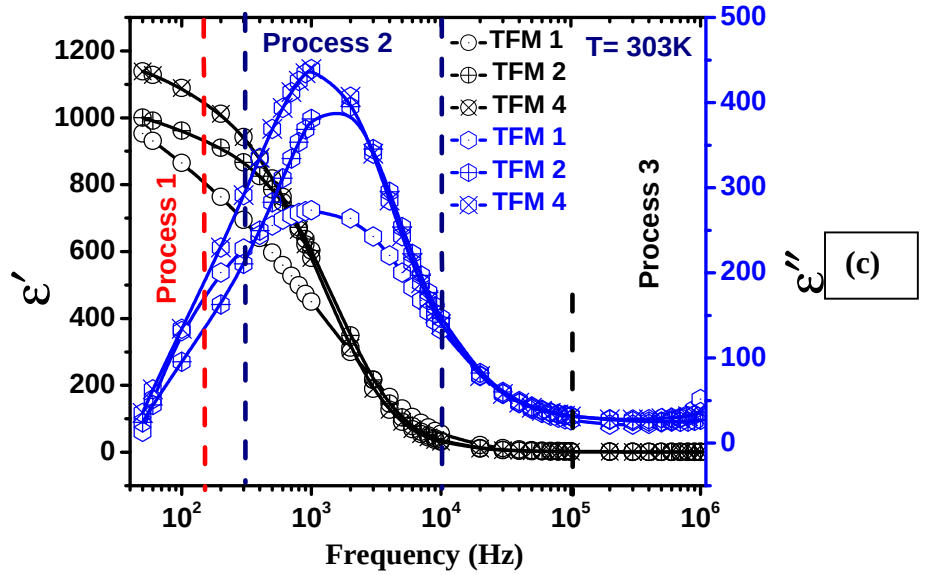
Process 2
-○-TFM 1
-⊕- TFM 2
-⊗- TFM 4
-⬡- TFM 1
-⊕- TFM 2
-⊗- TFM 4
T= 303K
Process 1
Process 3
ε′
ε″
(c)
Frequency (Hz)

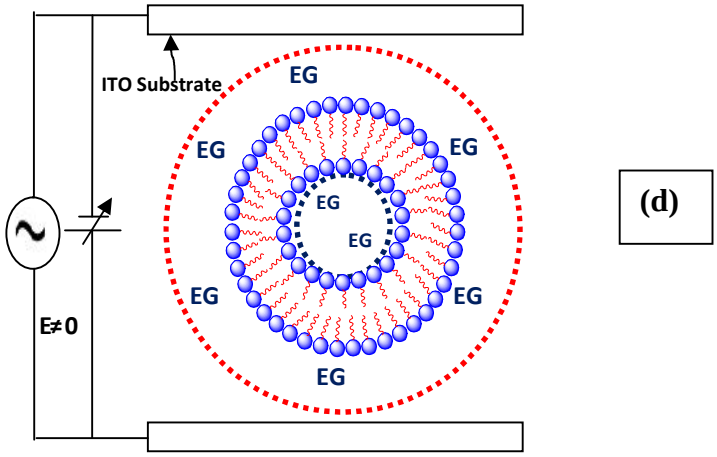

Figure 3.31: Variation of complex permittivity as function of frequency at 303K (a) tween 20 : ethylene glycol series (b tween 20 : water series (c) tween 20 : formamide series respectively. (d) schematic for dielectric process. Where M1=10:90wt%, M2= 30:70wt% and M4= 50:50wt% stands for concentration of respective solute: solvent.

Temperature dependent complex permittivity for three series is presented in the figure 3.32 (Col.1 and Col.2). The dielectric permittivity was found to be increased with the variation of the temperature for these systems in all series. Such behaviour implies that all the phases are ordered up to the studied temperature range (300-400K) either they were in vesicles geometries or in the miceller phase. However loss factor did not show any regular trend as it found to be increased in some series and decreased in others as evident from the figure 3.32 Col.2. Fluctuations in the loss behaviour in the intermediate temperature region attributed to the structural transitions in these systems at the expanse of the increasing temperature.

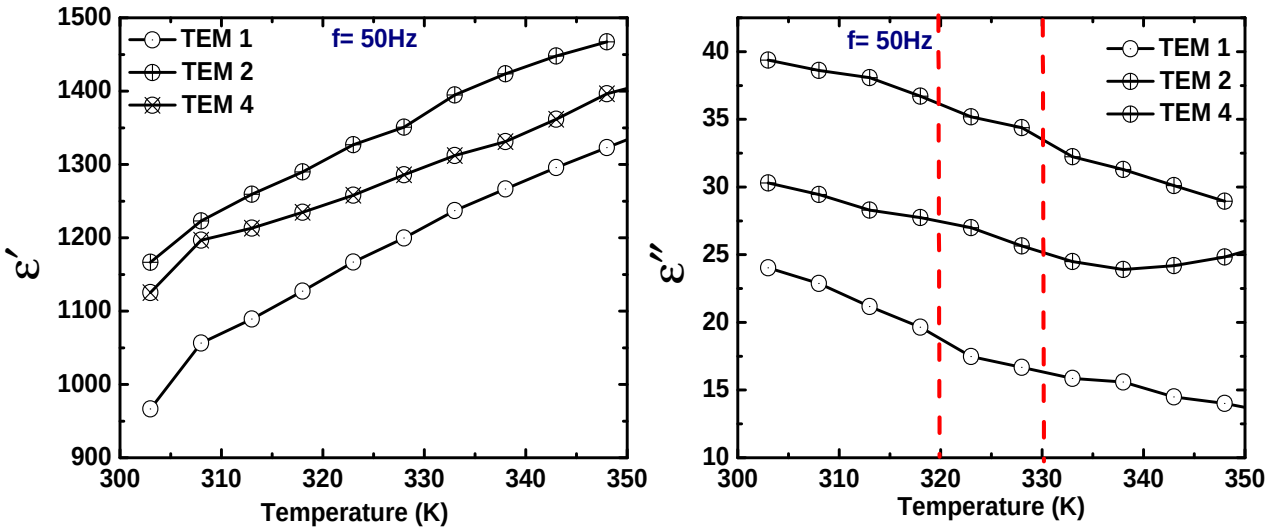

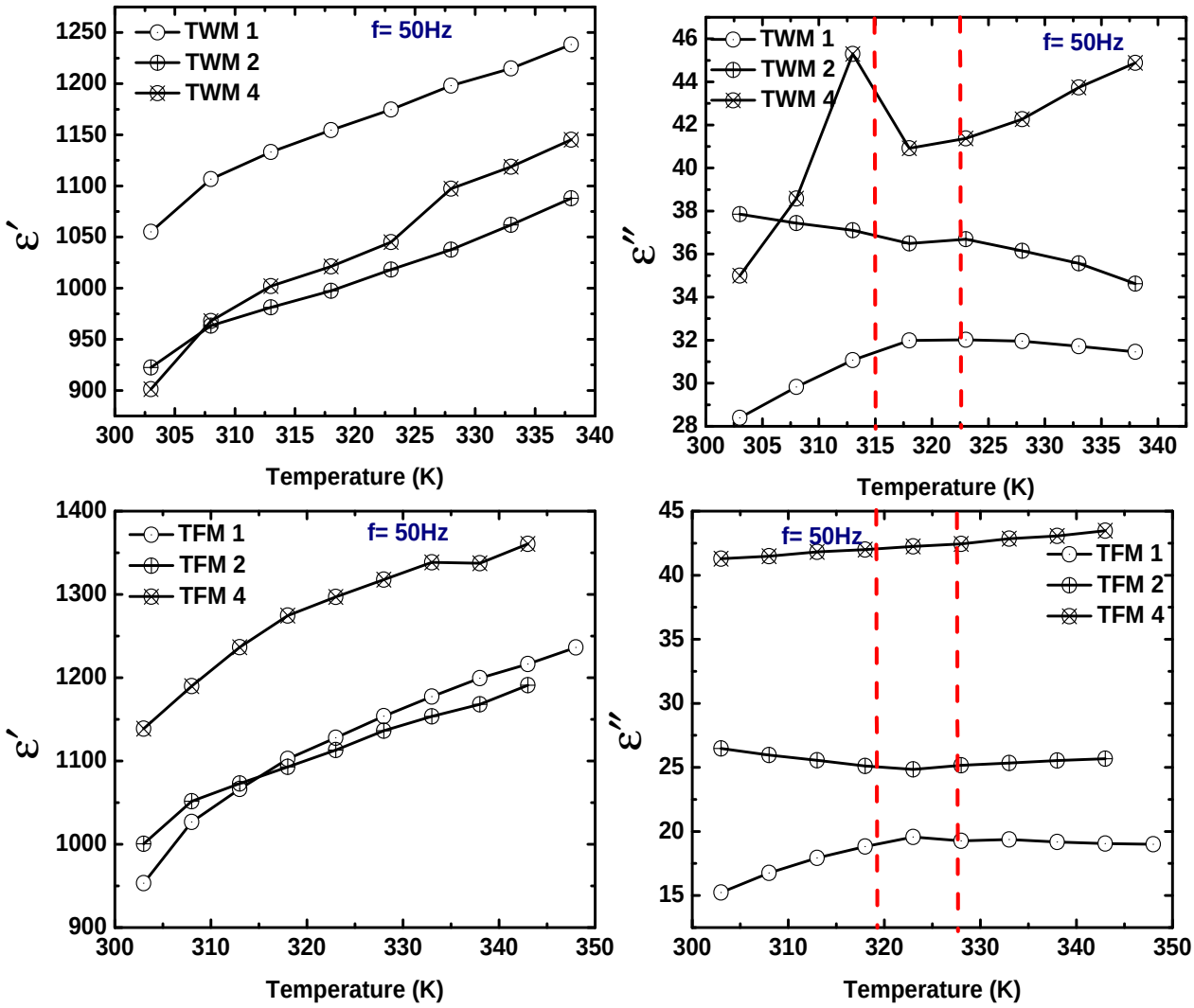

Figure 3.32: Variation of complex permittivity as function of temperature for tween 20: ethylene glycol series, tween 20: water series and tween 20 : formamide series respectively (Col.1) real part. (Col.2) imaginary part.

These single relaxation processes obtained for various mixtures of three series were best fitted with the Cole-Cole relaxation process as evident from the figure 3.33 (a-c). The variation of distribution parameter (α) ranging from 0.15 to 0.17 for T20: EG series, 0.14-0.17 for T20: W series and 0.12-0.2 for T20: F series. The corresponding relaxation parameters for these systems were computed by using the standard equations 3.9-3.11. The obtained magnitude of the relaxation parameters are given in the Table 3.16. Dielectric strength for T20: W series found to be decreased with the rise in the amphiphilic concentration, though, reverse trend was observed in T20: F series. T20: EG series shows some irregular trend of dielectric strength with the variation amphiphilic concentration as evident from the Table 3.16.

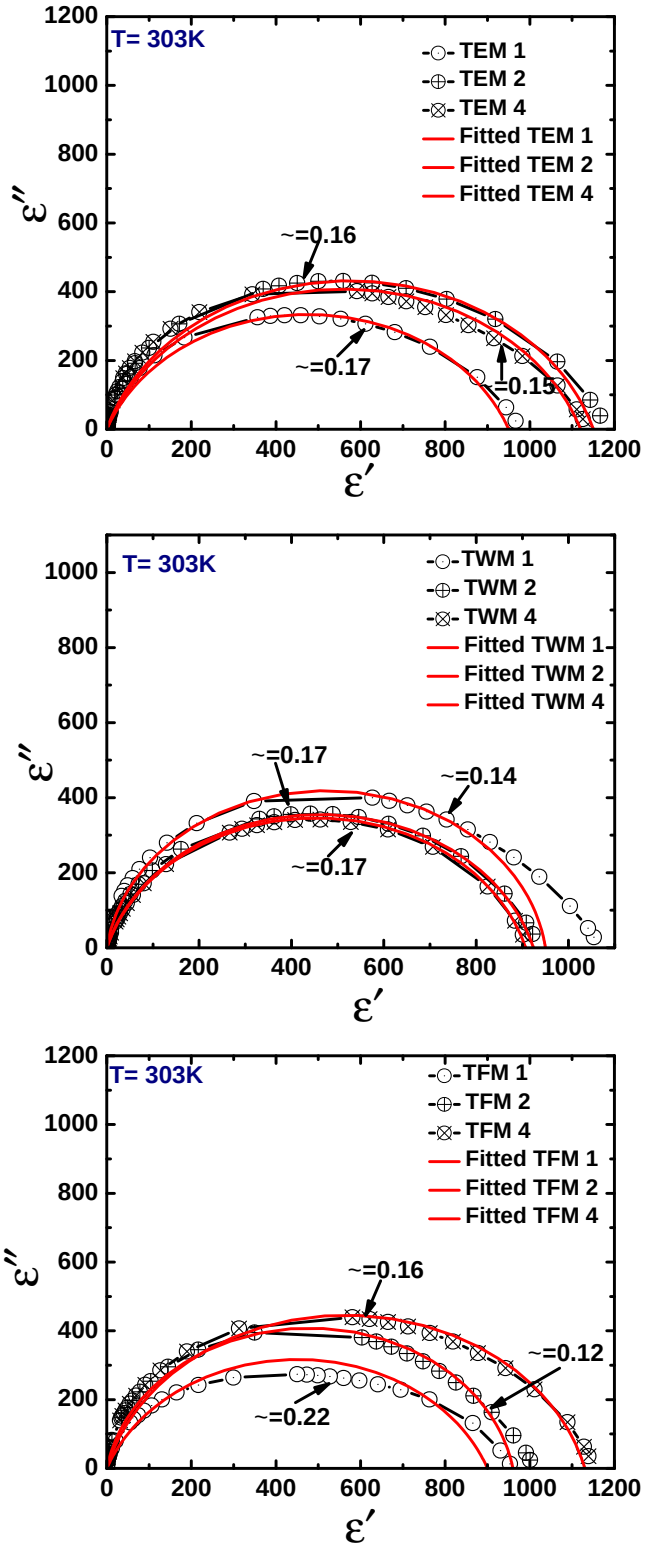

Figure 3.33: Cole-Cole plot at 303K (a) tween 20 : ethylene glycol series (b tween 20 : water series (c) tween 20 : formamide series respectively. Where M1=10:90wt%, M2= 30:70wt% and M4= 50:50wt% stands for concentration of respective solute: solvent.

The relaxation frequency noticed for these series is ranging from 603 to1503 Hz along with the low relaxation time of the micro second range.

Table 3.16: Relaxation parameters for T20: EG, T20: W and T20: F series

Tween 20: Ethylene glycol							
Mixtures	**ε′**	**Δε**	**f_r(Hz)**	**τ (μs)**	**Ea**		**n**
					Ist phase	**2nd phase**	
TEM 1	0966	0990	0646	246	12.00	9.60	1.43
TEM 2	1166	1159	0688	231	04.80	7.20	1.43
TEM 3	--	--	--	--	--	--	1.44
TEM 4	1125	1126	1276	124	18.60		1.45
TEM 5	--	--	--		--	--	1.46
Tween 20: Water							
TWM 1	1055	1034	1339	118	05.40	0.60	1.35
TWM 2	0922	0933	0713	223	01.20	3.30	1.44
TWM 3	--	--	--	--	--	--	1.45
TWM 4	0901	0909	0603	264	19.80	4.20	1.46
TWM 5	--	--	--	--	--	--	1.46
Tween 20: Formamide							
TFM 1	0953	0555	1288	123	09.60	0.60	1.46
TFM 2	1000	0957	1503	105	02.40	1.20	1.39
TFM 3	--	--	--	--	--	--	1.38
TFM 4	1138	1117	1060	150	01.20		1.46
TFM 5	--	--	--	--	--	--	1.47

3.3.4: Activation energy

Different biphasic region obtained at different concentrations and temperature scale were linearly fitted to compute the activation energy associated to these phases (graphs not shown here). The computed values of the activation energies for various series are listed in the Table 3.16. In T20:EG series at very low concentration first phase was found much stable than that of the second as it posses higher energy of activation to transit into the second phase (Table 3.16), however, in TEM 2 second phase seems to be more stable as it depicts relatively higher activation energy than that of first one. On the other hand the activation energy of first phase was found prominent for the T20: W and T20: F series. This analysis demonstrates that first phase of all the series was more stable than that of the second.

3.3.5: Refractive index

The magnitude of refractive index for the various series is given in the Table 3.16. We observed that value of **n** increased with the rise in the amphiphilic concentration for T20: EG and T20: F series, however T20: W series depicts decrease in the refractive index with rise in the T20 concentration up to TWM 3 and then again rise at higher concentrations of T20. Such behaviour of the refractive index owes to the increase in the viscosity of the systems.

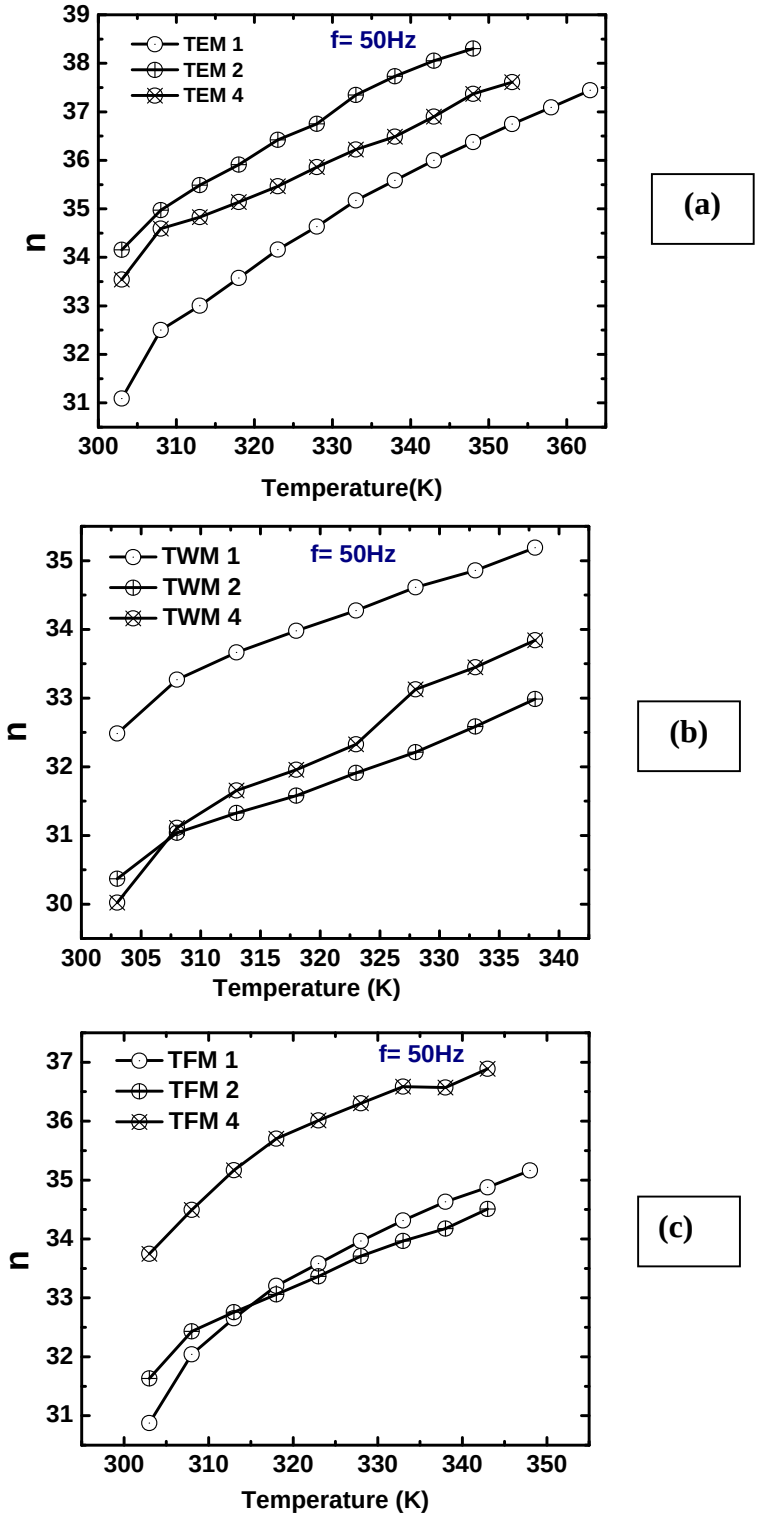

Figure 3.34: Variation of refractive index as a function of temperature (a) tween 20 : ethylene glycol series (b tween 20 : water series (c) tween 20 : formamide series respectively. Where M1=10:90wt%, M2= 30:70wt% and M4= 50:50wt% stands for concentration of respective solute: solvent.

However, the magnitude of the variation is very small. Variation of **n** as a function of temperature is presented in the figure 3.34 (a-c) for three series. The refractive index follows the same trend as discussed for the temperature dependent permittivity as it found to be increased with the rise in temperature and show various fluctuation regions as discussed earlier in dielectric behaviour.

3.4: Conclusions

In summary, from above studies we conclude that the non-aqueous solvents also prop up the self assembly process and results into more ordered layered lamellar and hexagonal phases in the lower and higher regimes of amphiphilic and solvent concentrations. It is worth noting that the polarity of the solvents and the quenching process play a vital role in the initialization of self assembly process and development of the lyotropic geometries in these systems. It is reasonable to say that these non-aqueous lyotropic mixtures are better alternative to replace water based systems as these systems shows more stable phase and up to the higher amphiphilic concentration than that of the water based systems. These systems were found stable with the variation of temperature and undergo liquid crystalline to liquid crystalline transition rather than isotropic transition in the temperature range 300-400K. The higher dielectric constant obtained for these systems is one of the key finding which enable their use as a component of the electrolytic capacitor. Higher dielectric strength and low relaxation time also facilitates these systems for capacitive applications. Systems with this range of refractive index could be used as a retarder film for the LCD applications.

3.5: References

[1] A. Ray, Nature, 231(1971) 313.

[2] A. Ray, J. Am. Chem. Soc., 91 (1969) 6511.

[3] A. Lattes , E. Perez, I. R.-Lattes, C. R. Chimie, 12 (2009) 45-53.

[4] H. N. Singh, S. M. Saleem, R. P. Singh, K. S. Birdi, J. Phys. Chem., 84 (1980) 2191.

[5] M. S. Akhter, S. M. Alawi, Colloids Surf. A, 173 (2000) 95.

[6] M. S. Akhter, S. M. Alawi, Colloids Surf. A, 219 (2003) 281.

[7] R.K Shukla, K.K. Raina, Int. J. Mod. Phys. B., 23 (2009) 5075.

[8] T. L. Greaves, C. J. Drummond, Chem. Soc. Rev., 37 (2008) 1709.

[9] C. Fong, T. Le, C. J. Drummond, Chem. Soc. Rev., 41(2012) 1297.

[10] M.K. Hossain, D.P. Acharya, , T. Sakai and H. Kunieda, J. Colloid Interface Sci., 277 (2004) 235-242.

[11] Y. Yamashita, H. Kunieda, , E. Oshimura and K. Sakamoto, J. Colloid Interface Sci., 312 (2007) 172-178.

[12] C. Tanford, J. Phys. Chem., 76 (1972) 3020-3024.

Chapter 4

Transition metal based Ternary non-aqueous LLC mixtures

This chapter summarizes structural, morphological, thermal, and optical analysis of non-aqueous ternary lyotropic liquid crystalline mixtures derived from the binary mixture of Cetyl pyridinium chloride: ethylene glycol(40:60wt%) and transition metal salt[TMS (zinc and cupric chloride)]in as prepared and quenched conditions. The origin of diverse lyotropic crystalline phases and phase transitions have been explored and discussed at lower and higher metal salt concentrations at 303K and elevated temperature. Refractive indices of these systems were explored to find the suitable application of investigated systems in technological areas.

The addition of additives like polymeric impurity, co-solvent, co surfactant and addition of inorganic salts influences the various structural and the packing parameters of the liquid crystalline mesophases. In general, addition of additives decrease the head group repulsion results in the decrease effective area at the interface and also the packing parameters. Anion and cation associated with these additives play an important role to the formation of mesostructure and solubility of the surfactants. The most advantageous prospective of these soft phases is their easily tailoring to desired mesophase by modulating the internal dimension of building blocks (head group and hydrophobic chain) via utilizing the variety of hydrophilic and hydrophobic additives. Such additives enhance the internal dimensions (like head group area and chain length), thus producing new stable and ordered LLC geometry. In this concern, new kinds of ternary systems like water, salt and surfactant (WSS) have been synthesized and characterized to facilitate the development of modified meso-structured, meso-porous materials via self assembly of ionic and non-ionic amphiphilic molecules [1-7]. They could offer confinement of the metal ions in definite ordered geometry even at lower concentration, better control on shape and size with higher yield [8-11]. However, due to the lack of stability at higher metal density and evaporation of water content from the media, these systems could not be exploited for the industrial applications [12-17]. The present study is an effort to develop some non-aqueous ternary mixture to overcome the difficulties faced in the WSS systems. Two types of transition metal salts (TMS) of varying concentrations have been employed to fabricate the ternary mixtures via dispersing the CPC: EG systems.

Ternary mixtures were prepared by dispersing the binary mixture CPC: EG (40:60 wt %) with varying concentrations (1, 2, 4, and 6, 10wt %) of transition metal salts [Zinc Chloride ($ZnCl_2$) and Cupric Chloride ($CuCl_2$). They were characterized via X-ray diffraction (XRD), polarizing optical microscopy (POM), differential scanning calorimetry (DSC) and optical techniques to confirm the development of diverse mesophase in the varying concentration regime of TMS in as prepared and quenched systems and to elucidate the corresponding thermal and optical behaviour.

4.1: Structural analysis

To confirm the distinct phases developed in three component systems XRD were employed at low angle in the 2θ range $1\text{-}10^0$. Binary mixture [CPC: EG (quenched)] exhibit well ordered neat bilayer mesophases as already described in the chapter 3 section 3.1.1. The as-prepared

ternary mixtures of $ZnCl_2$ and $CuCl_2$ did not reflect any diffraction peak indicating the absence of liquid crystalline ordering in the scanned 2θ range. Such behaviour of these systems may correspond to the lack of thermal equilibrium in these systems or metal salt hinder the self assembly process in the as prepared condition. XRD patterns for the quenched ternary mixtures are shown in the figure 4.1 (a-b) for $ZnCl_2$ and $CuCl_2$ based series respectively. System contained lower TMS ($ZnCl_2$) concentration (1wt %) diffract five lines. Last four lines were found in 1:√3: √4: √7 ratio corresponds to the hexagonal mesophase, however the first reflection at $2\theta=2.8^0$ indexed as characteristic of lamellar phase. Systems procured intermediate concentration (2, 4 and 6wt %) display four diffraction peaks, last three were indexed as characteristic reflections of hexagonal mesophase and first peak matched with lamellar mesophase. Three diffraction peaks observed at higher concentration (10 wt %) were found in 1:2:3 ratios indexed as characteristics reflection of lamellar mesophase. From the above XRD analysis it is quite evident that the addition of the TMS strongly influenced the packing of the micelles. Such modification in mesophases owing to the increase in the curvature of the head group which produce the repulsion in the alkyl chain, hence, give rise to hexagonal mesophase at lower and intermediate concentration of TMS. Though, at higher surfactant concentration repulsion at the head become more prominent drive the micelles to pack in bilayer lamellar structure. On the hand $CuCl_2$ dispersed systems did not diffract at any angle over the scanned 2θ scale at very low concentration (1wt %) as evident from the figure 4.1(b). Such disorderness in this system owing to the distortion of the LLC ordering with the addition of TMS as the neat binary system exhibit well defined lamellar phase (as already discussed in the chapter 3 section 3.1.1.). Four diffraction lines

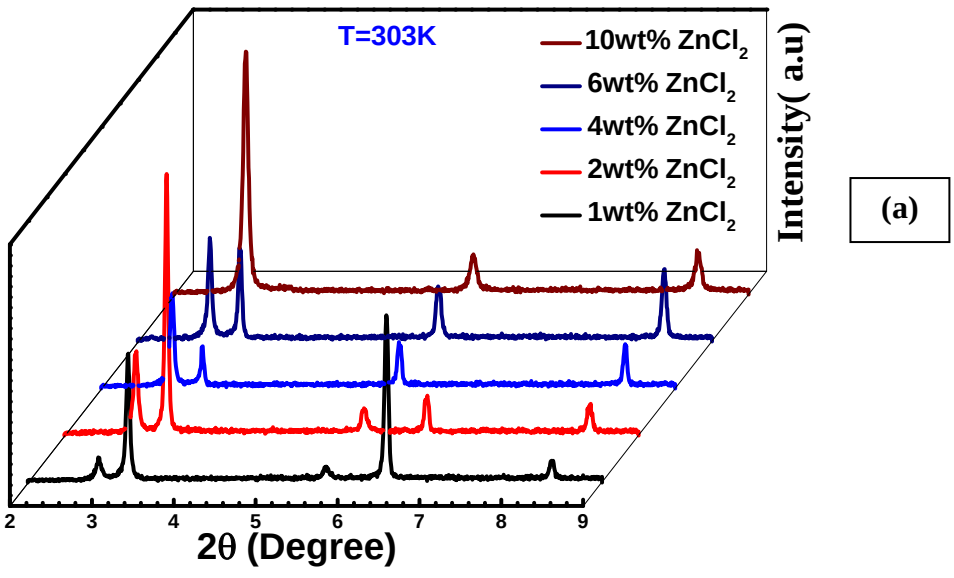

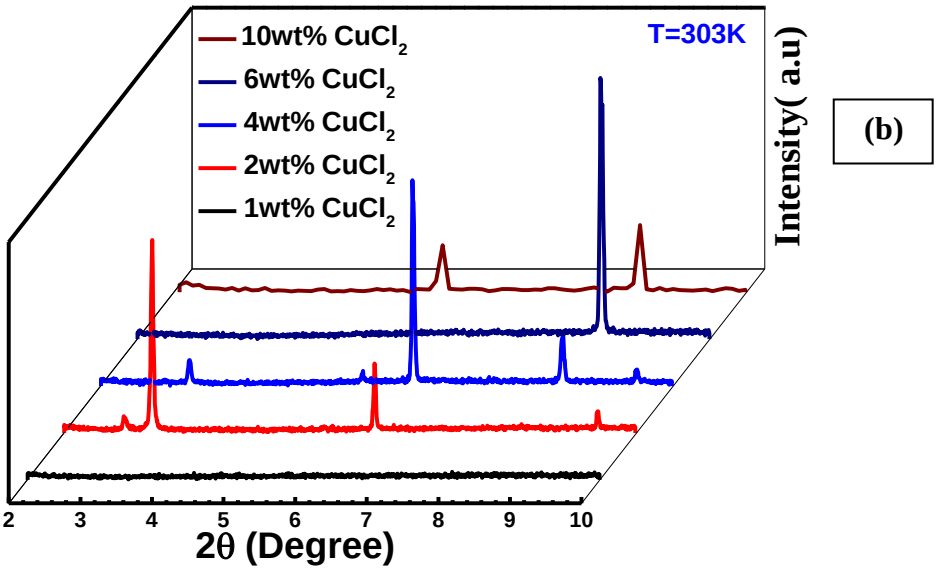

Figure 4.1: XRD profiles of quenched ternary mixtures at 303K (a) $ZnCl_2$ series (b) $CuCl_2$ series respectively.

were noticed for in 2 wt% mixture; last three lines were in 1:2:3 ratios indexed as characteristics reflection of lamellar mesophase, although, first peak was matched with hexagonal phase. Peaks observed at 4 wt% mixture were in 1:√3: √4: √7:√9 ratio, confirm the hexagonal mesophase. Single diffraction peak observed at 6wt% indexed as reflection of lamellar mesophase. However, at higher concentration system diffracts well defined highly intense peaks indexed with layered lamellar phase (were in 1:2:3 ratios) figure 4.1 (b). As prepared mixtures did not show any well ordered geometry at lower and higher concentrations of TMS (Texture not shown here) .Optical textures for the quenched mixtures are presented in the figure 4.2 Col.1 ($ZnCl_2$ series) Col.2 ($CuCl_2$ series) and Col.3 (aging effect for $CuCl_2$ series) respectively. Ordered fan like textures were seen at lower and intermediate concentrations signature of the hexagonal mesophase in the $ZnCl_2$ based series, however four lobe patterns observed at higher concentration (10wt %) was recognized as characteristic texture of lamellar phase. We noticed fanlike textures up to the intermediate concentration (1-4wt %) of $CuCl_2$ dispersed systems, though disrupted focal cones and dendritic geometry were seen at 6 and 10wt%. Interestingly some cubic rods, harvested at the nodal point of fan like texture were also found in 2 and 4wt% $CuCl_2$ concentrations. We presume that the growth of such well ordered cubic rods in the liquid crystalline moiety attributed to the confinement of released metal ions in the mesophase. Structural studies infer

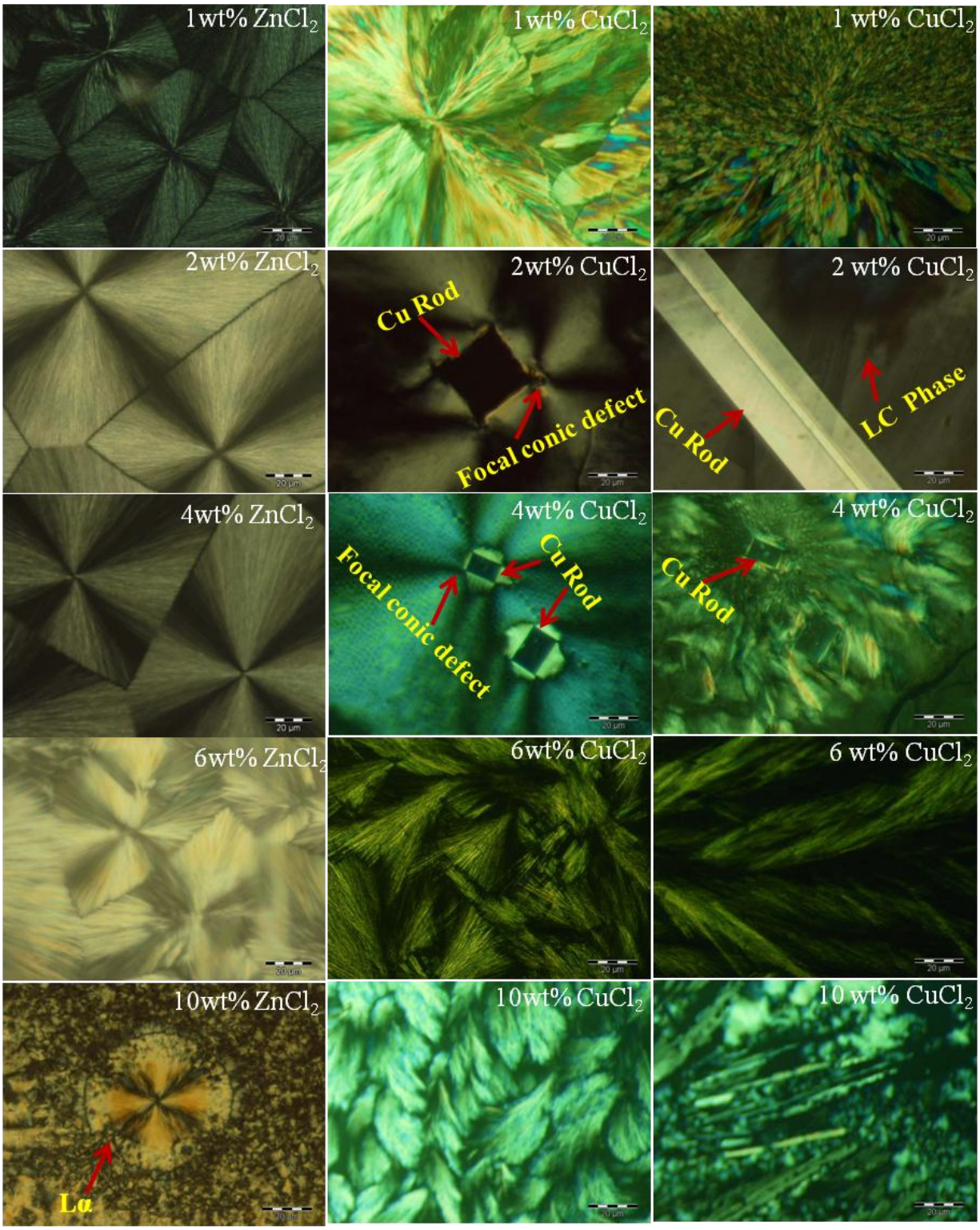

Figure 4.2: Texture patterns of quenched ternary mixtures at 303K (Col.1) $ZnCl_2$ series (Col.2) $CuCl_2$ series (Col.3) aging effect for $CuCl_2$ series respectively.

that at low metal salt concentrations, disordering in the system owe to the strong attractive electrostatic interactions between Cl^- ion and the positively charged head group. Growth of

ordered mesophases at 4 wt% (CCEM 3) corresponds to the increase in the aggregation of number of salt ions near the positively charged hydrophilic crown head group, which certainly enhance the repulsive force between hydrophobic chains (because of the increase in the curvature of hydrophilic crown) thus, resulting into hexagonal phase than that of layered lamellar mesophase. Aging effects studied for these ternary systems depicts hexagonal to lamellar transition up to 4 wt % concentrations as shown in the figure 4.2 Col. 3, however, lamellar phase remains preserved at higher concentrations. The cubic rods thus harvested at nodal point of the focal cone become eventually free from liquid crystalline moieties with the passage of time as system undergoes phase transition. A proposed model of the lamellar-hexagonal- lamellar transition observed from the textural and structural studies of $CuCl_2$ series is illustrated in figure 4.3. It is worth emphasizing to say that such transition in these systems owes to the undulation at the interface.

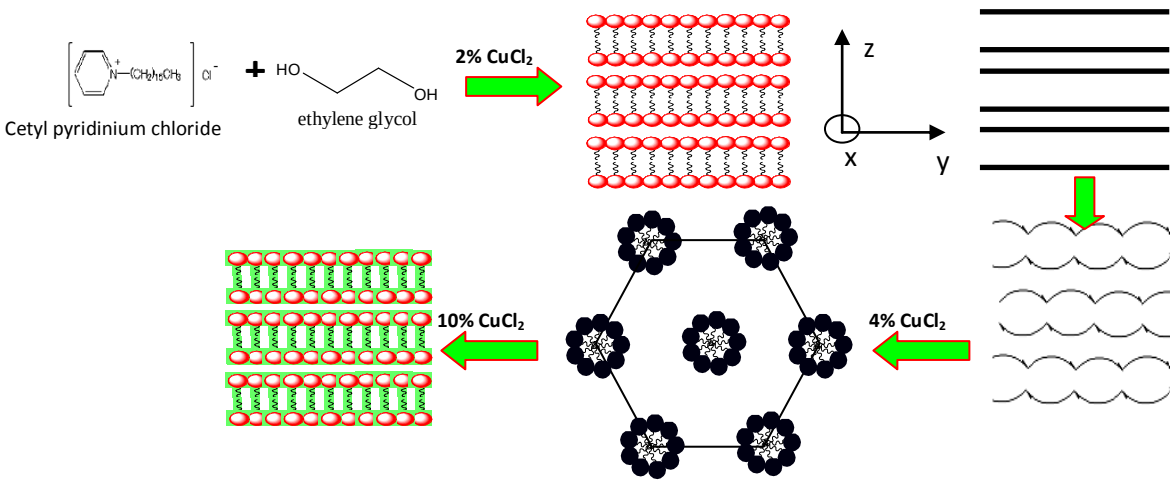

Figure 4.3: Illustration of lamellar- hexagonal- lamellar transition in $CuCl_2$ based non-aqueous ternary mixtures.

4.2: Thermal analysis

DSC profiles of neat precursor and $ZnCl_2$ based ternary mixture are depicted in the figure 4.4(a). Thermal behavior of the precursor materials was already discussed in the chapter 3. A single phase transition have been noticed for 1, 2 and 4 and 10wt% concentrations around 330K, however, system procured 4wt% $ZnCl_2$ display broad transition around 360K. These transitions either represent the amorphous to liquid crystal transition or liquid crystalline to liquid crystalline transitions, though; it is not possible to predict exact LC to isotropic transition in the studied temperature range (300-400K). The nature of reaction and order of

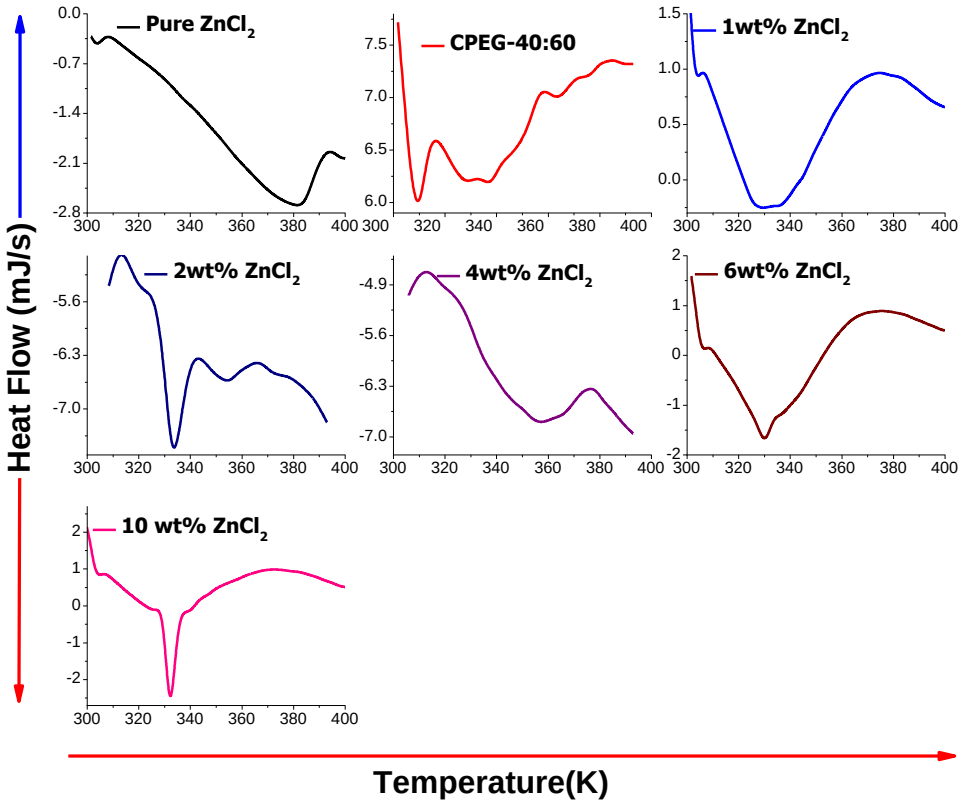
Pure ZnCl2
CPEG-40:60
1wt% ZnCl2
2wt% ZnCl2
4wt% ZnCl2
6wt% ZnCl2
10 wt% ZnCl2
Heat Flow (mJ/s)
Temperature(K)

(a)

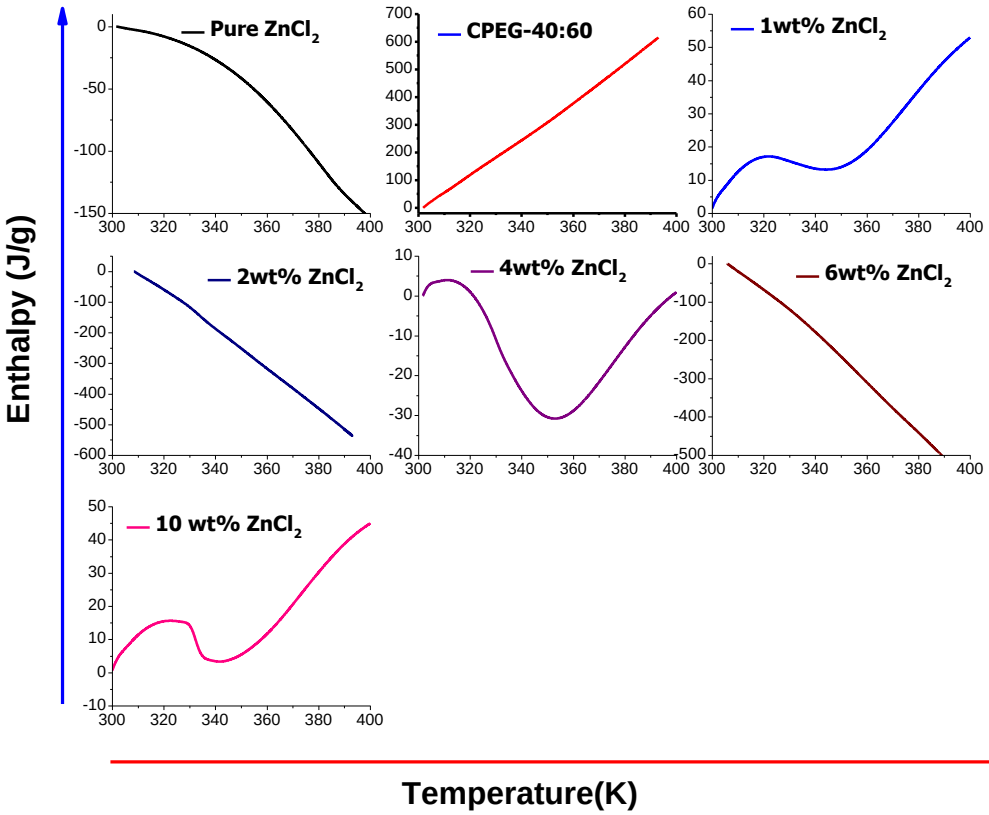
Pure ZnCl2
CPEG-40:60
1wt% ZnCl2
2wt% ZnCl2
4wt% ZnCl2
6wt% ZnCl2
10 wt% ZnCl2
Enthalpy (J/g)
Temperature(K)

(b)

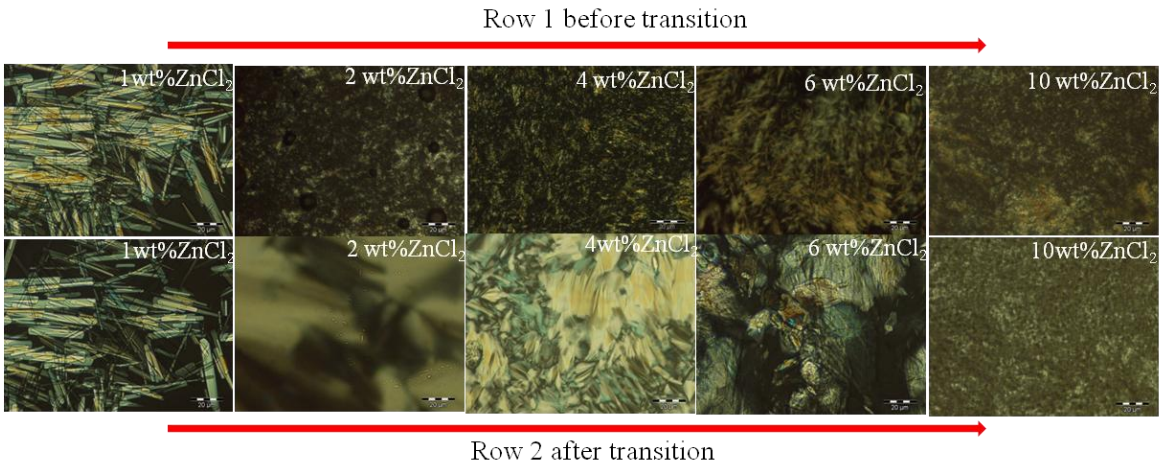

(c)

Figure 4.4: Variation of thermo-dynamical parameters for $ZnCl_2$ series (a) heat flow (b) enthalpy (c) thermo-optical analysis.

phase transitions for these calorimetric transitions are further confirmed from the variation of enthalpy and thermo-optical analysis at the expense of increasing temperature. Variation of enthalpy associated to the observed phase transitions for $Zncl_2$ based series is shown in figure 4.4(b). Pure $ZnCl_2$, binary mixture and systems procured 2 and 6 wt % $Zncl_2$ content shows continuous variation of enthalpy at transition represents the second order phase transition; however discontinuous variation of enthalpy in 1, 4 and 10 wt% represents the first order phase transition in these mixtures. Thermo-optical analysis for these systems is shown in the figure 4.4(c).Texture obtained after the transition reveals the nucleation of some new geometry in some cases, which indicates the amorphous to liquid crystalline transition in these systems. DSC profiles of precursors [pure $CuCl_2$ and Binary mixture CP: EG (40:60wt %)] and $CuCl_2$ based ternary mixtures are presented in the figure 4.5(a). Single transition peak obtained for the pure $CuCl_2$ at 380K attributed to the evaporation of coordinated water. The thermal behaviour of the binary systems (CPC: EG) is already described in the chapter 3 section 3.1.2. Single phase transition at 334, 355 and 355 K was observed up to intermediate concentrations of $CuCl_2$ (1, 2, 4wt%) though, mixture contain higher $CuCl_2$ content (6 and 10 wt%) depicts two transition peaks at 320K and 353K. The observed phase transition may correspond to the nucleation of new phase and melting or transformation of existing phases, which further confirm from thermo-optical analysis. Further to ascertain the nature and order of phase transition variation of enthalpy corresponding to these transitions is shown in the figure 4.5(b). All the mixtures depict endothermic nature as the ΔH is negative in all cases. The precursor and the prepared ternary mixtures were found continuous at the phase transition hints at the second order phase transition in these systems. Thermo-optical analysis

of these mixtures is presented in the figure 4.5(c). We noticed melting at very low concentration of $CuCl_2$ after transition as evident from the figure 4.5(c), however, other ternary systems depicts the growth of the new liquid crystalline phases.

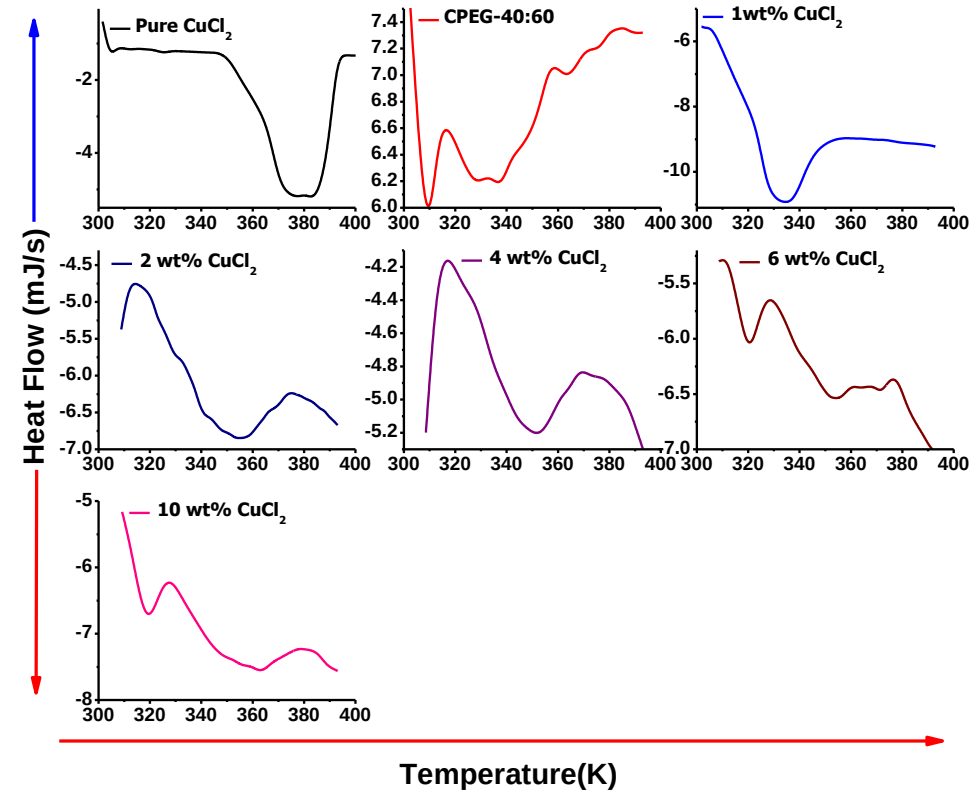

(a)

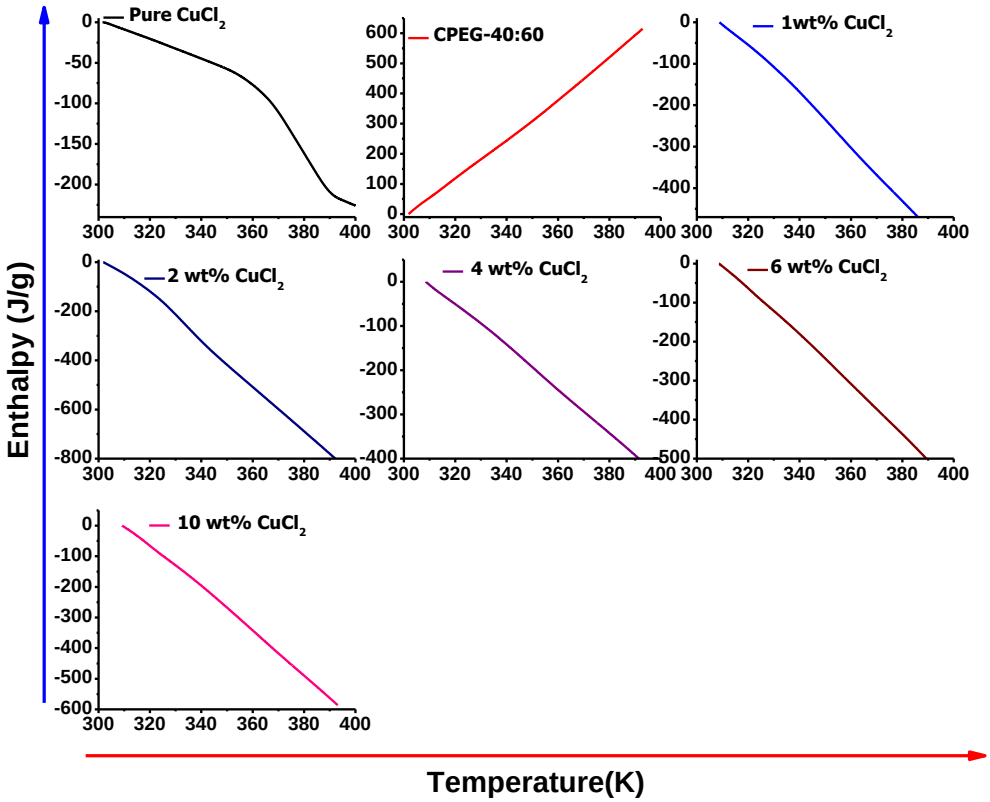

(b)

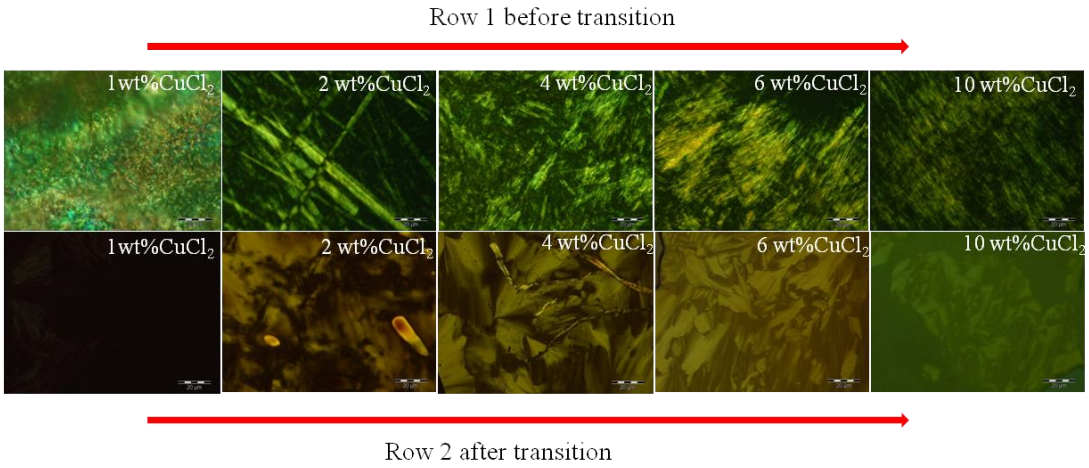

(c)

Figure 4.5: Variation of thermo-dynamical parameters for $CuCl_2$ series (a) heat flow (b) enthalpy (c) thermo-optical analysis.

All the textures observed for the nucleated phases matched with the layered lamellar structure. From these results it could be concluded that as prepared mixtures shows the amorphous to liquid crystalline transition with the variation in the temperature. These findings are found in good correlation with the thermo dynamical analysis.

4.3: Refractive index

Figure 4.6 (a-b) represents the variation of refractive index as function of $ZnCl_2$ and $CuCl_2$ concentration at 303K. It was noticed that **n** decreased with increase in the TMS concentration as evident from the figure 4.6(a). Such behavior of **n** in these mixtures attributed to the structural

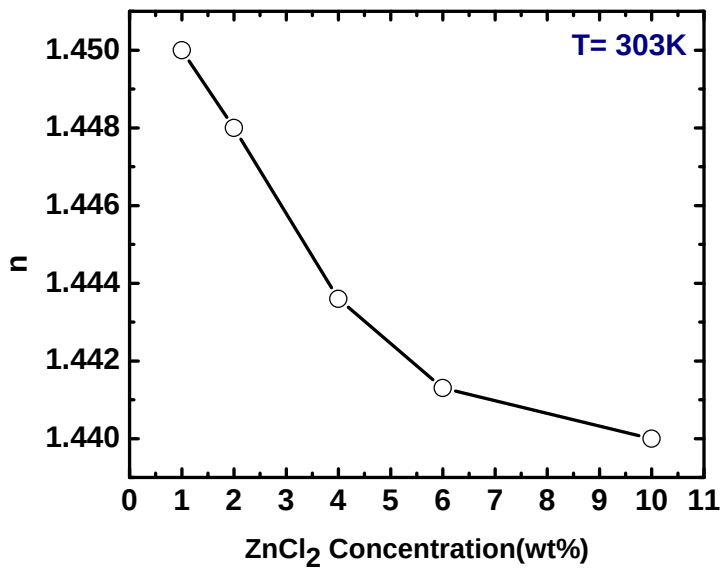

(a)

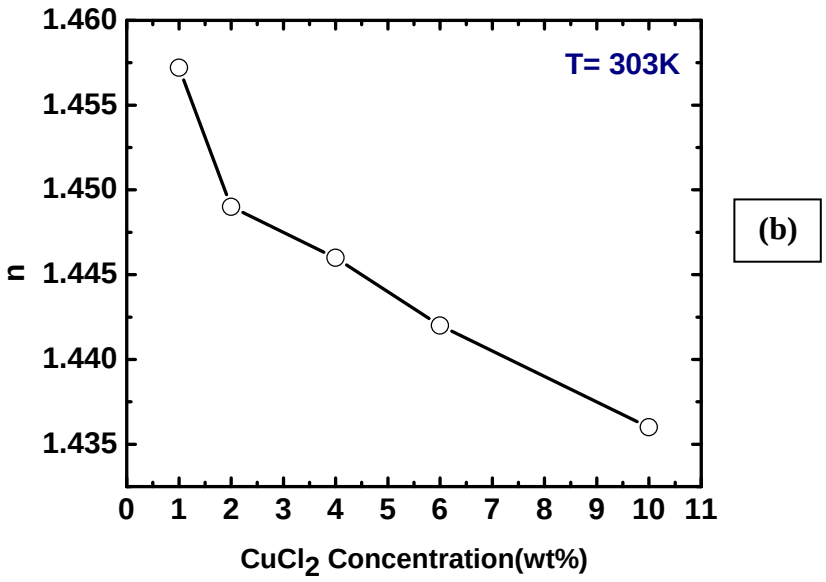

Figure 4.6: Variation of refractive index as function of TMS concentration (a) for $ZnCl_2$ based ternary mixtures (b) for $Cucl_2$ based ternary mixtures.

changes with the rise in TMS content as discussed in XRD analysis and also attributed to the random orientation of TMS ions at higher concentration distort the optical axis and hence, results lesser value of refractive index. Similar behaviour was noticed for the $CuCl_2$ based ternary mixtures as apparent from the figure 4.6(b).

4.4: Conclusions

It can be concluded from the above findings that the addition of metal salt play an important role to modulate the lyotropic phases. These ternary mixtures were found stable as they procured the lyotropic liquid crystalline phase up to higher TMS content. We noticed variety of mixed and neat lyotropic phases with the variation of the TMS content. The key finding with the addition of TMS are **a)** no phase separation have been seen at lower and higher content of the metal salt in as prepared and quenched systems, however, the phase observed were biphasic which need further experimentation to transit them in single phase, **b)** growth of the cubic rods in the $CuCl_2$ based systems prop up new possibility to grow in-situ micro and nanostructures in the non-aqueous lyotropic phases, **c)** these lyotropic phases may act as a stable soft template for the growth of variety of nanostructures and also as a conducting soft matrices. The refractive index found to be decreased with the rise of the TMS content. Further chemical analysis is in progress to understand self assembly mechanism in these complex ternary systems.

4.5: References

[1] T. Imura, Y. Hikosaka, W. Worakitkanchanakul, H. Sakai, M. Abe, M. Konishi, H. Minamikawa, D. Kitamoto, Langmuir, 23 (2007) 1659.

[2] H. Kawasaki, A. Sasaki, T. Kawashima, S. Sasaki, R. Kakehashi, I. Yamashita, K. Fukada, T. Kato, H. Maeda, Langmuir, 21 (2005) 5731.

[3] V. Percec, D. Tomazos, J. Heck, H. Blackwell, G. Ungar, J. Chem. Soc., Perkin Trans., 2 (1994) 31.

[4] M. Lee, B.K. Cho, Chem. Mater., 10 (1998) 1894.

[5] T. Otake, M. Ogasawara, K. Ito-Akıta,; N. Nishina, S. Ujiie, H. Ohno, T. Kato, Chem. Mater., 12 (2000) 782.

[6] B. Donnio, Curr. Opin. Colloid Interface Sci., 7 (2002) 371.

[7] H. Kunieda, G.Umizu, K. Aramaki, J. Phys. Chem. B, 104 (2000) 2005.

[8] O. Dag, A. Verma, G.A. Ozin, C.T. Kresge, J. Mater. Chem., 9 (1999) 1475.

[9] P.V. Braun, P. Osenar, S.I. Stupp, Nature, 380 (1996) 325.

[10] G.S. Attard, P.N. Barlett, N.R.B. Coleman, J.M. Elliott, J.R. Owen, J. H. Wang, Science, 278 (1997) 838.

[11] Y. Yamauchi, T. Momma, T. Yokoshima, K. Kuroda, T. Osaka, J. Mater. Chem., 15 (2005)1987.

[12] C. Albayrak, A.M. Soylu, O. Dag, Langmuir, 24 (2008) 10592.

[13] O. Celik, O. Dag, Ange. Chem. Inter. Ed., 40 (2001) 3800.

[14] O. Dag, S. Alayoglu, I. Uysal, J. Phy. Chem. B, 108 (2004) 8439.

[15] O. Dag, O. Samarskaya, C. Tura, A. Gunay, O. Celik, Langmuir, 19 (2003) 3671.

[16] R.K Shukla, K.K. Raina, Adv. Cond. Matt. Phys. Article ID 1747861 (2011) 1.

[17] R. K. Shukla, K. K. Raina, AIP conf. Proc., 1393 (2011) 341.

Chapter 5

Lyotropic colloidal mixtures

Present chapter deals with the structural, morphological, thermal, dielectric and refractive index analyses of ZnO based lyotropic liquid crystalline colloidal mixtures derived from the binary mixture of distinct surfactants and ethylene glycol [CPC: EG, SDS: EG, Tween 20: EG (10:90wt%)]. Various structural transitions and the nucleation mechanisms of new LC phases have been discussed at the expense of the increasing ZnO concentration. Thermo-dynamical parameters associated to these mixtures were explored to understand the stability of these colloids at the increasing temperature scale. In addition dielectric studies of these systems hint at the effects of electric field on the orientation of the impurity particles and their coupling with the LC domains. Refractive index of these systems has been measured at different temperatures (300K-400K range) to explore their suitable applications.

Self-assembly of micrometer and nanometer sized particles of various shapes and chemical compositions is of great interest from fundamental science and practical applications view point [1–10]. Anisotropic liquid crystal (LC) fluids are being used as host media for such colloidal self assembly is currently perhaps one of the most promising approaches [2–10]. It facilitate control of the medium-mediated inter particle forces by means of varying temperature, applying external fields, and utilizing the response of LC alignment to the presence of various chemical substances [3–10] and also enable one to achieve long range self assembly at the expanse of the long range orientational order of LC molecules. Most of the reports available in the literature dedicated to the nematic LC colloidal systems and few are for smectic [11-15] as already discussed in first chapter. The present study is an attempt to prepare lyotropic colloidal mixtures via dispersing ZnO micro particles in the binary mixtures of distinct amphiphiles (cationic, anionic and nonionic surfactants based) and ethylene glycol. The structural, thermal, dielectric and refractive index behaviour of prepared colloidal mixtures are examined and explored.

5.1: Pure Zinc oxide (ZnO)

Pure ZnO particles were prepared by standard co-precipitation method. The XRD pattern of as prepared ZnO is shown in figure 5.1(a). Highly intense peaks extended over 2θ scale infer about the crystalline nature of the material. The peaks observed at $2\theta=31.5^0$, 33.92^0,

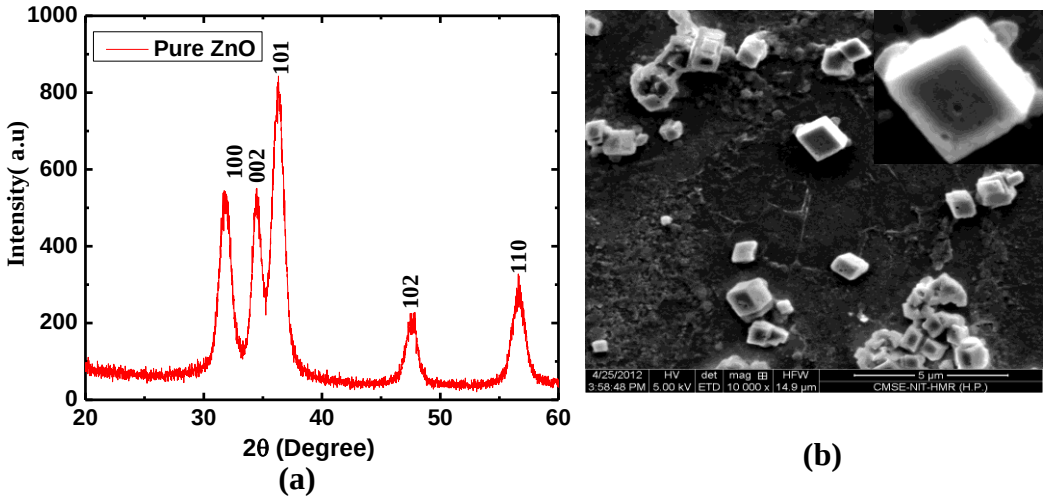

Figure 5.1: (a) XRD profile of pure ZnO (b) SEM image of ZnO.

35.93^0, 47.18^0 and 56.20^0correspondence to the lattice plane (100), (002), (101), (102) and (110) respectively, indicative of wurtzite hexagonal structure of ZnO. All the peaks were

matched with standard JCPDS card no. 50664. The scanning electron microscopy image of pure ZnO is presented in the figure 5.1(b). We noticed the cubic morphologies for these particles as evident from SEM image. The calculated average size of the particles is around 1µm. These particles were further utilized for the preparation of the lyotropic colloidal systems.

5.2: Lyotropic colloidal systems

Colloidal mixtures were prepared via dispersing the varying amount of zinc oxide particles (1µm) [(ZnO) 0.05, 0.1 and 0.5 wt%] in the binary mixtures of CPC: EG, SDS: EG, T20: EG (10:90wt %) respectively. They were characterized by X-ray diffraction (XRD), polarizing optical microscopy (POM), differential scanning calorimetry (DSC), dielectric spectroscopy and optical techniques to confirm the development of diverse mesophase in the varying concentration regime in as prepared and quenched conditions and also to instigate their thermal, dielectric and optical behaviours.

5.2.1: Structural analysis

To ascertain structure of nucleated phases and structural transition with the addition of the ZnO particles in the various binary systems (CPC: EG, SDS: EG, T20: EG), the as prepared and quenched mixtures were scanned in the $2\theta=1\text{-}8^0$ by X-rays. It was found that as prepared colloidal mixture did not diffract any angle over the scanned 2θ range (graphs not shown). It was worth noting that the quenching induces some ordering in these systems as we observed well defined peaks for the ZnO:SDS: EG based systems though, ZnO:CPC: EG and ZnO:T20: EG based systems did not diffract X-ray as evident from the figure 5.2 (a-c). In SDS: EG based systems [figure 5.2 (b)] peaks obtained at $2\theta= 3.5$ and 7^0 were found in 1:2 ratio characteristics of lamellar Lα mesophase phase. We observed hexagonal (quenched binary mixture SEM1 exhibit Hα phase) to lamellar transition with addition of ZnO particles in these systems. Such transition in these systems reflects that the addition of ZnO particles distort the cylindrical array of the micelles and the micelles packed into the bilayer structure as a result of decreasing repulsion in the hydrophobic crowns. Further to confirm the structures, these systems were studied by POM. The texture patterns for these quenched colloidal systems are presented in the figure5.3 (a) ZnO:CPC: EG, (b) ZnO:SDS: EG (c)ZnO:T20: EG respectively.

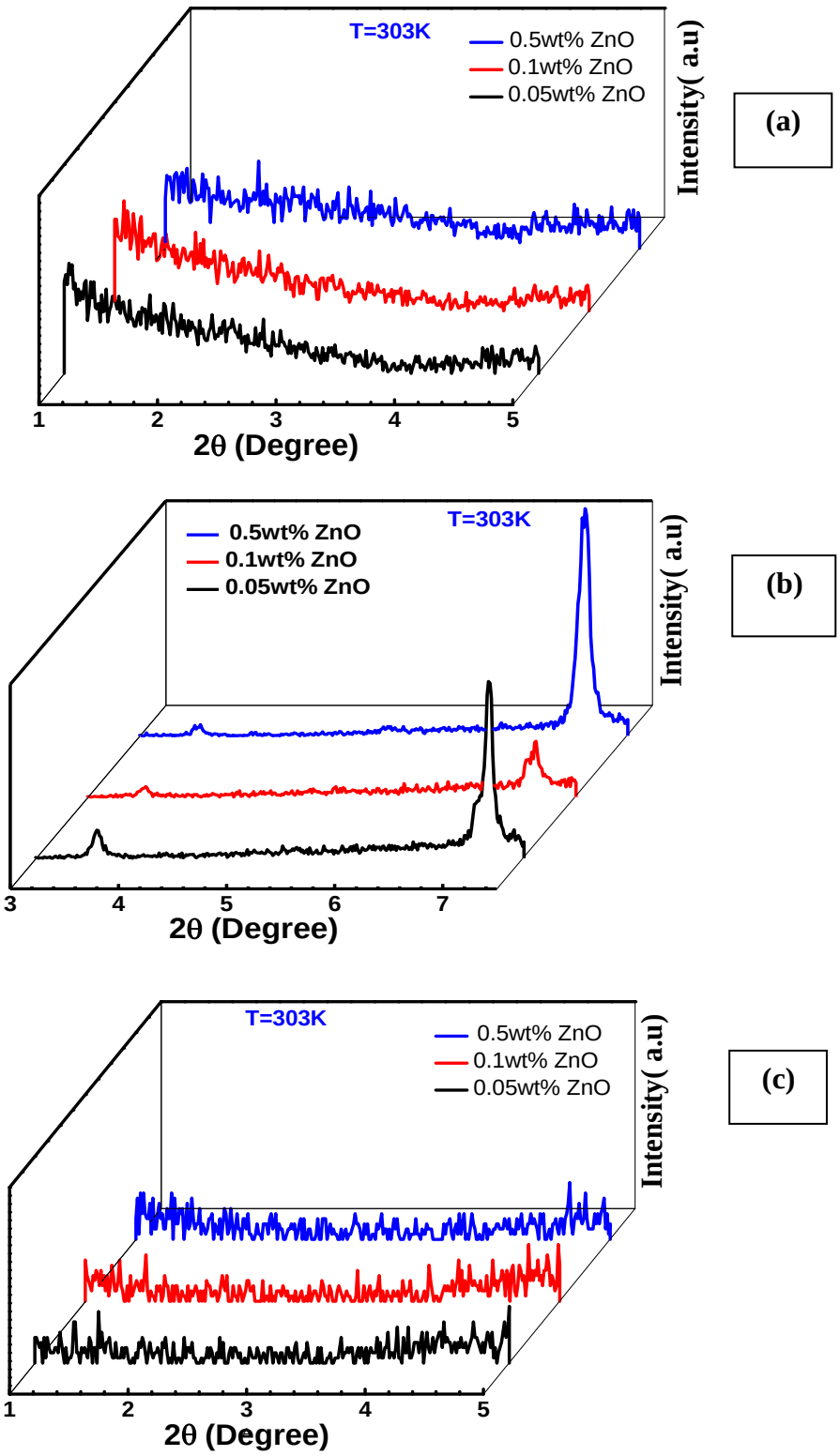

Figure 5.2: XRD profiles of quenched colloidal systems at 303K (a) zinc oxide: cetyl pyridinium chloride: ethylene glycol (b) zinc oxide: sodium dodecyl sulfate: ethylene glycol system (c) zinc oxide: tween 20: ethylene glycol system respectively.

In CPC: EG series brush like birefringent texture seen at 0.05wt% concentration, though, at higher concentrations (0.1 and 0.5wt %) characteristic textures of bilayer lamellar mesophase

along with the alignment of the particles in the direction of nodal point of the cone have been observed. Such alignment of the ZnO particles reflects the strong coupling between lyotropic

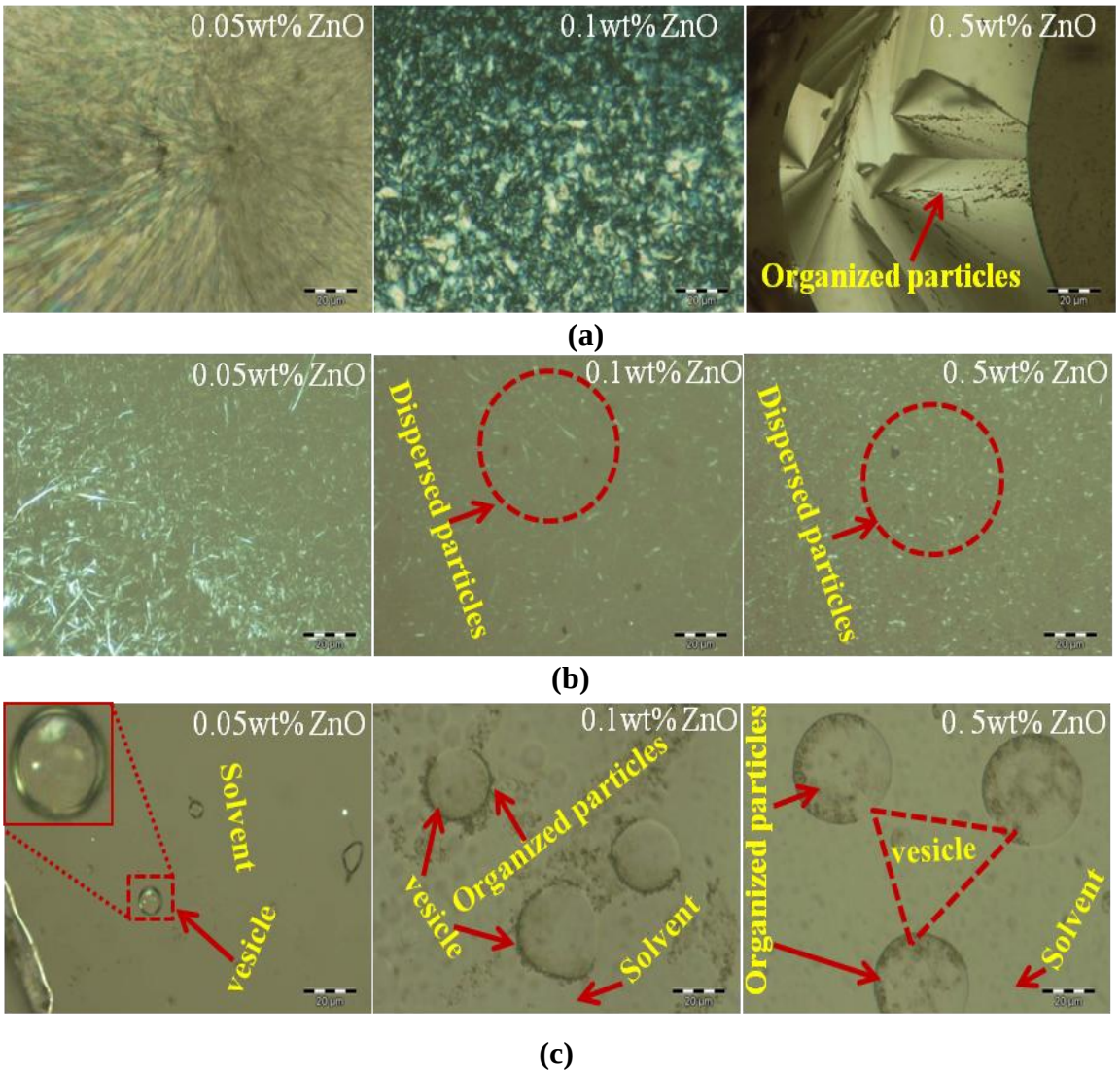

Figure 5.3: Textural variation of quenched colloidal systems at 303K at 100X magnification (a) zinc oxide: cetyl pyridinium chloride: ethylene glycol (b) zinc oxide: sodium dodecyl sulfate: ethylene glycol system (c) zinc oxide: tween 20: ethylene glycol system respectively.

domains and ZnO particles. Tiny needle like texture patterns obtained for ZnO:SDS: EG series as shown in the figure 5.3(b) predicts that these mixtures may possess liquid like and lamellar layered ordering. Interestingly vesicles like geometries and ordered arrangement of ZnO particles at the surface of the vesicles at 0.1wt% concentration and inside the vesicles at higher concentration (0.5wt %) have been noticed for ZnO: T20: EG systems as shown in the figure 5.3(c). On the basis of XRD and POM analysis it could be concluded that the addition

of ZnO particles affects the self assembly process in these systems, which results some phase transition (as we discussed above), however, ordered organization ZnO particles in some systems may depicts some interesting and enhanced properties.

5.2.2: Thermal analysis

To understand thermo-dynamical behaviour of colloidal systems for ZnO:CPC: EG series, variation of the thermal constraint are depicted in the figure 5.4 (a -b). The calorimetric transition for pure binary mixture and colloidal mixtures are shown in the figure 5.4(a). We

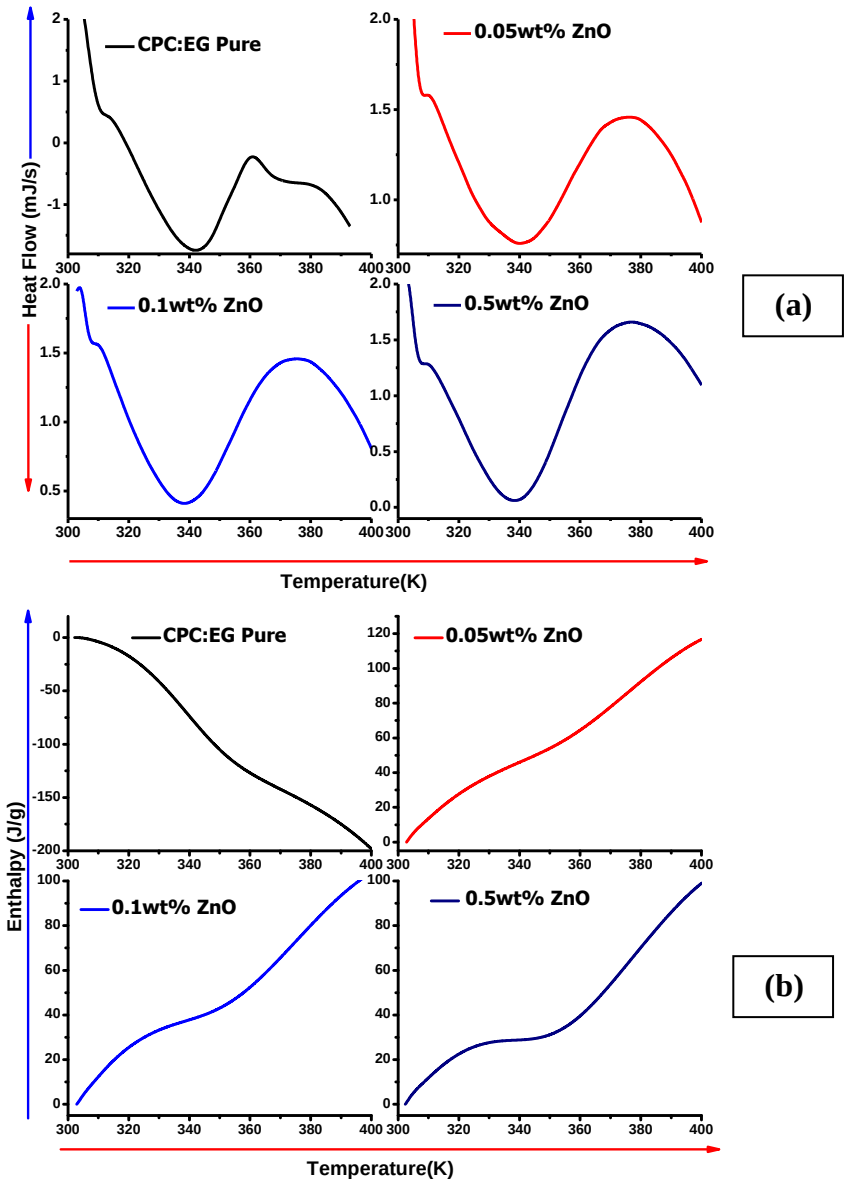

Figure 5.4: Variation of thermo-dynamical parameters for zinc oxide: cetyl pyridinium chloride: ethylene glycol based colloidal mixtures (a) heat flow (b) enthalpy respectively.

noticed the single phase transition for all the mixtures along with the decrease of 3K in the transition temperature. The transition temperatures for pure and colloidal systems are listed in the Table 5.1. These transitions may correspond to the structural transition in these systems which further confirmed from the thermo-optical analysis. To further examine the nature of reaction and the order of phase transition variation of enthalpy for these colloids is presented in the figure 5.4(b). It was noticed that all the three colloidal systems (ZnO 0.05-0.5wt%) exhibit endothermic nature, however the pure CPC:EG binary system posses exothermic nature, which means the additional heat is supplied to the systems at these transition inferring about the strong coupling in the ZnO particles and the LLC domains. The variation of the enthalpy is found to be continuous for pure binary mixture and display continuous to discontinuous transition as ZnO concentration raise to the higher side. Such behaviour of the enthalpy at calorimetric transition hint at the second order phase transition in pure binary mixture and first order phase transition in colloidal systems. To further confirm the origin of first and second order calorimetric transitions thermo-optical behaviour for colloidal systems is presented in the figure 5.5(a). We observed the nucleation of ordered phase after transition which implies that the mixtures undergo miceller to the liquid crystalline transition at the expanse of thermal energy. These findings were found in good agreement with the calorimetric studies and confirm that the transitions in these colloidal systems are of first order. Similar behaviour has been observed for the ZnO:SDS: EG, ZnO:T20: EG series (graphs not shown) and the corresponding parameters are given in the Table 5.1.

Table 5.1: Thermal parameters for the colloidal systems

Zinc Oxide :Cetyl pyridinium chloride: Ethylene glycol			
Mixtures	**Phase**	**T_C (K)**	**Order**
CPC:EG Pure	L_α+H_α	341.00	2^{nd}
0.05wt% ZnO	L_α	341.00	1^{st}
0.1wt% ZnO	L_α	338.00	1^{st}
0.5wt% ZnO	L_α	338.00	1^{st}
Zinc Oxide :Sodium dodecyl sulphate : Ethylene glycol			
SDS:EG Pure	H_α	340.00	2^{nd}
0.05wt% ZnO	L_α	340.00	1^{st}
0.1wt% ZnO	L_α	340.00	1^{st}
0.5wt% ZnO	L_α	338.00	1^{st}
Zinc Oxide :Tween 20 : Ethylene glycol			
T20:EG Pure	Vesicles	340.00	2^{nd}
0.05wt% ZnO	Vesicles	337.00	1^{st}
0.1wt% ZnO	Vesicles	340.00	1^{st}
0.5wt% ZnO	Vesicles	340.00	1^{st}

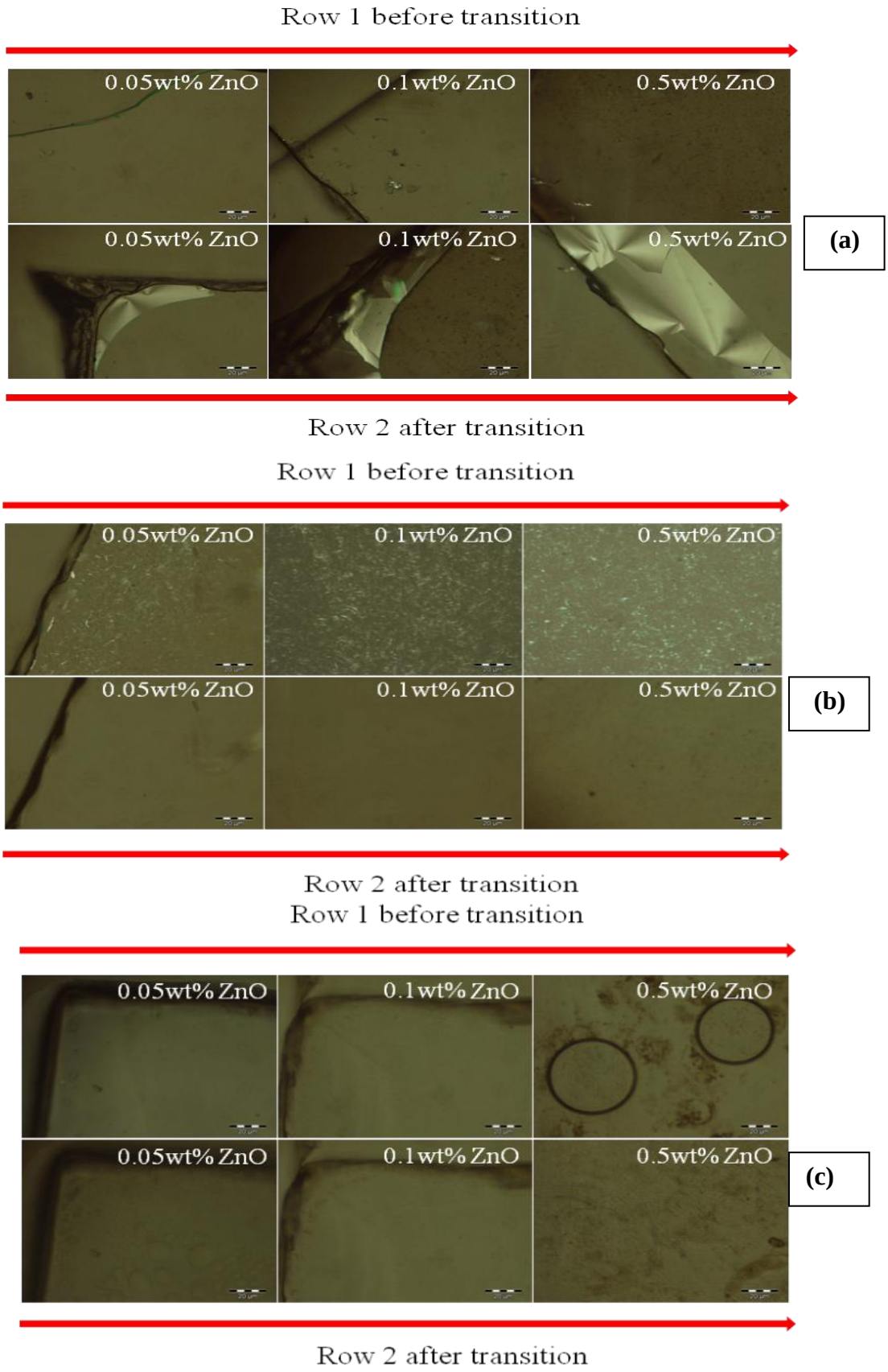

Figure 5.5: Thermo-optical analysis for the ZnO dispersed colloidal systems (a) zinc oxide: cetyl pyridinium chloride: ethylene glycol (b) zinc oxide: sodium dodecyl sulfate: ethylene glycol system (c) zinc oxide: tween 20: ethylene glycol system respectively.

It was observed that addition of ZnO particles did not affect the T_c much inferring that these colloids are entropically stable. The thermo-optical analysis for the ZnO:SDS: EG and ZnO:T20: EG based series shows the reverse behaviour than that of the ZnO:CPC: EG as evident from the figure 5.5(b-c), rather than nucleation of ordered geometries these systems showed deformation of the ordered patterns, which may corresponds to the liquid crystalline to miceller transitions.

5.2.3: Dielectric spectroscopy

The complex permittivity of pure CPC:EG and colloidal systems (ZnO =0.05,0.1 and 0.5wt%) at 303K in the frequency range of 50Hz-1MHz is shown in figure 5.6(a). Well defined exponential decay behaviour with the progression of frequency has been seen for the real part of dielectric permittivity along with the well accounted peaks in the loss factor in KHz frequency range. 18.5 (at 0.05wt %) and around 45% (at higher concentrations) increase in the dielectric permittivity have been noticed in comparison to pure CPC: EG binary systems with the addition of the ZnO at lower and higher concentration, which results large dispersion in the lower frequency range. Increase in the permittivity in these colloidal mixtures attributed to the strong coupling between the ZnO particles and the lyotropic domains and also to the increase in the mesophase ordering. In neat binary mesophasic systems (CEM as already described in the chapter 3), large permittivity owing to the dipolar motion of the micelles head group and the counter ion, we presume that the rise in the permittivity of the colloidal mixture also corresponds to the alignment of ZnO particle at the interface in the direction of dipoles via self assembly process. The loss factor for these mixtures was found minimum at lower frequencies. Single

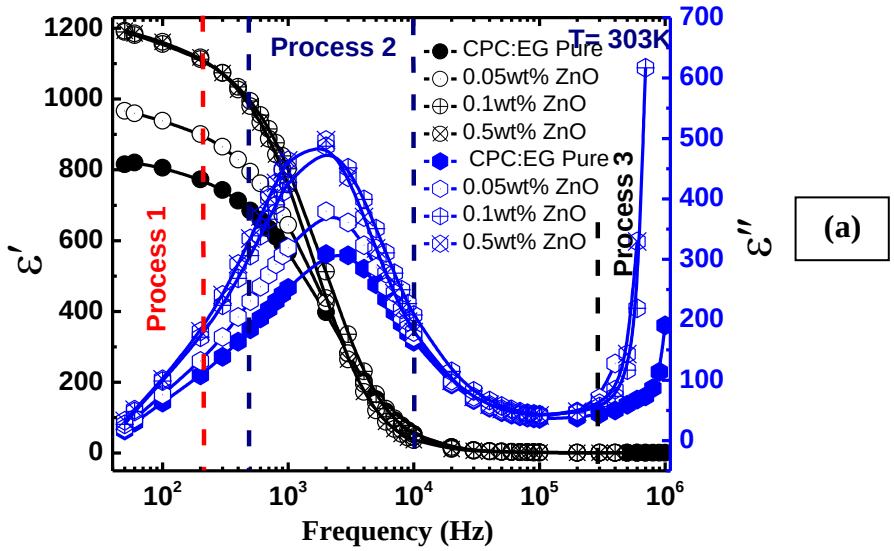

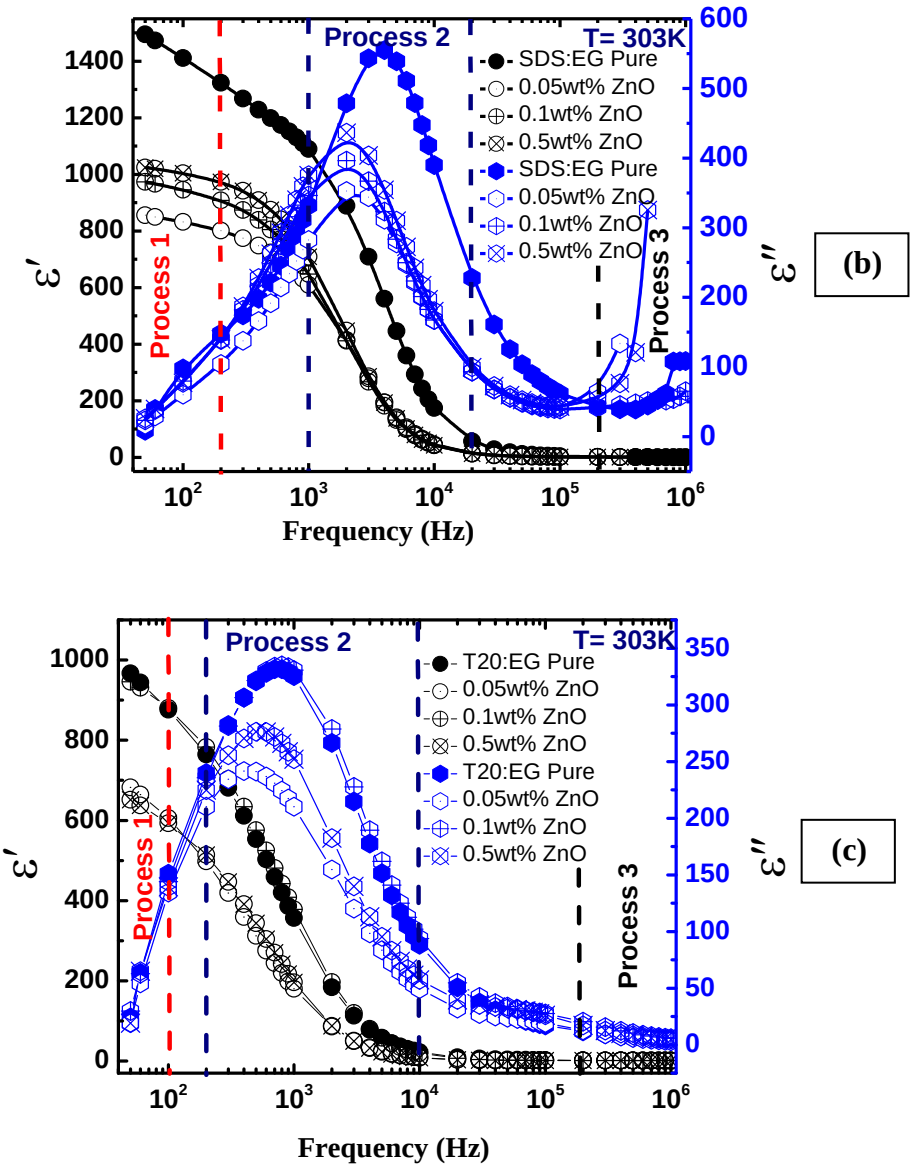

Figure 5.6: Variation of complex permittivity as a function of frequency for colloidal systems at 303 K (a) zinc oxide: cetyl pyridinium chloride: ethylene glycol (b) zinc oxide: sodium dodecyl sulfate: ethylene glycol system (c) zinc oxide: tween 20: ethylene glycol system respectively.

relaxation peaks obtained in the KHz frequency region designated as the process 2 corresponds to the relaxation of the counter ion in the charged layer with the rise in the frequency. In similar fashion the colloids derived from the ZnO:SDS: EG and ZnO:T20: EG binary systems also display well defined dielectric behaviour along with the single loss peak, though, dielectric permittivity decreased with the addition of ZnO particles in these systems. We noticed 43%, 35% and 31% decrease in the permittivity with the rise in the ZnO concentration in ZnO:SDS: EG system, however, 29, 2, 32.6% reduction have been observed for ZnO:T20: EG systems. Such decrease in the permittivity in these systems may correspond

to the structural transitions. Some anomalous trend in the ZnO:T20: EG based systems owes to the organization of the particles on the surface and inside the vesicles.

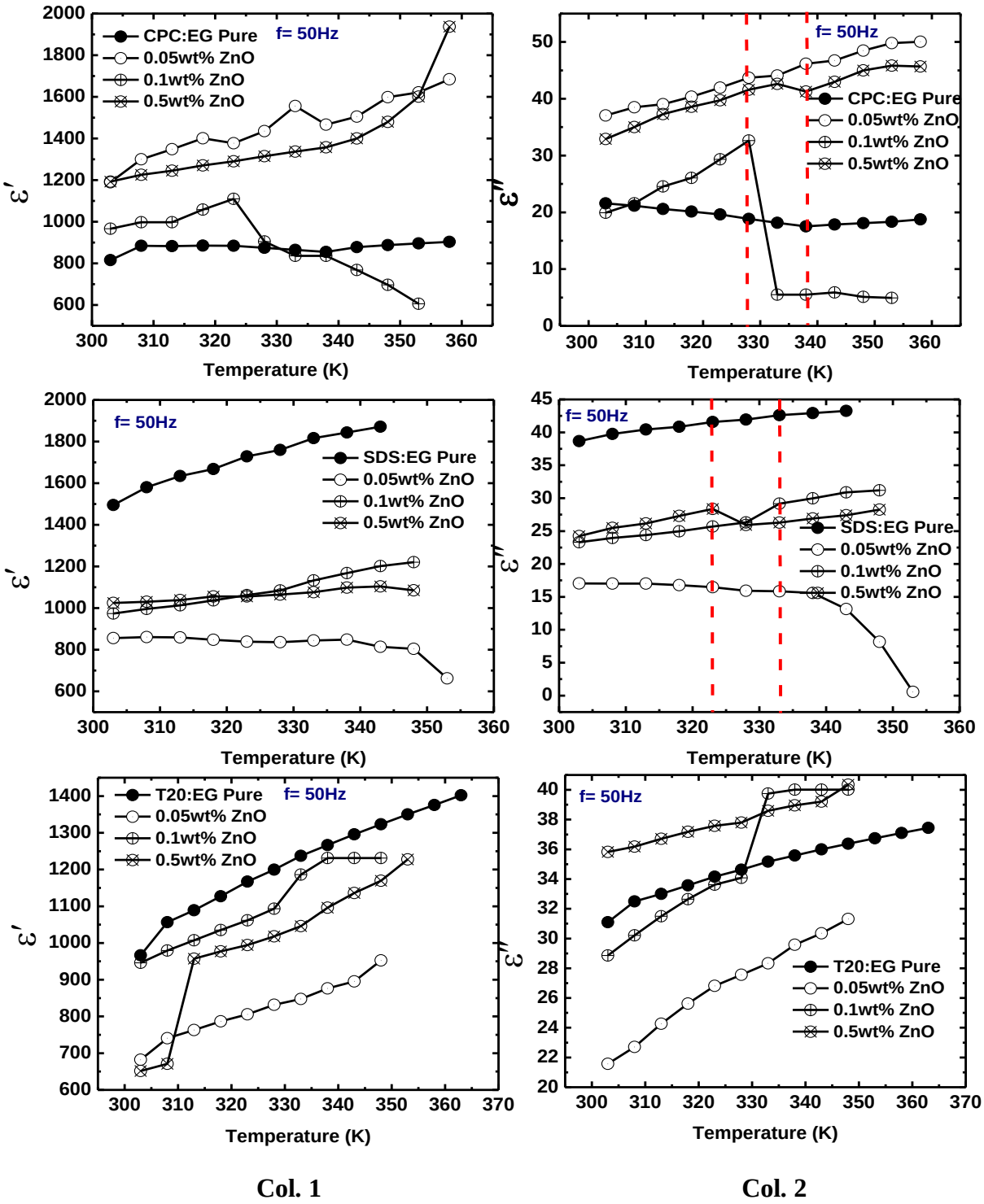

Figure 5.7: Variation of complex permittivity as a function of temperature for zinc oxide: cetyl pyridinium chloride: ethylene glycol, zinc oxide: sodium dodecyl sulfate: ethylene glycol system and zinc oxide: tween 20: ethylene glycol system respectively Col.1 real part Col. 2 Imaginary part .

Temperature dependent dielectric permittivity for these colloidal systems is shown in the figure 5.7 (Col. 1 real part and Col. 2 imaginary part respectively). All the systems show the increase in the dielectric permittivity with the rise in the temperature except 0.1wt% concentration of ZnO in CPC: EG system. Such behaviour of the permittivity hints that these systems transit from one liquid crystalline phase to another Liquid crystalline phase rather than isotropic phase. The loss factor for these systems also follows the same trend as discussed for the real part. Distinct regions as marked in the figure 5.7 Col.2 separate the two phases in the temperature range 325-340K hints at the phase transition and were found in good correlation with calorimetric studies. Relaxation process observed for these colloids was best fitted with the Cole-Cole relaxation process as all the systems show well defined semicircle with the distribution parameters of the range 0.11-0.15for ZnO:CPC:EG systems, 0.2 -0.24 for ZnO:SDS:EG systems and 0.1-0.17 for T20:EG systems respectively as shown in the figure 5.8(a-c).

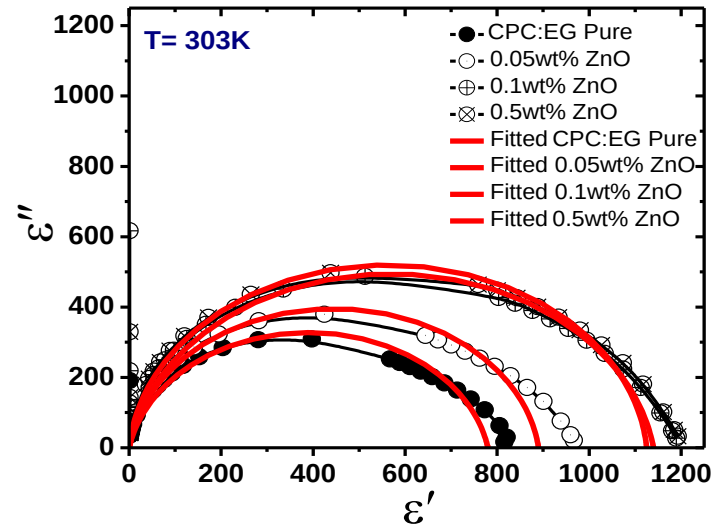

(a)

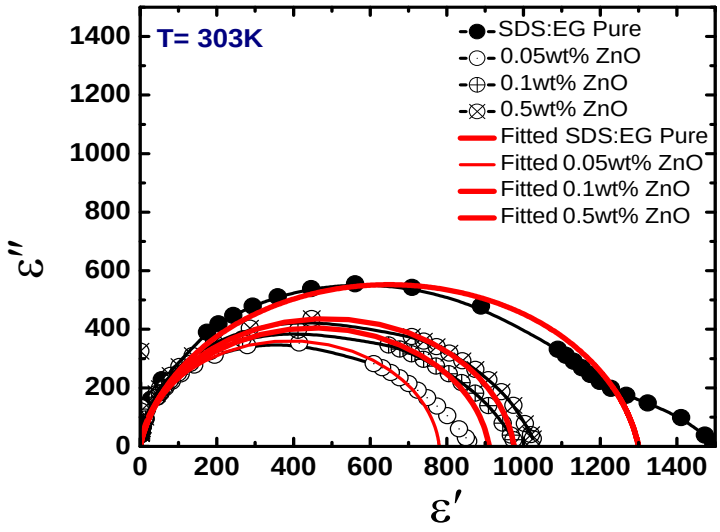

(b)

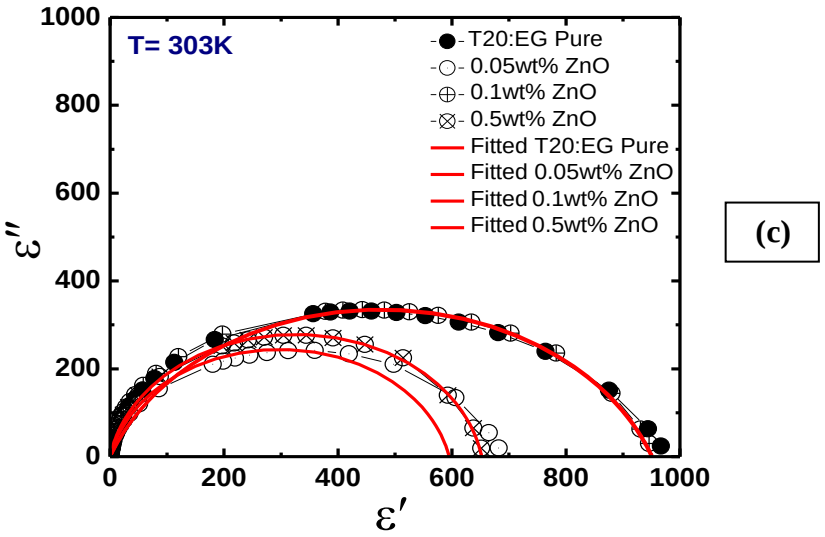

Figure 5.8: Cole-Cole plots for colloidal systems at 303 K (a) zinc oxide: cetyl pyridinium chloride: ethylene glycol (b) zinc oxide: sodium dodecyl sulfate: ethylene glycol system (c) zinc oxide: tween 20: ethylene glycol system respectively.

The corresponding relaxation parameters for colloidal systems are listed in the Table 5.2 We found higher dielectric strength for the ZnO:CPC:EG colloidal systems than that of the other two series. Relaxation frequency (f_r) found to be decreased with the addition of the ZnO particles at lower concentration (0.05wt %) and then become constant with further increase in

Table 5.2: Relaxation parameters for colloidal systems.

Zinc Oxide :Cetyl pyridinium chloride: Ethylene glycol							
Mixtures	**ε′**	**Δε**	**f_r(Hz)**	**τ (μs)**	**E_a**		**n**
					Ist phase	**2nd phase**	
CPC:EG Pure	0815	0797	2400	066	05.00	3.30	1.40
0.05wt% ZnO	0966	0922	1992	079	06.00	0.70	1.44
0.1wt% ZnO	1189	1180	2040	078	05.70	0.30	1.44
0.5wt% ZnO	1192	1188	2040	078	01.80	2.20	1.45
Zinc Oxide :Sodium dodecyl sulphate: Ethylene glycol							
SDS:EG Pure	1495	1169	4000	039	25.20	76.0	1.41
0.05wt% ZnO	0855	0823	1990	080	02.40	313.0	1.41
0.1wt% ZnO	0975	0910	1990	080	04.20	4.50	1.41
0.5wt% ZnO	1024	0999	1990	080	06.00	4.20	1.42
Zinc Oxide :Tween 20: Ethylene glycol							
T20:EG Pure	0966	0990	0646	246	12.00	9.60	1.42
0.05wt% ZnO	0682	0648	0476	334	08.30	5.40	1.45
0.1wt% ZnO	0945	0900	0770	206	05.40	0.40	1.45
0.5wt% ZnO	0651	0646	0540	294	01.80	1.80	1.40

ZnO content for CPC and SDS based colloidal system, though T20:EG system shows some anomalous trend. All the systems display very low relaxation time in the range of micro

second, though magnitude is quite high for the T20 based systems which attributed to the bulkiness of the higher chain length of T20 amphiphiles.

5.2.4: Activation energy

The Arrhenius plots for ZnO:CPC:EG colloidal systems are depicted in the figure 5.9 (a-c). Biphasic regions were linearly fitted to compute the activation energy for these systems. The computed value of activation energy is given in the Table 5.2. In ZnO:CPC:EG system first phase was found more stable as it acquire higher energy of activation to transit to the second

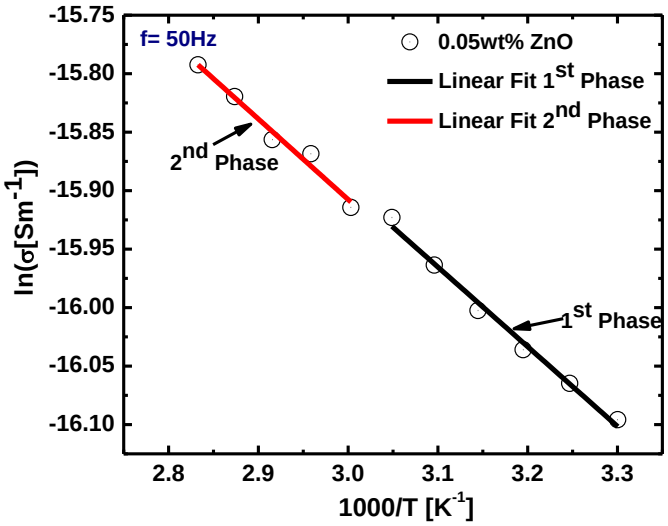

(a)

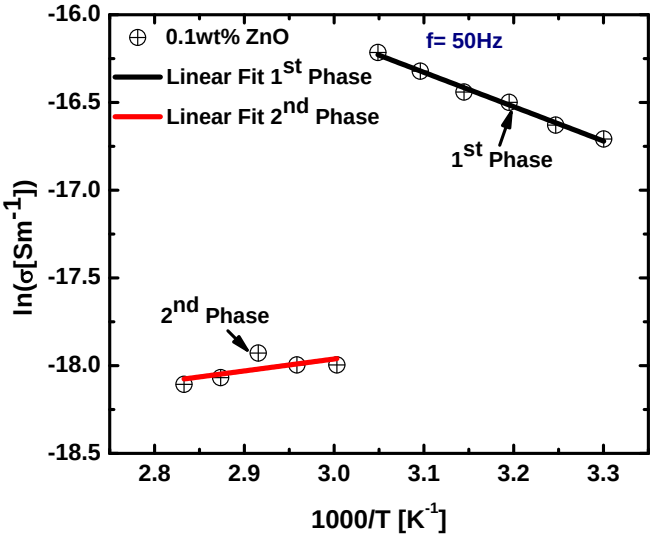

(b)

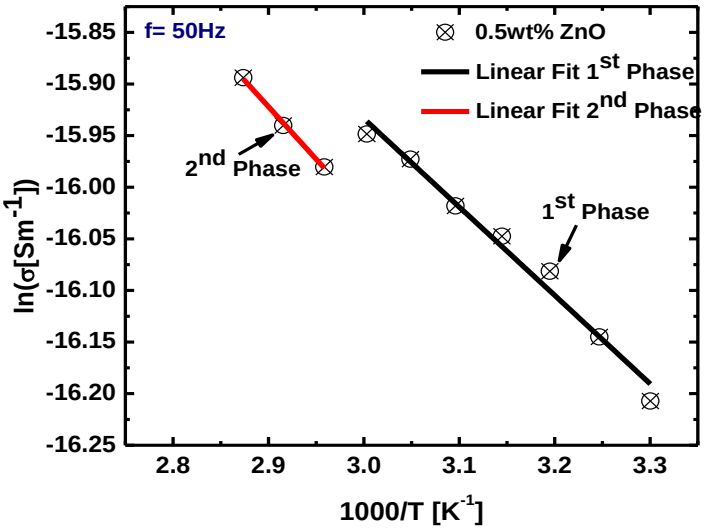

(c)

Figure 5.9: Arrhenius plot for zinc oxide: cetyl pyridinium chloride: ethylene glycol colloidal systems (a) 0.05wt% ZnO (b) 0.1wt% ZnO (c) 0.5wt% ZnO respectively.

phase. In similar fashion we computed the activation energy of ZnO:SDS: EG and ZnO:T20:EG systems by linearly fitting the biphasic regions (graphs not shown here). The obtained magnitude for various systems is listed in the Table 5.2.We observed that second phase procured higher energy of activation for SDS: EG based colloidal systems, though, the activation energy of first phase were found prominent in the T20 based systems.

5.2.5: Refractive index

Concentration based refractive index (**n**) of all colloidal mixtures is given in the Table 5.2. We observed that the **n** increased very sharply with the addition of the ZnO particles at low concentration, however, the variation with increasing ZnO content is not that much pronounced in the ZnO:CPC:EG and ZnO:SDS:EG systems. Reverse trend in the T20 based

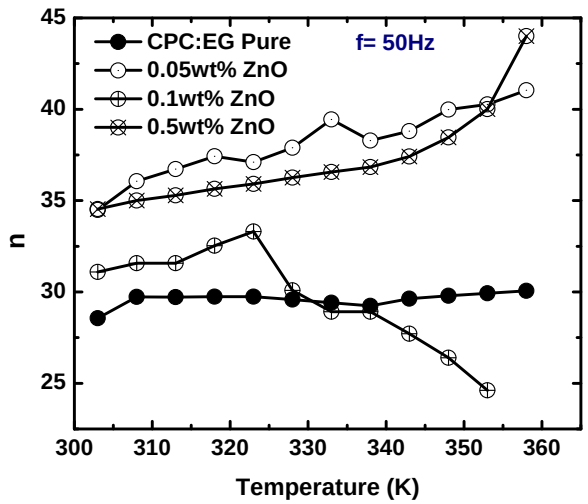

(a)

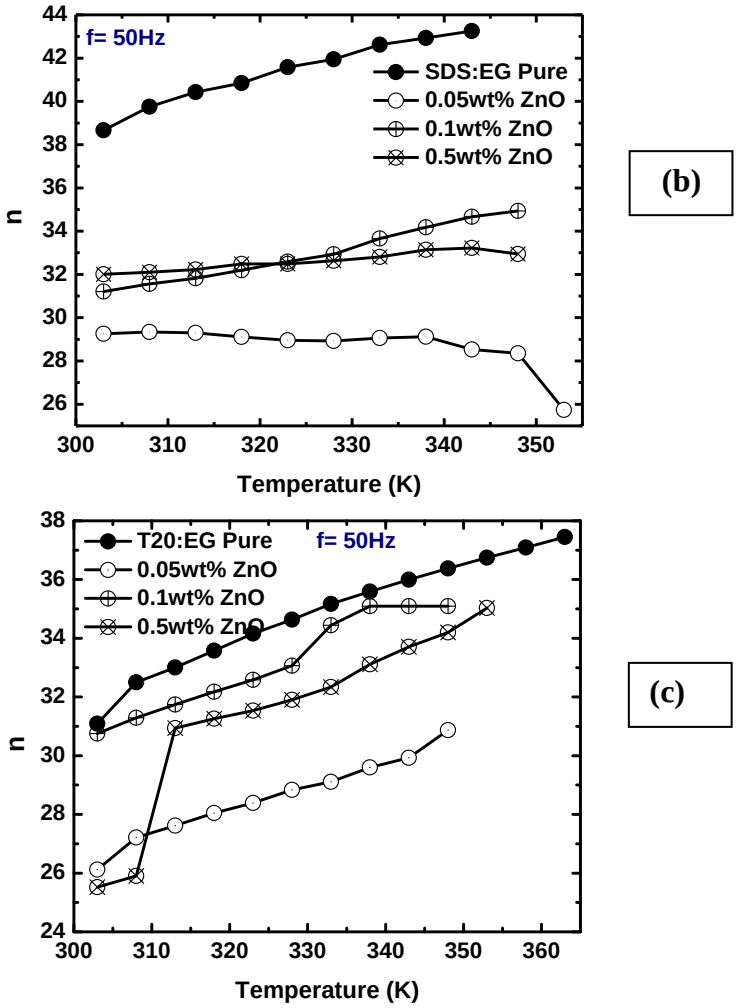

Figure 5.10: Variation of refractive index as function of temperature (a) zinc oxide: cetyl pyridinium chloride: ethylene glycol (b) zinc oxide: sodium dodecyl sulfate: ethylene glycol system (c) zinc oxide: tween 20: ethylene glycol system respectively.

systems have been seen as refractive index first increase and then decline at higher ZnO content. Such behaviour of **n** attributed to the increase in the viscosity of the systems with the rise in the ZnO content. However the variation in the magnitude **n** is very less. Variations of refractive index as function of temperature for colloidal mixtures are shown in the figure 5.10 (a-c). Temperature dependent refractive index follows the same trend as we have observed in the temperature dependent dielectric permittivity (discussed in section 5.2.3).

5.3: Conclusions

We noticed various mixed to pure and hexagonal to lamellar phase transitions in the colloidal mixtures. CPC based colloidal mixtures were found more ordered as they exhibit the mixed L_α+H_α to pure L_α phase transition with the insertion of ZnO particles and also shows

enhancement in the dielectric permittivity with the rise in the ZnO content. Though, SDS and T20 based colloidal systems display fall in the permittivity with the addition ZnO particles owing to the structural transition in these systems. The relaxation time was found minimum for the CPC and SDS based systems than that of the T20 based colloidal systems which may attribute to the higher chain length of the Tween 20 amphiphiles. No significant variation in the transition temperature has been noticed for these colloidal mixture reveals that ZnO impurities are well organized in the systems and they were entropically stable. From these findings, we concluded that cationic surfactant based colloidal mixture are best among three and can be utilized for the potential capacitor application. Further studies are in progress to explore the optical properties of these colloidal systems.

5.4: References

[1] P. Poulin, S. Holger, T.C. Lubensky, D.A. Weitz, Science, 275 (1997) 1770.

[2] M.M. Skarabot, U. Tkalec, M. Ravnik, S. Zumer, Science, 313(2006) 954.

[3] T.C. Lubensky, D. Pettey, N. Currier, H. Stark, Phys Rev E., 57 (1998) 610.

[4] C.P. Lapointe, T.G. Mason, I.I. Smalyukh, Science, 326 (2009)1083

[5] L. Ramos, M. Zapotocky, T.C. Lubensky, D.A .Weitz, Phys Rev E, 66 (2002) 031711.

[6] M. Ravnik, G.P. Alexander, J.M. Yeomans, S. Zumer, Faraday Discuss, 144 (2010) 159.

[7] T. Yamamoto, H. Yokoyama, Y. Tabe, Mol Cryst Liq Cryst, 478 (2007) 967–975.

[8] J.C. Loudet, P. Barois, P. Poulin, Nature, 407 (2000) 613.

[9] M. Zapotocky, L. Ramos, P. Poulin, T.C. Lubensky, D.A. Weitz, Science, 283 (1999) 209.

[10] O.P. Pishnyak, S. Tang, J.R. Kelly, S.V. Shiyanovskii, O.D. Lavrentovich, Phys Rev Lett., 99 (2007) 127802.

[11] Y. Kim, D. Yoon, H. Jeong, O. Lavrentovich, H. Jung, Adv. Funct. Mater., 21 (2011) 610.

[12] Y. Kim, D. Yoon, H. Jeong, H. Jung, Soft Matter, 6 (2010) 1426.

[13] Y.H. Kim, D.K. Yoon, H.S. Jeong, J.H. Kim, E.K. Yoon, H.-T. Jung, Adv. Funct. Mater., 19 (2009) 3008.

[14] J. P.F. Lagerwall, G. Scalia, Cur. App. Phys., 12 (2012) 1387.

[15] T. Sun, J. Y. Ying, Nature, 389 (1997)704.

Chapter 6

Conclusions and future scope

6.1: Conclusions

1. This study involves the development of novel non-aqueous lyotropic liquid crystalline phases in binary mixtures of cationic anionic and non-ionic amphiphiles at low and high concentration regime of the varying polarity solvents (ethylene glycol, water, formamide) in as prepared and quenched conditions. The quenched systems were found more ordered than as prepared. It is worth noting that polarity of the solvent and the nature of the building blocks (chain length, head group area and the counter ion) play vital role in the self assembly of these systems. Amphiphiles with lower chain length (SDS) results hexagonal mesophase though the amphiphiles having moderate (CPC) and higher chain lengths (Tween 20) facilitates the bilayer vesicles ordering. Various structural transitions at the expanse of increasing amphiphilic concentration have been discussed for these systems. We concluded that diverse non-aqueous mesophases obtained in this study could be better prospective to replace the aqueous mesophases in order to reduce the chances of phase transition and fulfill the requirement in the water sensitive application. We believe that these non-aqueous LLC phases will be of great interest in fundamental and technological view points and offer potential applications in diverse fields.
2. Calorimetric studies of these systems hints at their stability, nucleation and growth of new phases at the varying temperature scale. Most of these phases were stable in the temperature range of 330-345K after which they transit to another LLC phase. Most of the studied systems show second order phase transition (which implies that the systems transit from one structural phase to another rather than one state to other). Thermo-dynamical and thermo-optical analysis gives deep insight understanding about the higher ordering of the quenched phases. Though, more thermal parameters need to be analyzed to define the exact mechanism of higher ordering in quenched phases. It is difficult to predict the exact isotropic temperature for these phases in the studied temperature range (303K) range as we have found many lyotropic to lyotropic transition in these systems and in other

prospective if we raise the temperature to higher extent, these systems may transit to the thermo tropic LC phases before isotropic.

3. Higher dielectric permittivity obtained for these soft lyotropic phases is another key finding of the present study. Higher dielectric constant for various LLC mesophases (derived from the cationic, anionic and non-ionic amphiphiles) attributed to the interfacial phenomenon's and found directly proportional to the polarity of the solvent and aggregation number of the amphiphiles. Low loss factor and the relaxation phenomena observed in these mesophases. Different two phase regions obtained in the dielectric measurements and Arrhenius analysis predicts the higher stability of the first phase (higher activation energy). The higher capacitance, high dielectric permittivity, low loss, higher dielectric strength and low relaxation time enable these soft materials for the capacitive applications and also as potential component of the electrolytic capacitors.
4. Ternary mixtures (derived via TMS dispersion in binary mixture of CPC: EG) were found more stable and also hints that the TMS play a vital role to tune the desired mesophase in these soft lyotropic systems. The growth of cubic rods at low TMS concentrations open up new possibility to fabricate new micro and nano structured materials using these ternary phases. The soft TMS based mixture could also be utilized as conducting matrices for further development of LLC soft composite systems.
5. The lyotropic colloidal mixture prepared via dispersing zinc oxide (ZnO) in the binary mixtures (cationic, anionic and non-ionic) gives enhancement in the permittivity for the mesophases derived from cationic amphiphiles than that of the anionic and non-ionic. From these findings, we conclude that physical properties of these colloidal mixtures strongly depend upon ordering of the phase, alignment of the particles and counter ion of the systems.
6. Refractive index of the phases did not show any significant variation in binary and colloidal mixtures at varying concentration of amphiphiles and ZnO. To explore the optical properties of these colloidal systems further work need to be done like UV-Vis spectroscopy and the Fluorescence spectroscopy.

6.2: Future scope

Diverse neat and mixed lyotropic ordered and stable phases have been developed, although lot of work remains to understand their physics and technological prospective. These non-aqueous phases further can be utilized as soft template for the growth of nano structured materials. More experimentation and fundamental understanding is needed to exploit them for high capacitance electrolytic capacitors. Ordered lyotropic liquid crystalline colloidal systems could be studied further for optical applications using UV-Vis spectroscopy and the Fluorescence spectroscopy.